

MTP-AERO-63-31  
April 26, 1963

N 64 10105\*

203p.

Con. auctio:  
NASA

CODE-1

**GEORGE C. MARSHALL**

**SPACE  
FLIGHT CENTER**

602 703

HUNTSVILLE, ALABAMA

(NASA TM<sup>#</sup>-X-51044)

MTP-AERO-  
63-31)

A WIND TUNNEL INVESTIGATION TO DETERMINE SOME  
AERODYNAMIC HINGE MOMENTS ON THE MODEL ENGINES  
OF A SATURN I, BLOCK I CONFIGURATION

By

Glenn T. Boyd

Apr. 26, 1963 203 P ref

OTS PRICE

XEROX \$ 14.00 pl

OTS: \$14.00 pl, \$6.29 mf

MICROFILM \$ 6.29 mf.



UNITED STATES NATIONAL AERONAUTICS AND SPACE ADMINISTRATION

GEORGE C. MARSHALL SPACE FLIGHT CENTER

---

MTP-AERO-63-31

---

A WIND TUNNEL INVESTIGATION TO DETERMINE SOME  
AERODYNAMIC HINGE MOMENTS ON THE MODEL ENGINES  
OF A SATURN I, BLOCK I CONFIGURATION

By

Glenn T. Boyd

ABSTRACT

This report documents the data acquired during an investigation to determine aerodynamic hinge moments caused by external flow on nozzles of the Saturn I, Block I configuration. The model used for this investigation exhausted air through small nozzles which simulated the jet spread angle, thus simulating the base flow geometry and base pressures. The data, presented in pressure coefficient distribution form, were acquired for angles of attack from 0 to -8 degrees, free stream Mach numbers from 1.60 to 2.87, various engine gimbal angles, base shroud configurations, and for nozzle internal flow and no flow conditions.

GEORGE C. MARSHALL SPACE FLIGHT CENTER

---

MTP-AERO-63-31

---

April 26, 1963

A WIND TUNNEL INVESTIGATION TO DETERMINE SOME  
AERODYNAMIC HINGE MOMENTS ON THE MODEL ENGINES  
OF A SATURN I, BLOCK I CONFIGURATION

By

Glenn T. Boyd

EXPERIMENTAL AERODYNAMICS BRANCH  
AEROBALLISTICS DIVISION

## LIST OF ILLUSTRATIONS

<u>Figure</u>	<u>Title</u>	<u>Page</u>
1	Axis System and Sign Convention .....	10
2	Test Model Geometry .....	11-12
3	Model Pressure Instrumentation Locations .....	13-15
4	Test Model Configurations .....	16-17
5	Variation of Nozzle Exit Mach Number with Jet Static Pressure Ratio to Simulate Prototype Initial Jet Spread Angle .....	18
6	Variation of Wind Tunnel and Prototype Trajectory Jet Static Pressure Ratios with Mach Number .....	19
7-30	Pressure Distribution over the Surface of a Nozzle with Various Shroud Configurations .....	20-115
	a. Model Angle of Attack = 0 degrees	
	b. Model Angle of Attack = -2 degrees	
	c. Model Angle of Attack = -4 degrees	
	d. Model Angle of Attack = -8 degrees	
31-38	Effects of Mach Number on Star and Base Pressure Ratios at Various X/D's .....	116-147
	a. $\alpha$ = 0 degrees	
	b. $\alpha$ = -2 degrees	
	c. $\alpha$ = -4 degrees	
	d. $\alpha$ = -8 degrees	
39-41	Variation of Center Star to Base Pressure Ratio with Mach Number .....	148-159
	a. $\alpha$ = 0 degrees	
	b. $\alpha$ = -2 degrees	
	c. $\alpha$ = -4 degrees	
	d. $\alpha$ = -8 degrees	

LIST OF ILLUSTRATIONS (Cont'd)

<u>Figure</u>	<u>Title</u>	<u>Page</u>
42-49	Results of Wind Tunnel Tests Showing Variation of Shroud Pressures .....	160-191
	a. $\alpha = 0$ degrees	
	b. $\alpha = -2$ degrees	
	c. $\alpha = -4$ degrees	
	d. $\alpha = -8$ degrees	
50	Variation of Nozzle Aerodynamic Hinge Moments with Nozzle Gimbal Angle at Various Mach Numbers for Shroud Configurations .....	192-195
	a. 1	
	b. 2	
	c. 3	
	d. 4	

### DEFINITION OF SYMBOLS\*

<u>Symbol</u>	<u>Definition</u>
$M_\infty$	free-stream Mach number
$M_e$	nozzle exit Mach number
$\gamma$	ratio of specific heats (1.40 for air)
$P_\infty$	free-stream static pressures - psia
$q$	free-stream dynamic pressure - psia
$P$	nozzle external local surface static pressure - psia
$P_b$	base and star pressure - psia
$P_e$	nozzle exit static pressure - psia
$P_c$	nozzle plenum chamber pressure - psia
$P_l$	shroud local static pressure - psia
$d$	model reference diameter = 4.000 inches across tanks, (see Figure 2).
$f$	distance from gimbal point to nozzle exit plane, 1.54 inches, 96.5 inches full scale
$X$	distance from model base centerline, inches
$d_e$	nozzle internal exit diameter = .714 inches
$A_e$	nozzle exit area
$A_*$	nozzle throat area
$A_e/A_*$	nozzle expansion ratio (3.065)
$x$	distance along a nozzle longitudinal station - inches
$X/d$	normalized parameter for star and base pressure orifice

---

\*Positive direction of moments and angles are indicated by arrows in Figure 1.

## DEFINITION OF SYMBOLS (Cont'd)

<u>Symbol</u>	<u>Definition</u>
$\alpha$	model angle of attack - degrees
$\beta$	nozzle gimbal angle, measured from 6° cant, degrees
$\Delta\theta$	initial jet spread angle - degrees
$C_h$	nozzle aerodynamic hinge moment, referenced at gimbal station (100 inches full scale),  $\frac{\text{Hinge Moment}}{q A_e \int}$
$\phi$	model shroud angular orifice position, degrees
$\theta$	model nozzle angular orifice position, degrees
x/D	normalized parameter for nozzle pressure orifice locations, distance from nozzle exit.

## CONFIGURATION NOMENCLATURE

- A zero gimbal angle (Figure 4a)
- B No. 2 nozzle, maximum gimbal angle - out (Figure 4a)
- C No. 2 nozzle, maximum gimbal angle - in (Figure 4a)
  
- 1 basic shroud lengths - single flare (Figure 4b)
- 2 basic shroud length - double flare (Figure 4b)
- 3 shroud cut to heat shield (Figure 4b)
- 4 shroud cut to firewall (Figure 4b)
- 5 pressure shroud (Figure 3c and 4b)

GEORGE C. MARSHALL SPACE FLIGHT CENTER

---

MTP-AERO-63-31

---

A WIND TUNNEL INVESTIGATION TO DETERMINE SOME  
AERODYNAMIC HINGE MOMENTS ON THE MODEL ENGINES  
OF A SATURN I, BLOCK I CONFIGURATION

By

Glenn T. Boyd

SUMMARY

10105

This report presents final data from an investigation to determine nozzle aerodynamic hinge moments on a typical Saturn I vehicle model with varying engine shroud configurations. Wind tunnel tests were conducted during April and May, 1961, at the Langley Research Center Unitary Plan Wind Tunnel. Test variables for this investigation included Mach number, jets on and off, angle of attack, nozzle gimbal angle, and engine shroud configuration.

Data presented in this report primarily depict the pressure rise over the surface of a nozzle and the influences caused by Mach number, jet on and off, angles of attack, gimbal angles, and engine shroud configuration. Also included in this report are center star (flame shield) and base pressure distributions and the local static pressure distribution over one quadrant of the model afterbody.

No attempt has been made to analyze the data contained herein except to insure accuracy of the data. Some representative hinge moment data in coefficient form are presented with a brief explanation of the trends.

A UTH&R

INTRODUCTION

The investigation to determine nozzle aerodynamic hinge moments was initiated in June, 1960, after it became apparent that a stability and control problem would exist due to the substitution of the lighter weight, high energy upper stages. An increase in the control engines gimbal capability was considered mandatory to eliminate the possibility of under control. When increased from the existing seven-degree circular

pattern to the ten-degree square pattern, it was evident that the control engines would hit the shroud before reaching the maximum possible gimbal angle. Two solutions to this problem were considered:

- a. Flare the control engine shrouds an additional six degrees, beginning at station 54.
- b. Remove that portion of the shroud aft of station 54.

To determine nozzle aerodynamic hinge moment magnitudes for the following base configurations, an experimental test program was conducted at the Unitary Plan Wind Tunnel, Langley Research Center, during April and May, 1961. Configurations investigated were:

- a. Current SA-1 base shroud extending to station 22
- b. Base shroud flared six degrees from station 54
- c. Base shroud removed aft of stations 54 (heat shield)
- d. Base shroud removed aft of station 110 (firewall).

#### DESCRIPTION

##### Facility

The low speed test section of the Unitary Plan Wind Tunnel at Langley Research Center has a design Mach number range from 1.50 to 2.87. The test section is of the asymmetric sliding-block, closed-working section type with a working section four feet high, four feet wide and approximately seven feet long. This tunnel permits variation of Mach number at any desired increment through its range with the tunnel operating.

##### Model and Instrumentation

The model used for this investigation was designed and fabricated by the Marshall Space Flight Center. The core of the model was a steel weldment assembly containing a plenum chamber with an integral strut support, housing four high pressure air supply lines. The model conformed to a modified Saturn SA-1 configuration by simulated tanks, fairings and shrouds attached to the weldment assembly. Figure 2 presents test model geometry and a photograph of the model installed in the Langley UPWT. The four outboard nozzles could be gimbaled manually, but because of the complex pressure tubing routing, the base had to be disassembled. In determining hinge moments by use of pressure integration, it is desirable to obtain as many orifices as possible.

A total of thirty pressure orifices could be placed on the Number 2 nozzle, instrumented for this purpose. In addition, twenty static orifices were placed on the Number 3 nozzle as a check for instrumentation accuracy, and as a check between nozzles, since an identical pressure distribution should be felt by both. The location of these pressure orifices is shown in Figure 3a. Although this was primarily a nozzle hinge moment investigation, base and center star (flame shield) pressure distributions were also obtained. Locations of these orifices are shown in Figure 3b. Static pressure distribution was also acquired over the external surface of one quadrant of the shroud. The shroud pressure orifice locations were as shown in Figure 3c. Additional pressure measurements were made at the nozzle exit and in the nozzle plenum chamber for exit static and stagnation pressures. Pressure measurements were made using pressure transducers with scanivalves.

Configurations tested during this investigation included:

- a. SA-1 base shroud extending to station 22
- b. Base shroud flared six degrees from station 54 - double flare
- c. Base shroud removed aft of station 54 (heat shield)
- d. Base shroud removed aft of station 110 (firewall).

Figure 4 presents details of the various test model configurations including the magnitude and direction of engine gimbaling.

#### Tests

The model, being single-strut supported, was pitched negatively at zero yaw to eliminate any interference from the strut and to obtain the maximum combined angle of attack and gimbal angle relationship. Results of an investigation conducted previously on a "no flow" model indicated no strut interference for the top-side nozzles and an approximate data deviation of two per cent for the lower nozzles. Table I presents a run schedule with pertinent test variables included.

No corrections have been applied to the angles of attack due to tunnel flow misalignment. Depending on test Mach number, flow misalignment in this tunnel is less than  $1.5^\circ$  as defined by calibrations.

Matching Parameters

Several approaches may be used in the determination of nozzle aerodynamic hinge moments, any of which would yield valid trends. Absolute magnitudes, however, may be determined only by simulation of the full scale geometry and exact duplication of flow parameters.

The method used for determining nozzle hinge moments in this investigation involved passing high pressure air through the nozzles to simulate internal flow characteristics. Hinge moments are obtained by integrating measured pressures radially and longitudinally over the nozzle external surface. Simulation requirements include duplication of the exhaust plume shape and vehicle base pressures which require alteration of the nozzle internal geometry. However, a change in the internal geometry affects the external shape of the nozzle making duplication of the exact configuration impossible. This shows that compromises must be made as to which simulation parameters are considered the most important.

Given the jet exit Mach number of the prototype engine and known jet gas specific heat ratios of both the model and prototype, the model jet exit Mach number may be determined by methods presented in Reference 1. Having ascertained jet exit Mach number, the required nozzle expansion ratio (area ratio) may easily be found, thus yielding the proper diameter ratio (exit to throat). Previous studies show that the derived nozzle shape approximates the shape of that derived by the method of characteristics within a deviation of  $\pm 3\%$ , when an area ratio of  $A_e/A_s = 3.065$  is used, the nozzle exit angle is simulated, a throat radius of curvature of one and one-half times the throat radius is selected, and a general bell mouth shape is used. However, these relationships are valid in the strictest sense for a pressure ratio  $P_e/P_\infty = 1$ . The deviation of actual jet spread angle from optimum spread angles for pressure ratios greater than one is relatively small particularly for the range of test pressure ratios considered. Figure 5 shows these deviations in jet spread angle vs pressure ratio for the prototype and model nozzles. Prandtl-Meyer expansion expressions were used to compute the initial spread angles. The dashed curve in Figure 5 indicates jet spread angle variation with jet static pressure ratio for the test nozzles. Note also the test nozzle exit Mach number variation required to duplicate the prototype spread angles through the test range of pressure ratios. As mentioned previously, however, the test nozzle ( $M_e = 2.66$ ) provides jet spread angles in close agreement with the prototype nozzle ( $M_e = 3.20$ ). Presented in Figure 6 is the variation in range of jet static pressure ratios for the test model and for a typical prototype trajectory with test Mach number. Although altitude was not matched, the model nozzle chamber pressure was adjusted so that jet static pressure ratio was matched to that of the prototype at each test Mach number.

### PRESENTATION OF DATA

The data in this report are shown as pressure ratio distributions. It was originally intended to present all nozzle pressure data in hinge moment form. However, tests showed that the only configuration applicable to the Saturn base shroud configuration was that of the SA-1. Examination of the nozzle pressure distribution plots showed no appreciable pressure rises for the SA-1 configuration, hence, negligible hinge moments.

Figures 7 through 30 present the variation of pressure distribution over the nozzle surface for various model shroud configurations. The plots for a given figure number are arranged in negatively increasing model angles of attack. Figures 7 through 14 present curves for a gimbal angle of  $0^\circ$ . Plots are arranged in order of increasing free-stream Mach number with odd figure numbers containing jet-on data and even figure numbers, jet-off data. Figures 15 through 22 are arranged in the same general order for a gimbal angle of  $+6^\circ$ . The data presented in Figures 23 through 30 are also arranged in this order for a gimbal angle of  $-9^\circ$ .

Figures 31 through 38 present the effect of Mach number on center star (flame shield) and base pressure ratios in the base and star regions. These plots are arranged by configuration with the odd numbered figures denoting jet-on runs and the even numbered, the jet-off runs. Jet-on values of the pressure ratio ( $P_e/P_\infty$ ) are indicated in Table I and on the first figure of each set.

Data presented in Figures 39 through 41 are the results of evaluating the data presented in Figures 31 through 38. Center star to base pressure ratio variation with Mach number is shown where the center star value chosen is the peak pressure in the star region and the base pressure is taken as an average value from the preceding plots. These plots are presented for configurations A-1, A-2, and A-3. Data for configuration A-4 are not shown because the base pressure instrumentation was eliminated when the shrouds were removed at the firewall position.

Figures 42 through 49 depict the variation of static pressure distribution over the surface of one control engine shroud of the A-1 configuration. The plots are arranged in order of increasing Mach number with the even numbered figures containing jet-on data and the odd numbered, jet-off.

Figure 50 contains a representative selection of the nozzle pressure data reduced to hinge moment coefficient form. These data were obtained by integrating, circumferentially and longitudinally, the nozzle surface pressure distribution and resolving the moment about the gimbal point (station 100, full scale) in a plane  $45^\circ$  to the pitch plane of the model.

This report does not present all data acquired during the test program. A certain amount of pressure data (for example, the Number 3 engine surface pressures) was taken primarily as a check of the Number 2 engine pressure instrumentation malfunctioned. A visual comparison was made of the data obtained from both nozzles, the deviation being within the data accuracy.

#### DISCUSSION

A representative selection of nozzle aerodynamic hinge moment data is included in this report. Figure 50 shows that for the SA-1 configuration no hinge moments of any consequence appear. This is due to the fully shrouded condition at the base. As was anticipated, nozzle hinge moments for configuration 2 (double flared shroud) corresponded very closely with configuration 1. Although configurations such as 3 and 4 do not now exist, it is interesting to note the magnitude of  $C_h$  compared to that of the SA-1 type configuration.

TABLE I

<u>Run No.</u>	<u>Configuration</u>	<u>M</u>	<u><math>\alpha</math></u>	<u>P<sub>c</sub></u>	<u>P<sub>e</sub>/P<sub><math>\infty</math></sub></u>
15	A-2	1.60	Range	--	jet off
16		1.60		114.8	2.9
17		2.00		--	jet off
18		2.00		114.5	5.4
19		2.40		--	jet off
20		2.40		115.2	9.7
21		2.87		--	jet off
22		2.87		116.2	20.1
23	A-3	1.60		--	jet off
24		1.60		138.4	3.4
25		2.00		--	jet off
26		2.00		138.7	6.2
27		2.40		--	jet off
28		2.40		139.7	11.3
29		2.87		--	jet off
30		2.87		139.9	23.2
31	A-4	1.60		--	jet off
32		1.60		129.6	3.4
33		2.00		--	jet off
34		2.00		130.5	6.2
35		2.40		--	jet off
36		2.40		130.5	11.3
37		2.87		--	jet off
38		2.87		130.6	23.2
40	A-1	1.60		--	jet off
41		1.60		131.0	3.4
44		2.00		--	jet off
45		2.00		130.3	6.2
47		2.40		131.9	11.3
48		2.40		--	jet off
51		2.40		--	jet off
53		2.87		--	jet off
55		2.87		132.0	23.2
57	B-4	1.60		--	jet off
58		1.60		131.6	3.4
59		2.00		--	jet off
60		2.00		131.5	6.2
61	B-4	2.40		--	jet off
62		2.40		132.3	11.3
63		2.87		--	jet off
64		2.87		132.2	23.2
65	B-3	1.60	-2°, -4°, -8°	--	jet off
66		1.60	Range	129.7	3.4
67		2.00		--	jet off

TABLE I (Cont'd)

<u>Run No.</u>	<u>Configuration</u>	<u>M</u>	<u><math>\alpha</math></u>	<u>P<sub>c</sub></u>	<u>P<sub>e</sub>/P<sub><math>\infty</math></sub></u>
68	B-3	2.00	Range	130.4	6.2
69		2.40		--	jet off
70		2.40		130.1	11.3
71		2.87		--	jet off
72		2.87		130.3	23.2
73	B-2	1.60		--	jet off
74		1.60		130.5	3.4
75		2.00		--	jet off
76		2.00		129.9	6.2
77		2.40		--	jet off
78		2.40		132.1	11.3
79		2.87		--	jet off
80		2.87		131.9	23.2
81	B-1	1.60		--	jet off
82		1.60		131.8	3.4
83		2.00		--	jet off
84		2.00		131.6	6.2
85		2.40		--	jet off
86		2.40		130.8	11.3
87		2.87		--	jet off
88		2.87		132.3	23.2
89	C-1	1.60		--	jet off
90		1.60		132.3	3.4
91		2.00		--	jet off
92		2.00		133.5	6.2
93		2.40		--	jet off
94		2.40		132.7	11.3
95		2.87		--	jet off
96		2.87		132.8	23.2
97	C-2	1.60		--	jet off
98		1.60		131.2	3.4
99		2.00		--	jet off
100		2.00		130.7	6.2
101		2.40		--	jet off
102		2.40		130.7	11.3
103		2.87		--	jet off
104		2.87		131.8	23.2
105	C-3	1.60		--	jet off
106		1.60		130.0	3.4
107		2.00		--	jet off
108		2.00		130.4	6.2
109		2.40		--	jet off
110		2.40		130.7	11.3
111		2.87		--	jet off
112		2.87		131.9	23.2

TABLE I (Cont'd)

<u>Run No.</u>	<u>Configuration</u>	<u>M</u>	<u><math>\alpha</math></u>	<u><math>P_c</math></u>	<u><math>P_e/P_\infty</math></u>
113	C-4	1.60	Range	--	jet off
114		1.60		125.6	3.4
115		2.00		--	jet off
116		2.00		126.6	6.2
117		2.40		--	jet off
118		2.40		124.9	11.3
119		2.87		--	jet off
120		2.87		125.3	23.2
125	5-A-1	1.60		--	jet off
126		1.60		130.2	3.4
127		2.00		--	jet off
128		2.00		129.7	6.2
129		2.40		--	jet off
130		2.40		130.2	11.3
131		2.87		--	jet off
132		2.87		130.5	23.2

Range =  $0^\circ$ ,  $-2^\circ$ ,  $-4^\circ$ ,  $-8^\circ$

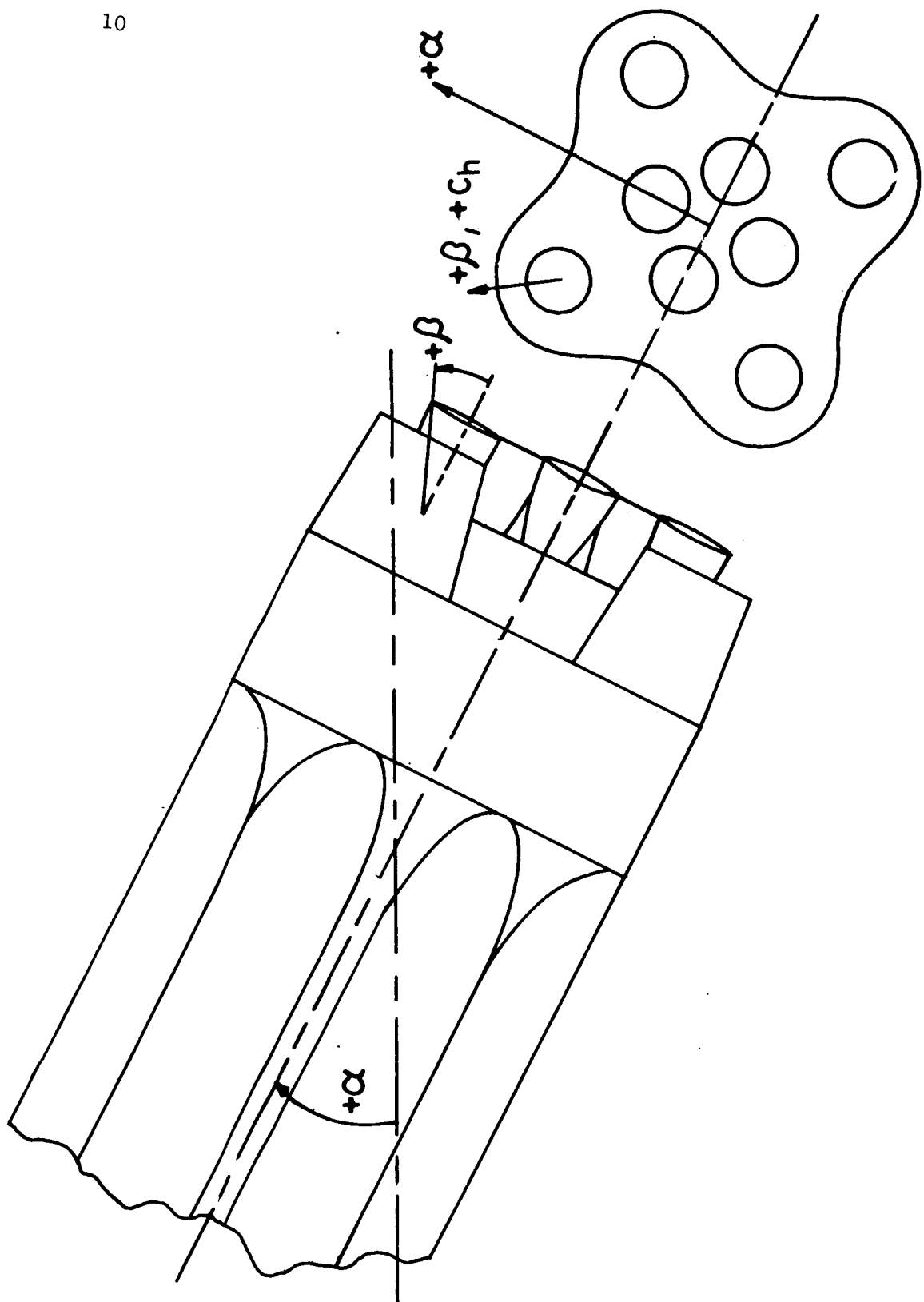


FIGURE I AXIS SYSTEM AND SIGN CONVENTION

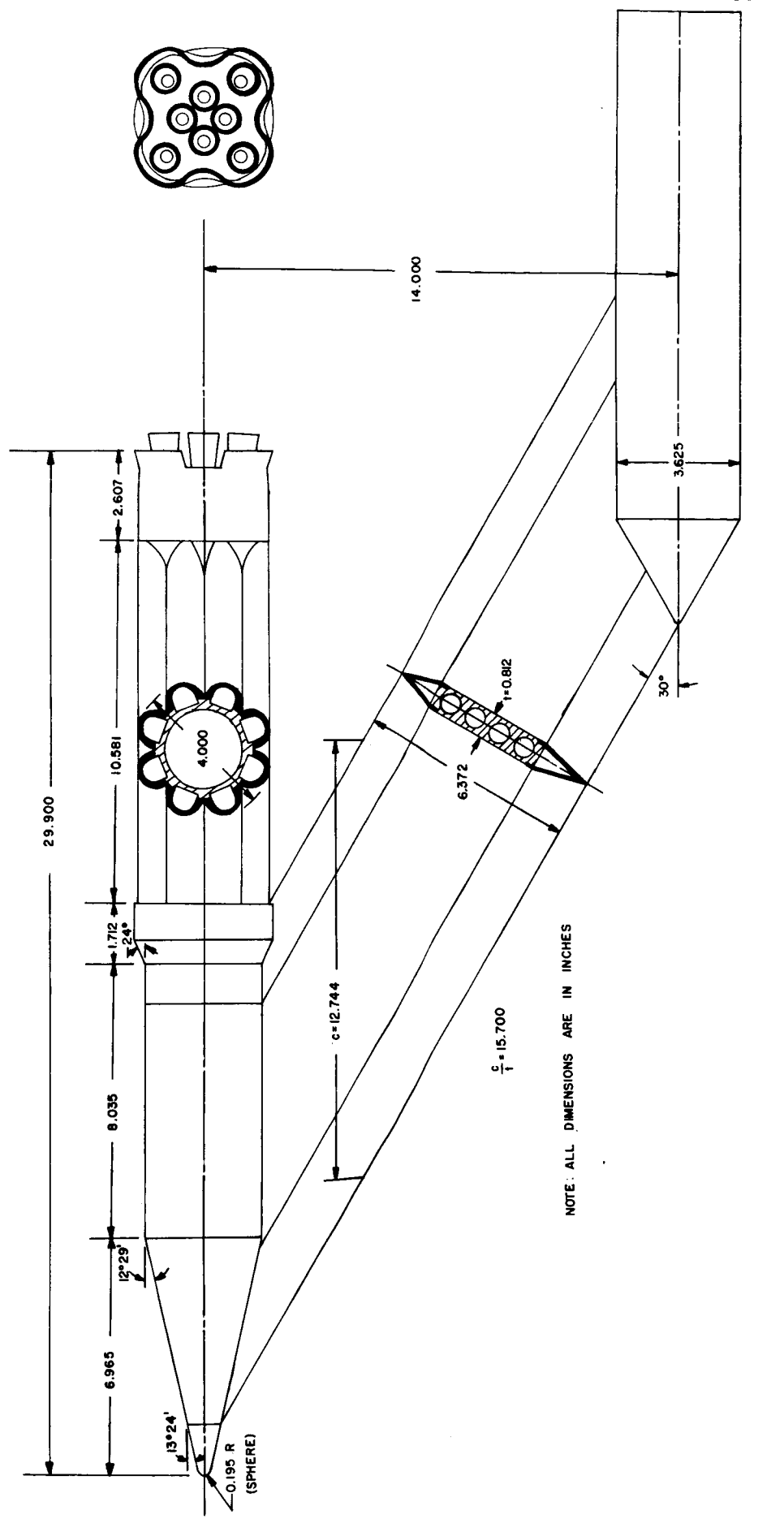
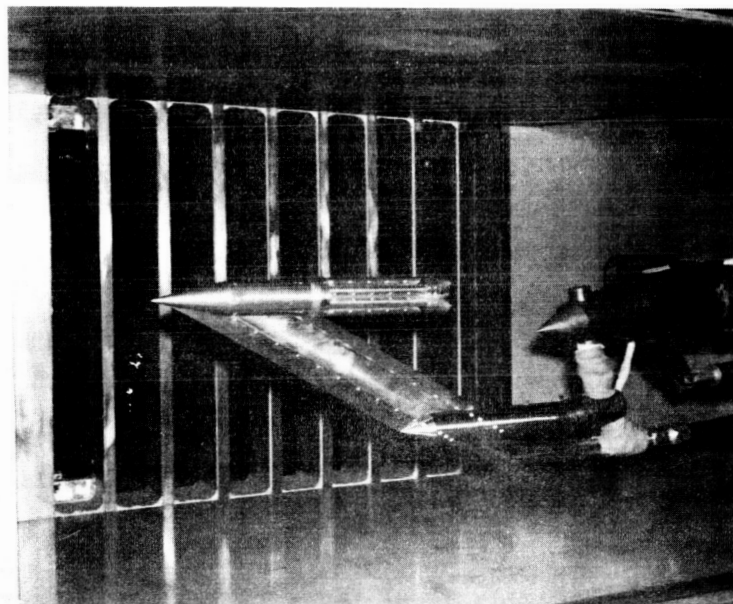
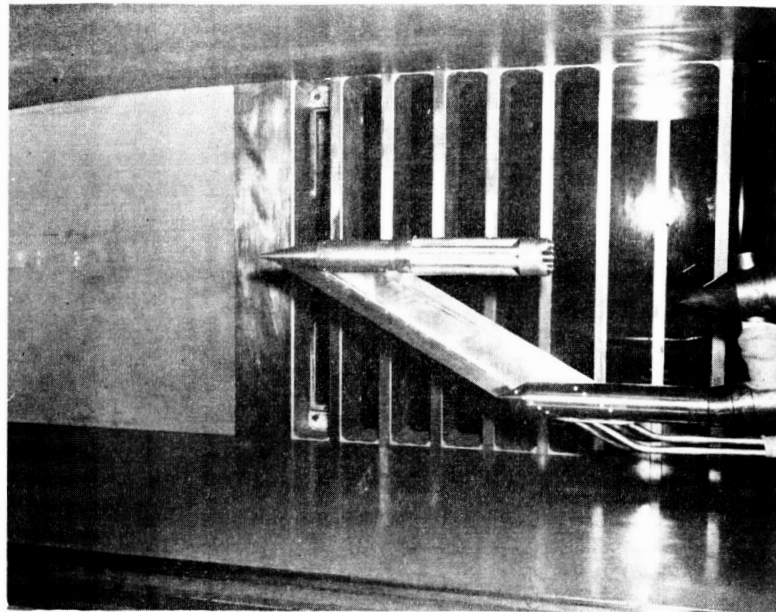
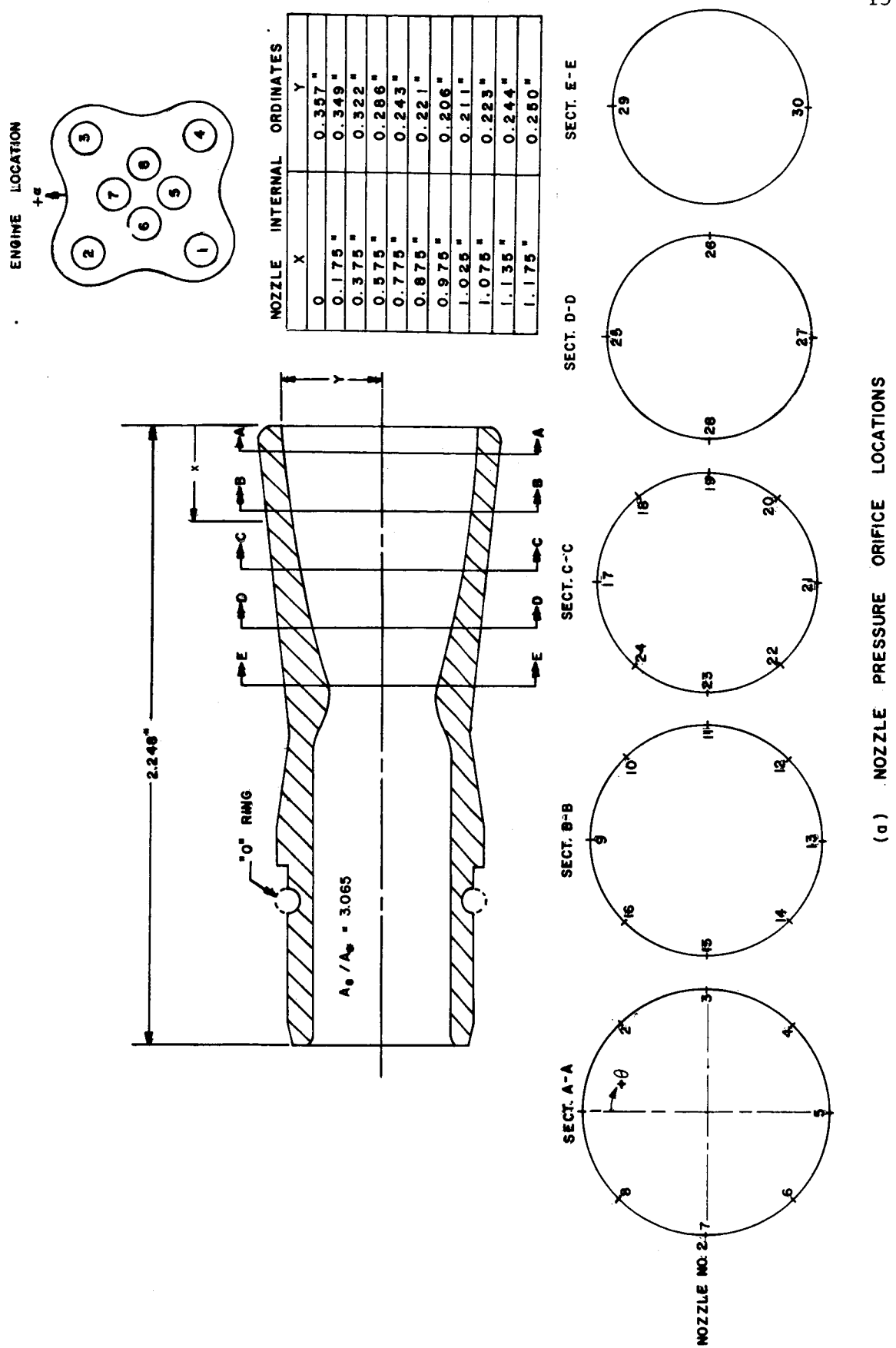


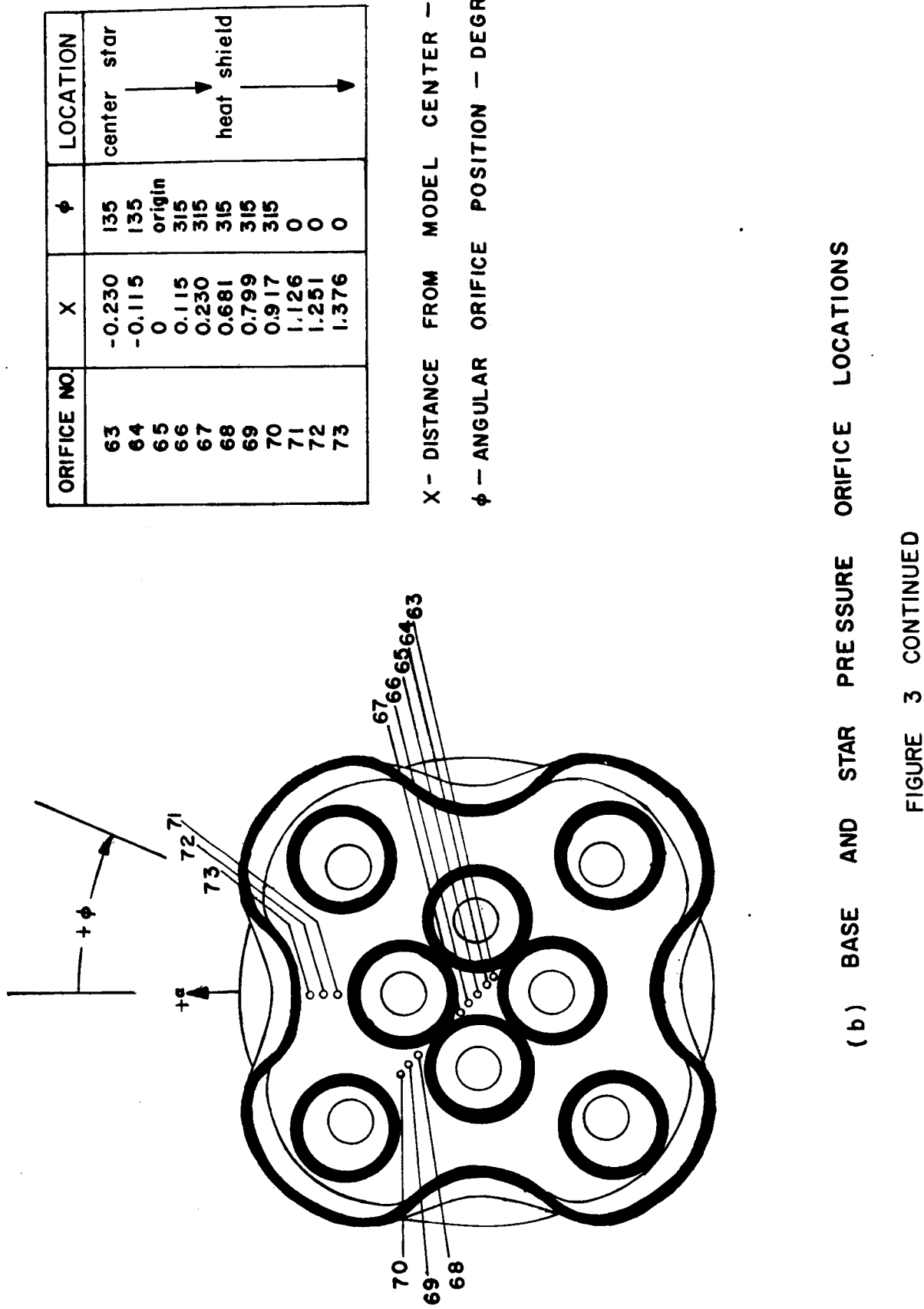
FIGURE 2 TEST MODEL GEOMETRY

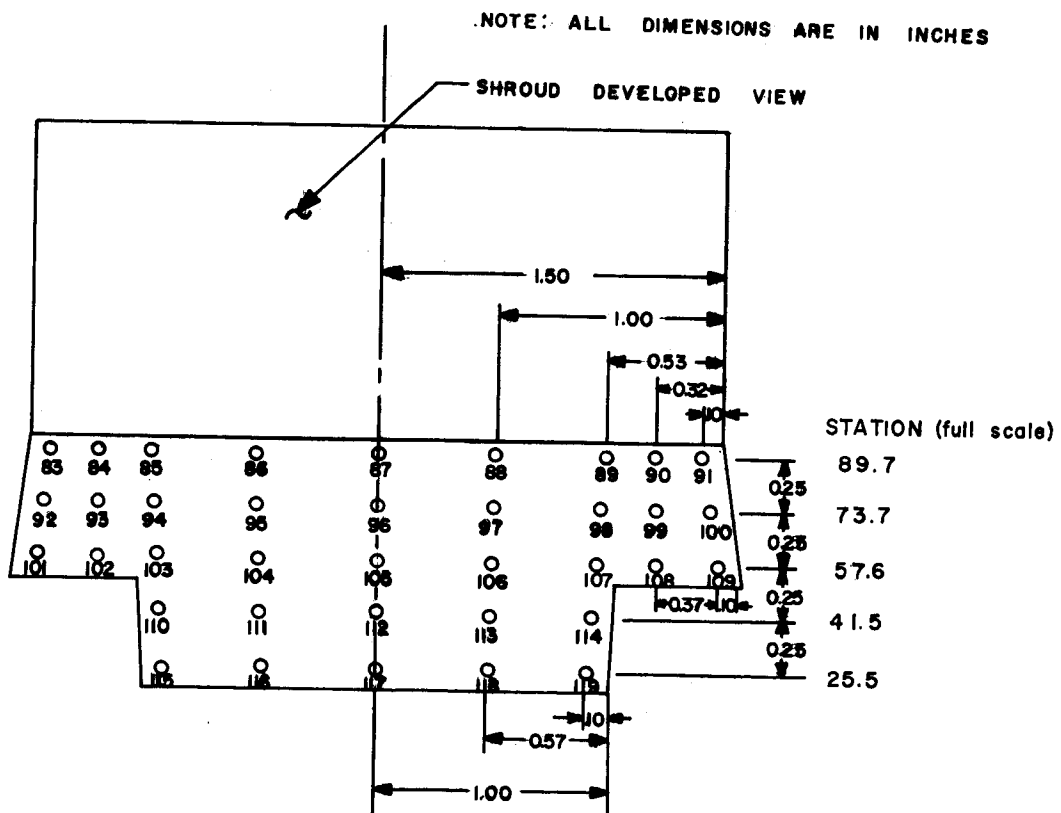
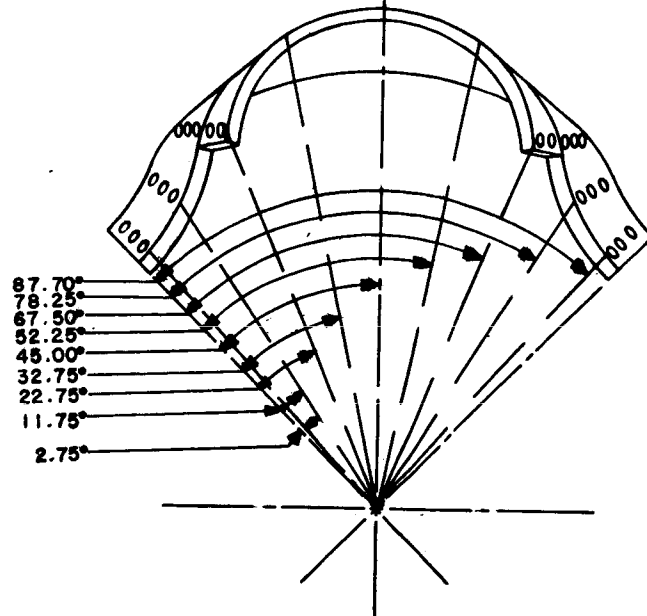


(b) PHOTOGRAPH OF SATURN SA-1 COLD FLOW  
MODEL INSTALLED IN THE LANGLEY UNITARY  
PLAN WIND TUNNEL

FIGURE 2 CONCLUDED

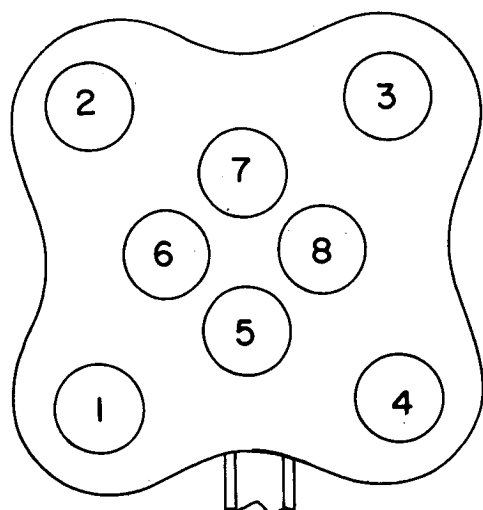




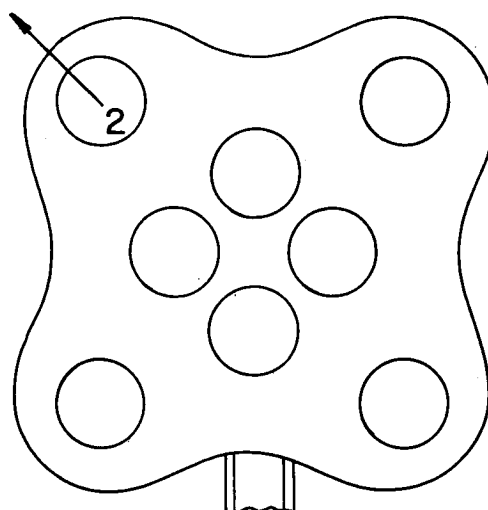


(c) SHROUD PRESSURE ORIFICE LOCATION AND IDENTIFICATION

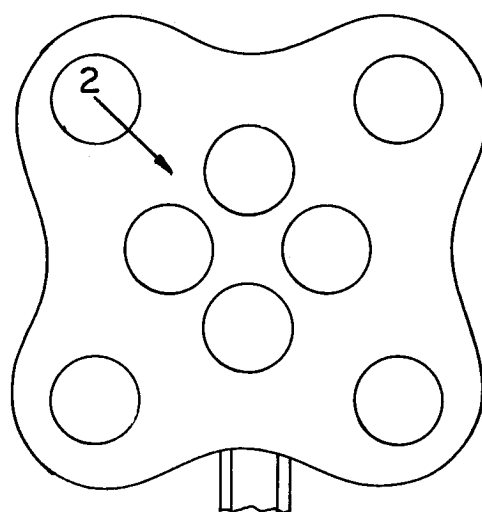
FIGURE 3 CONCLUDED



Configuration A  
 $\beta = 0^\circ$



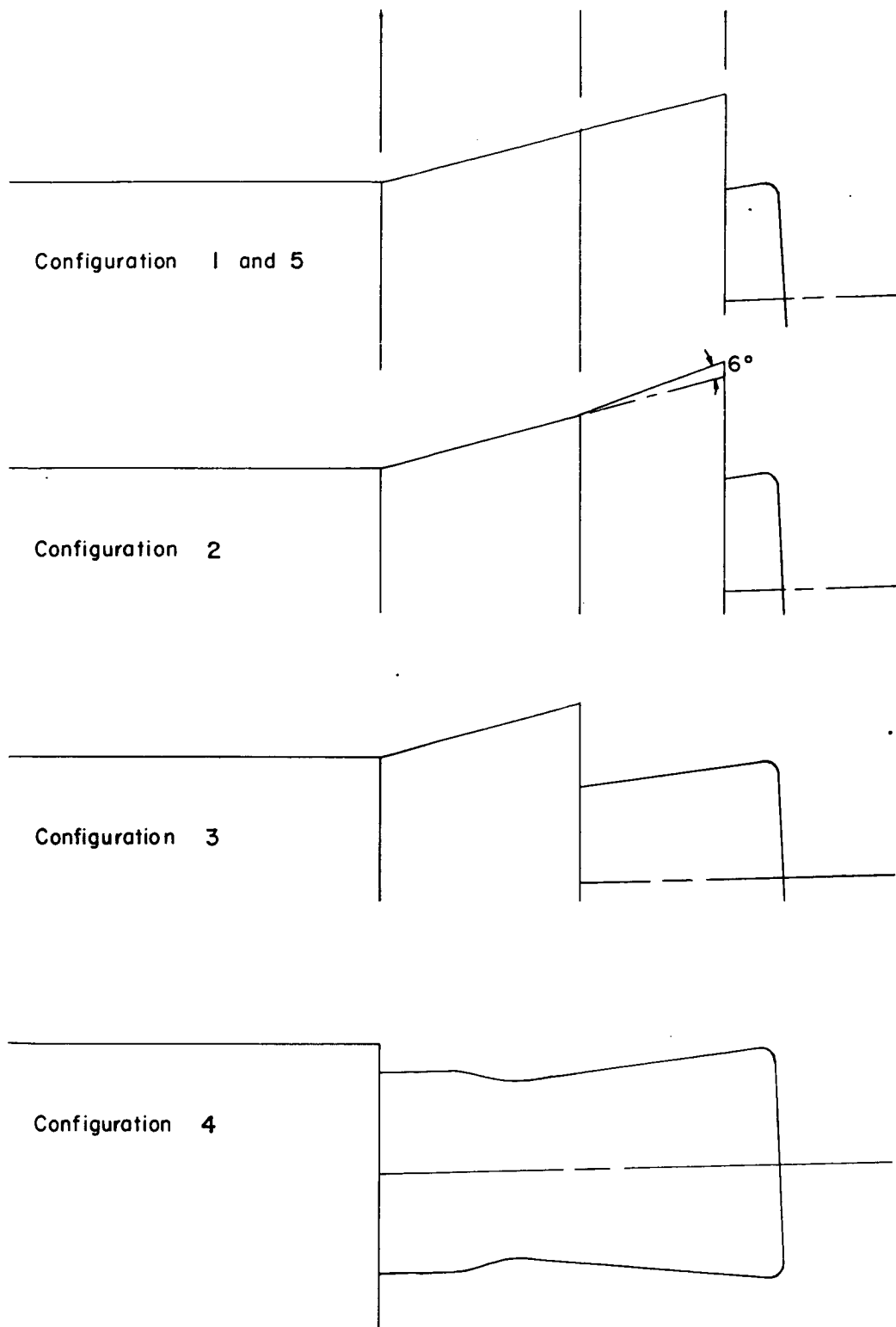
Configuration B  
 $\beta = 6^\circ$



Configuration C  
 $\beta = -9^\circ$

(a) Nozzle Gimbal angle configurations

Figure 4 Test model configurations



(b) Shroud Configurations

Figure 4 Concluded

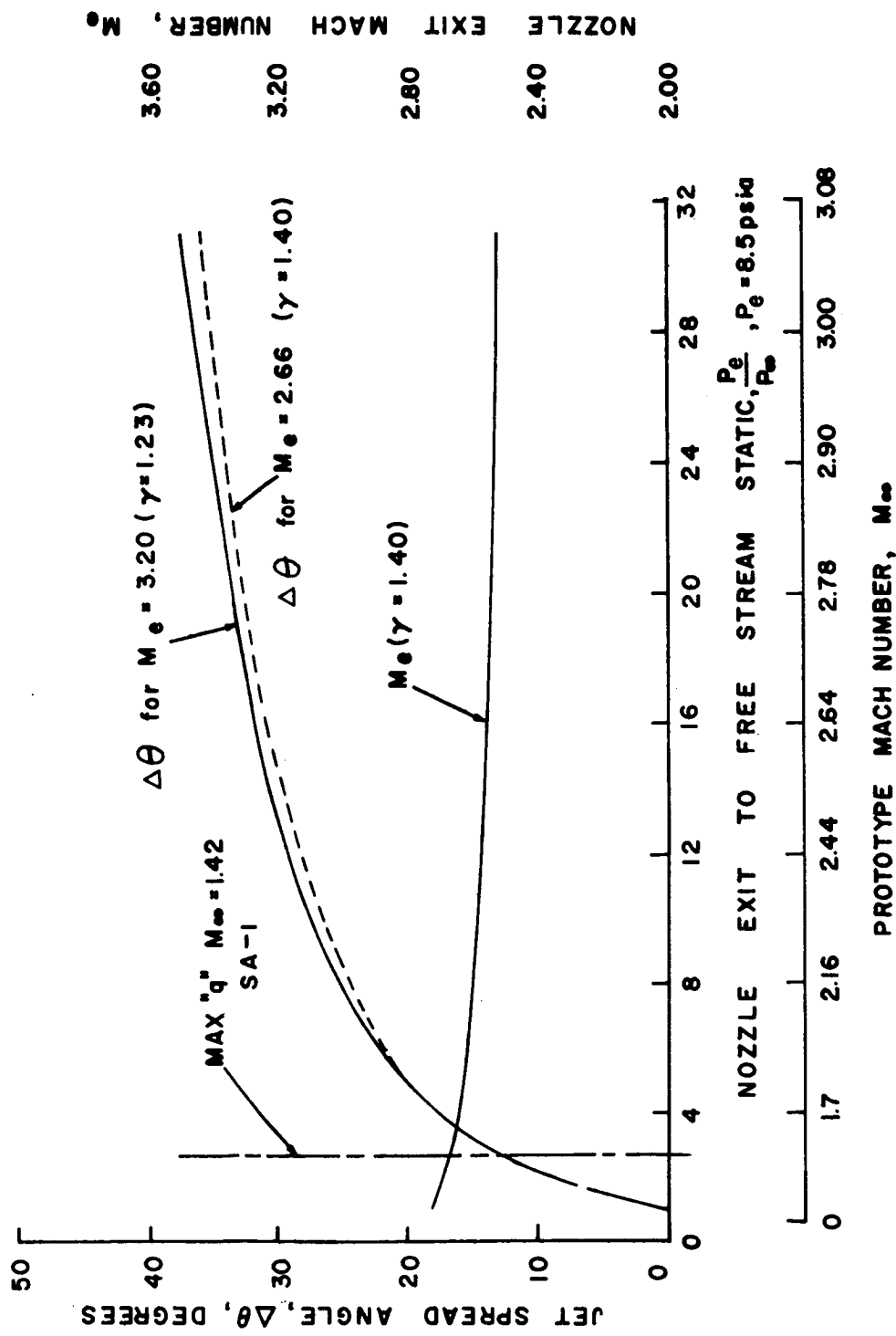


FIGURE 5 VARIATION OF NOZZLE EXIT MACH NUMBER (cold flow technique) WITH JET STATIC PRESSURE RATIO TO SIMULATE PROTOTYPE INITIAL JET SPREAD ANGLE

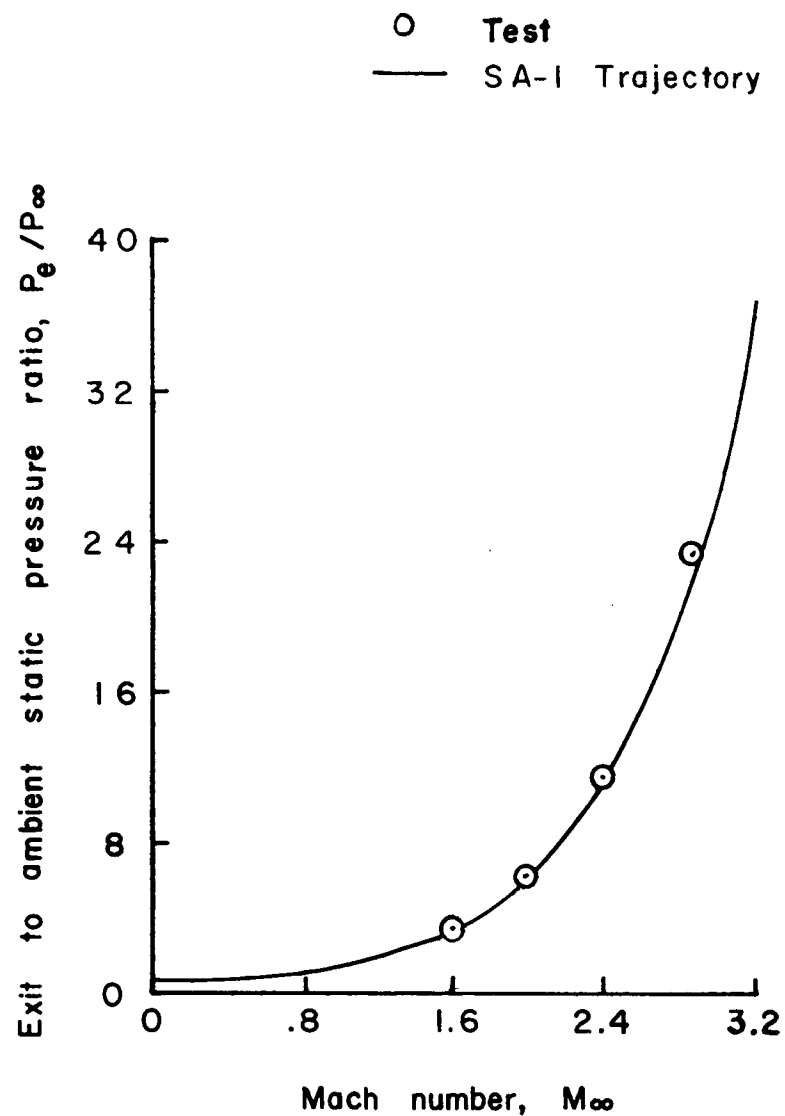


Figure 6 Variation of wind tunnel and prototype trajectory jet static pressure ratios with Mach number

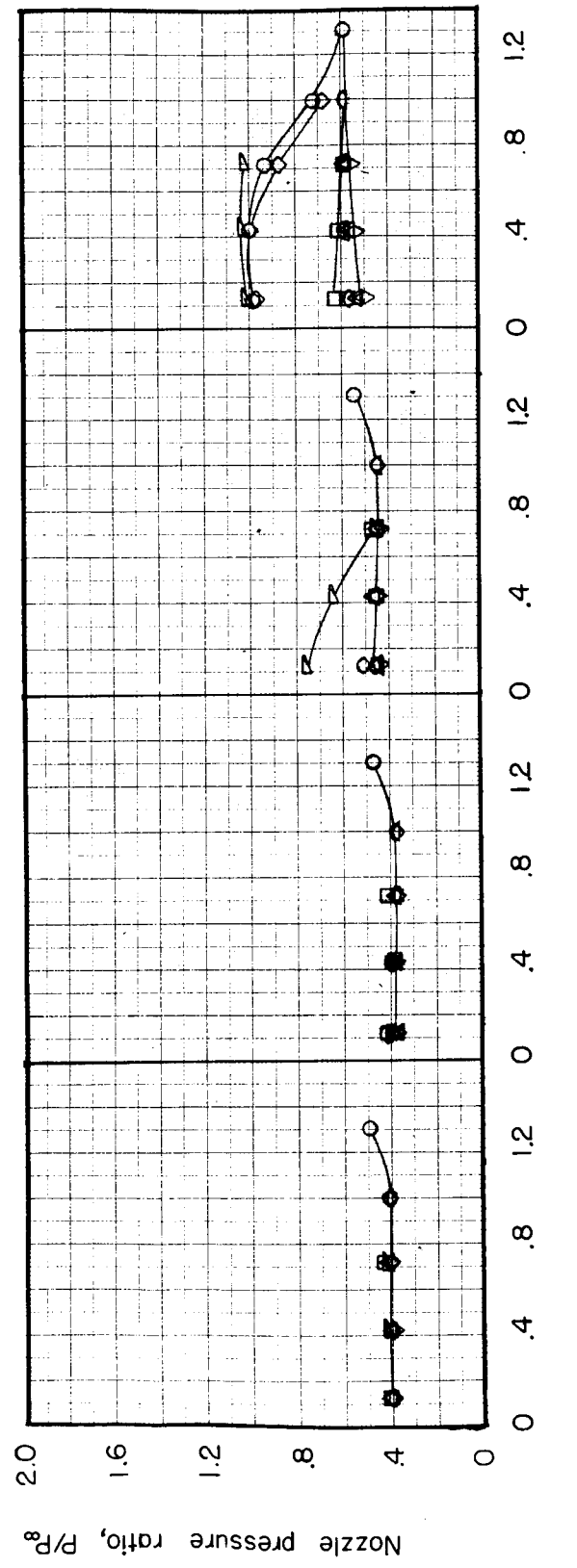
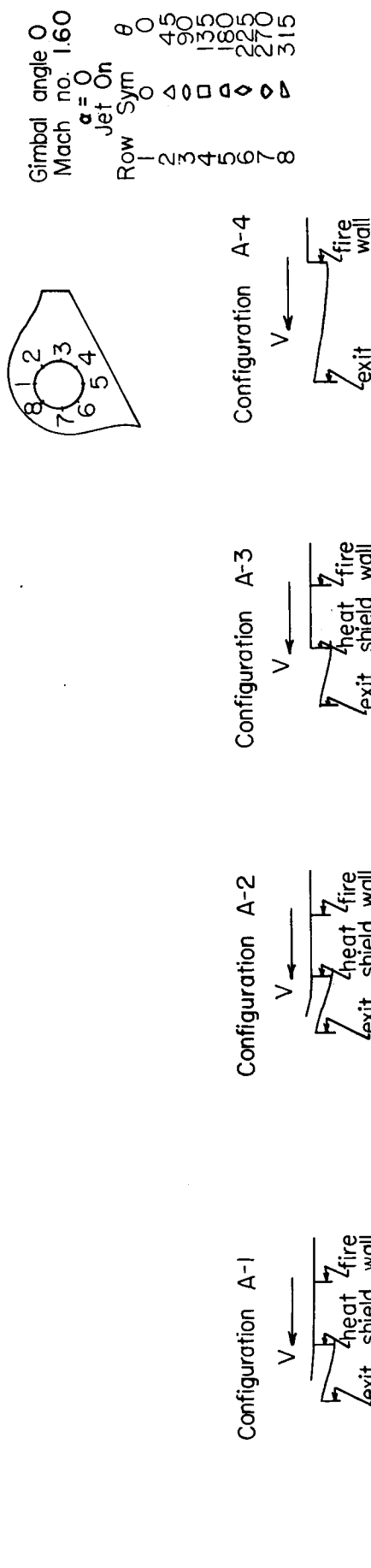


Figure 7q Pressure distribution over the surface of a nozzle with various shroud configurations

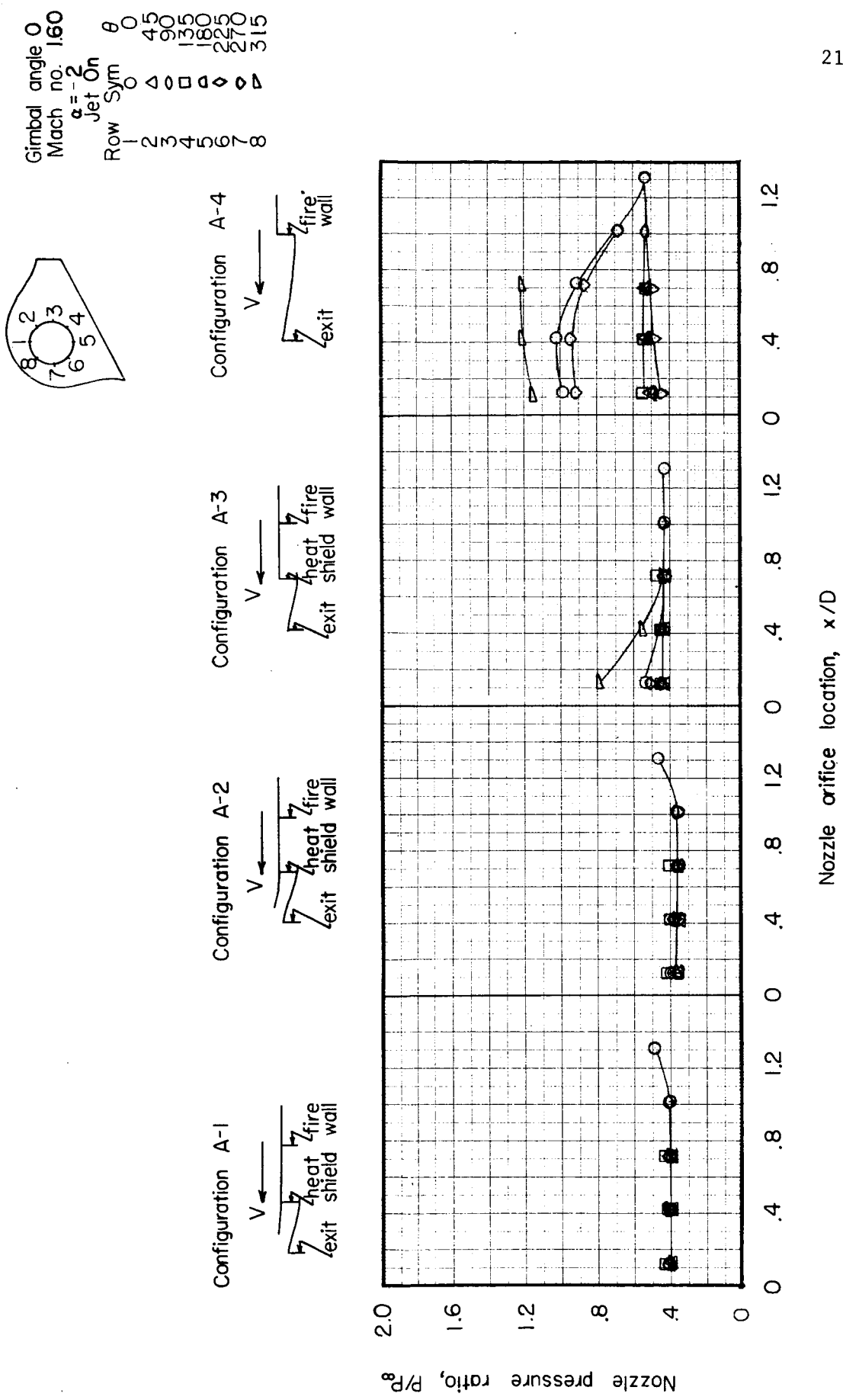


Figure 7b Pressure distribution over the surface of a nozzle with various shroud configurations

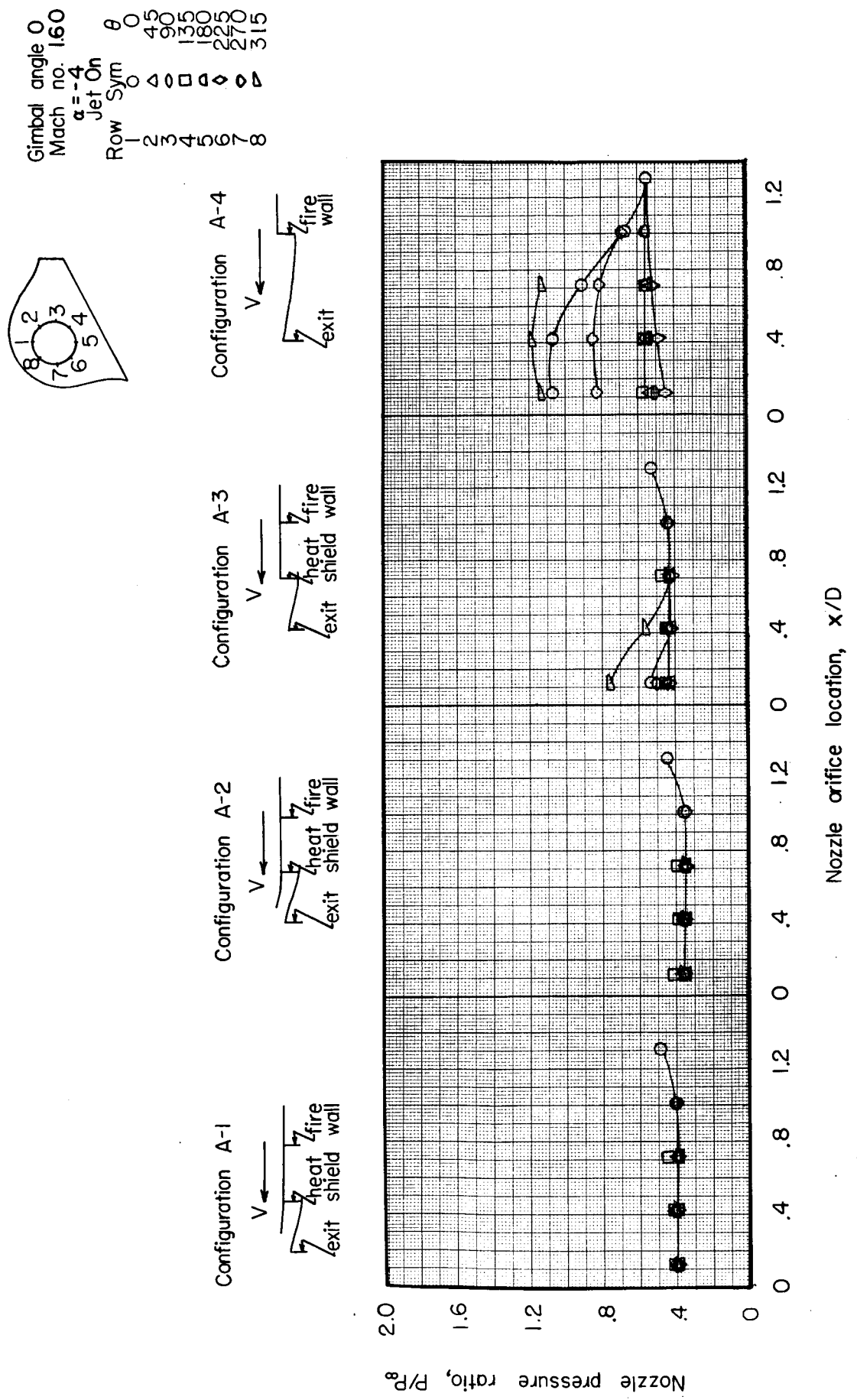


Figure 7c Pressure distribution over the surface of a nozzle with various shroud configurations

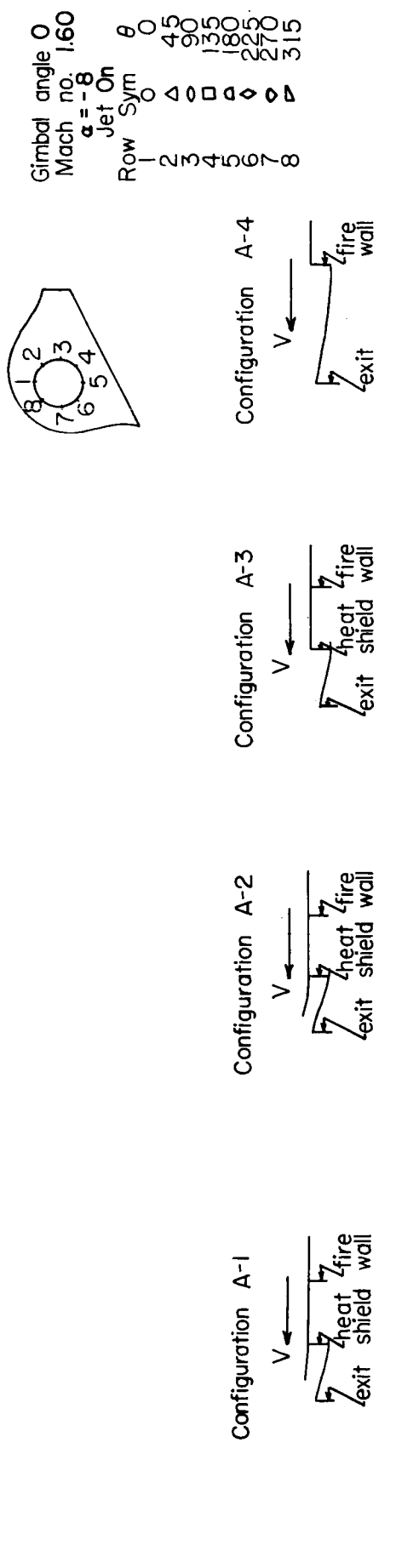


Figure 7d Pressure distribution over the surface of a nozzle with various shroud configurations

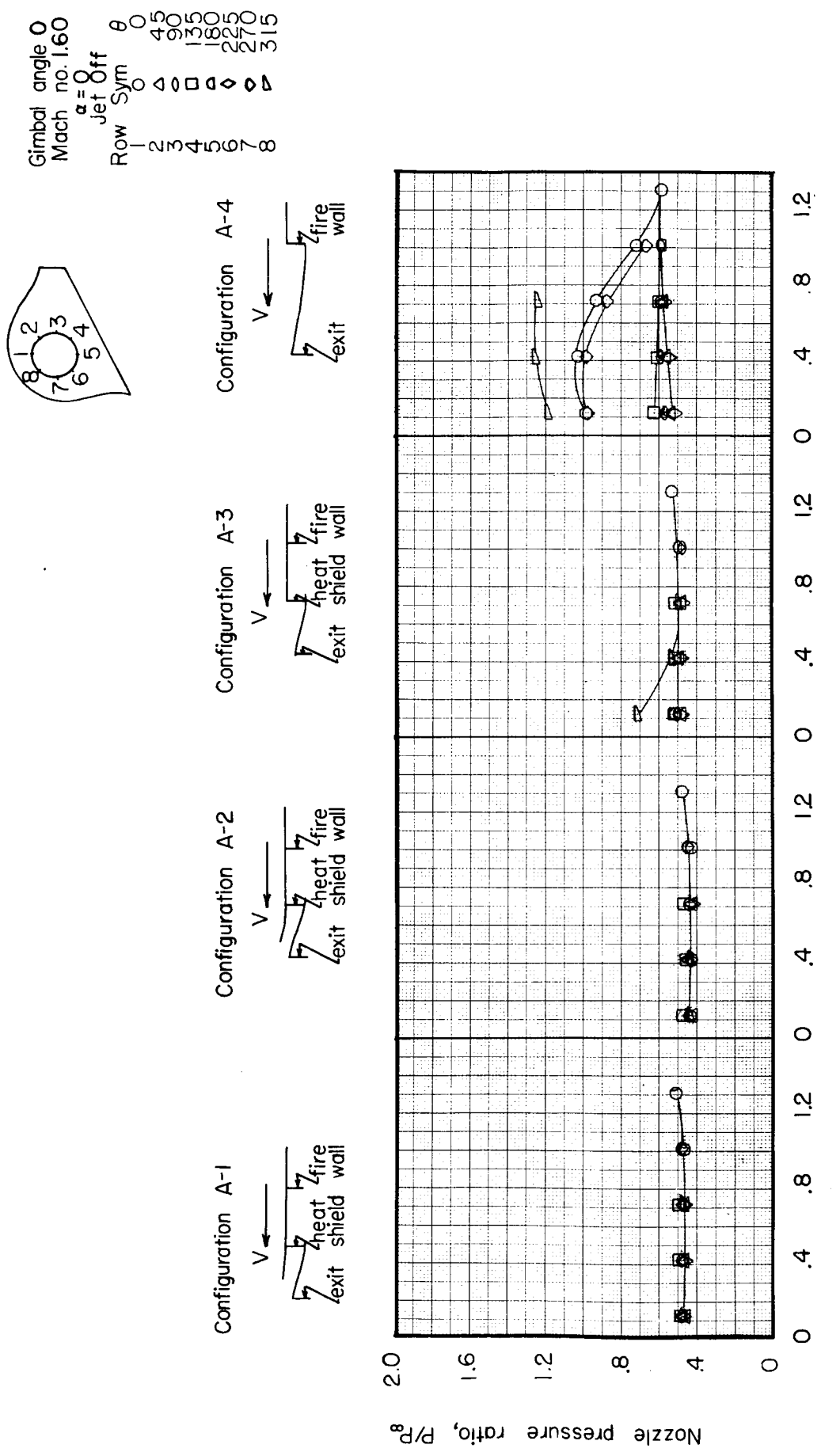


Figure 8a Pressure distribution over the surface of a nozzle with various shroud configurations

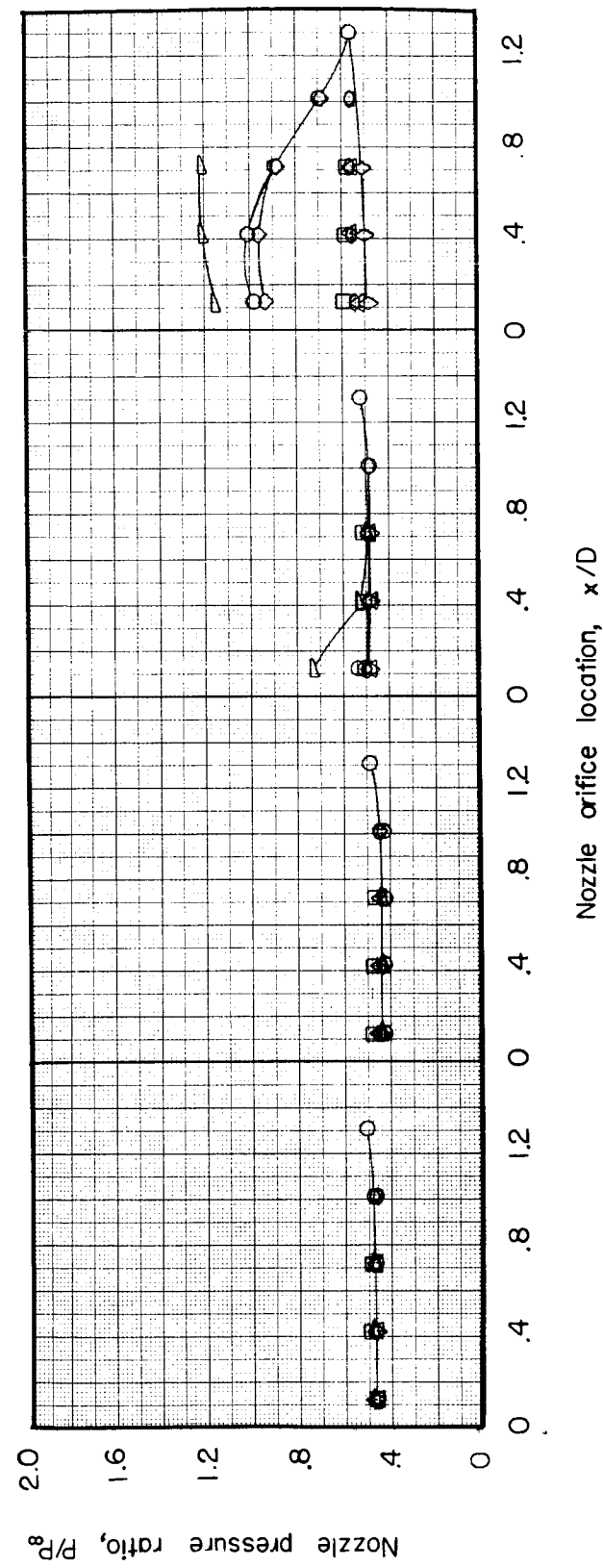
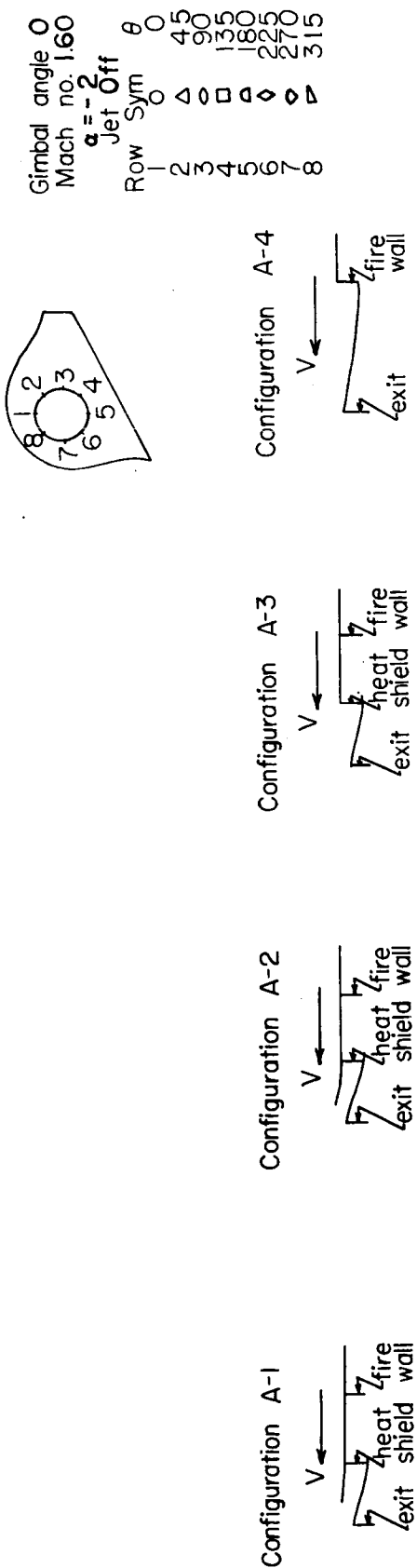


Figure 8b Pressure distribution over the surface of a nozzle with various shroud configurations

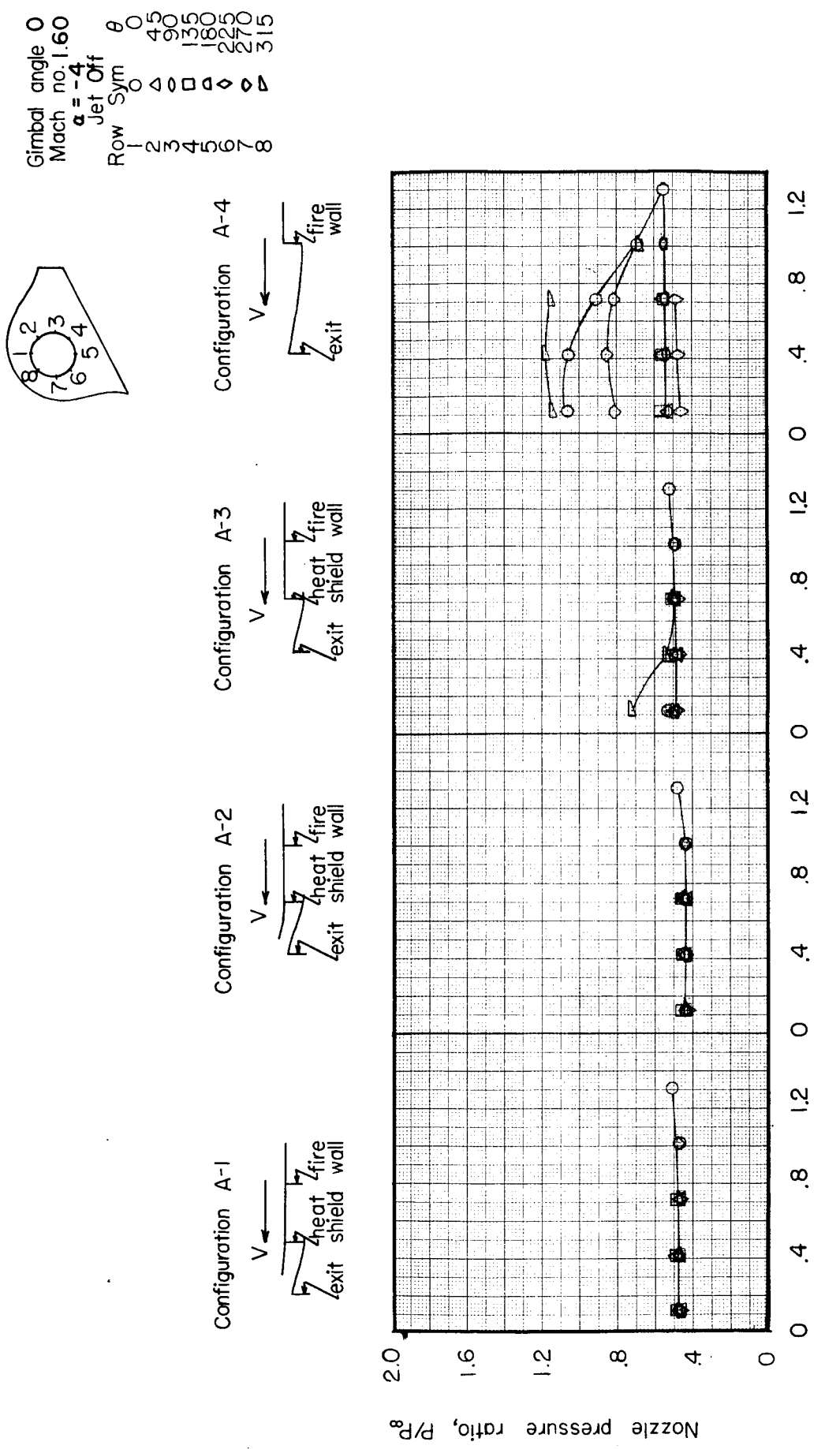


Figure 8c Pressure distribution over the surface of a nozzle with various shroud configurations

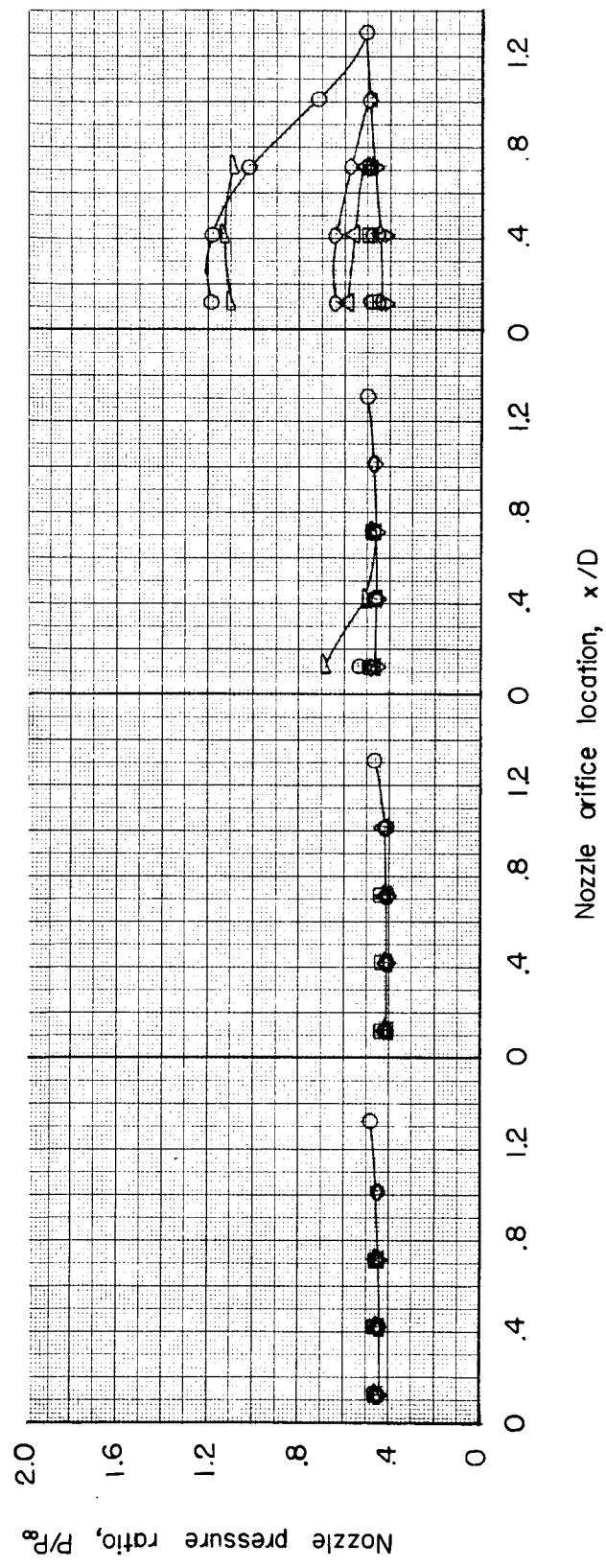
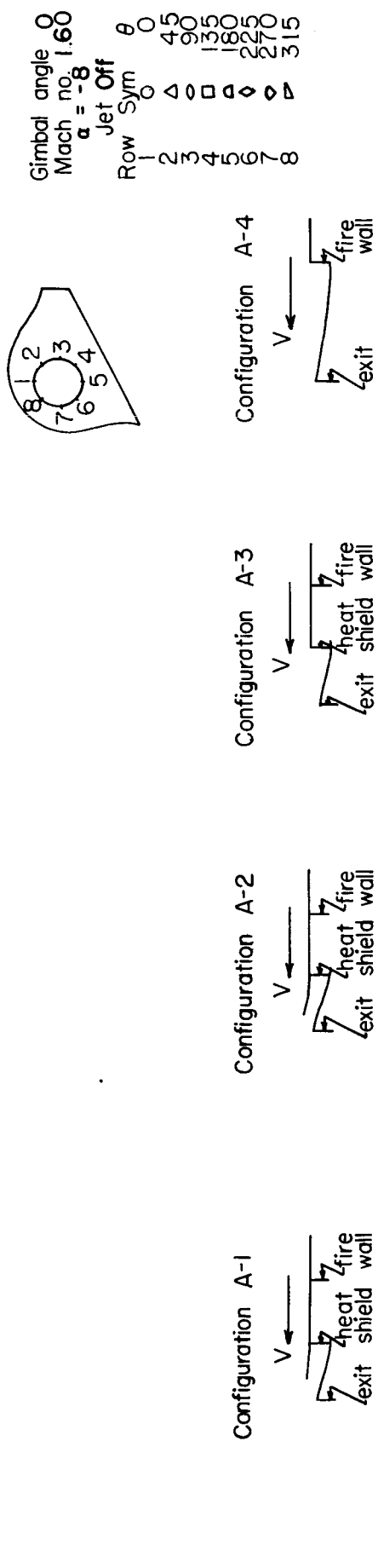


Figure 8d Pressure distribution over the surface of a nozzle with various shroud configurations

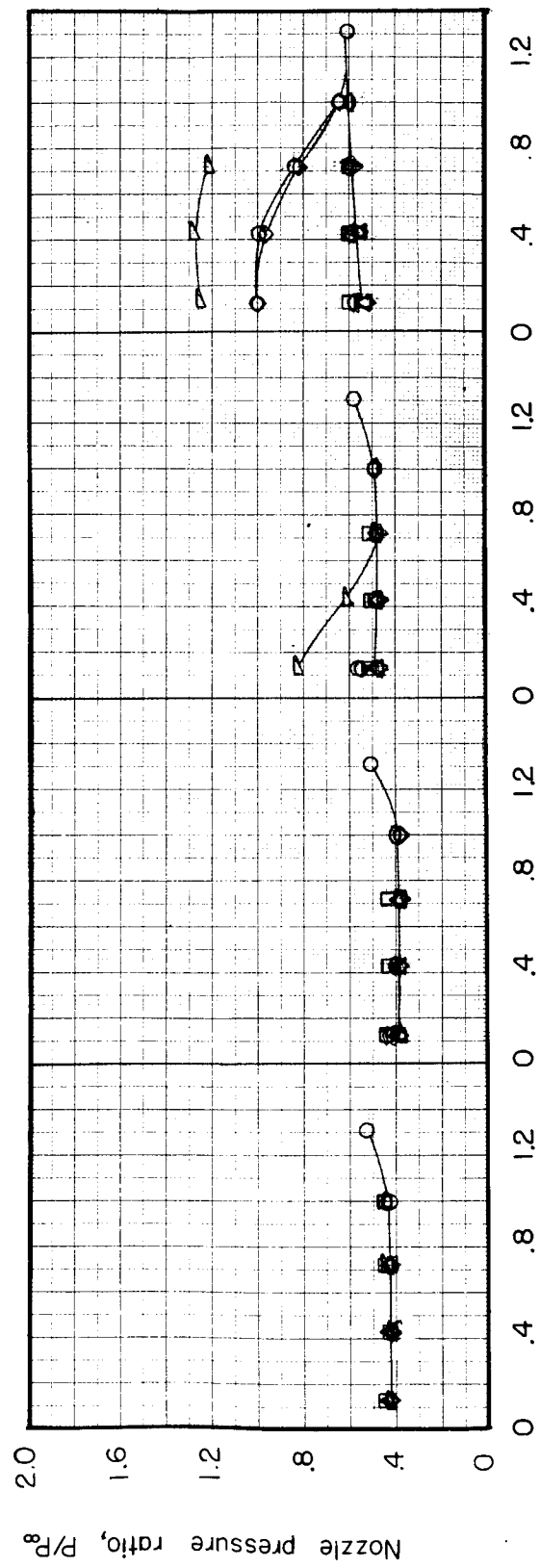
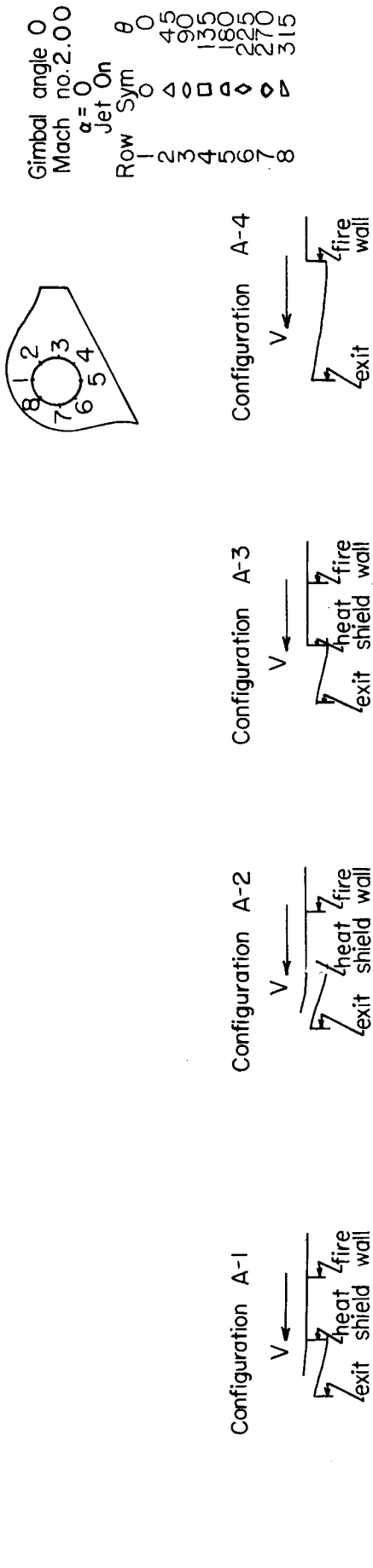
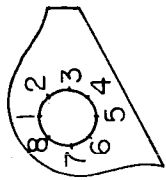


Figure 9d Pressure distribution over the surface of a nozzle with various shroud configurations

Gimbal angle 0  
Mach no. 2.00  
 $\alpha = -2^\circ$   
Jet On  
Row Sym 0  
2 3 4 5 6 7 8  
2 3 4 5 6 7 8



Configuration A-1  
V ←  
heat shield wall  
exit  
Z<sub>fire</sub> wall

Configuration A-2  
V ←  
heat shield wall  
exit  
Z<sub>fire</sub> wall

Configuration A-3  
V ←  
heat shield wall  
exit  
Z<sub>fire</sub> wall

Configuration A-4  
V ←  
heat shield wall  
exit  
Z<sub>fire</sub> wall

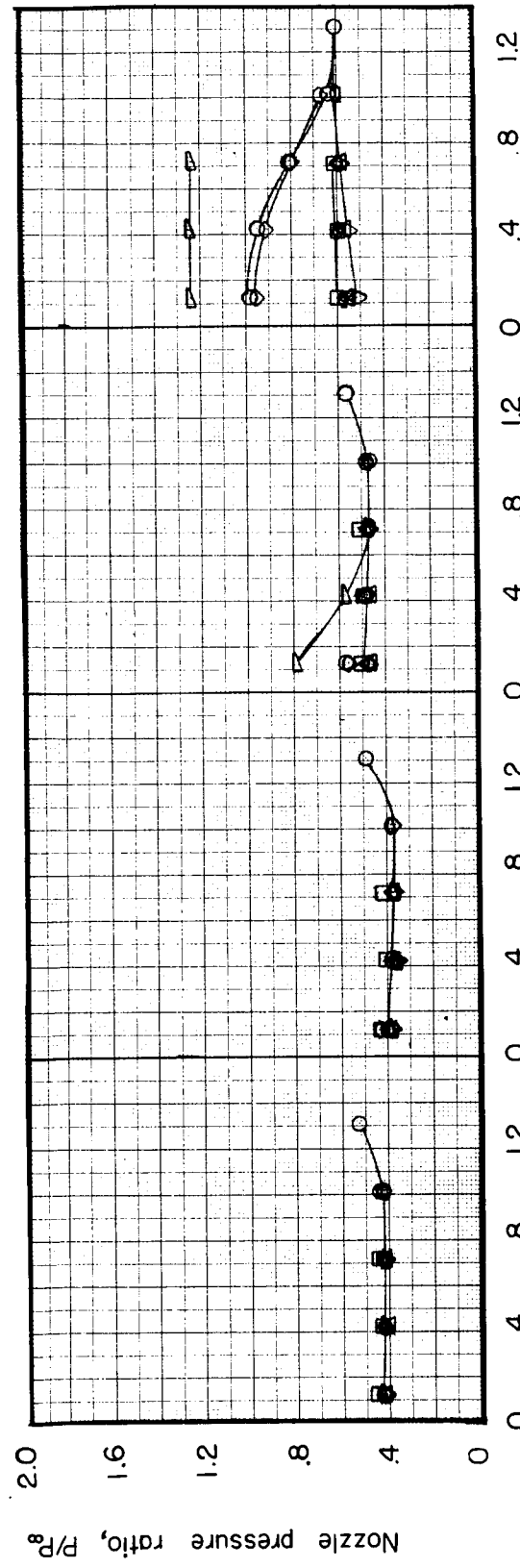


Figure 9b Pressure distribution over the surface of a nozzle with various shroud configurations

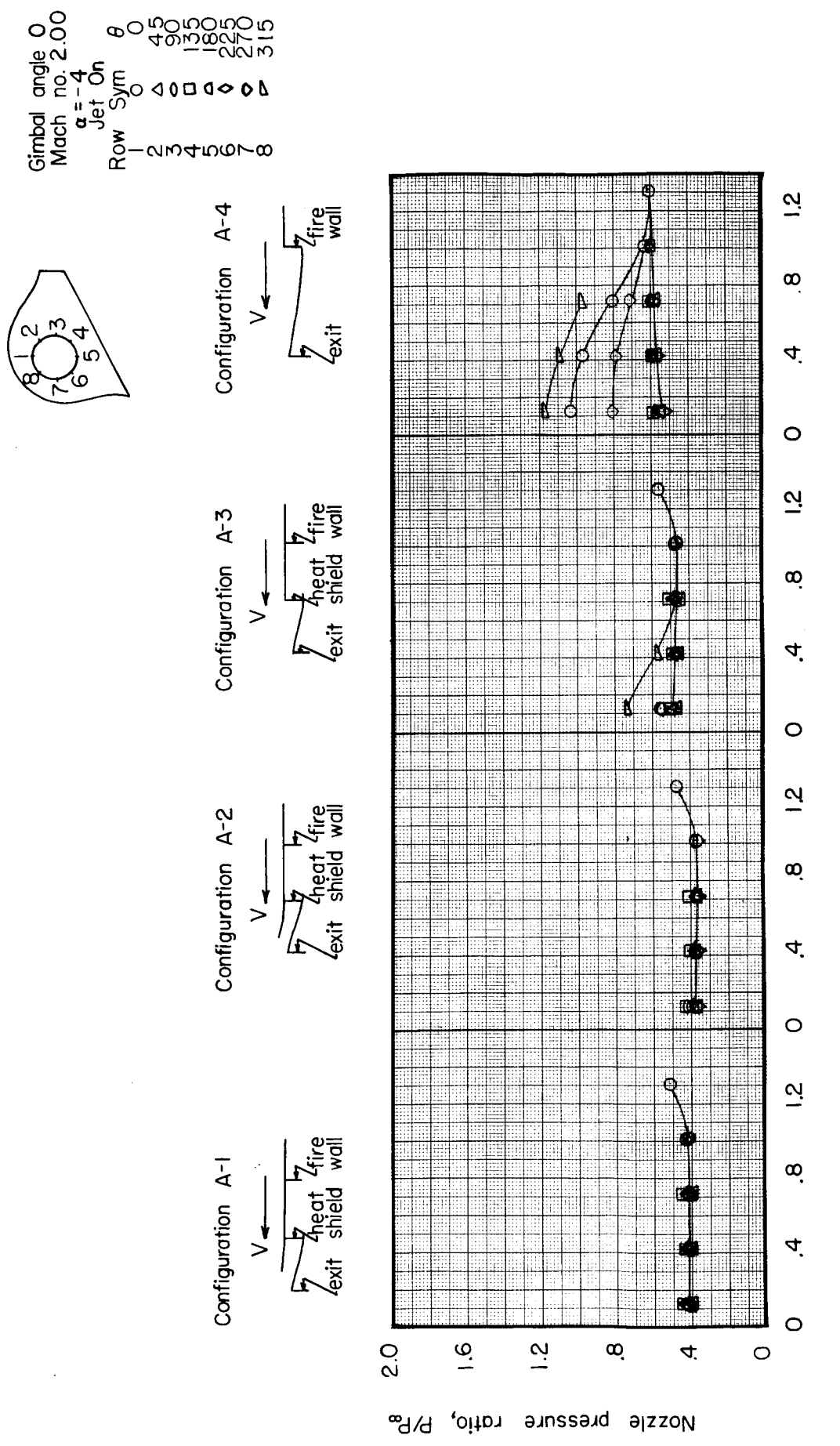


Figure 9c Pressure distribution over the surface of a nozzle with various shroud configurations

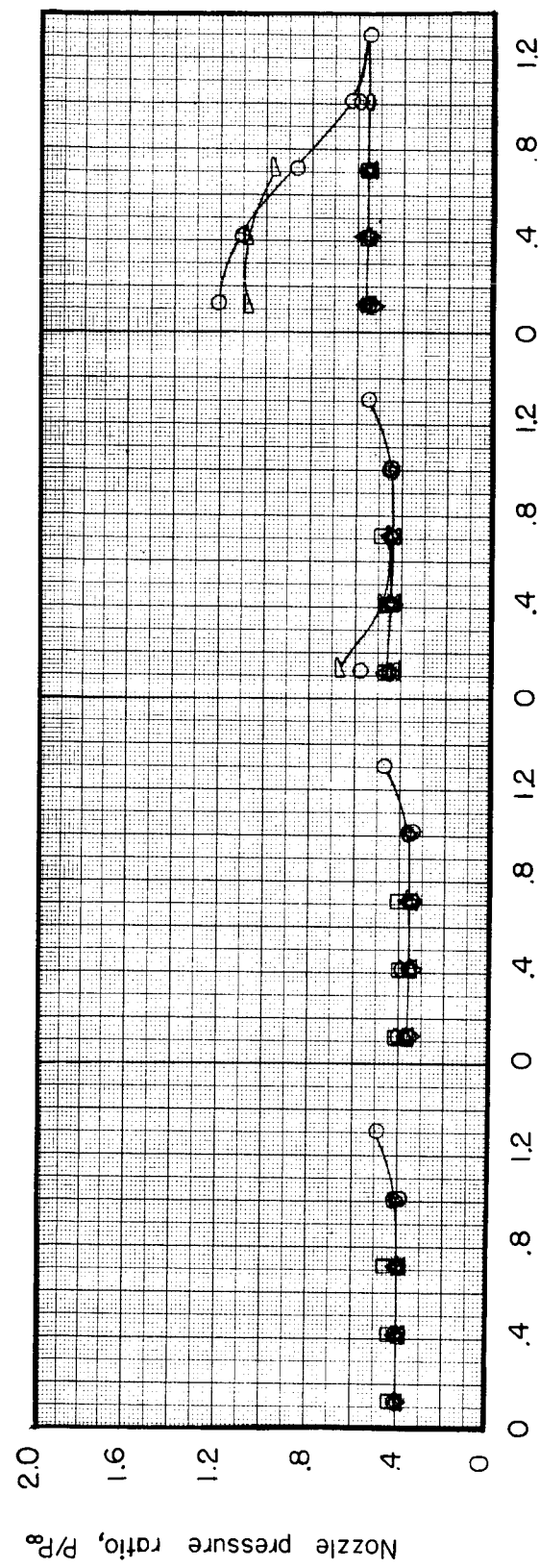
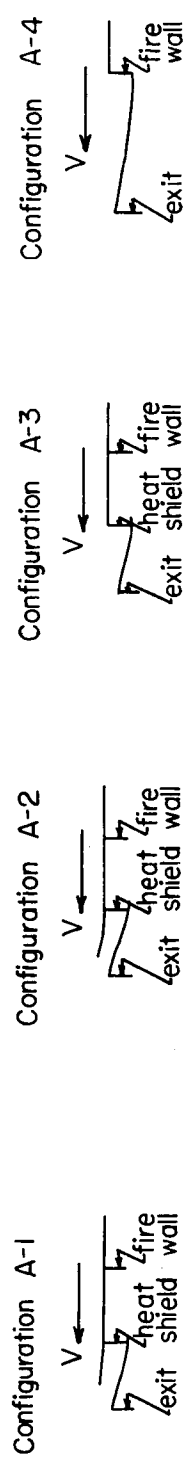
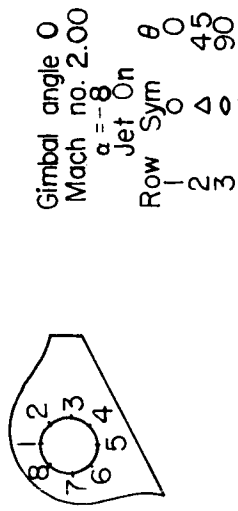


Figure 9d Pressure distribution over the surface of a nozzle with various shroud configurations

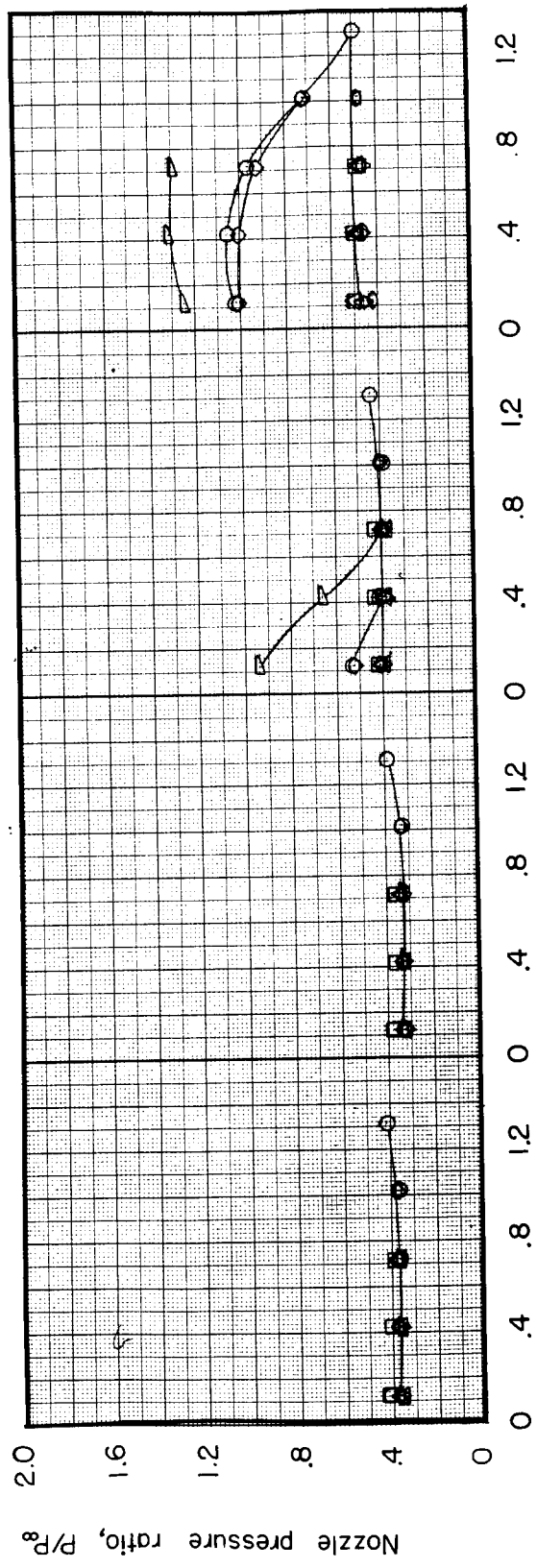
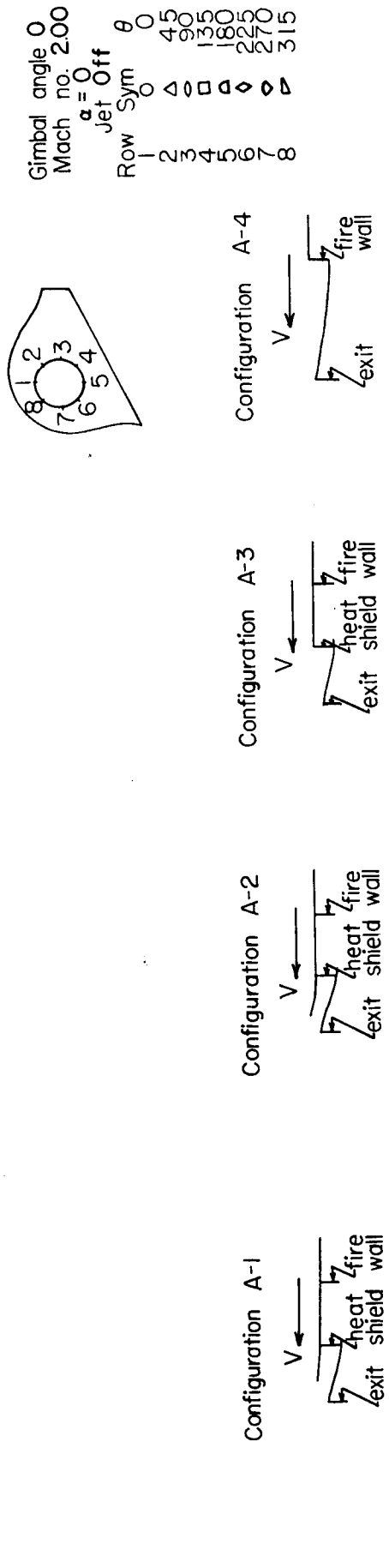


Figure 10a Pressure distribution over the surface of a nozzle with various shroud configurations

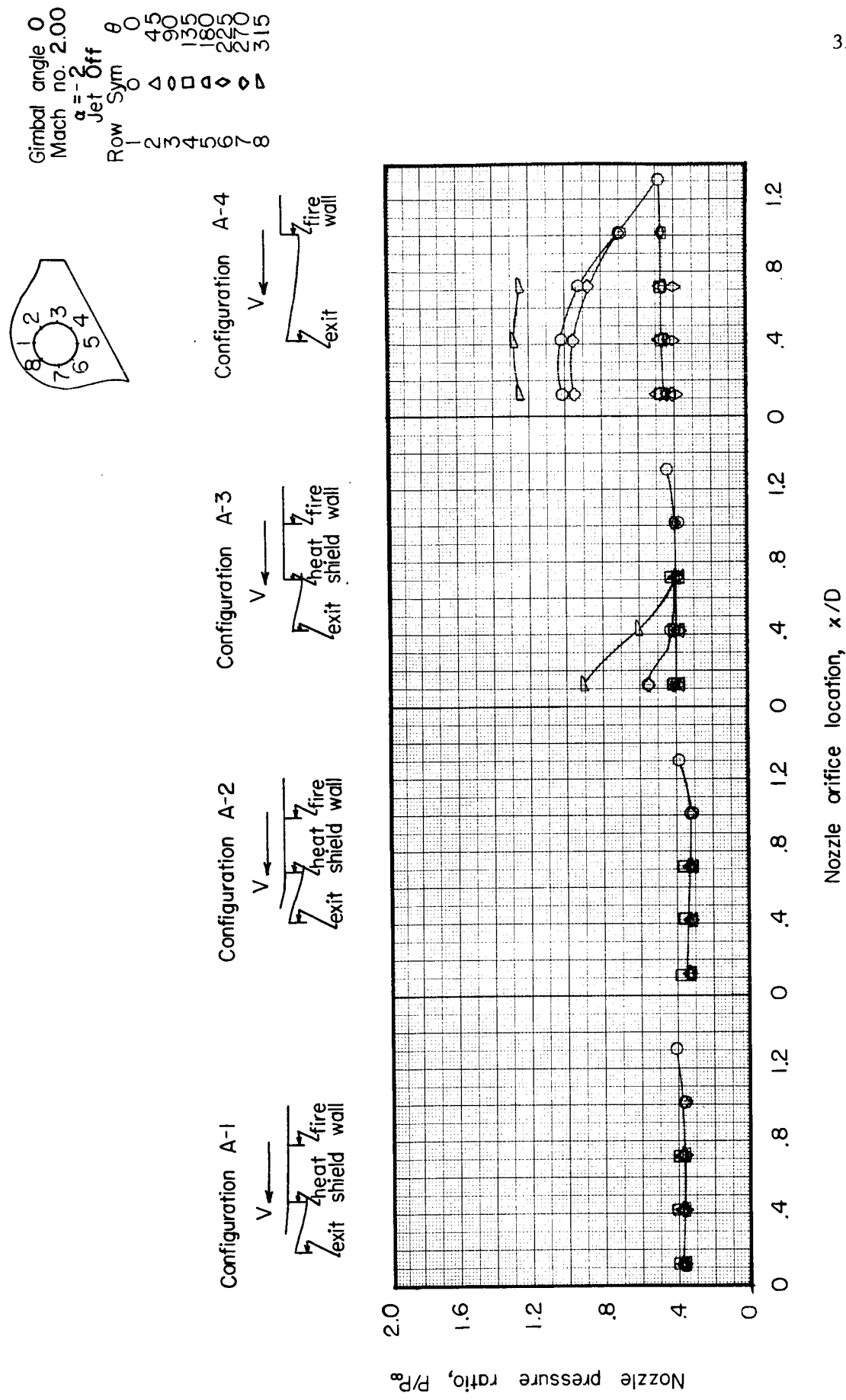


Figure 10 b Pressure distribution over the surface of a nozzle with various shroud configurations

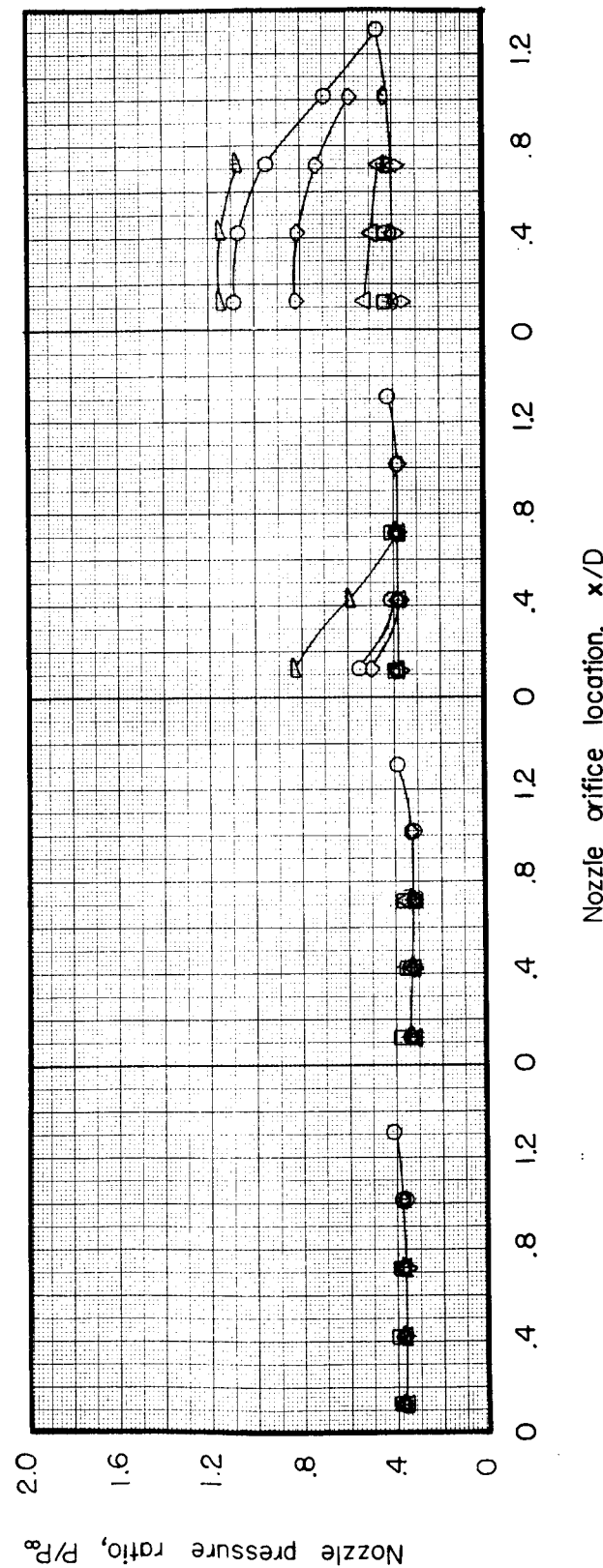
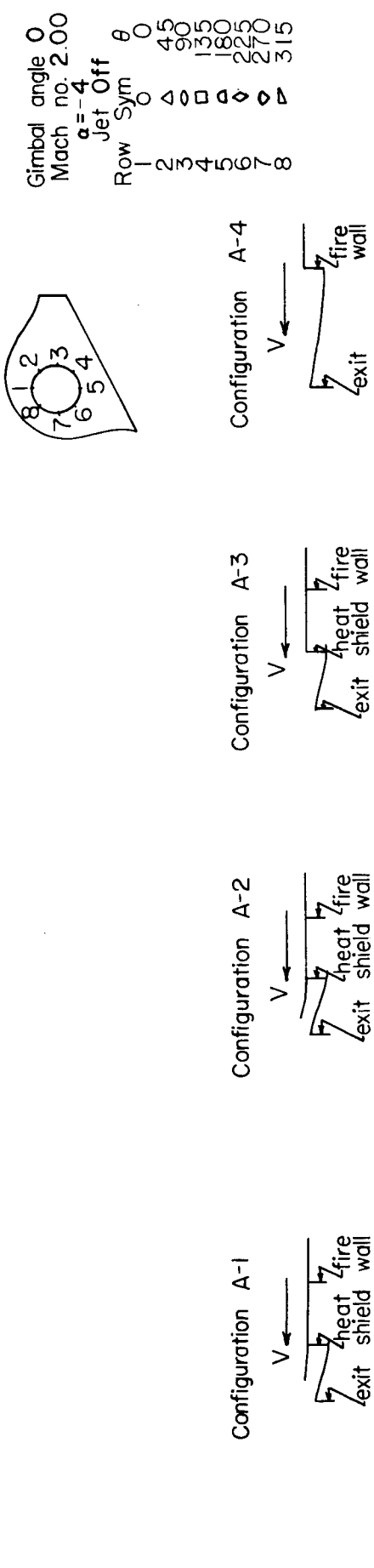


Figure 10c Pressure distribution over the surface of a nozzle with various shroud configurations

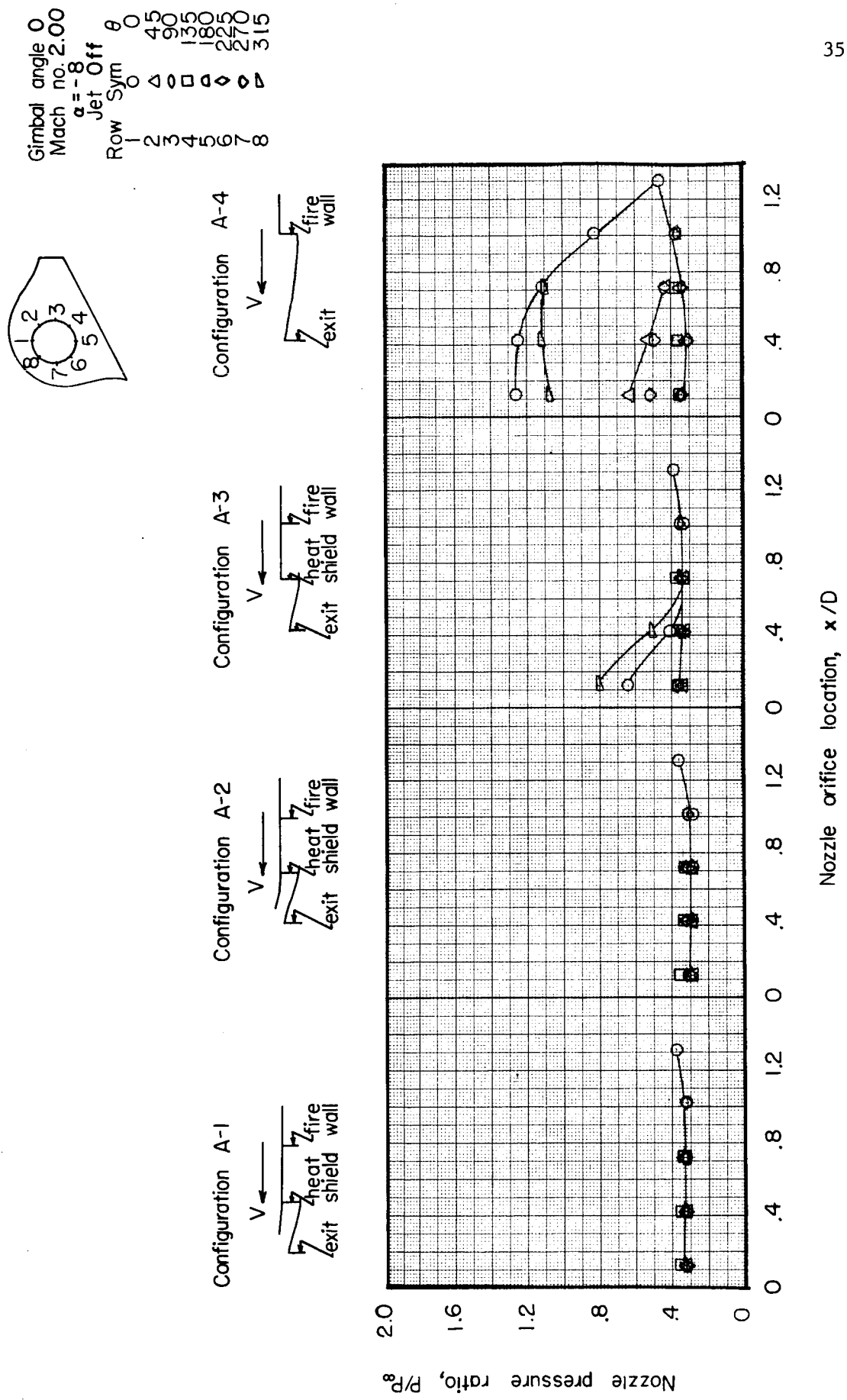


Figure 10d Pressure distribution over the surface of a nozzle with various shroud configurations

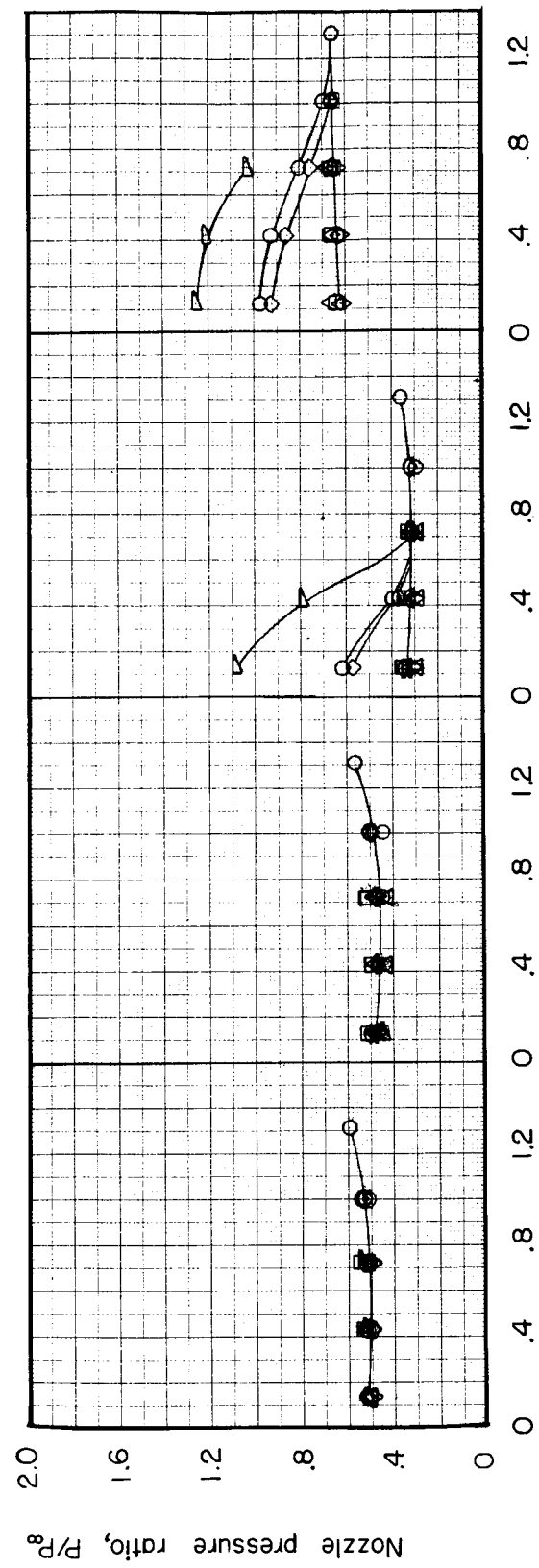
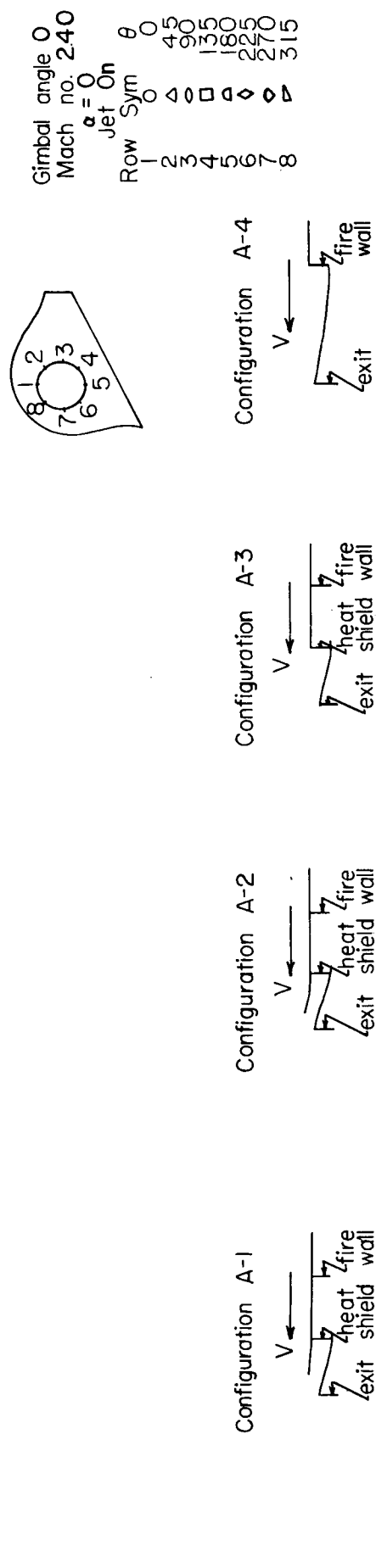


Figure 11a Pressure distribution over the surface of a nozzle with various shroud configurations

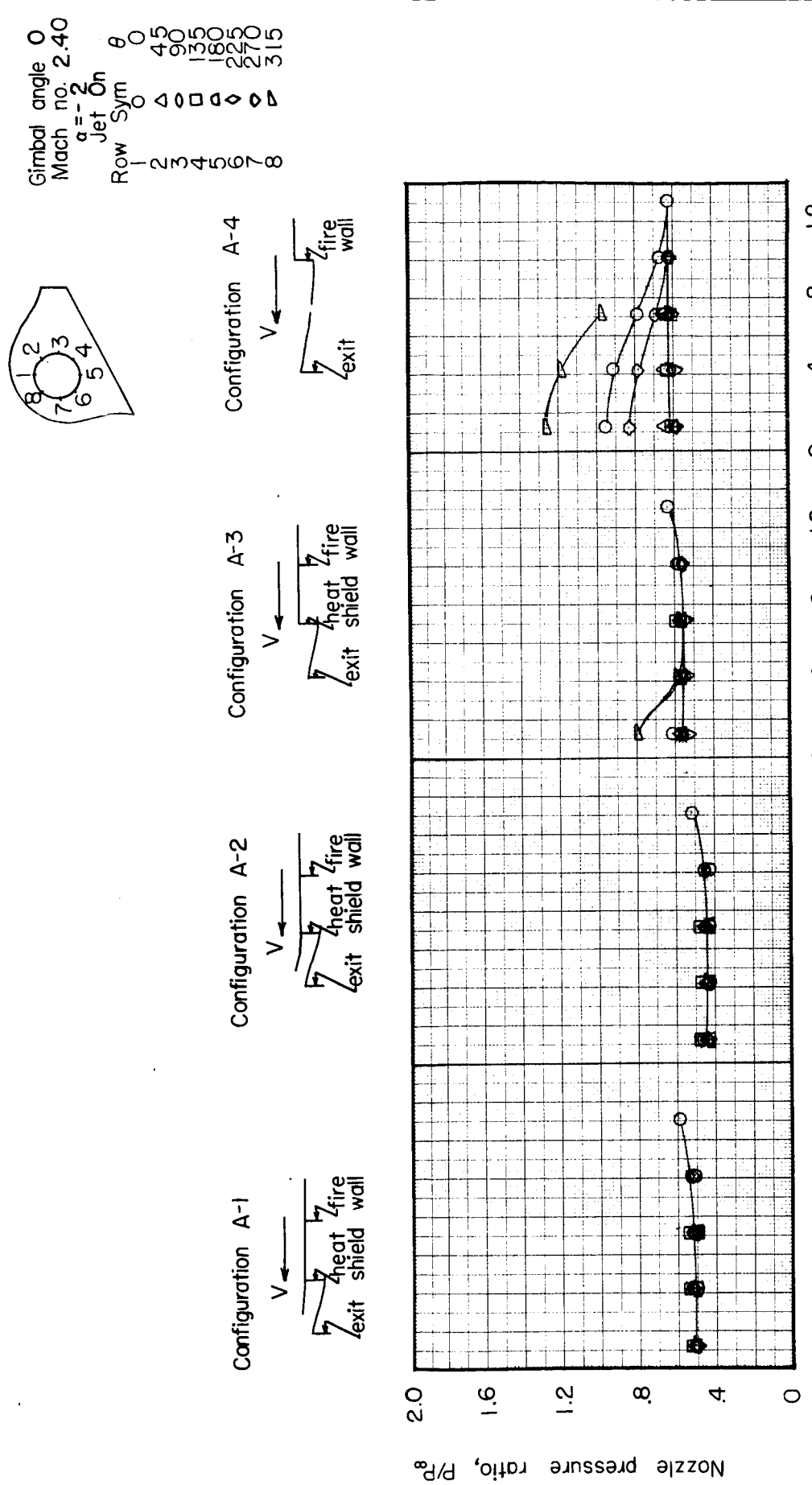


Figure 11b Pressure distribution over the surface of a nozzle with various shroud configurations

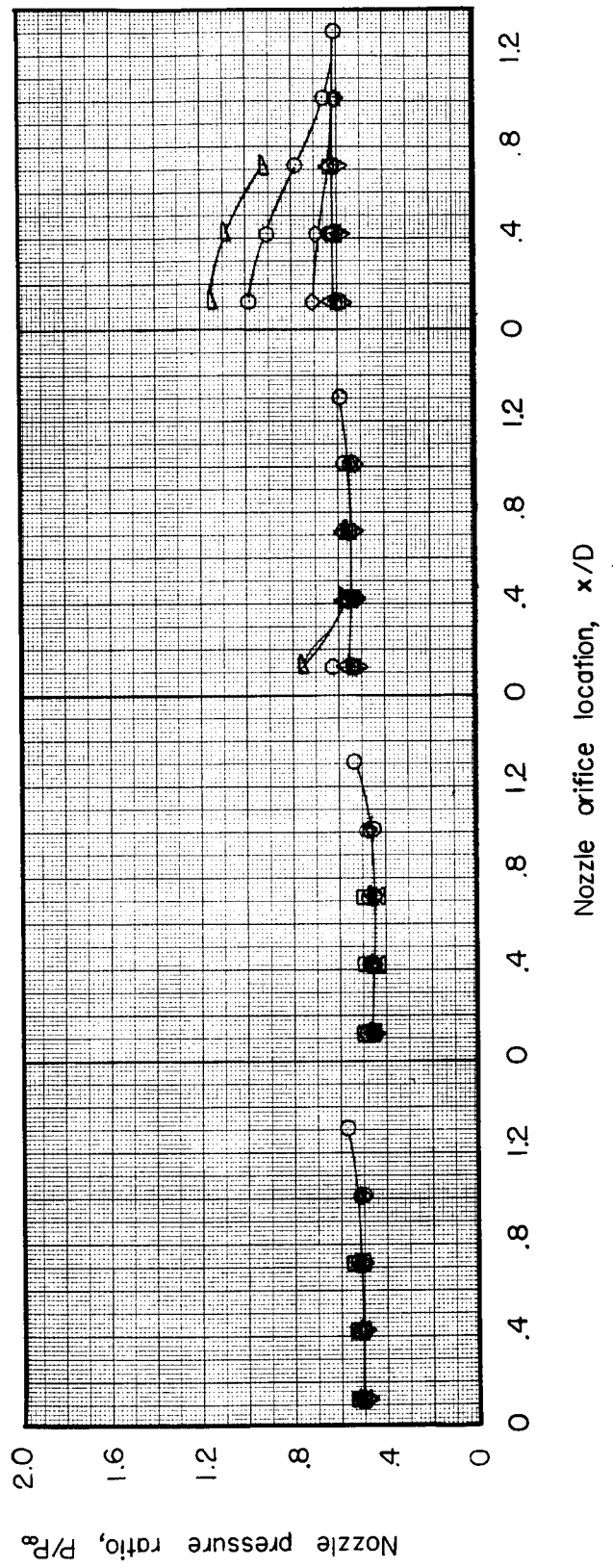
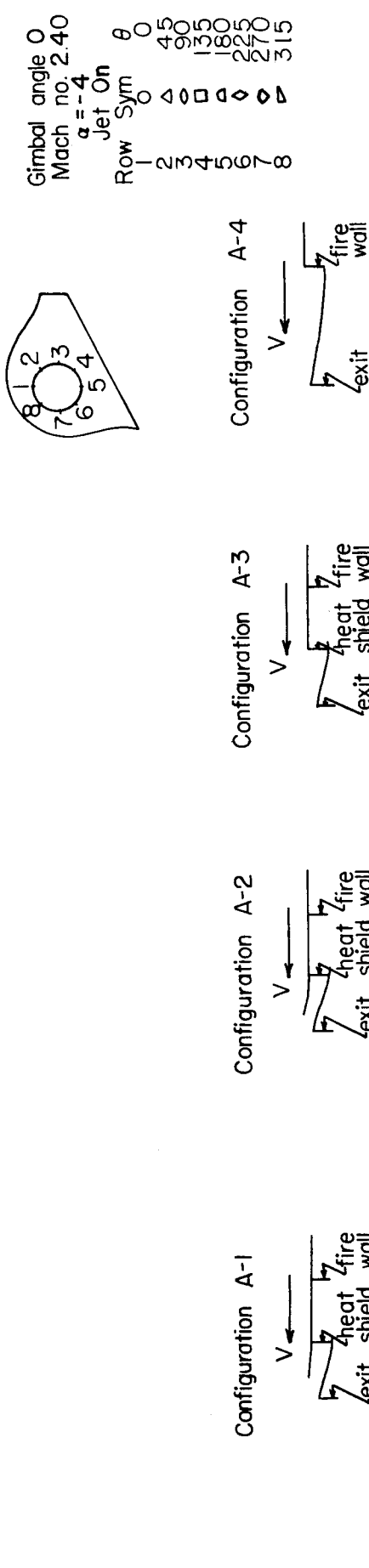


Figure IIc Pressure distribution over the surface of a nozzle with various shroud configurations

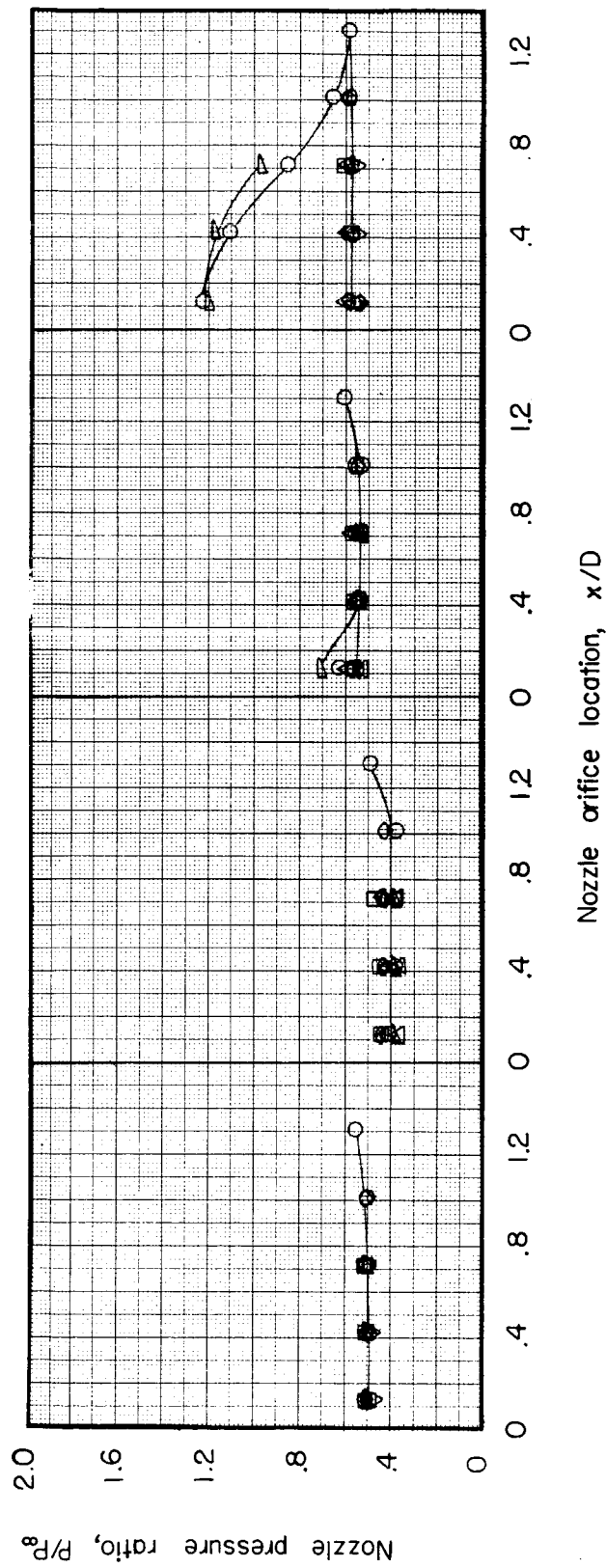
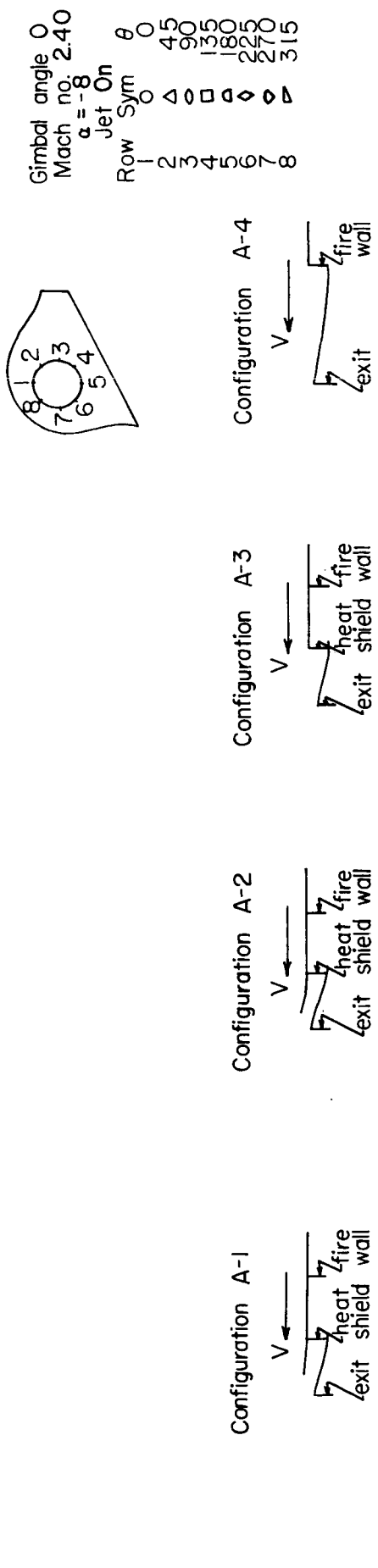


Figure 11d Pressure distribution over the surface of a nozzle with various shroud configurations

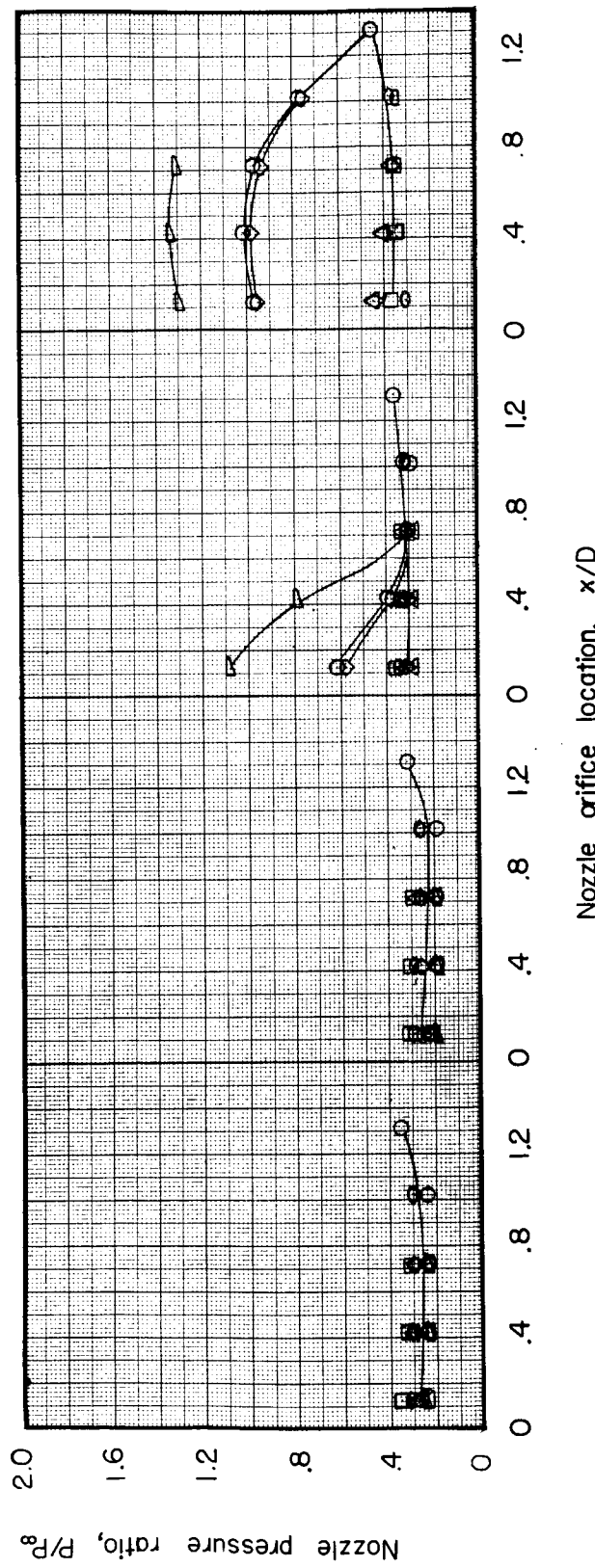
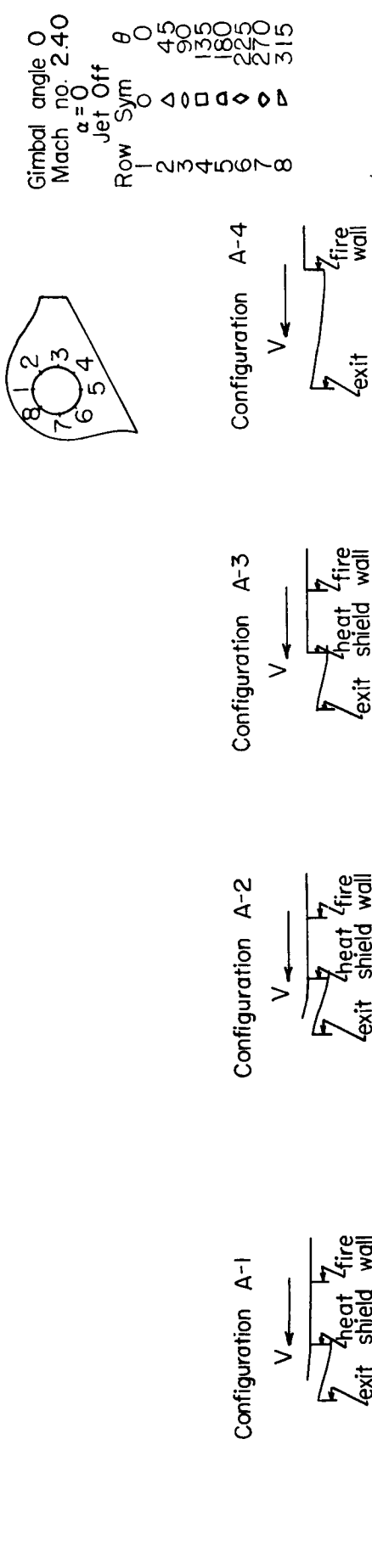


Figure 12a Pressure distribution over the surface of a nozzle with various shroud configurations

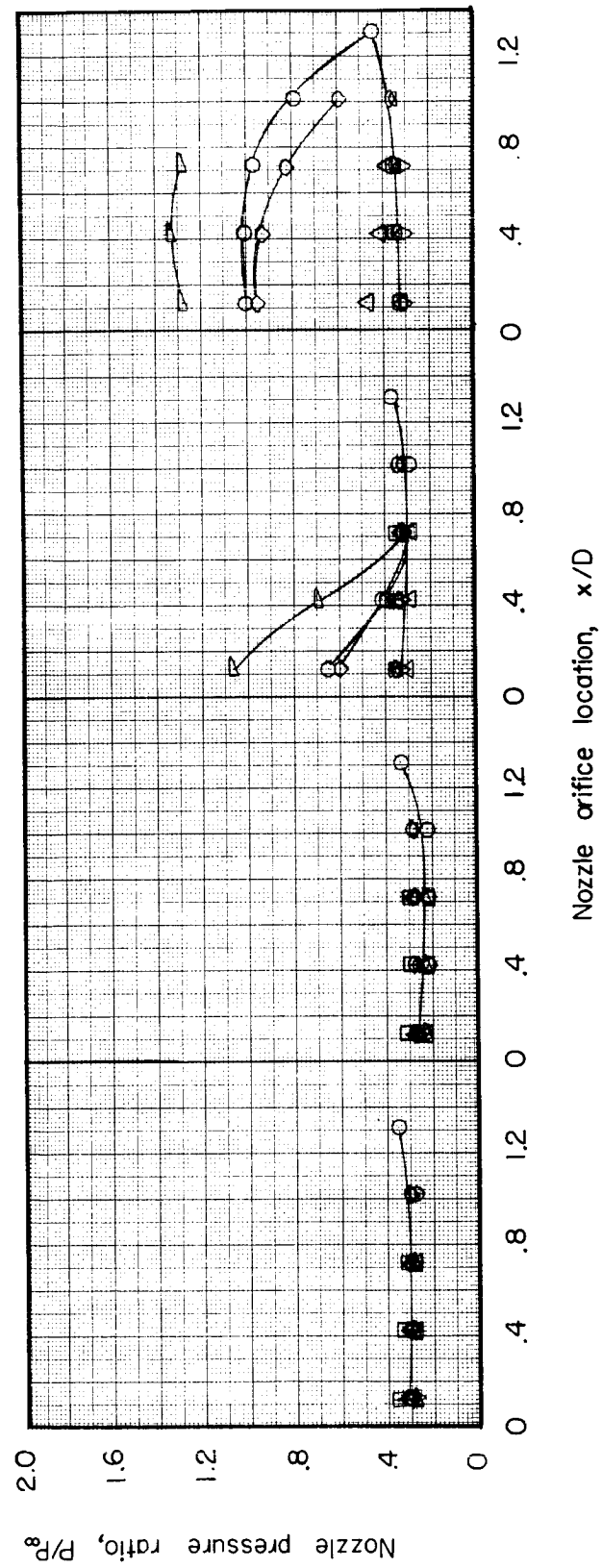
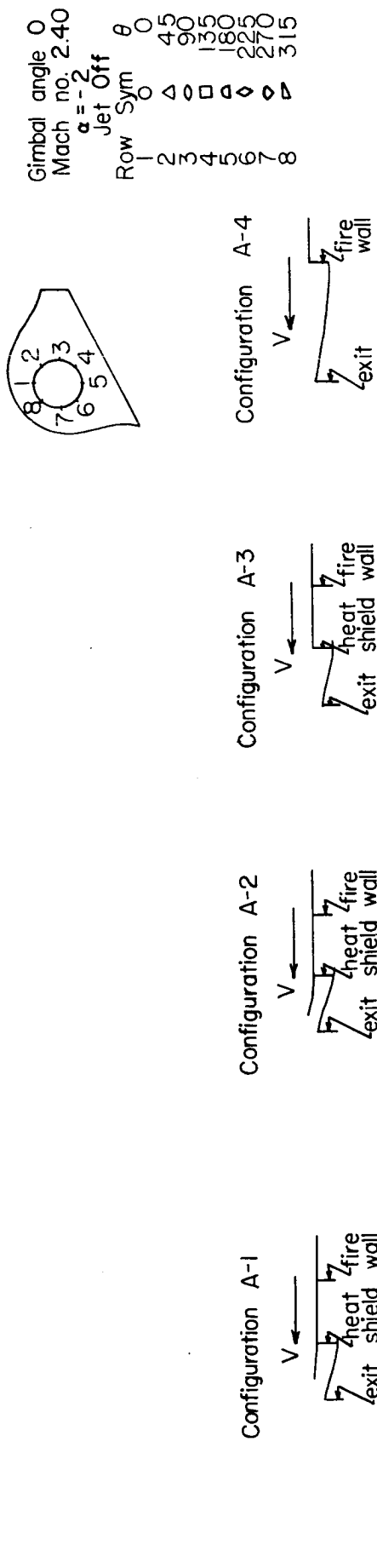


Figure 12b Pressure distribution over the surface of a nozzle with various shroud configurations

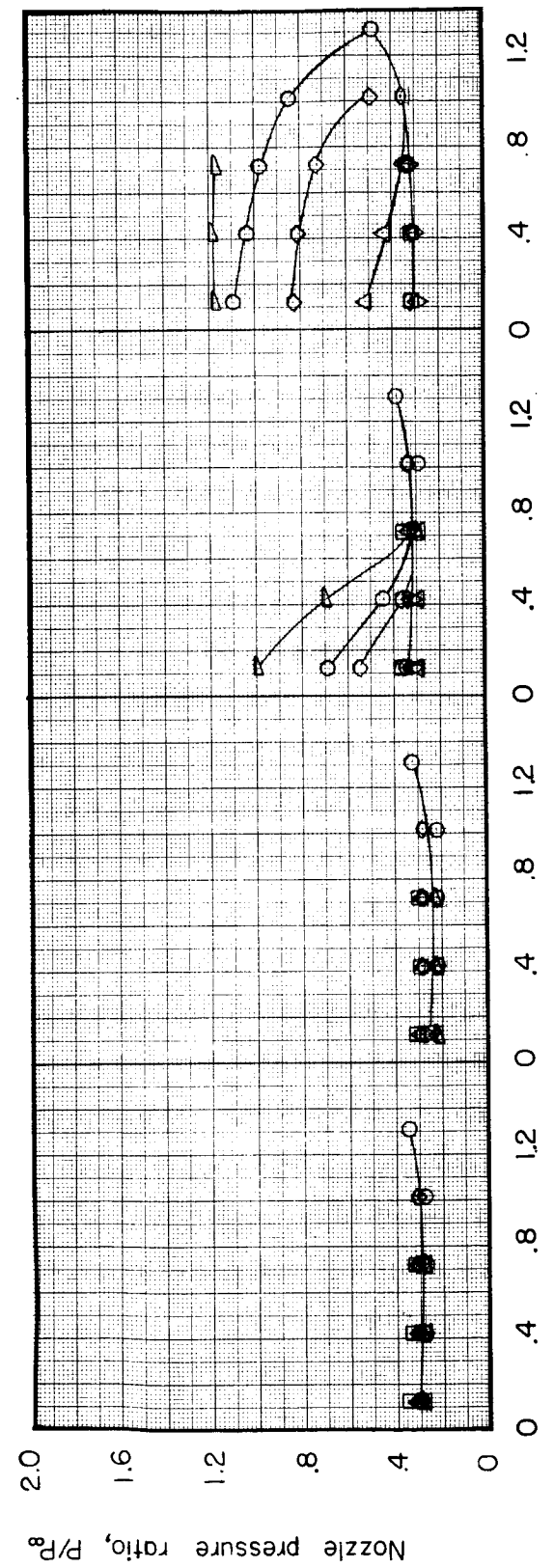
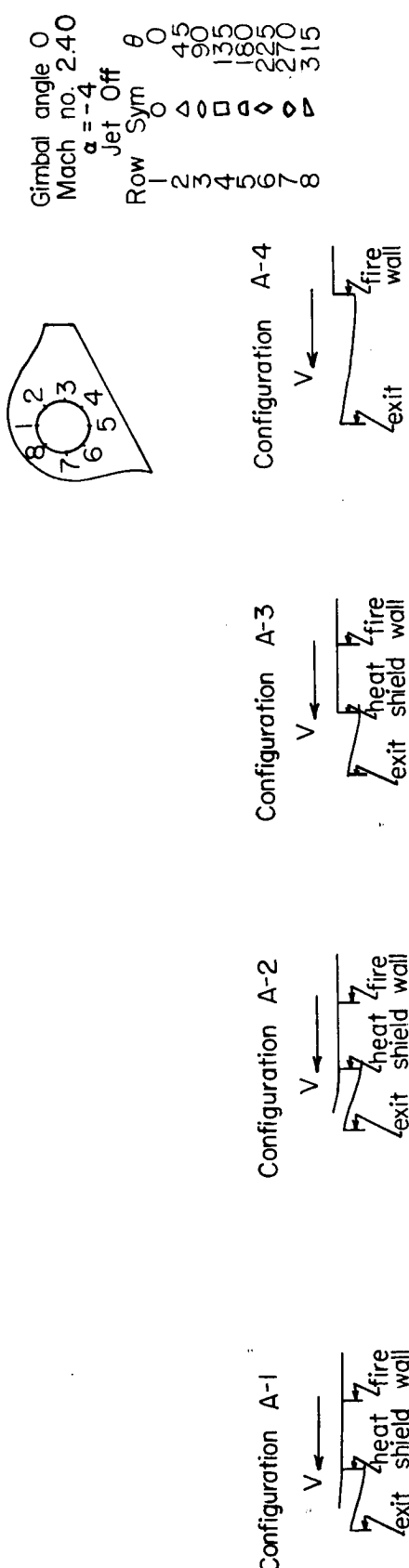


Figure 12c Pressure distribution over the surface of a nozzle with various shroud configurations

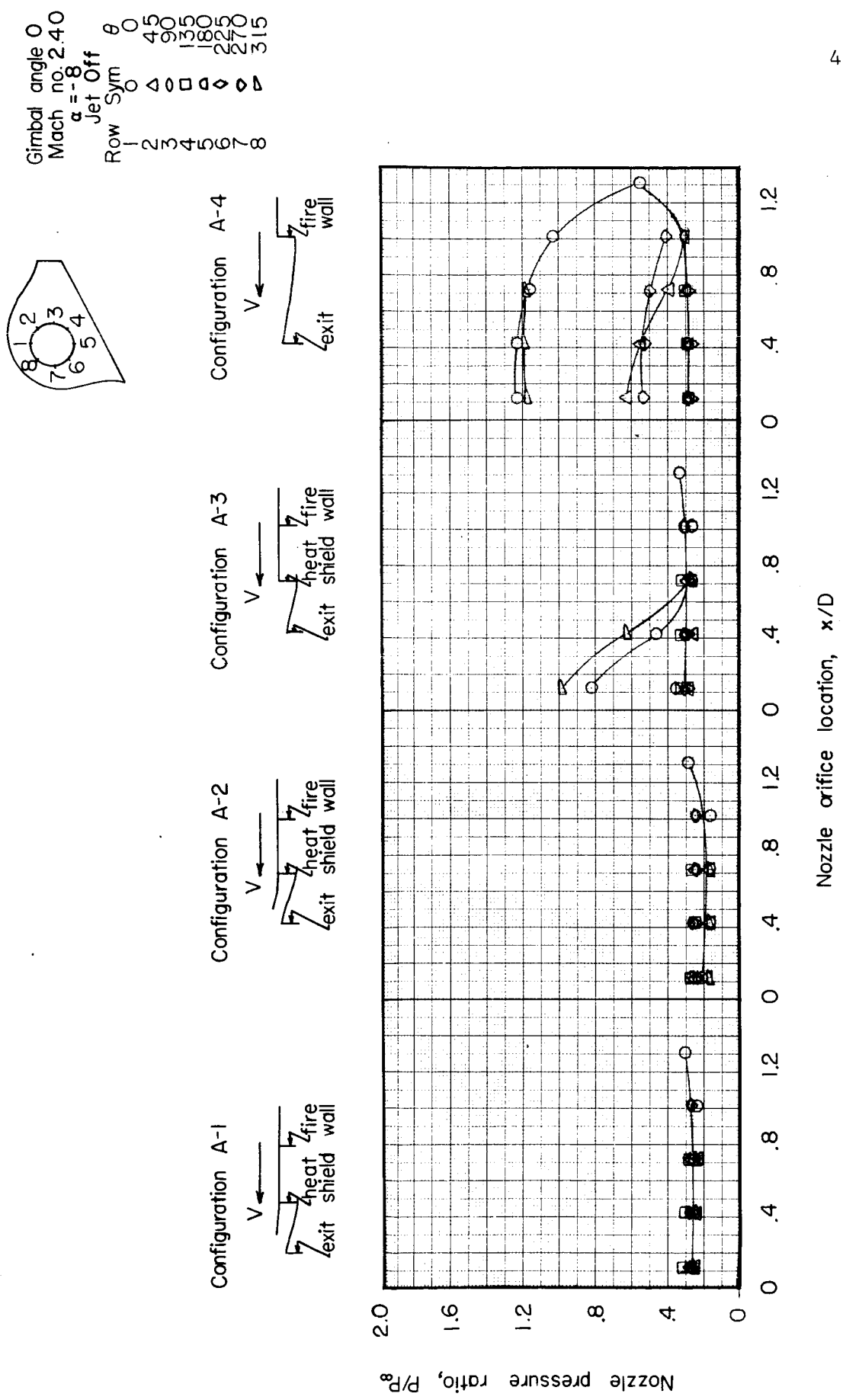


Figure 12.4 Pressure distribution over the surface of a nozzle with various shroud configurations

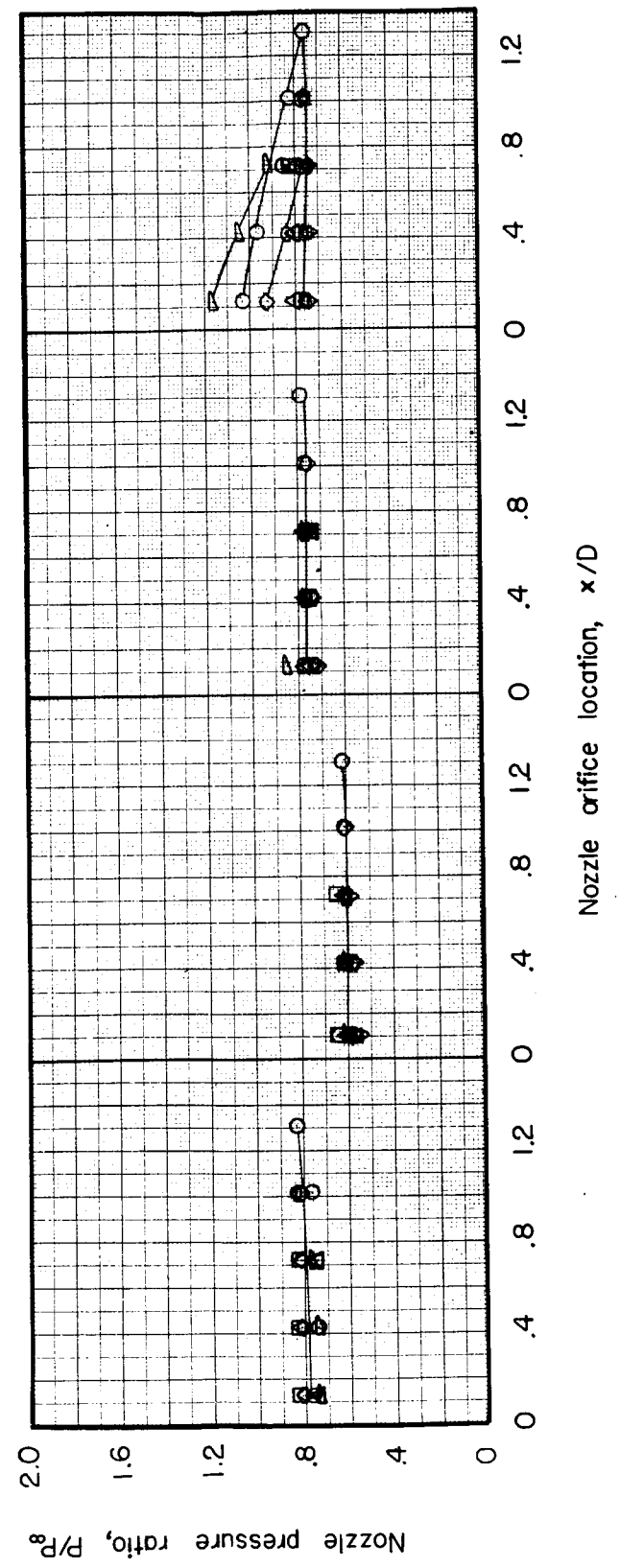
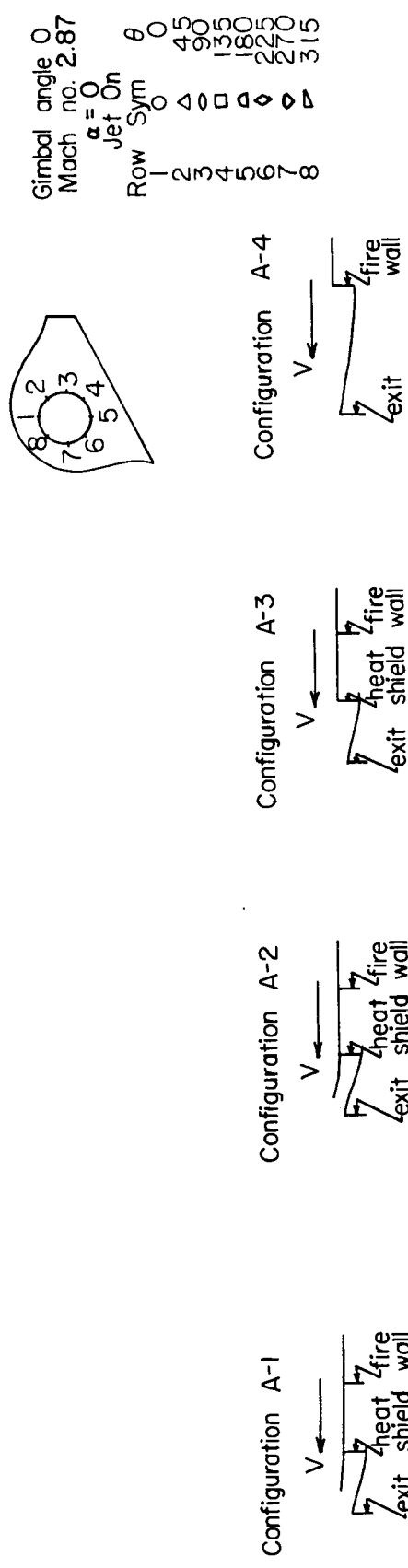
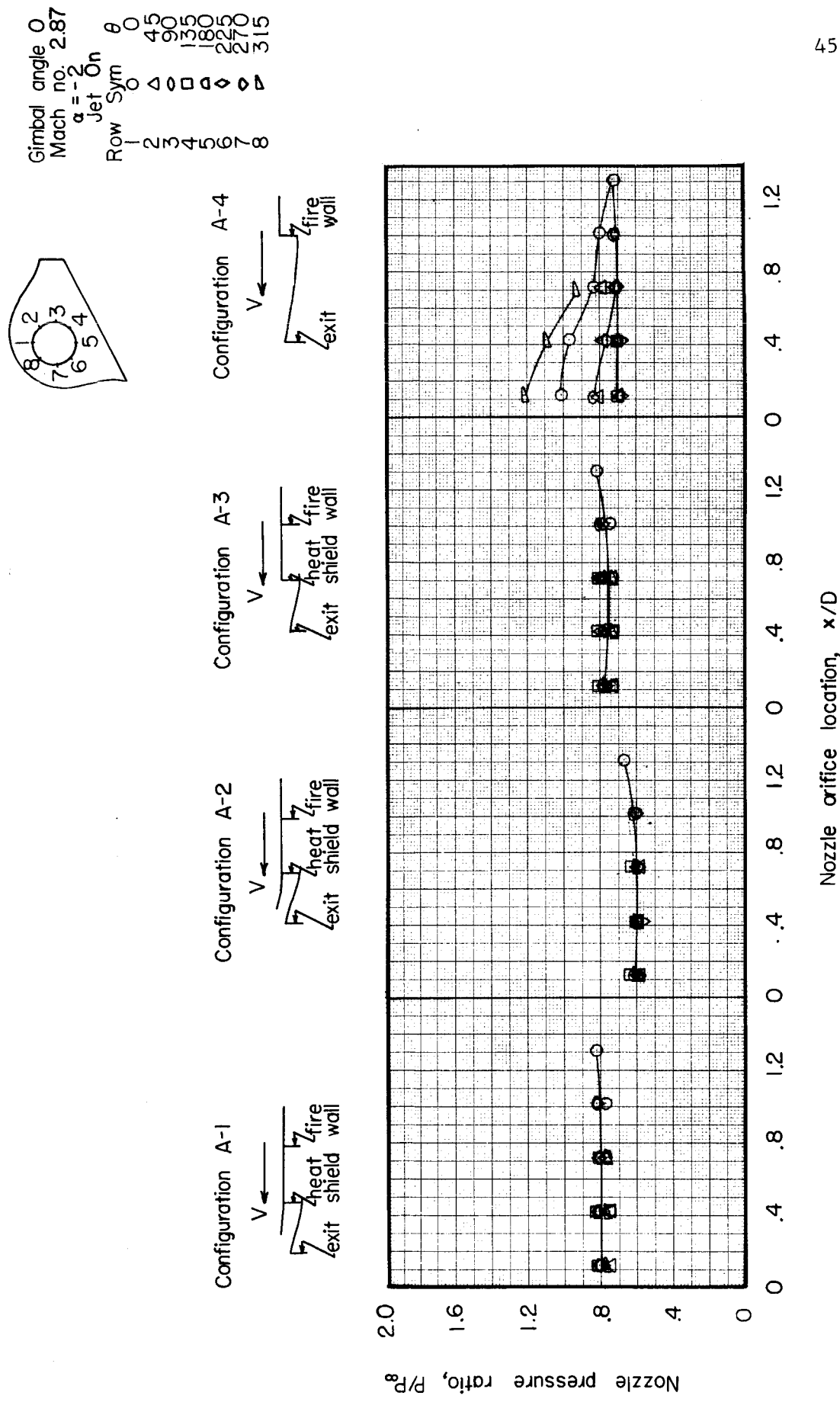


Figure 13a Pressure distribution over the surface of a nozzle with various shroud configurations



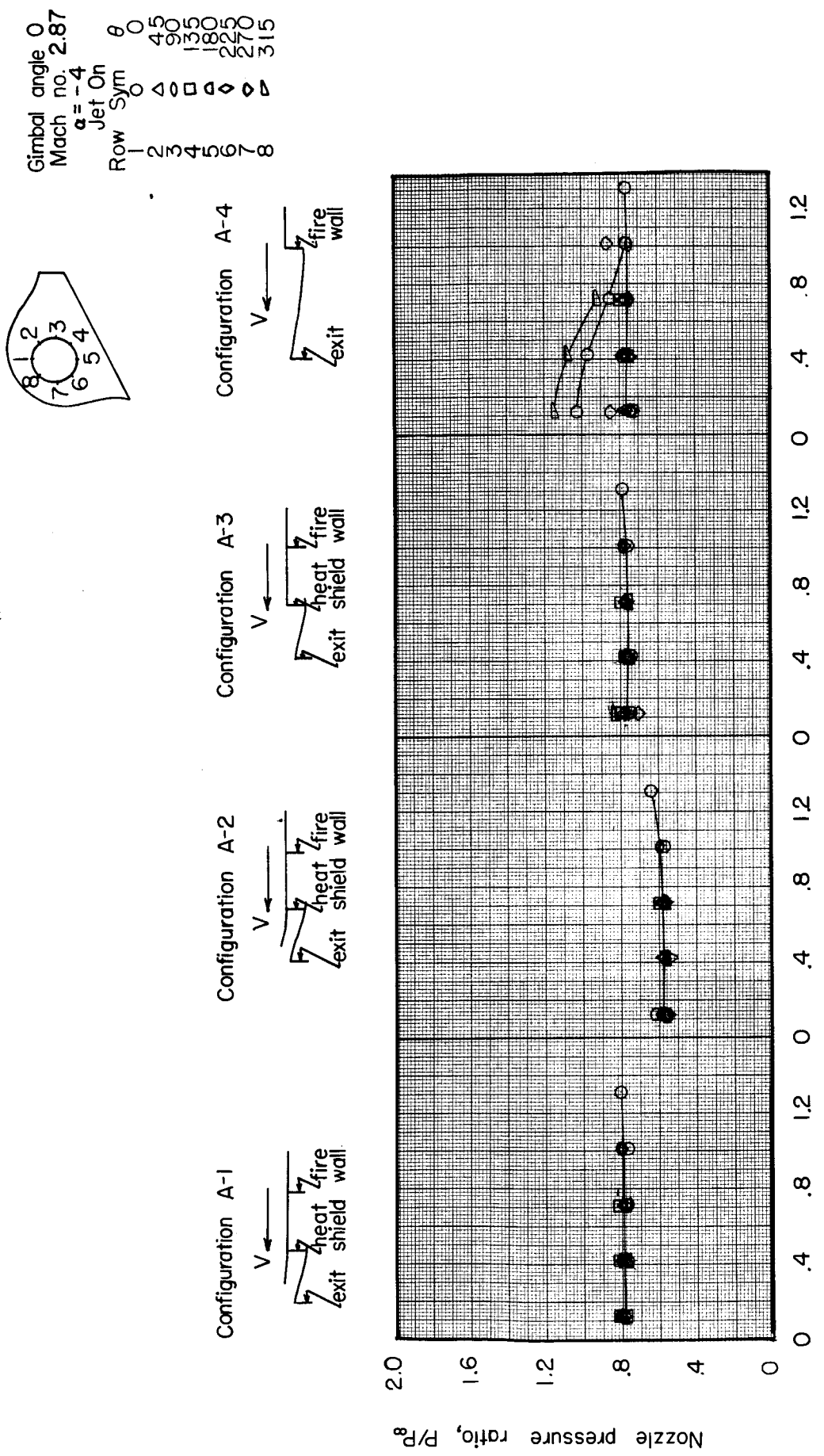


Figure I3c Pressure distribution over the surface of a nozzle with various shroud configurations

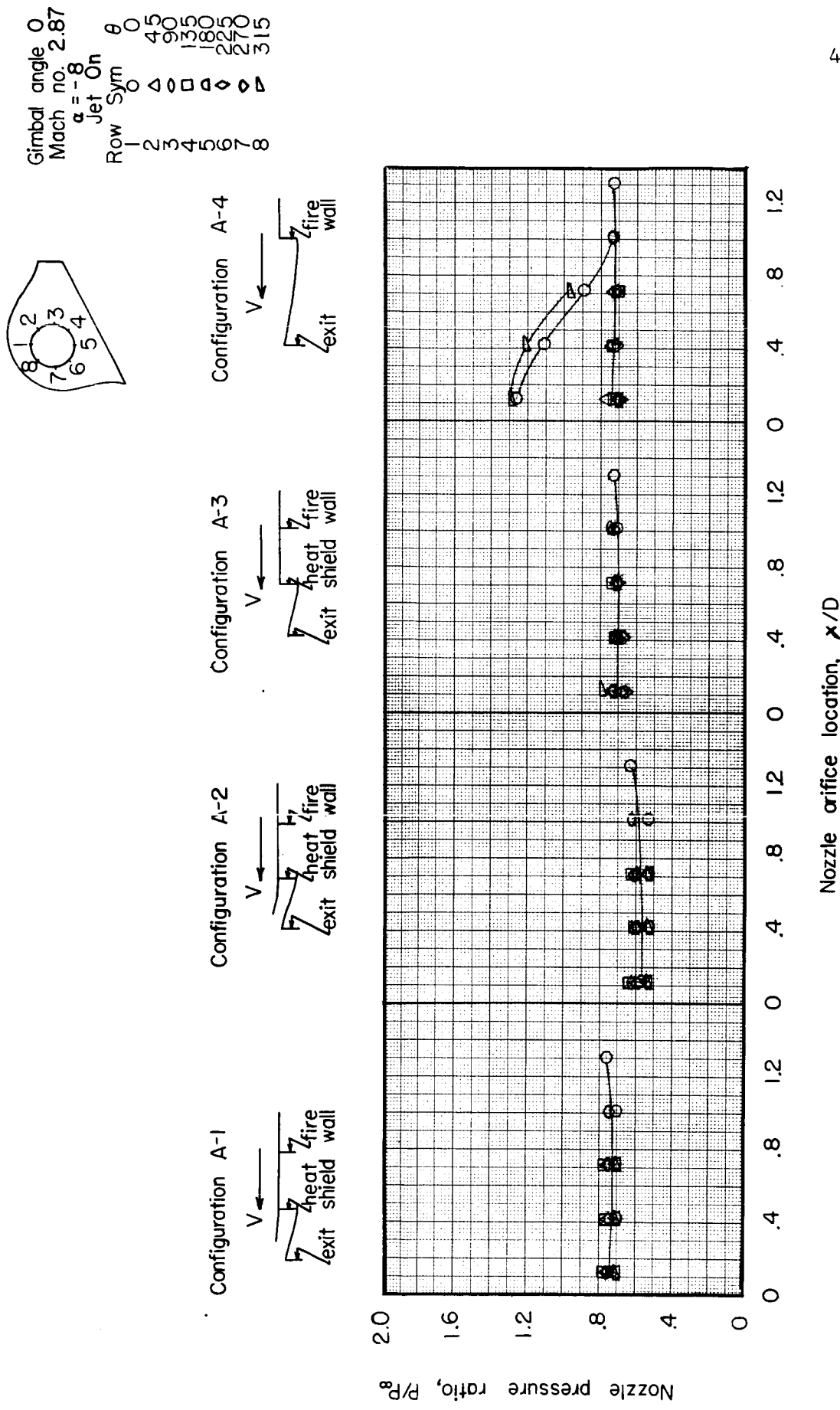


Figure 13d Pressure distribution over the surface of a nozzle with various shroud configurations

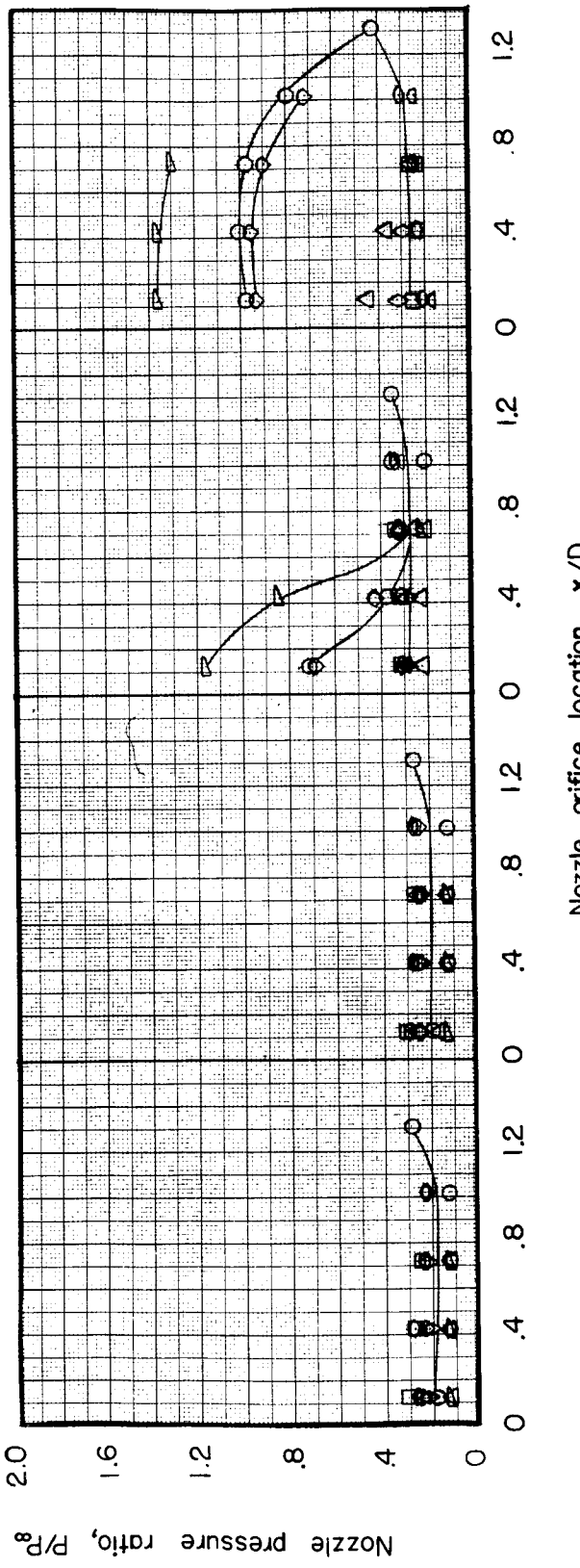
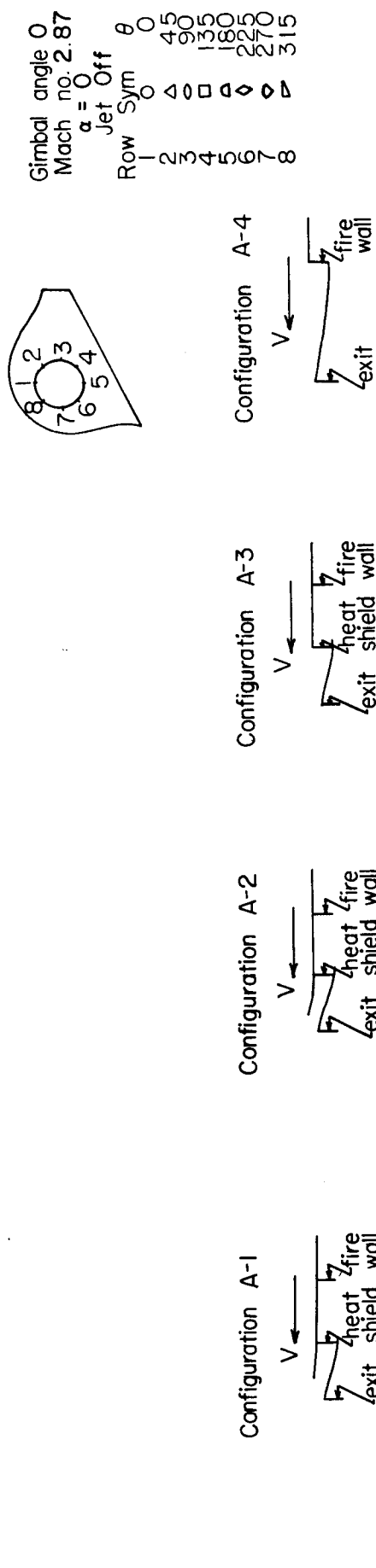


Figure 14a Pressure distribution over the surface of a nozzle with various shroud configurations

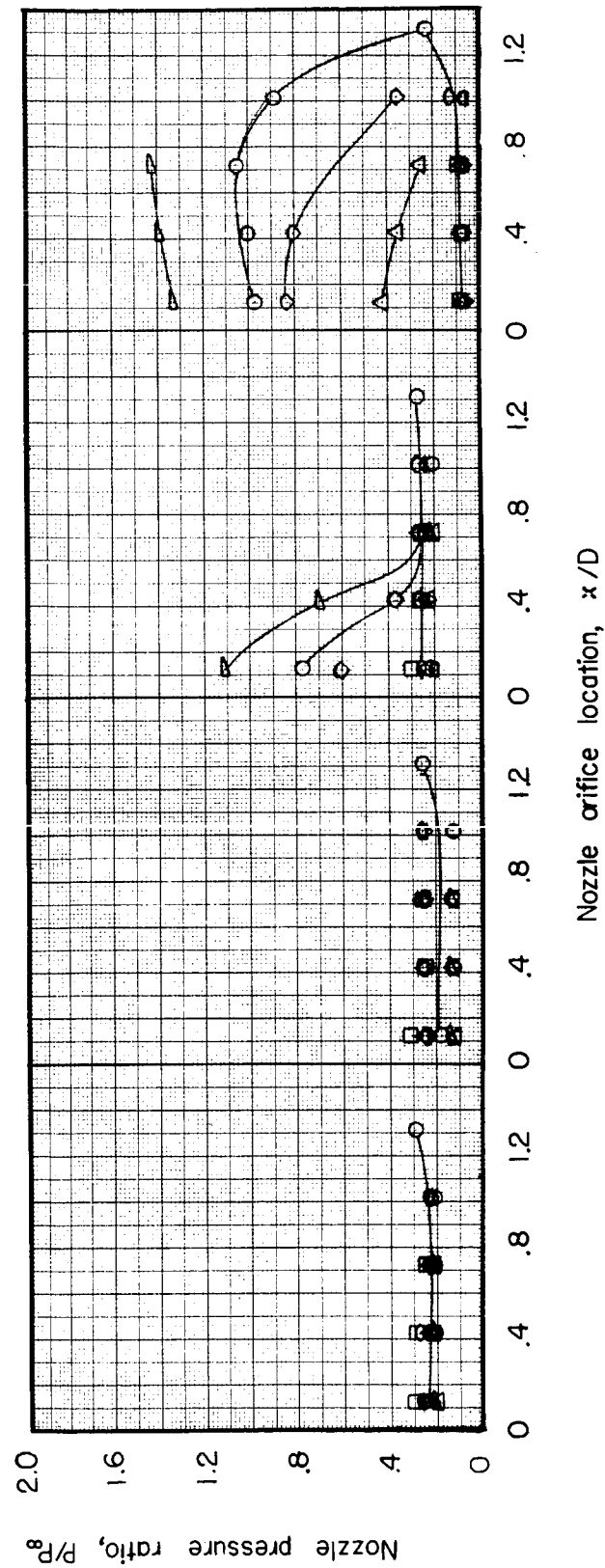
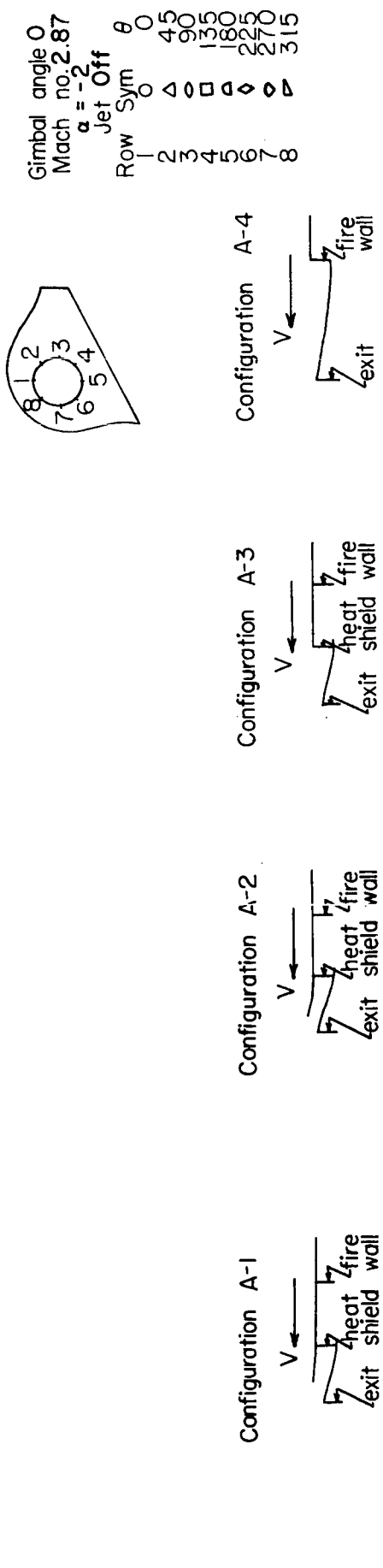


Figure 14b Pressure distribution over the surface of a nozzle with various shroud configurations

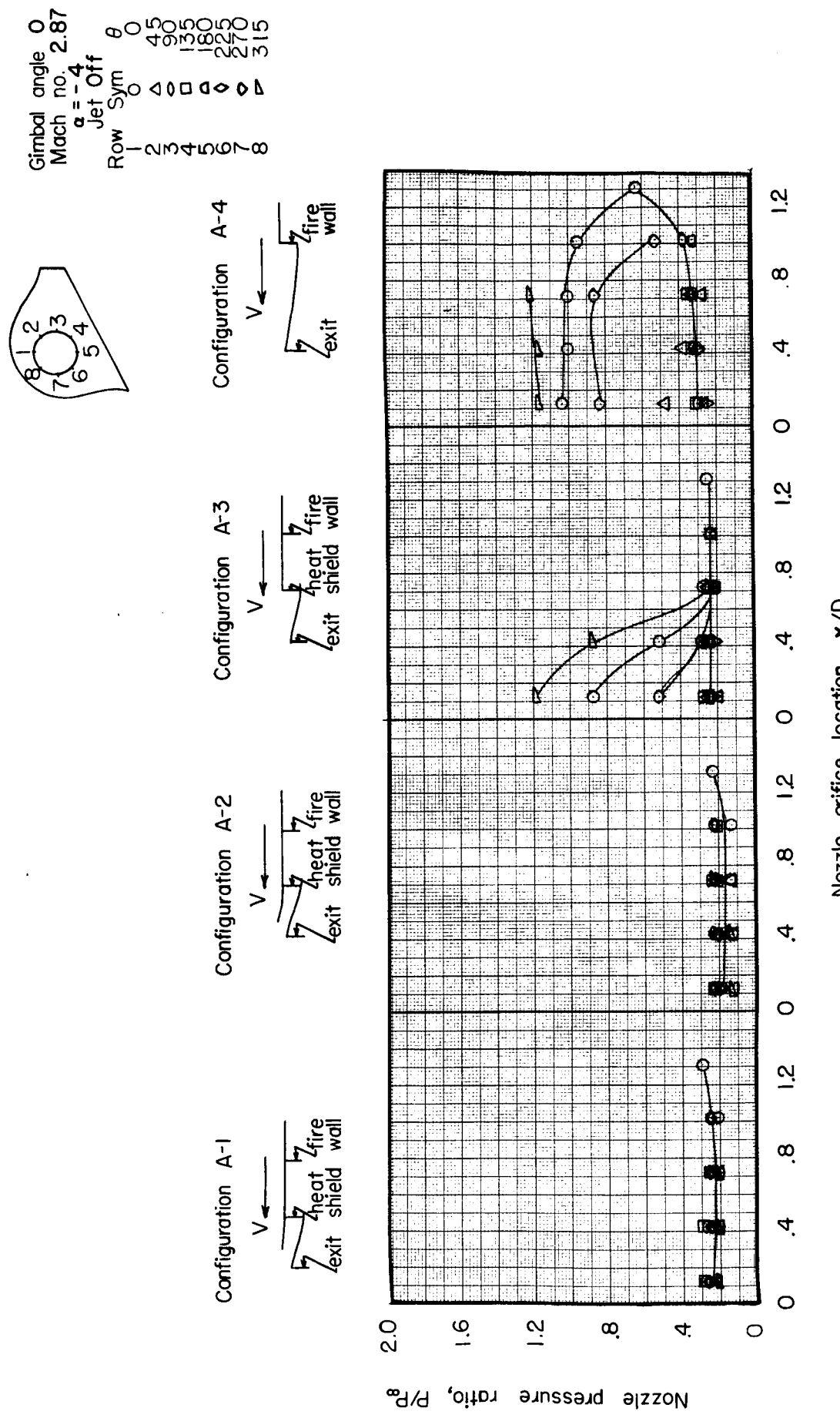


Figure 14c Pressure distribution over the surface of a nozzle with various shroud configurations

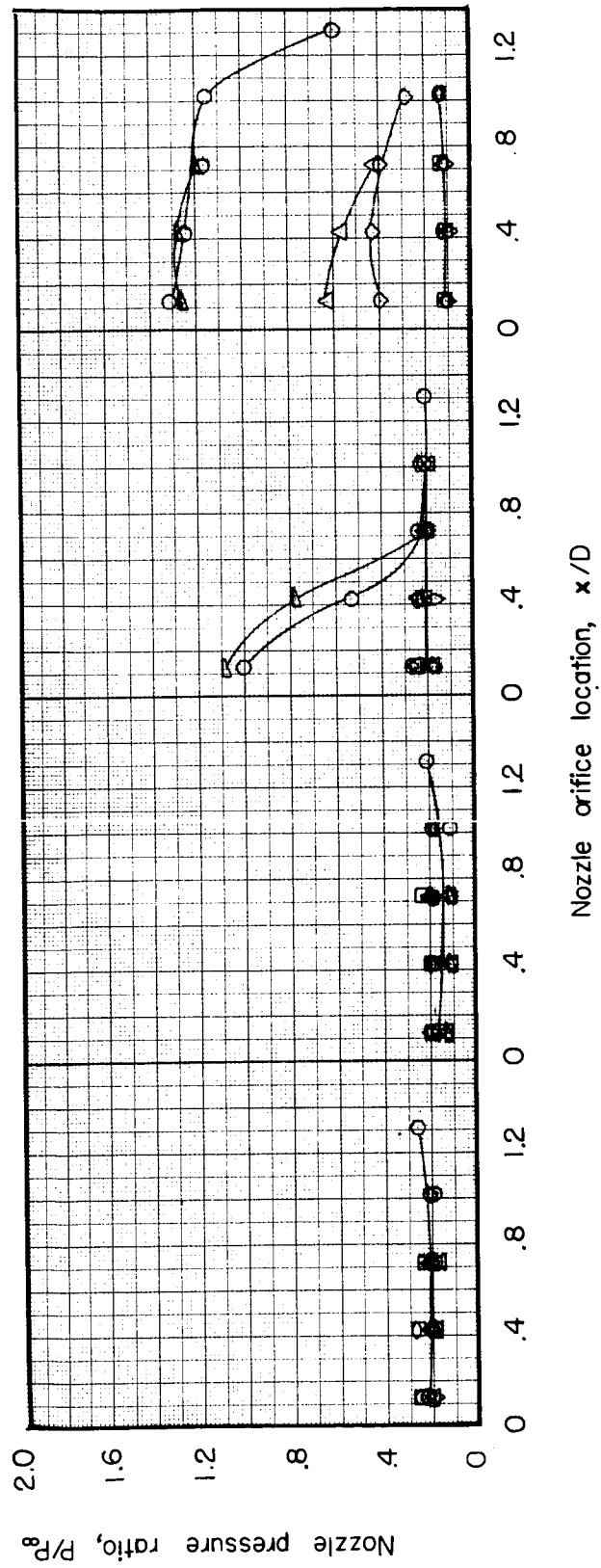
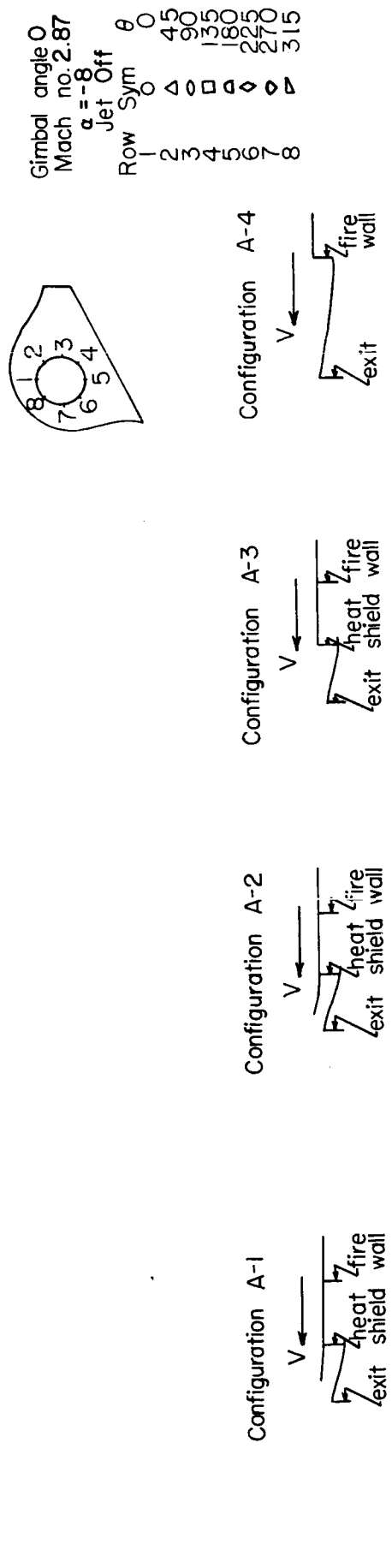


Figure 14d Pressure distribution over the surface of a nozzle with various shroud configurations

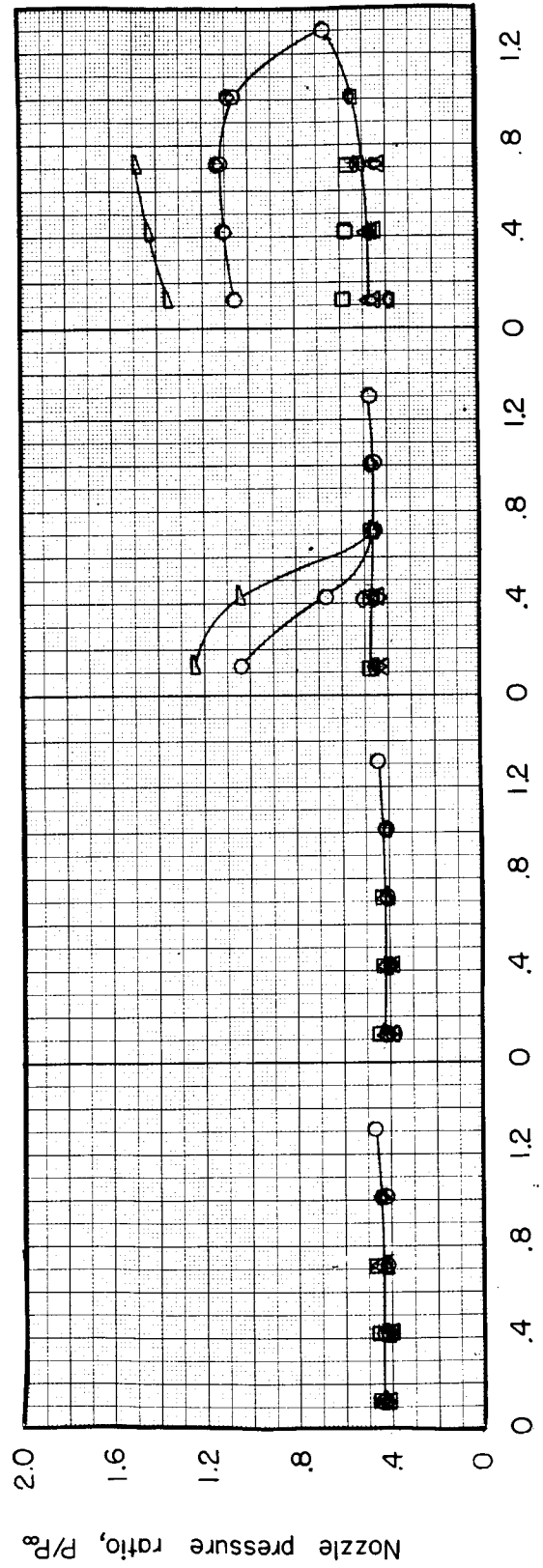
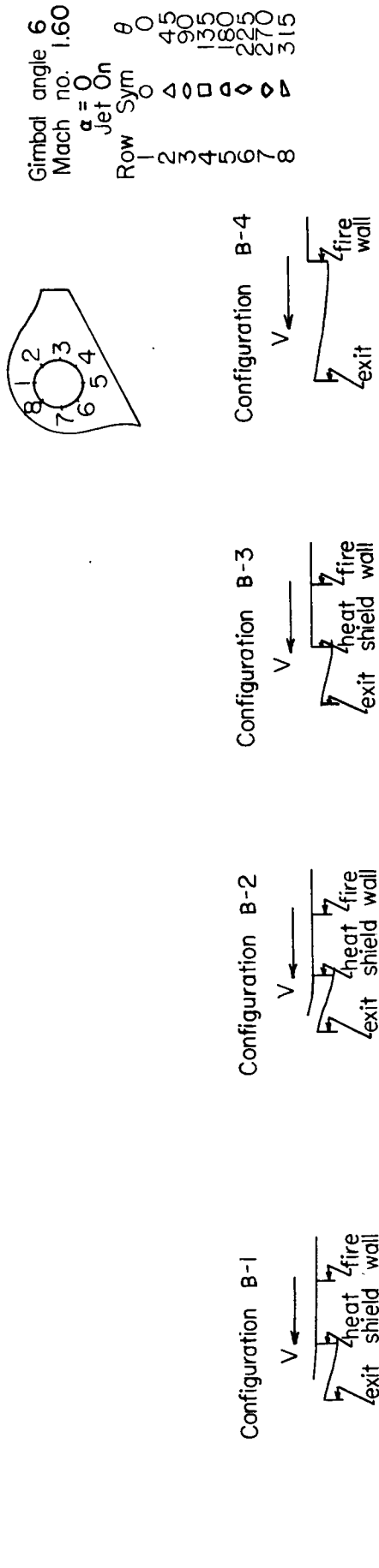
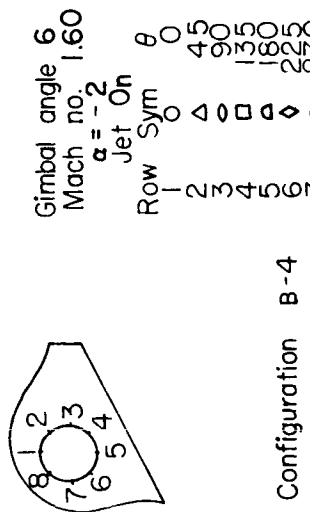


Figure 15a Pressure distribution over the surface of a nozzle with various shroud configurations



Configuration B-1  
 $V \leftarrow$   
 exit heat fire wall  
 Configuration B-2  
 $V \leftarrow$   
 exit heat fire wall  
 Configuration B-3  
 $V \leftarrow$   
 exit heat fire wall

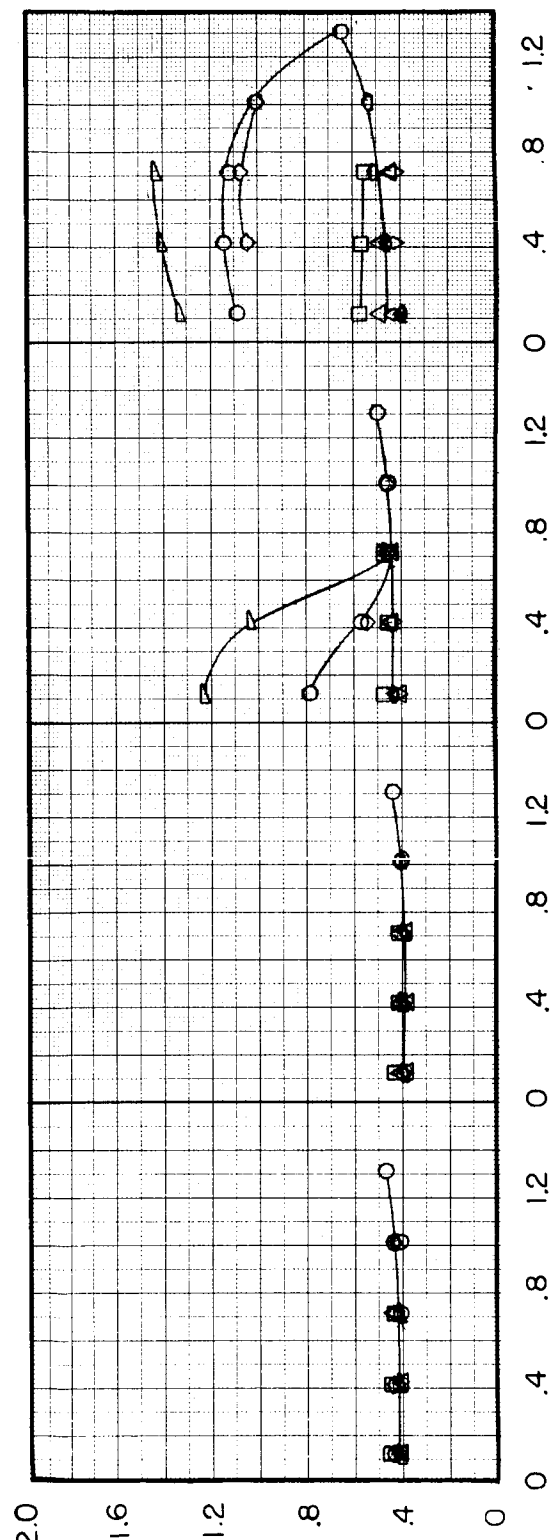


Figure 15 b Pressure distribution over the surface of a nozzle with various shroud configurations

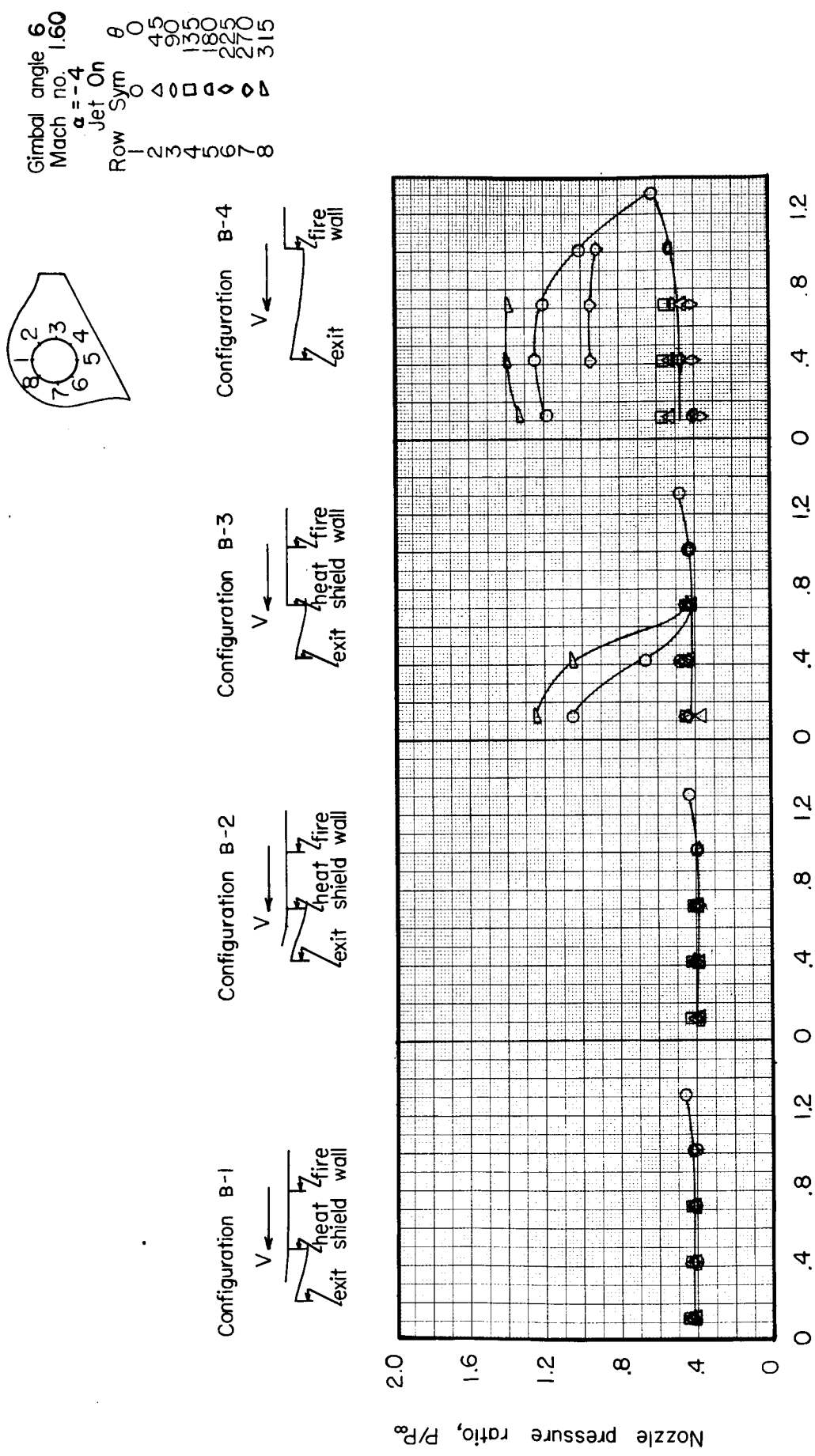
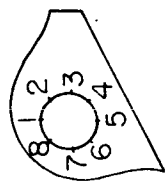


Figure 15c Pressure distribution over the surface of a nozzle with various shroud configurations

Gimbal angle 6  
Mach no. 1.60  
 $\alpha = -8^\circ$   
Jet On Sym 0  
Row 1 2 3 4 5 6 7 8  
1 2 3 4 5 6 7 8  
2 3 4 5 6 7 8  
3 4 5 6 7 8  
4 5 6 7 8  
5 6 7 8  
6 7 8  
7 8  
8



Configuration B-1  
V ←  
exit fire wall  
heat shield wall

Configuration B-2  
V ←  
exit fire wall  
heat shield wall

Configuration B-3  
V ←  
exit fire wall  
heat shield wall

Configuration B-4  
V ←  
exit fire wall

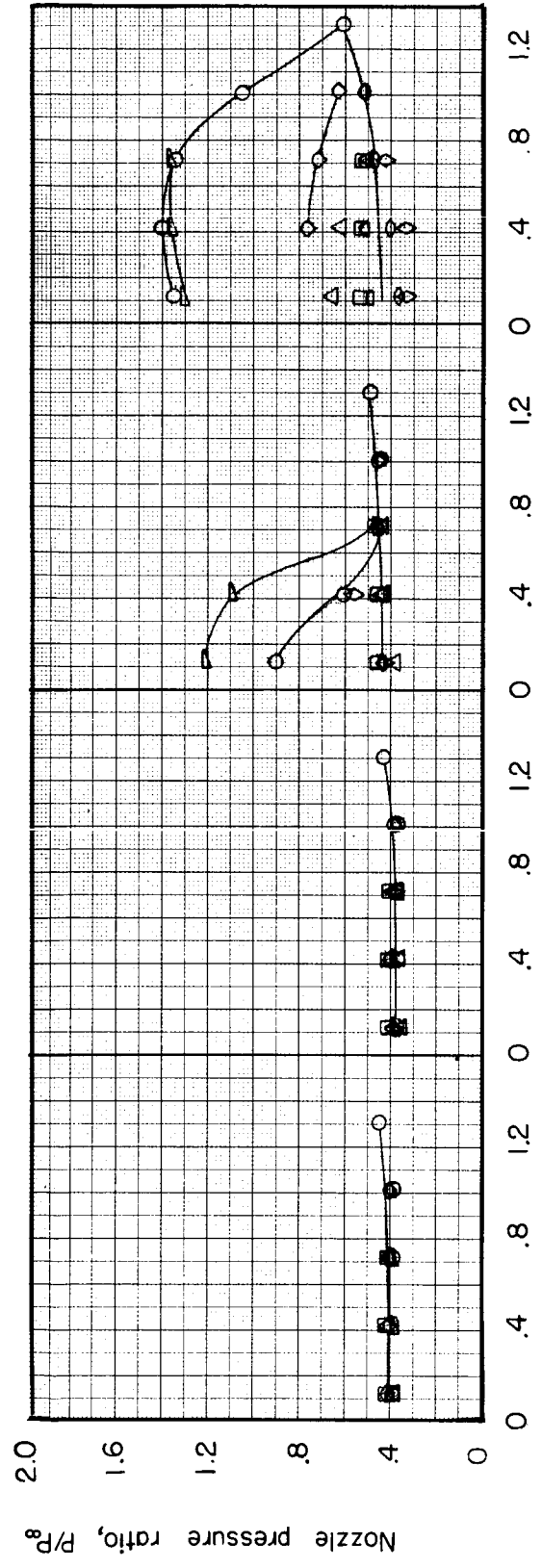


Figure 15d Pressure distribution over the surface of a nozzle with various shroud configurations

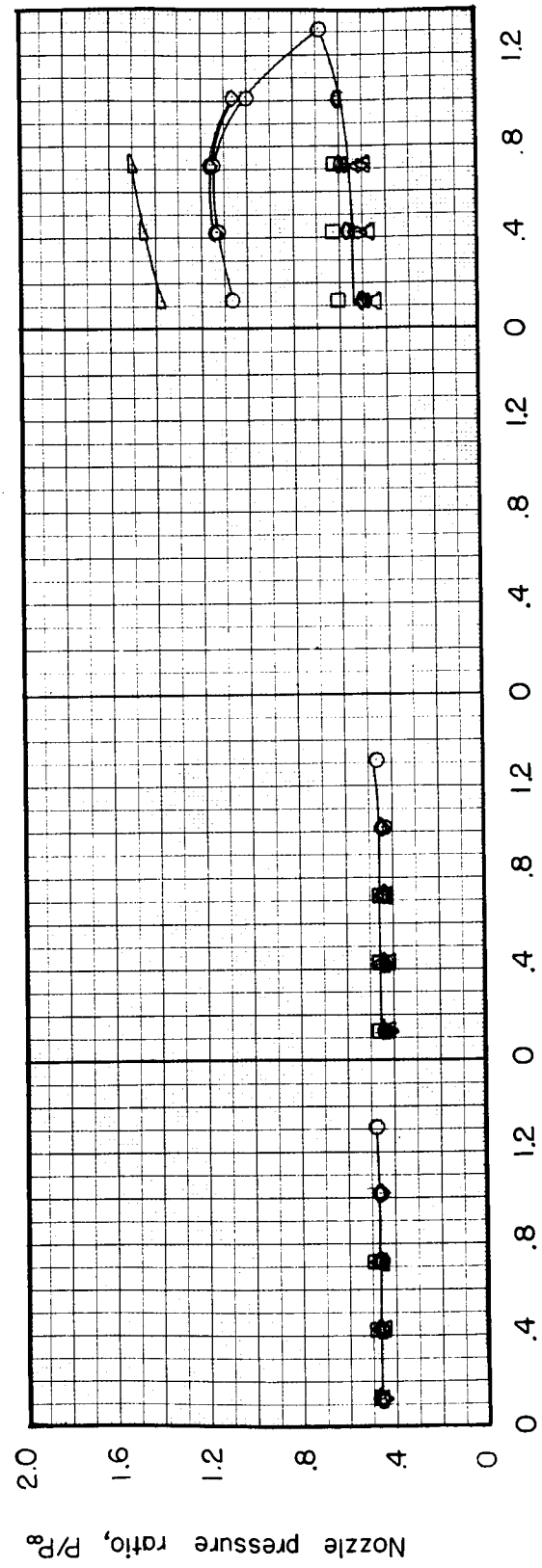
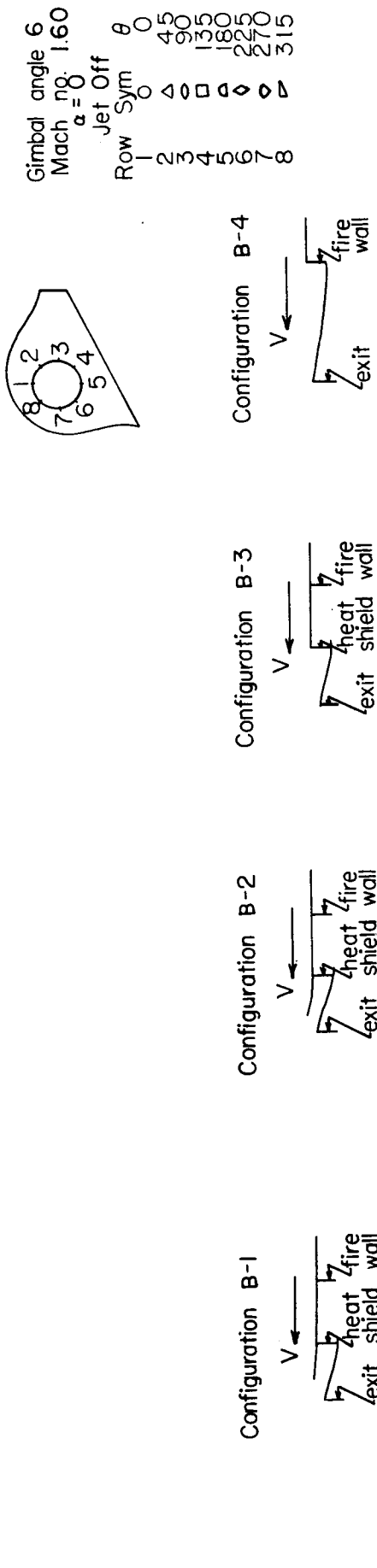


Figure 16a Pressure distribution over the surface of a nozzle with various shroud configurations

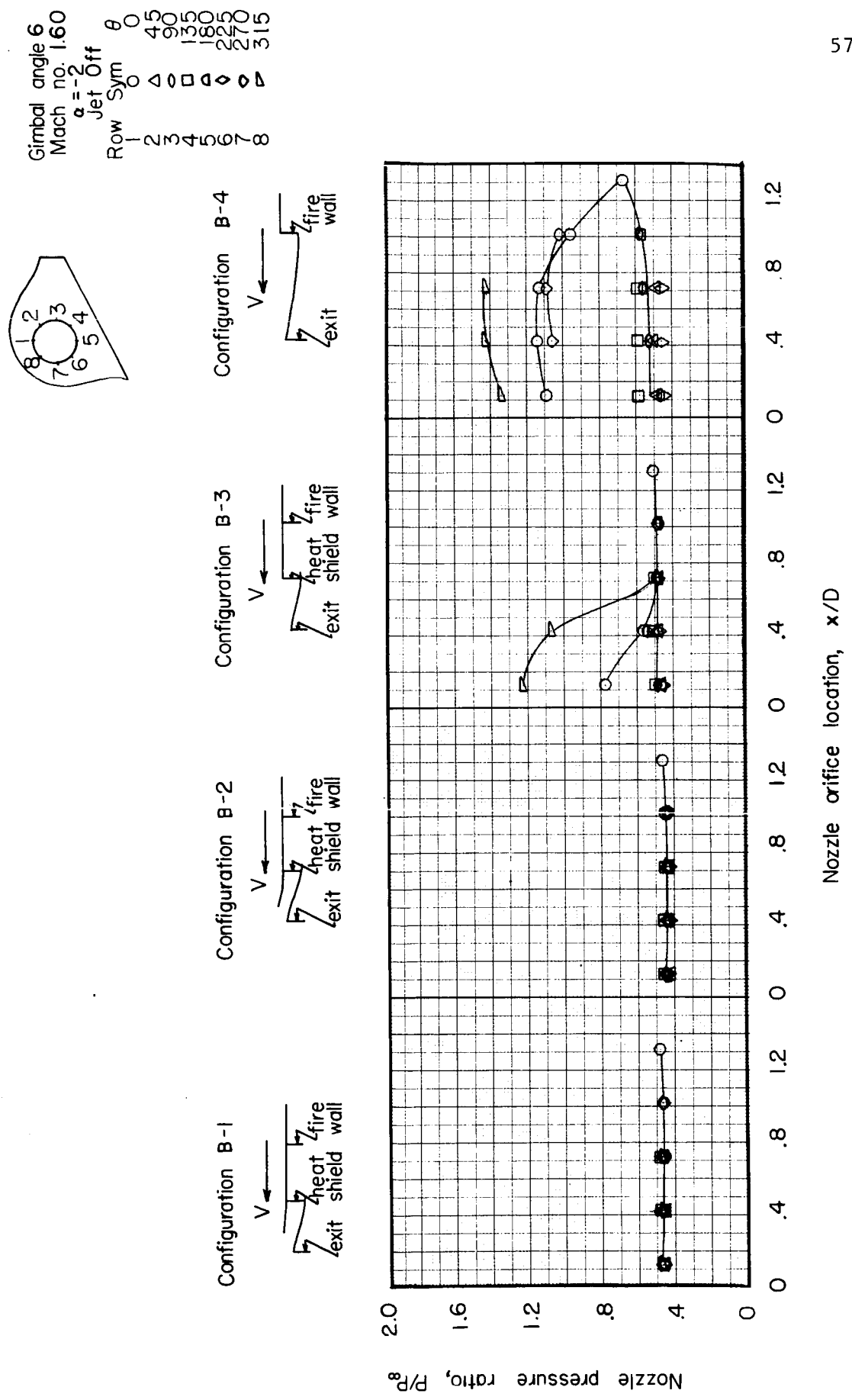


Figure 16b Pressure distribution over the surface of a nozzle with various shroud configurations

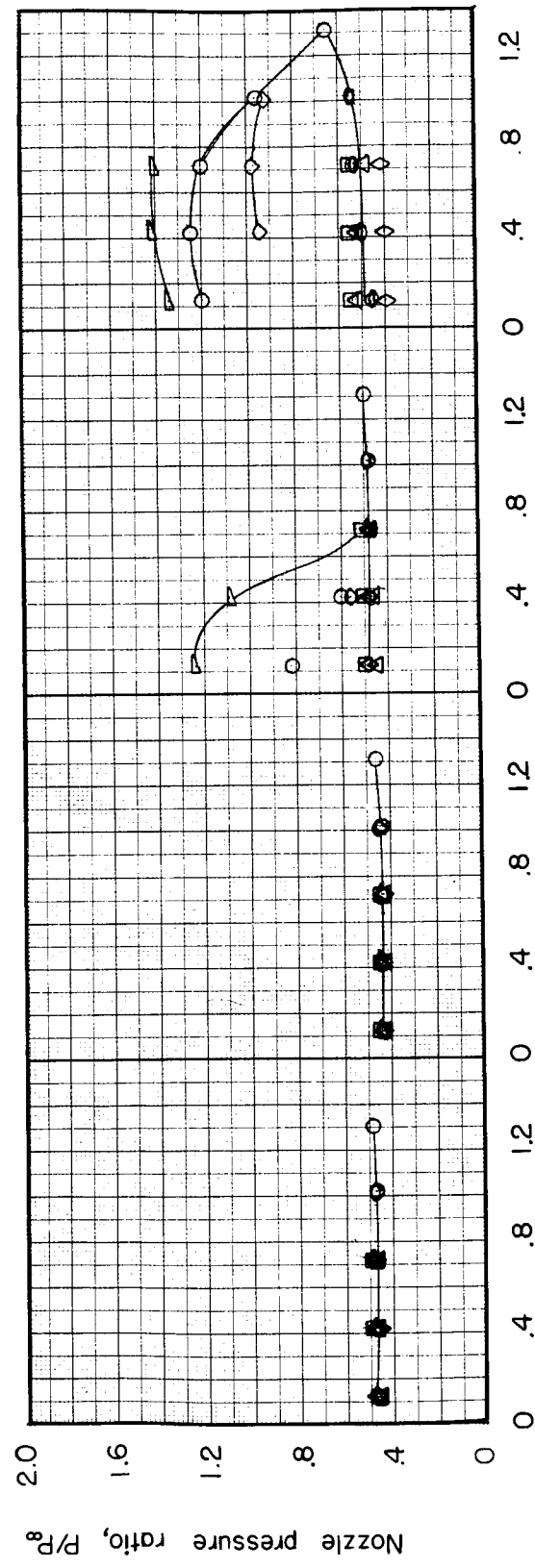
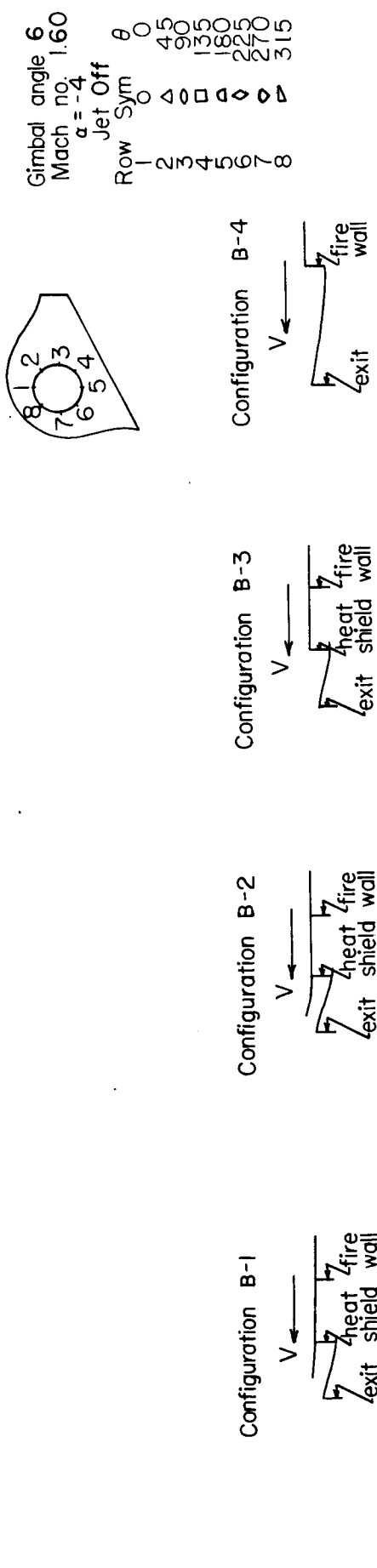


Figure 16c Pressure distribution over the surface of a nozzle with various shroud configurations

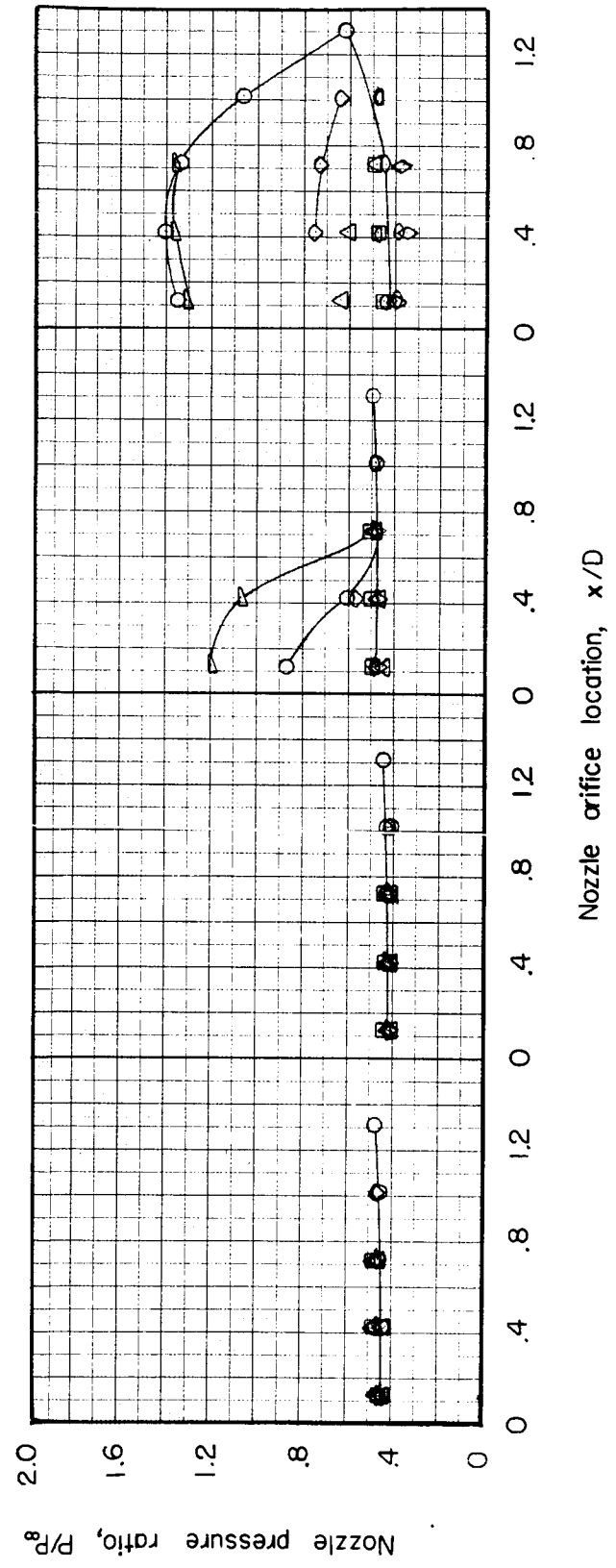
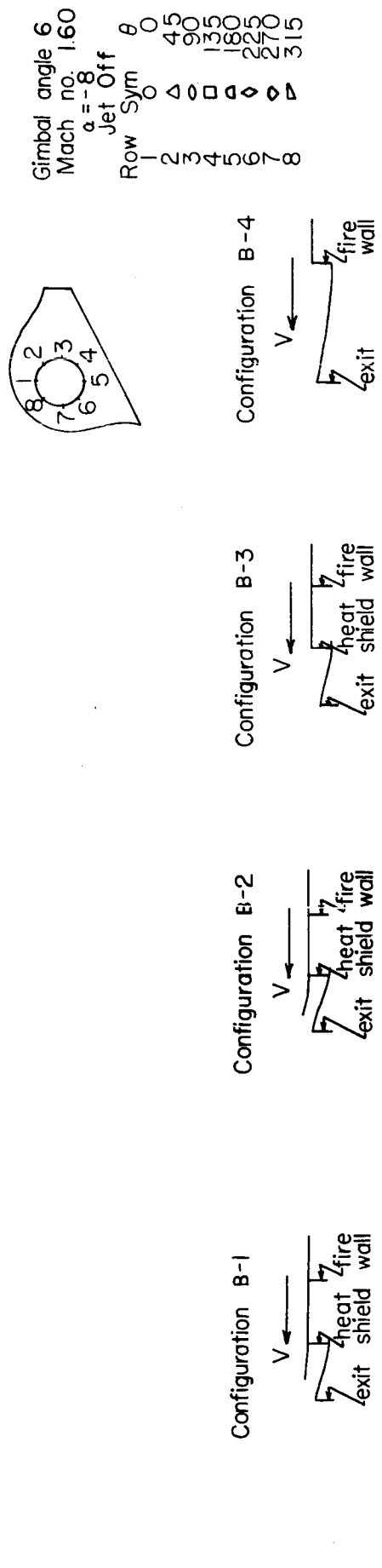


Figure 16d Pressure distribution over the surface of a nozzle with various shroud configurations

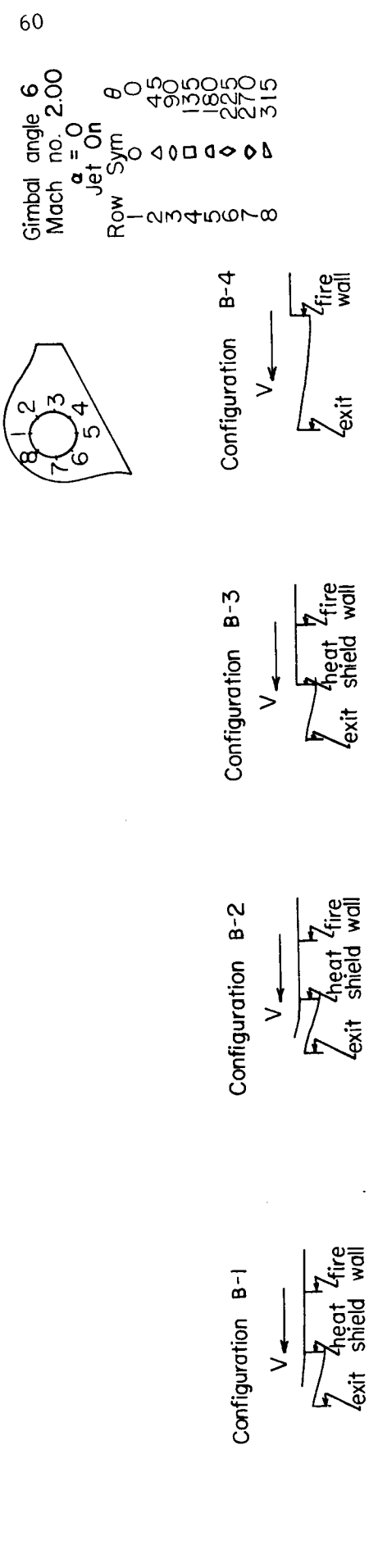


Figure 17a Pressure distribution over the surface of a nozzle with various shroud configurations

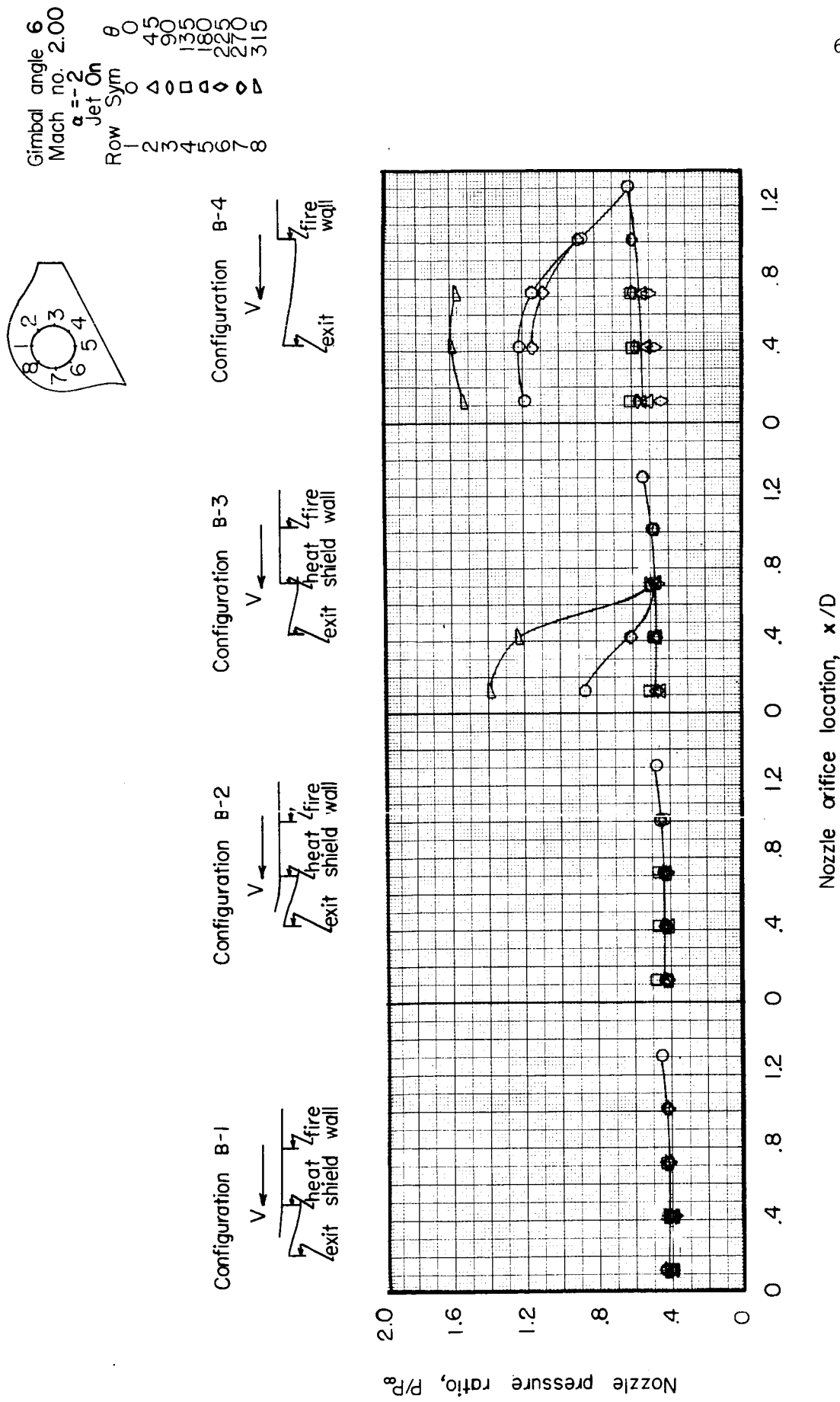


Figure 17b Pressure distribution over the surface of a nozzle with various shroud configurations

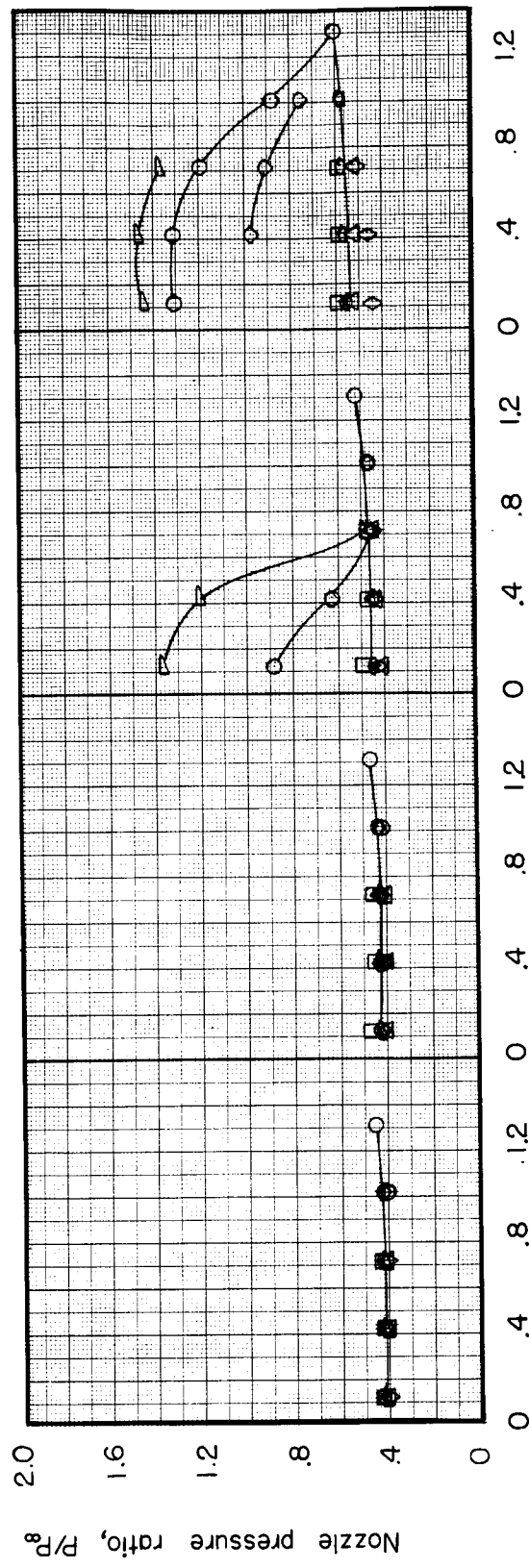
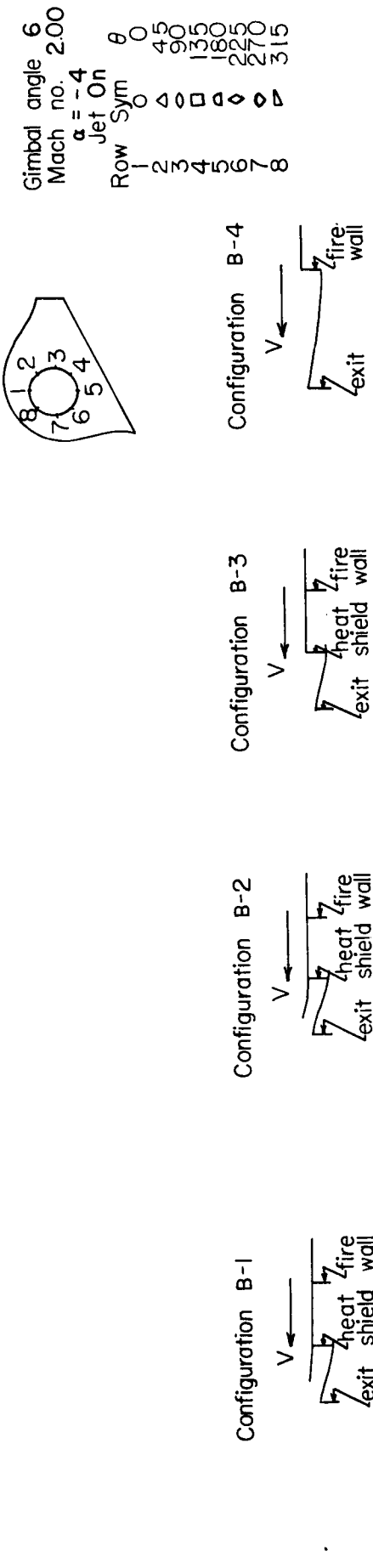


Figure I7c Pressure distribution over the surface of a nozzle with various shroud configurations

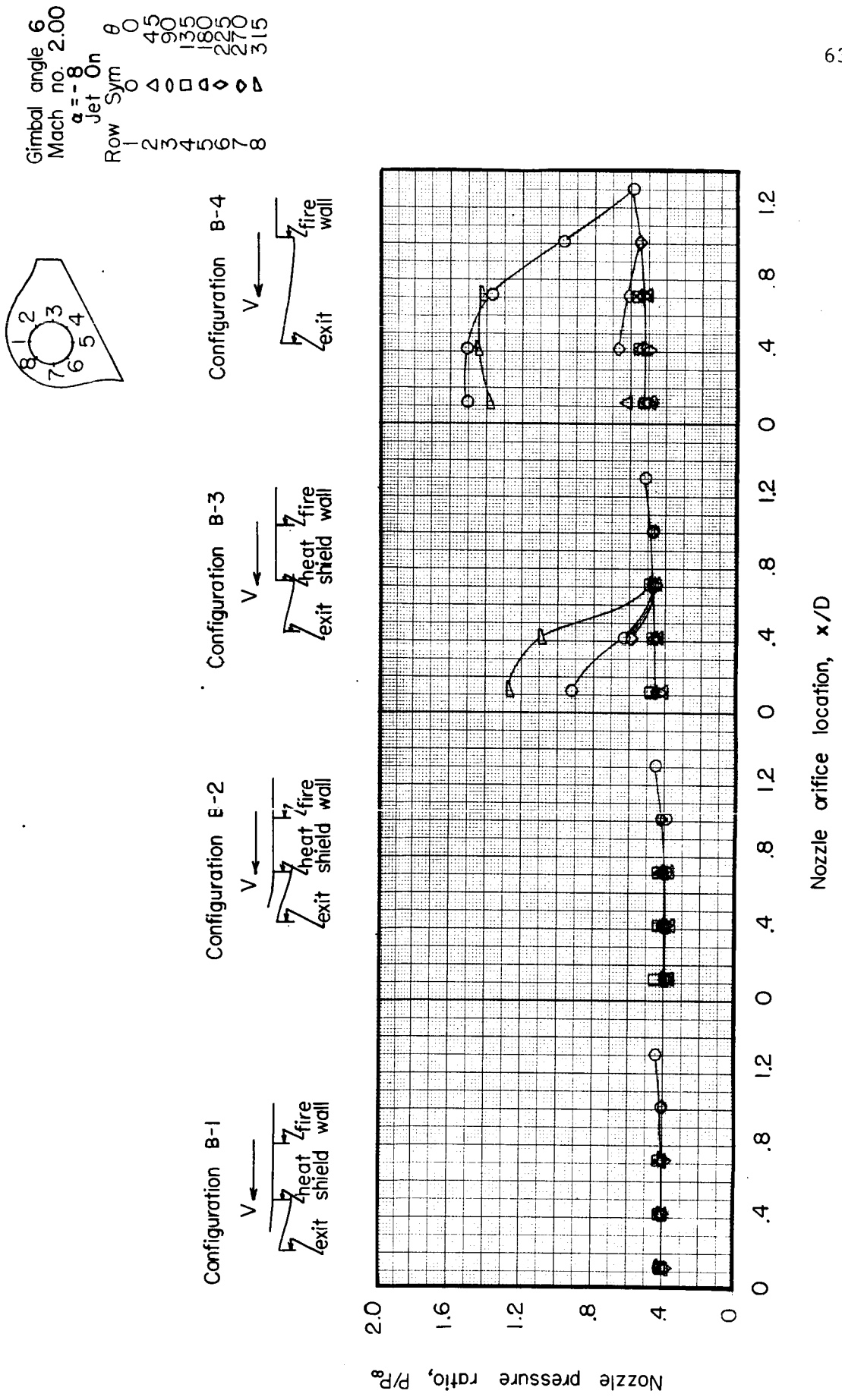


Figure 17d Pressure distribution over the surface of a nozzle with various shroud configurations

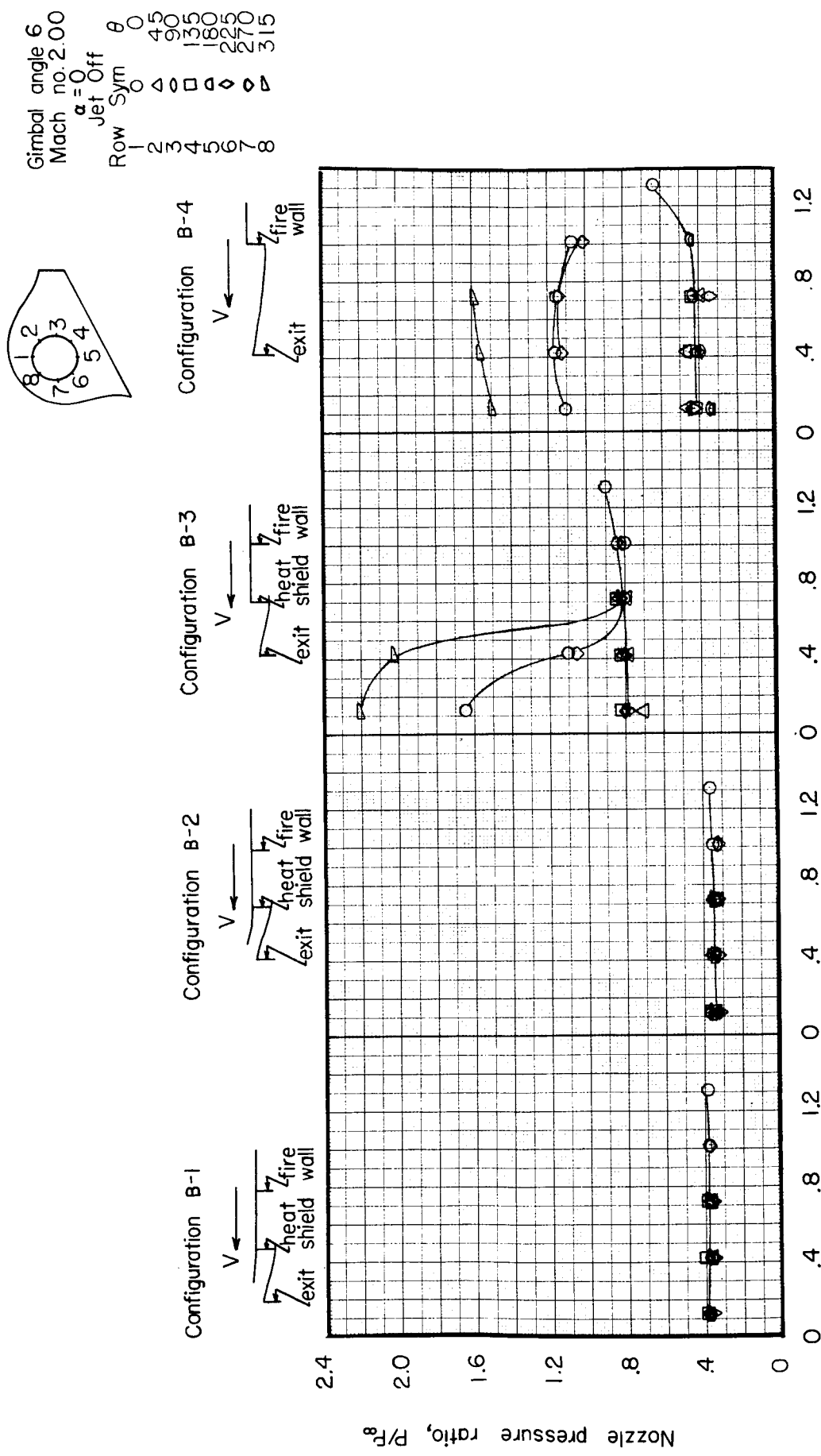


Figure 18a Pressure distribution over the surface of a nozzle with various shroud configurations

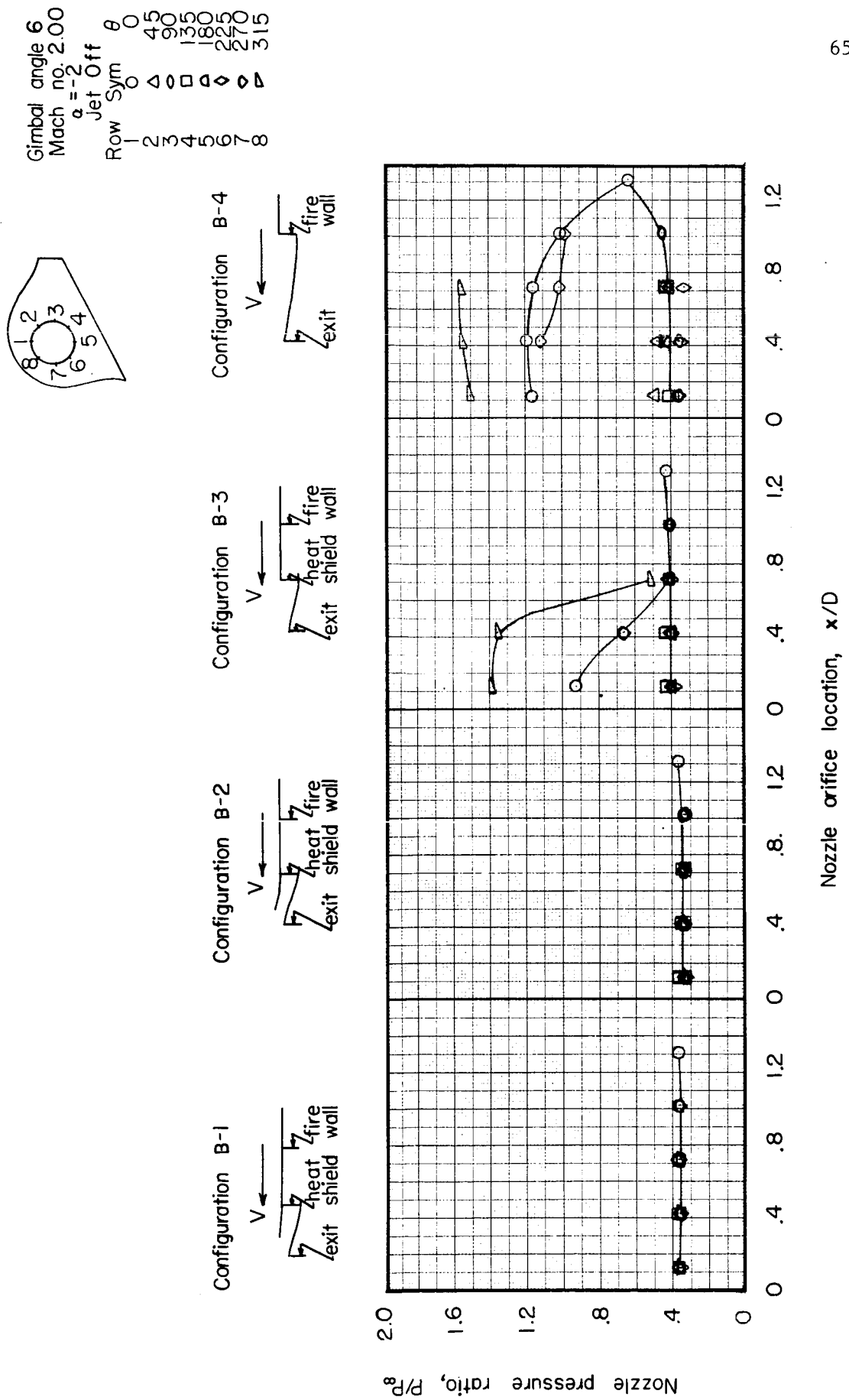


Figure 18 b Pressure distribution over the surface of a nozzle with various shroud configurations

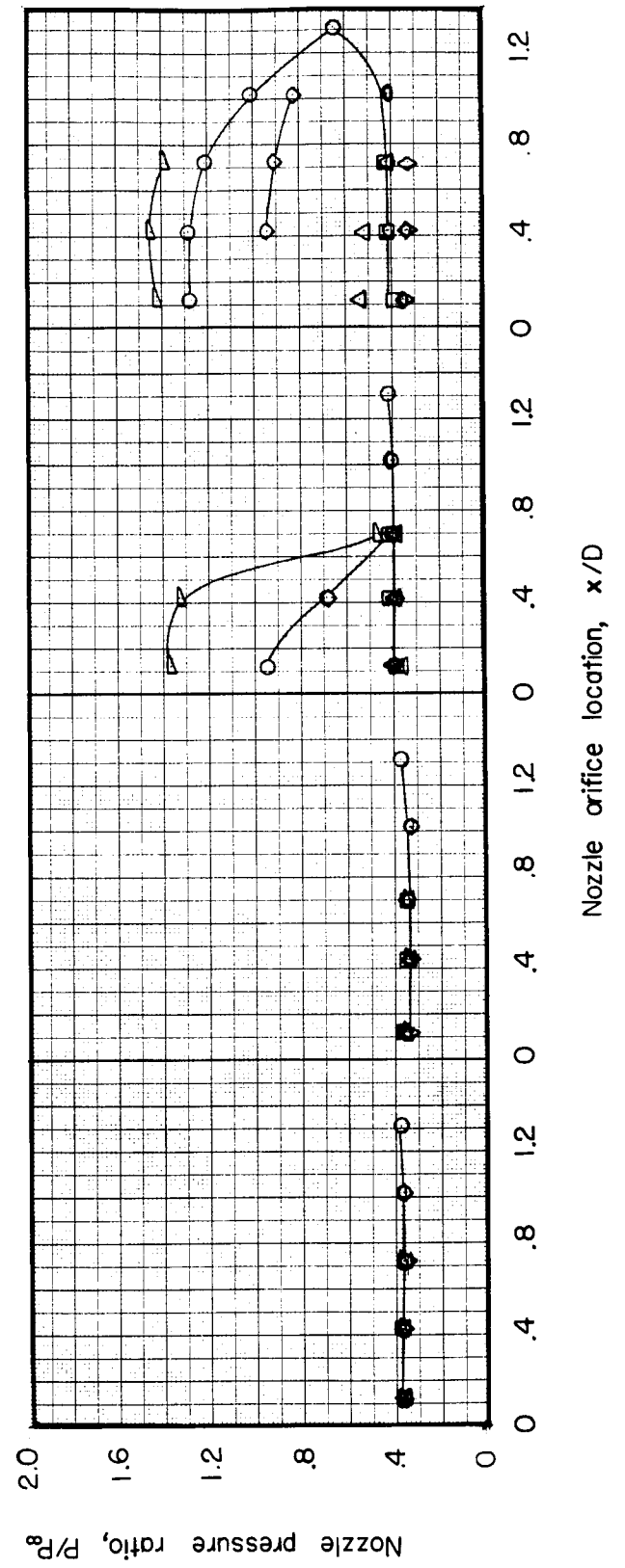
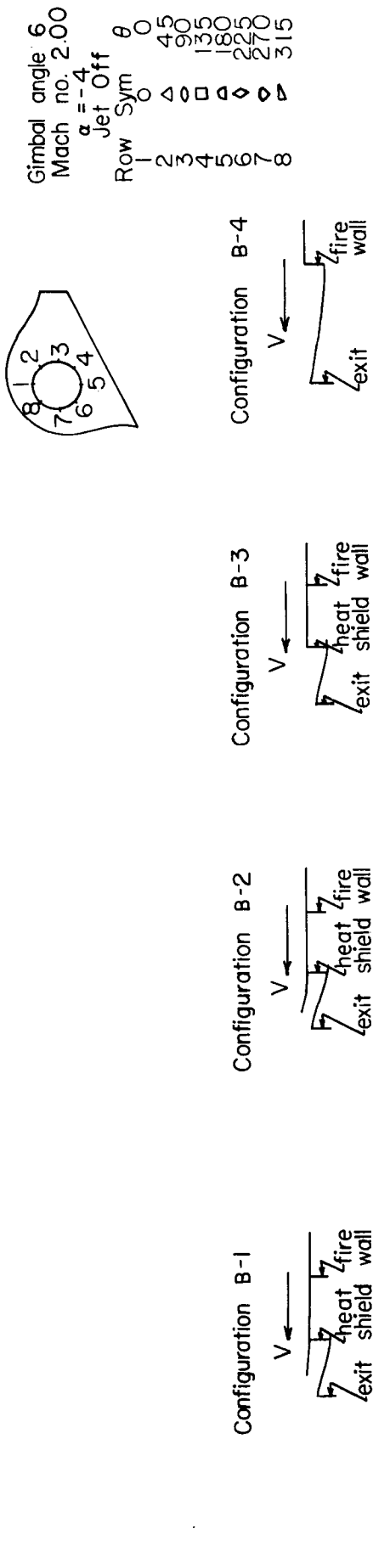


Figure 18c Pressure distribution over the surface of a nozzle with various shroud configurations

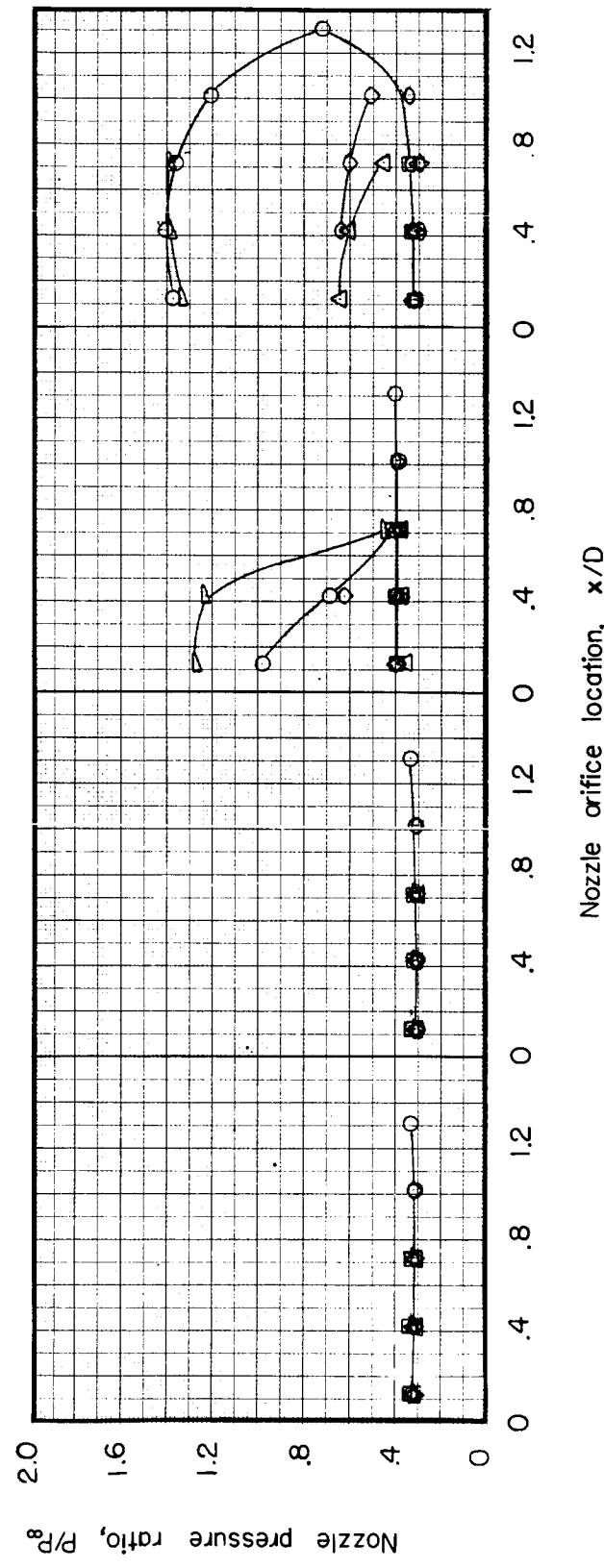
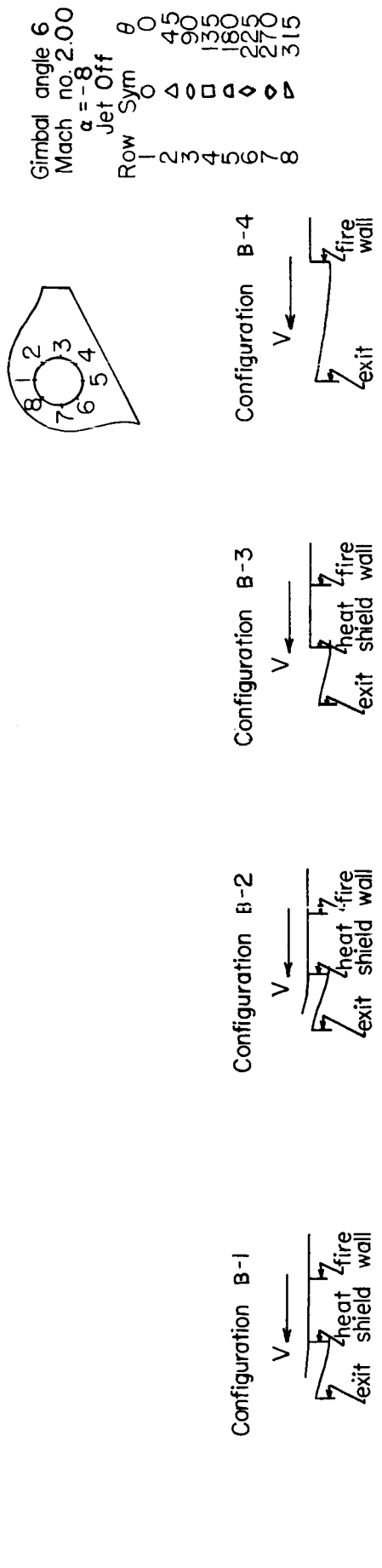


Figure 18d Pressure distribution over the surface of a nozzle with various shroud configurations

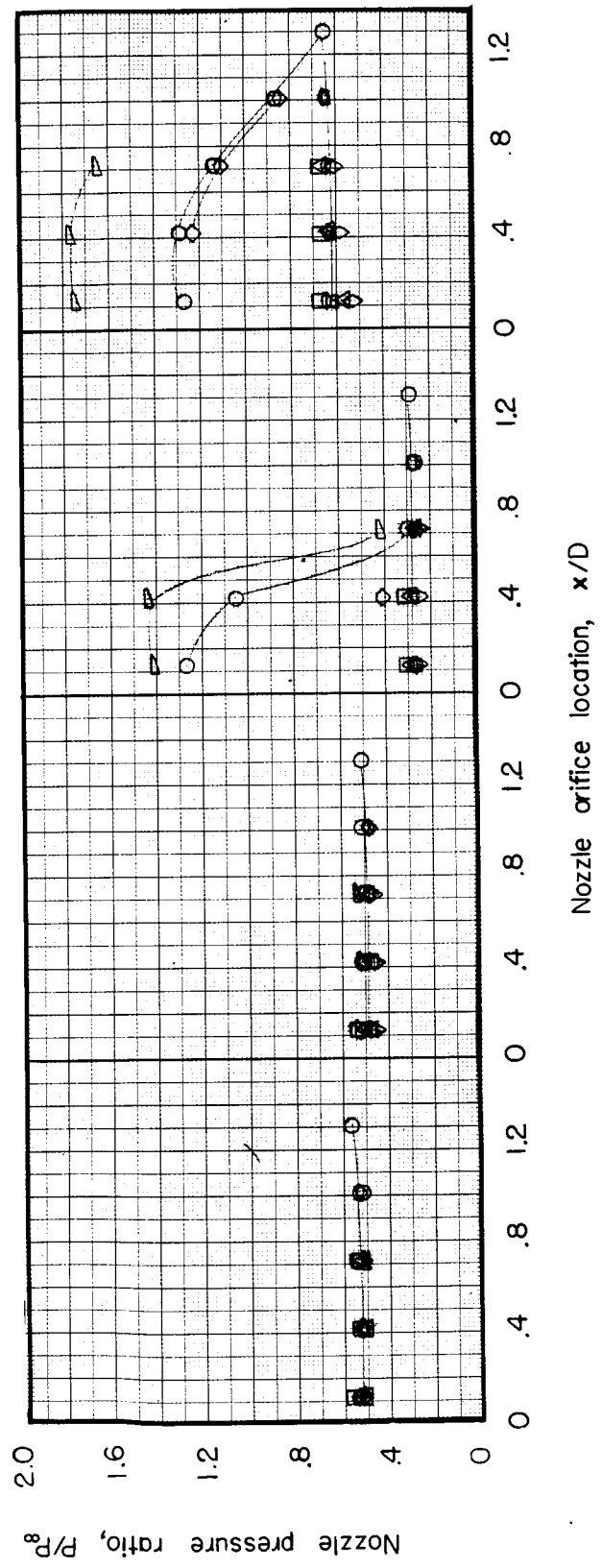
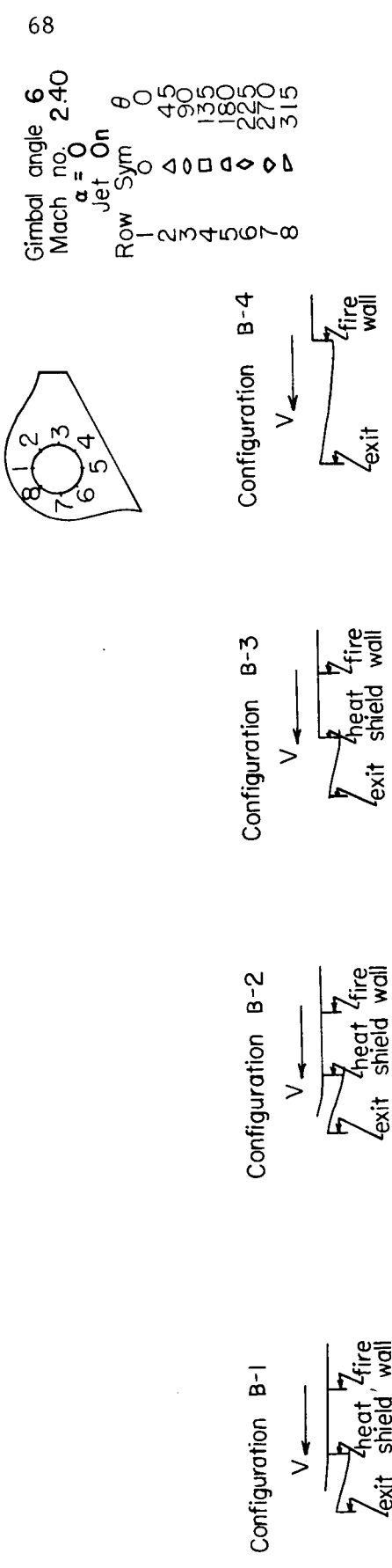


Figure 19a Pressure distribution over the surface of a nozzle with various shroud configurations

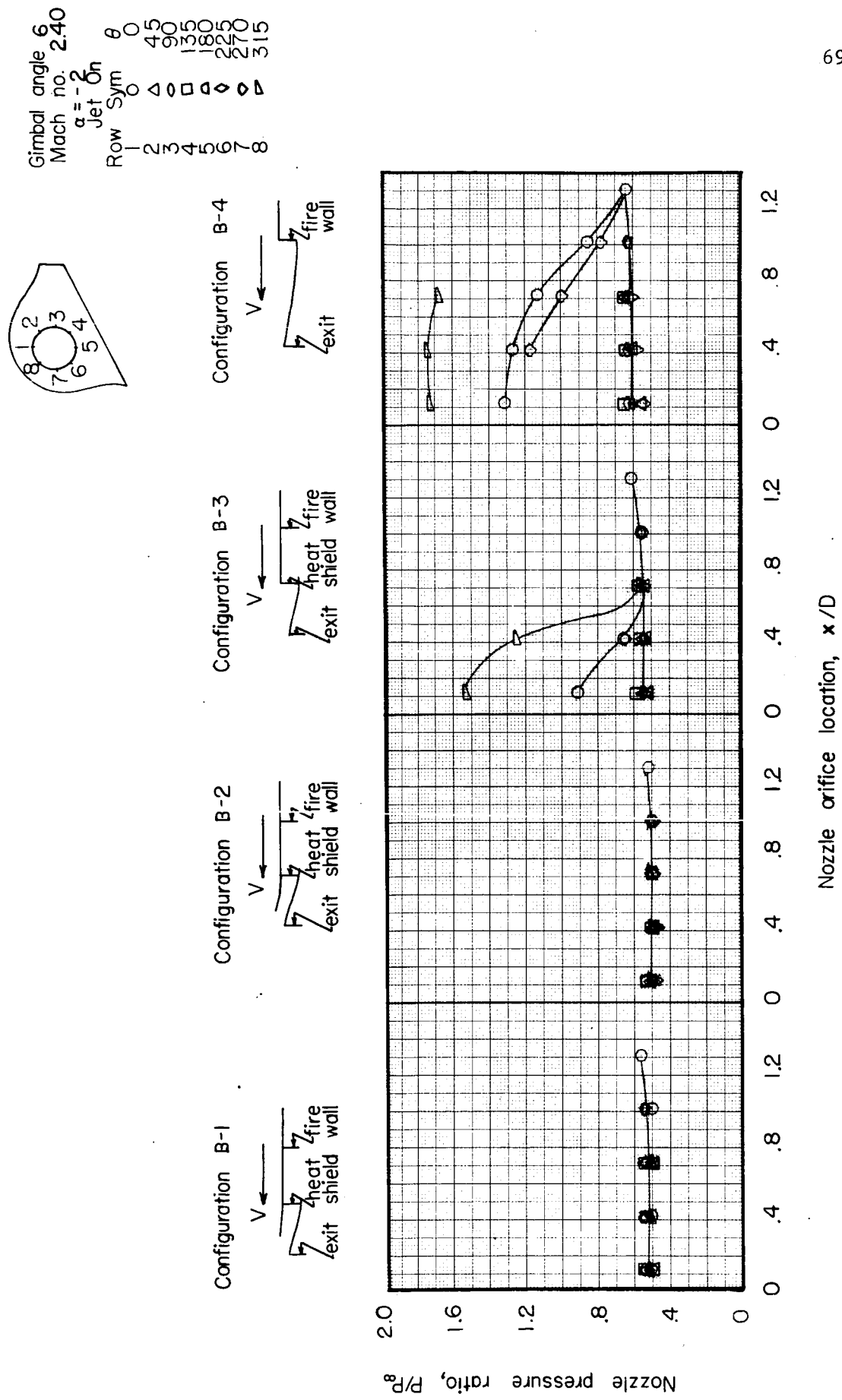


Figure 19b Pressure distribution over the surface of a nozzle with various shroud configurations

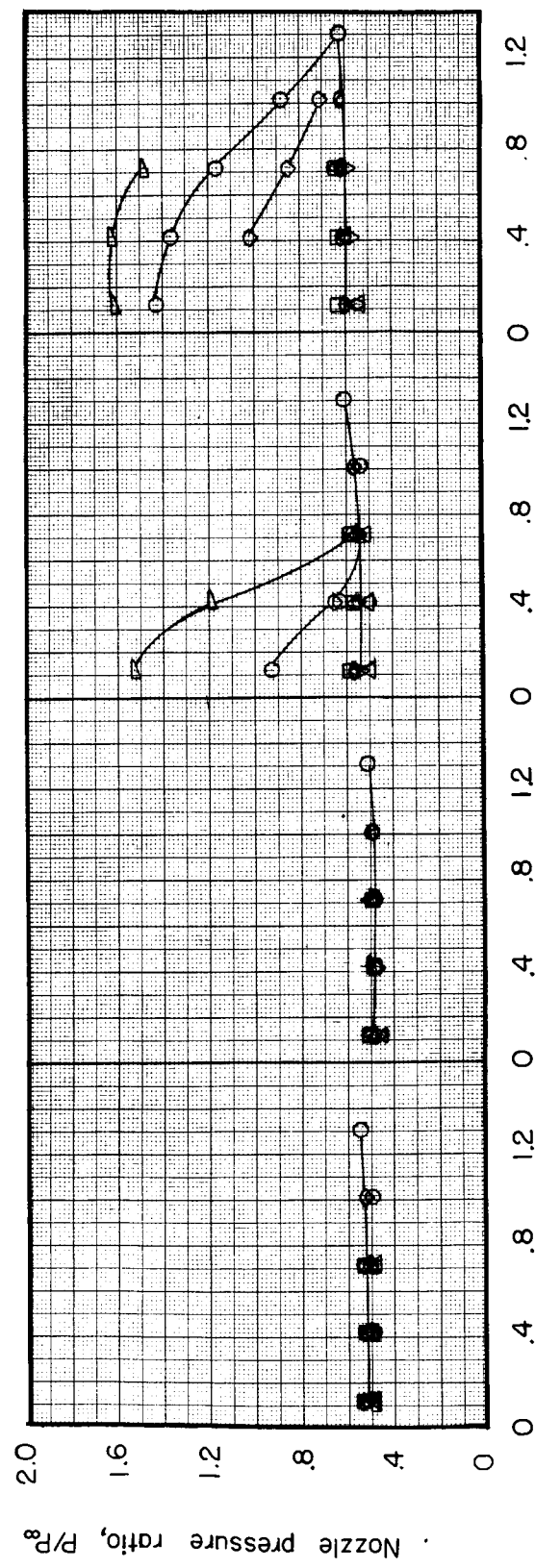
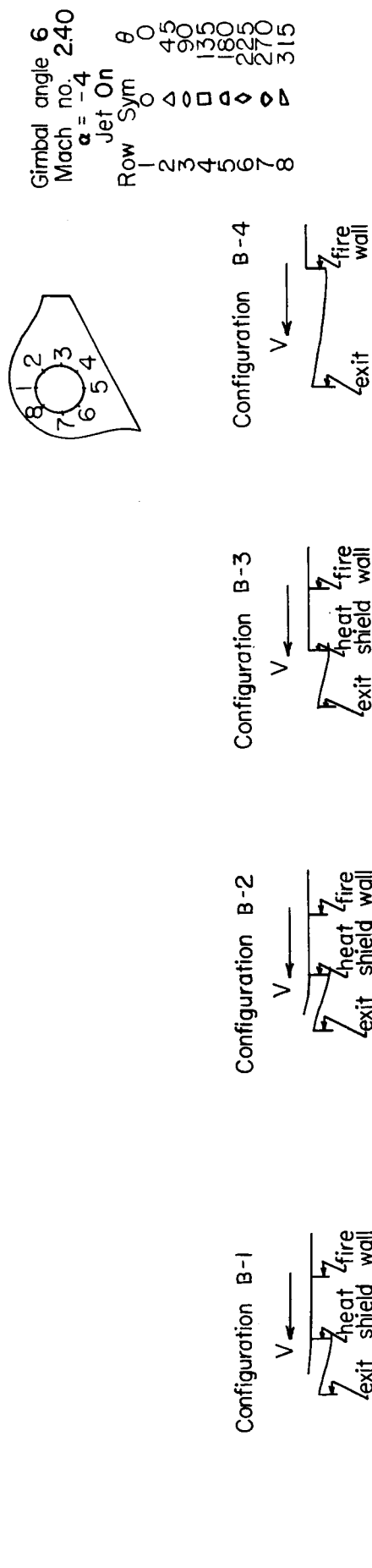


Figure 19c Pressure distribution over the surface of a nozzle with various shroud configurations

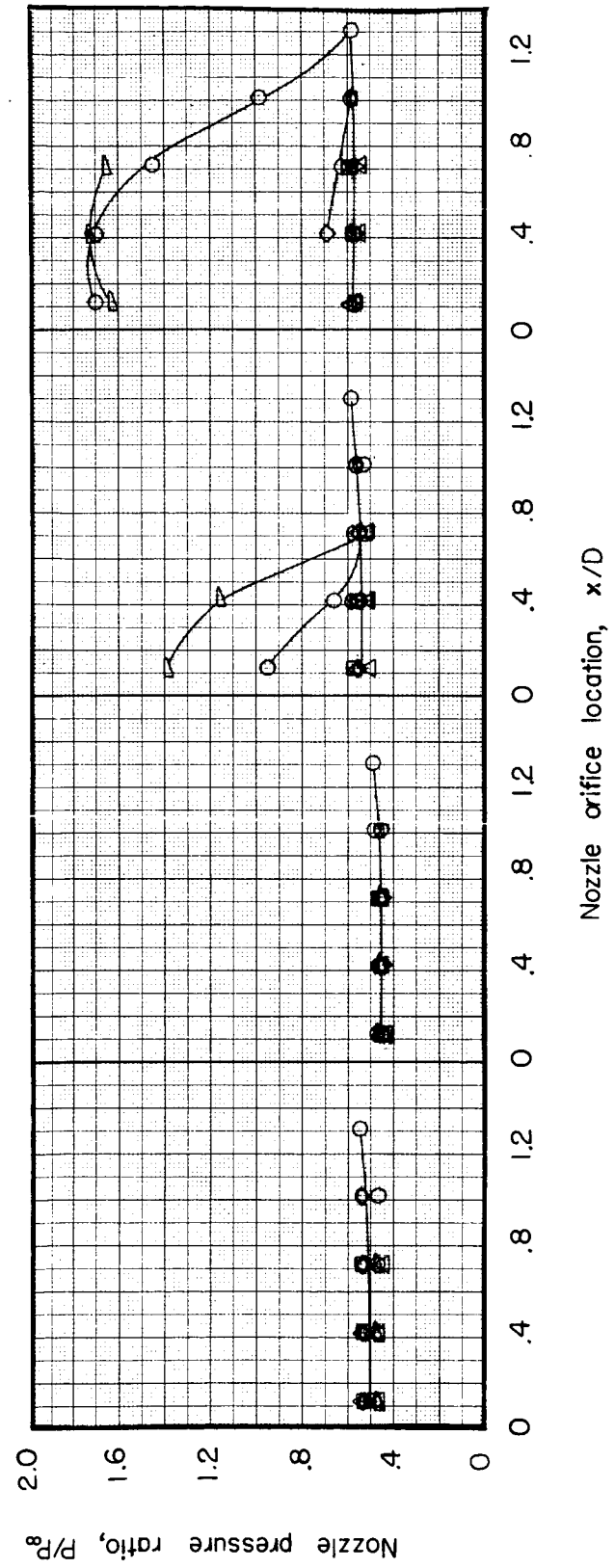
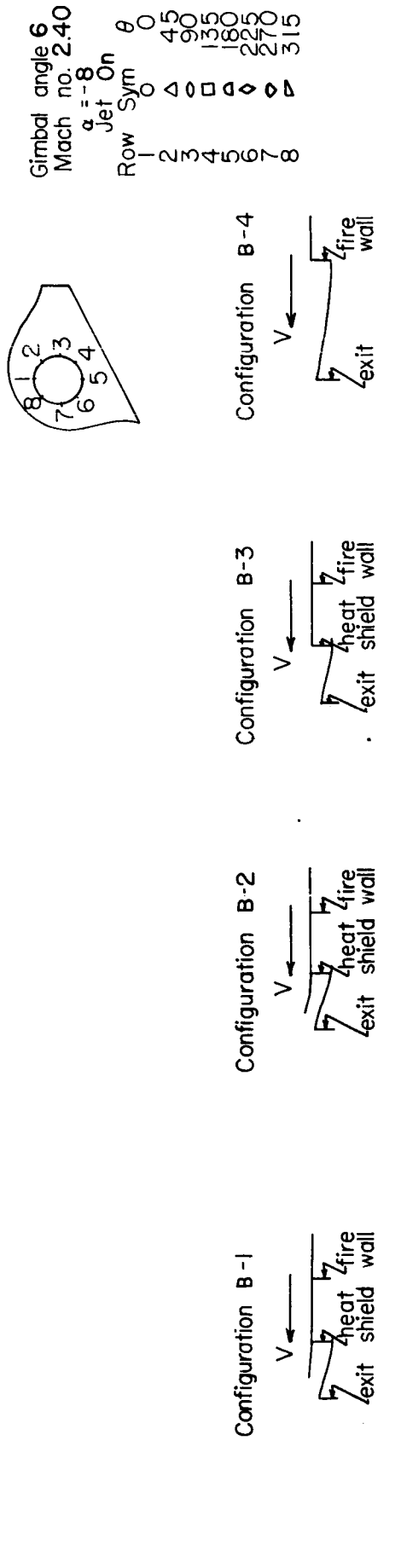


Figure 19d Pressure distribution over the surface of a nozzle with various shroud configurations

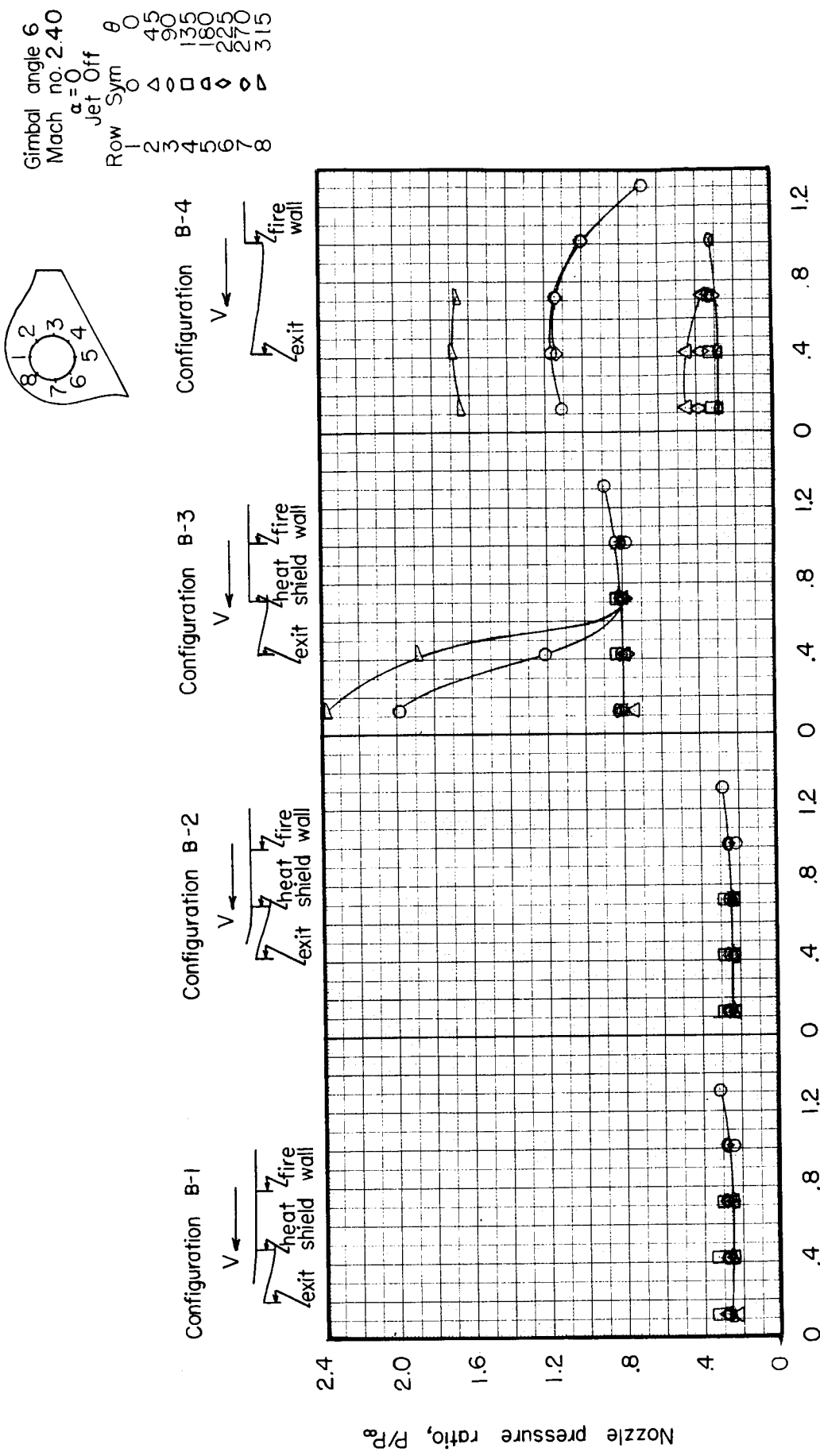


Figure 20a Pressure distribution over the surface of a nozzle with various shroud configurations

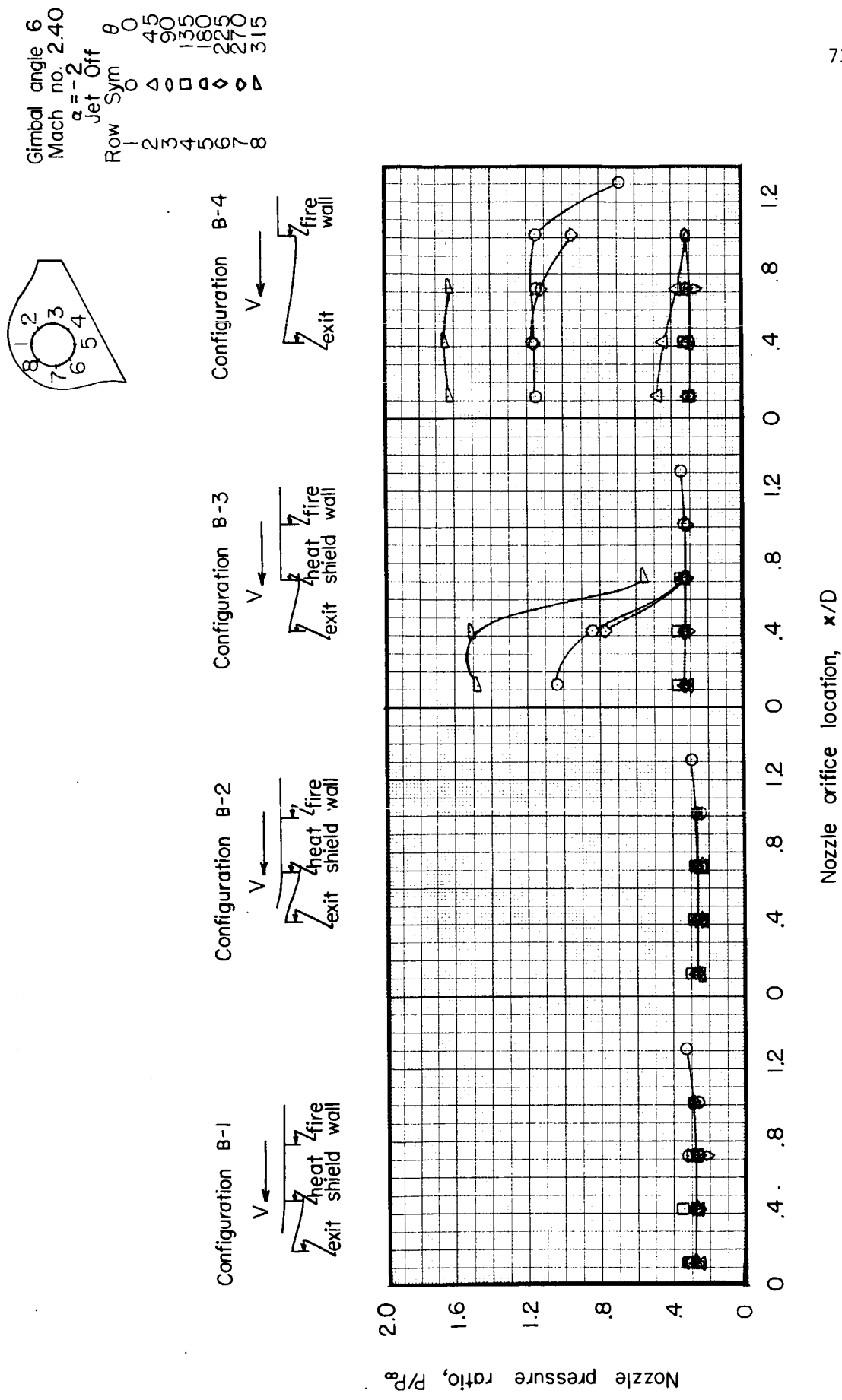


Figure 20b Pressure distribution over the surface of a nozzle with various shroud configurations

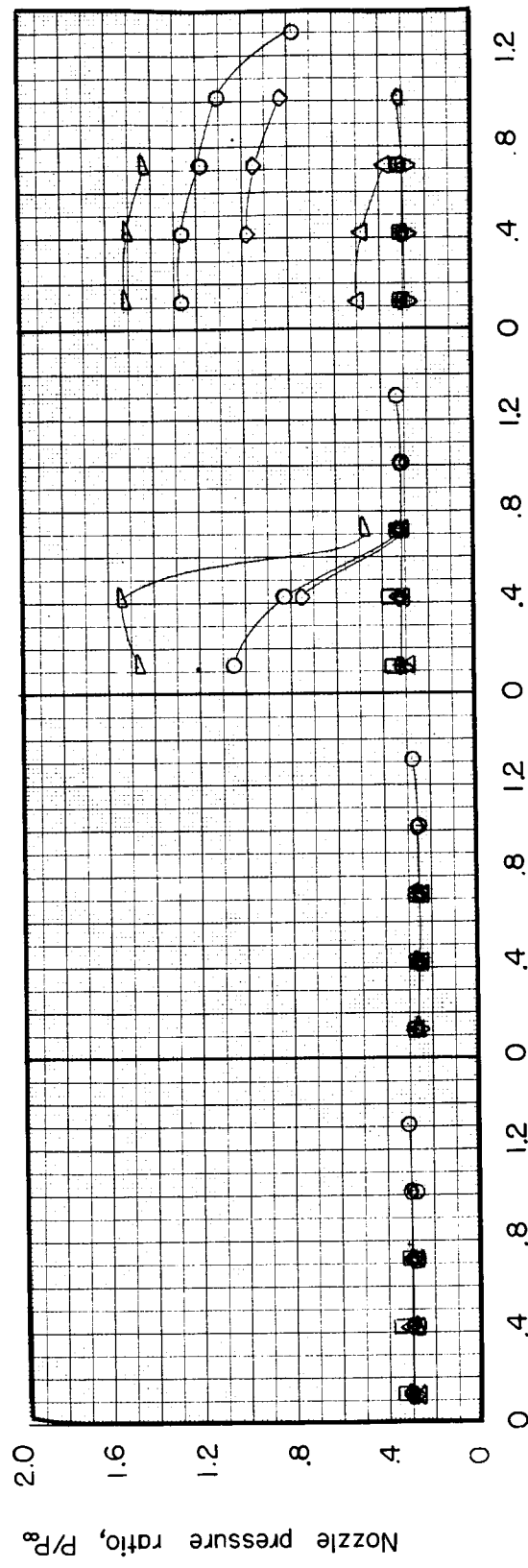
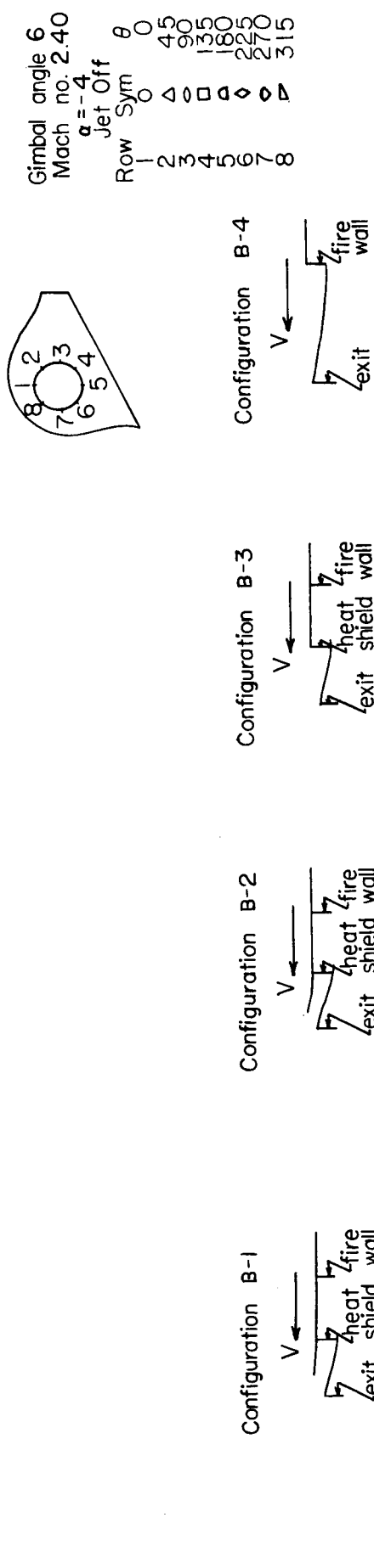


Figure 20c Pressure distribution over the surface of a nozzle with various shroud configurations

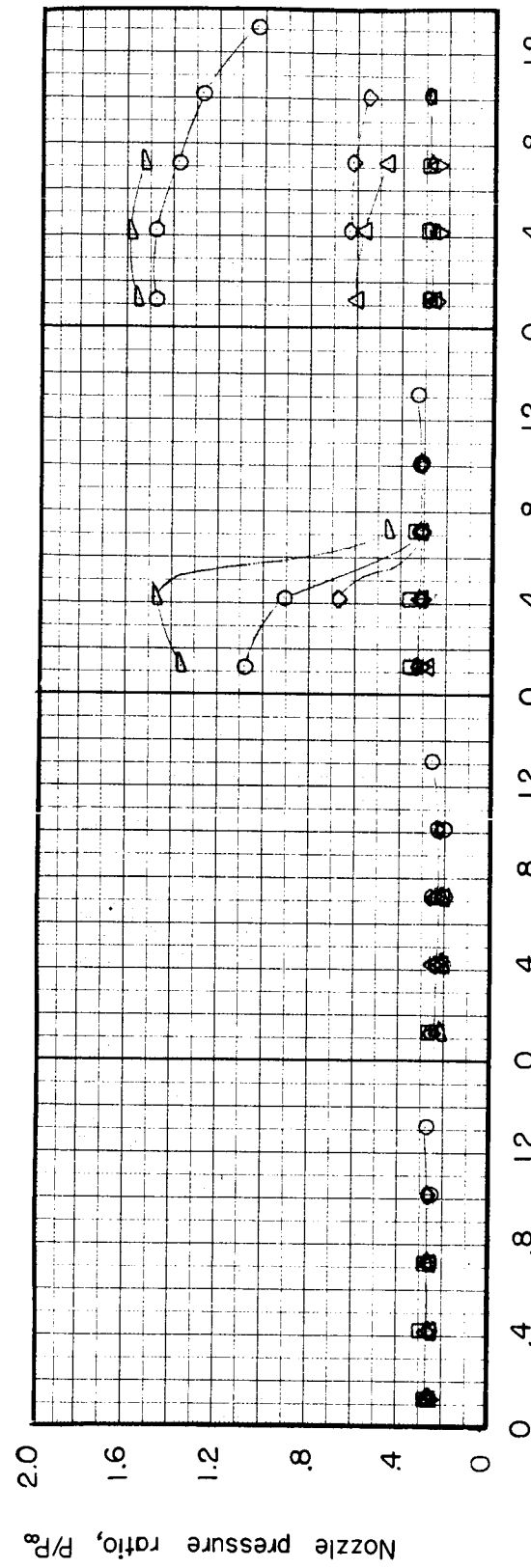
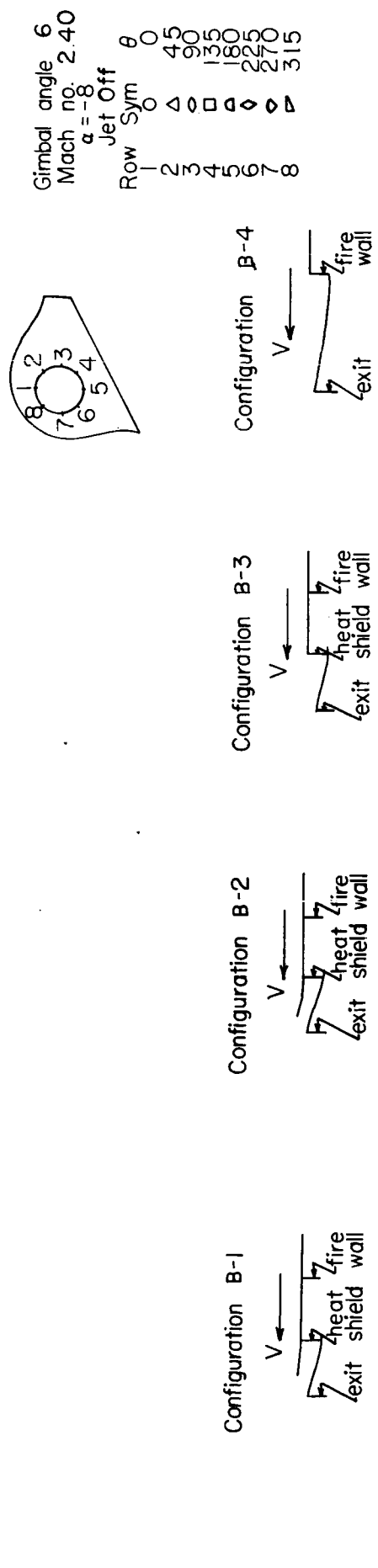


Figure 20d Pressure distribution over the surface of a nozzle with various shroud configurations

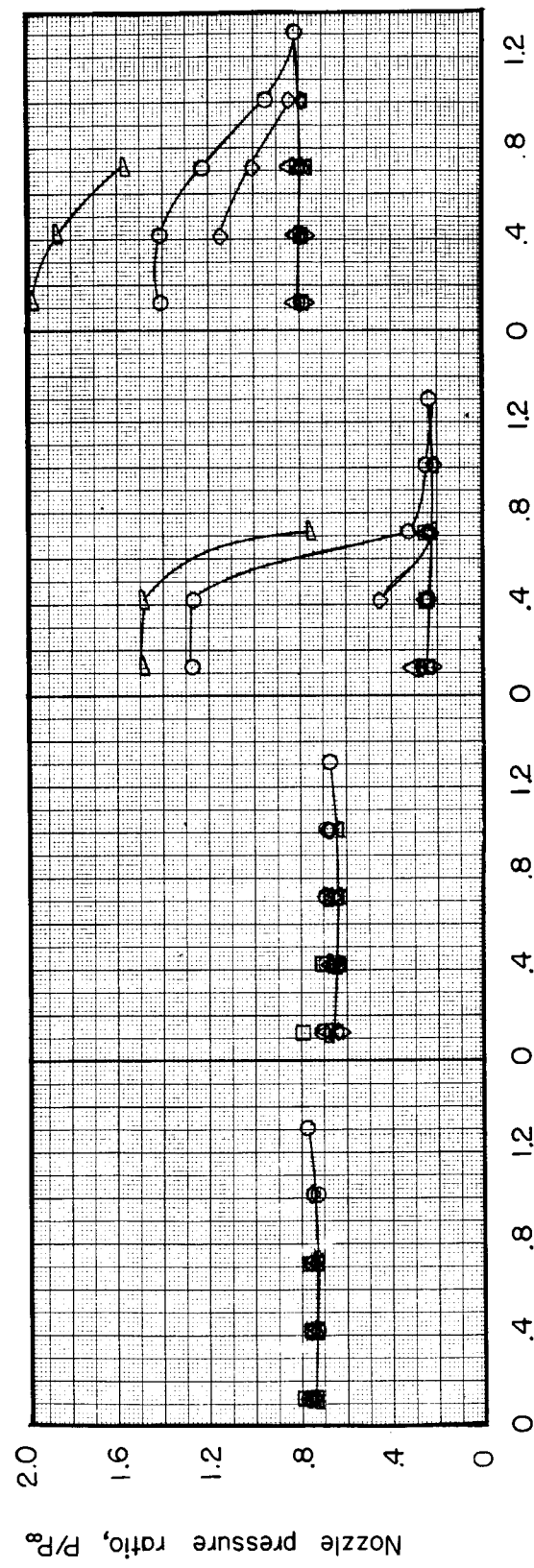
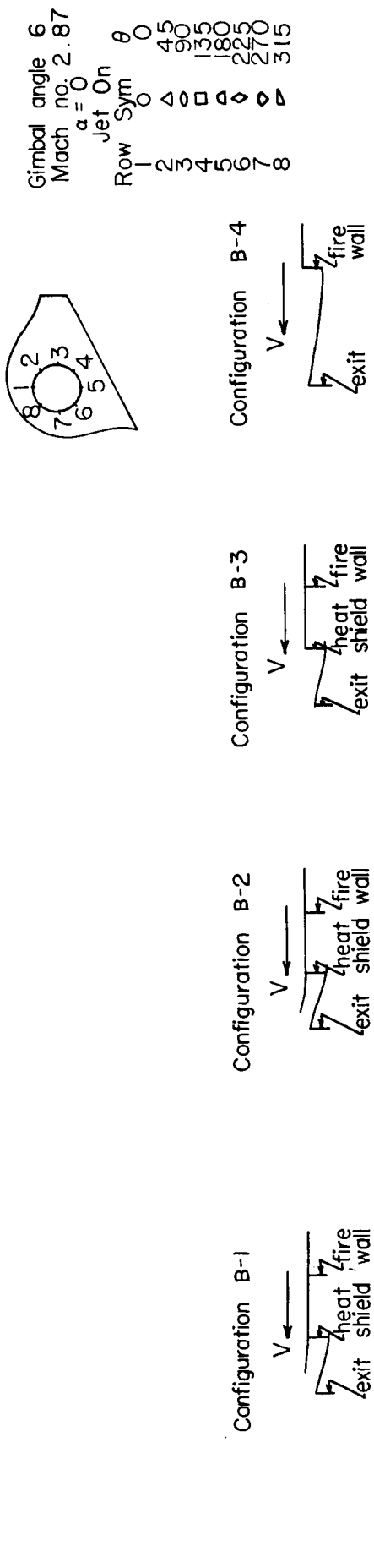


Figure 21a Pressure distribution over the surface of a nozzle with various shroud configurations

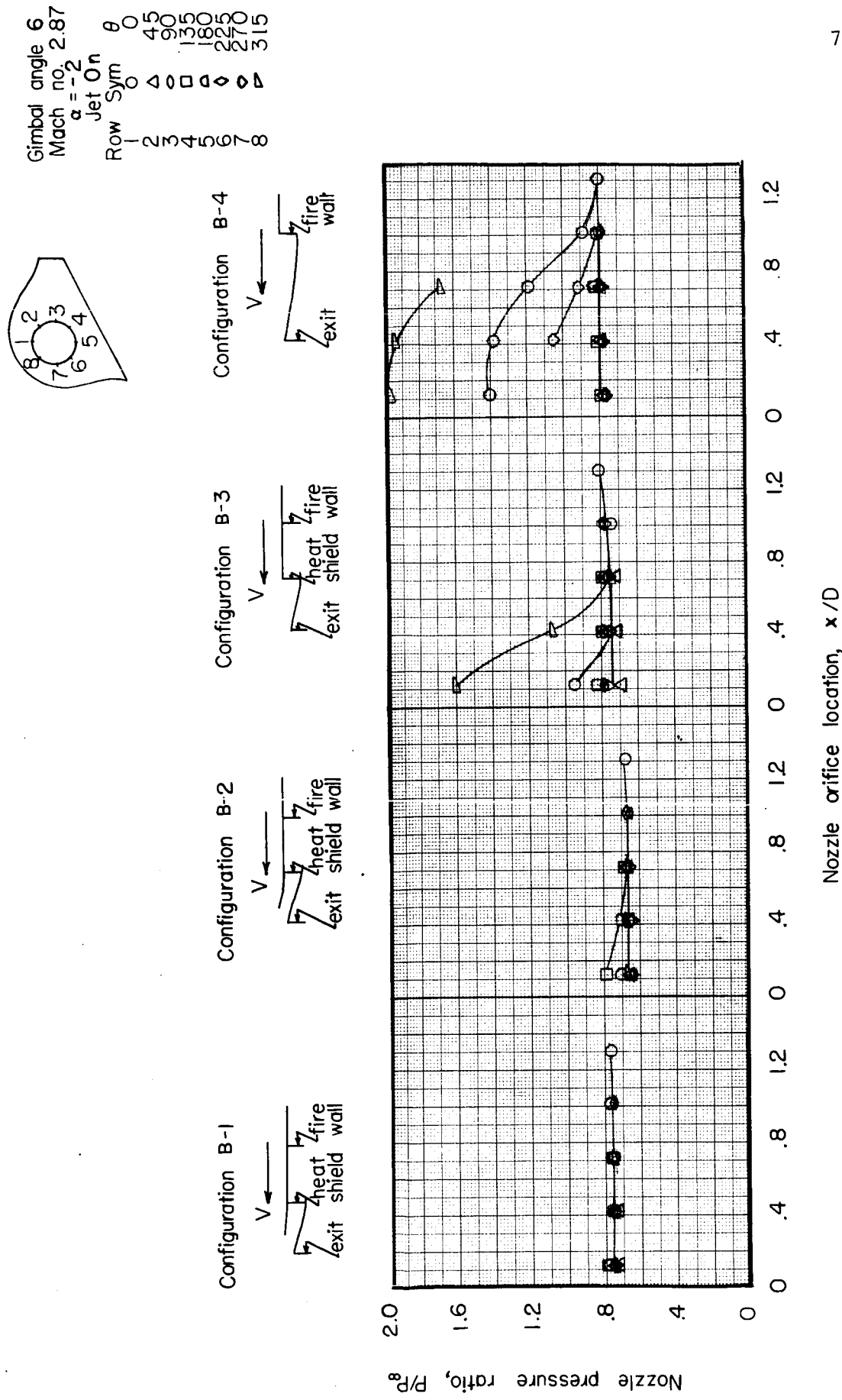


Figure 21b Pressure distribution over the surface of a nozzle with various shroud configurations

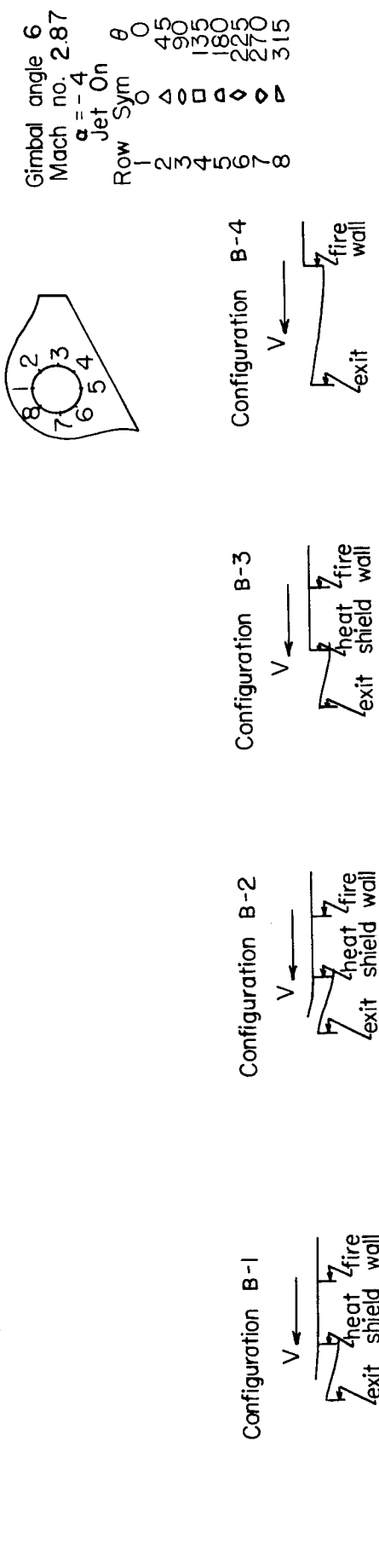


Figure 21c Pressure distribution over the surface of a nozzle with various shroud configurations

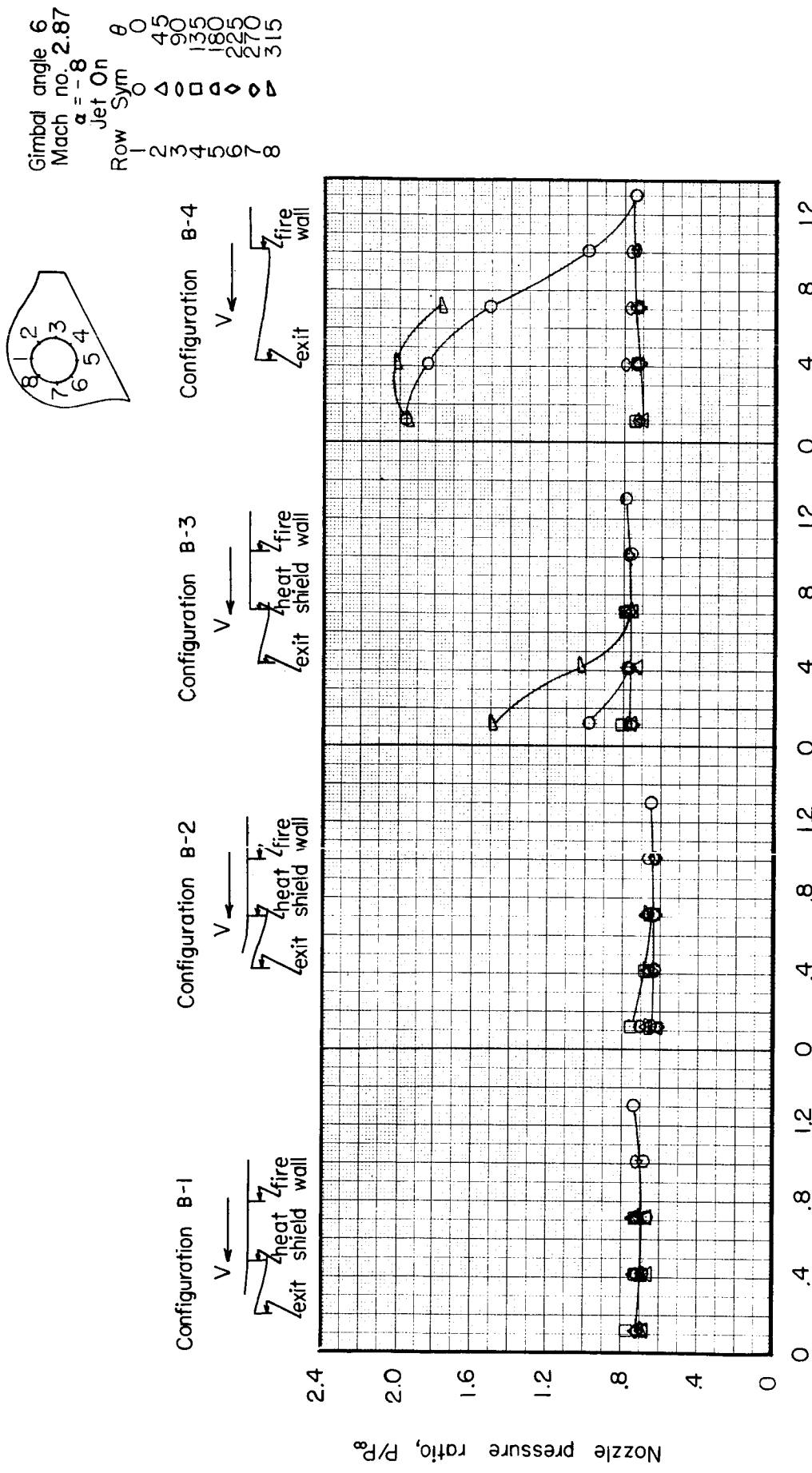


Figure 21d Pressure distribution over the surface of a nozzle with various shroud configurations

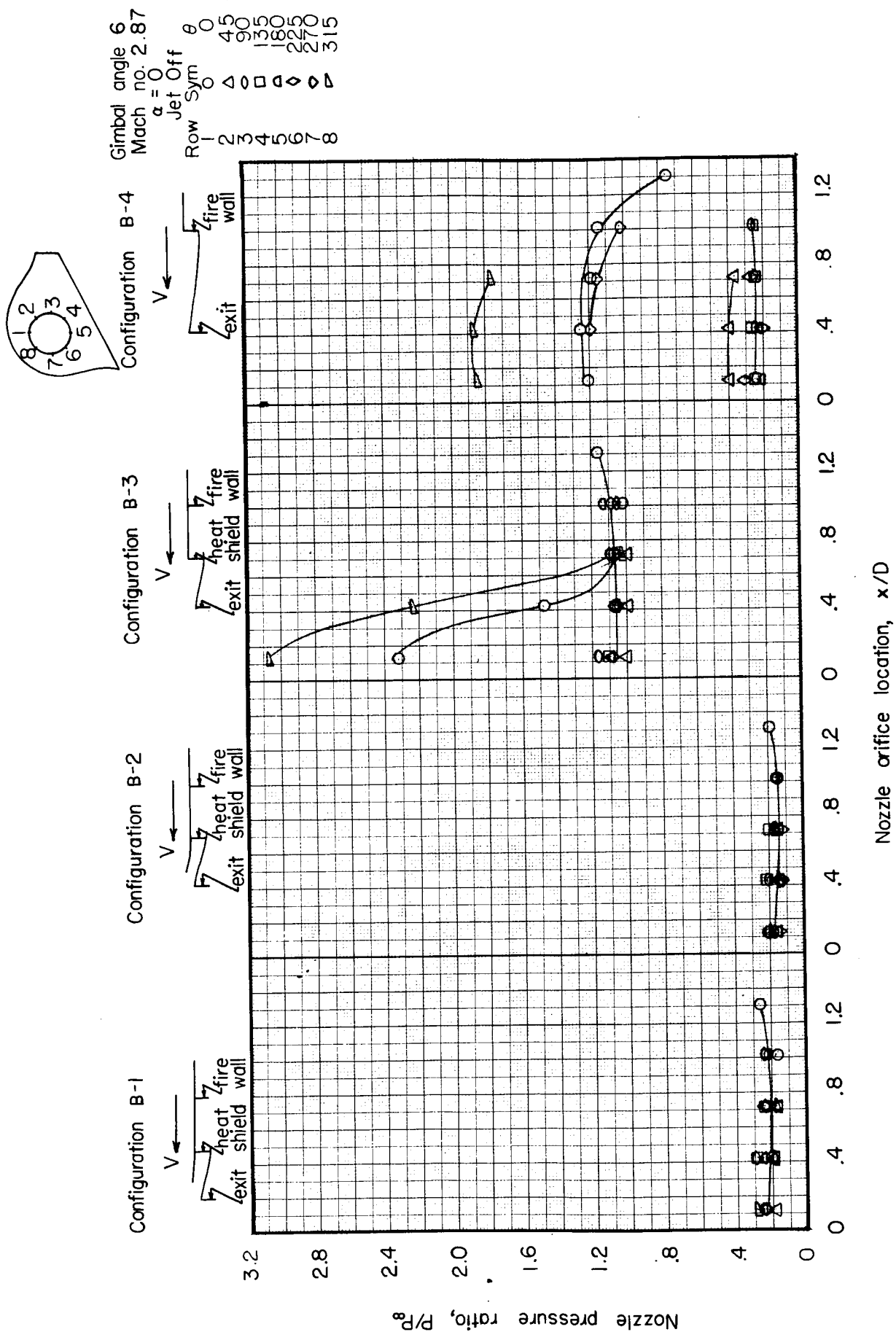


Figure 22a Pressure distribution over the surface of a nozzle with various shroud configurations

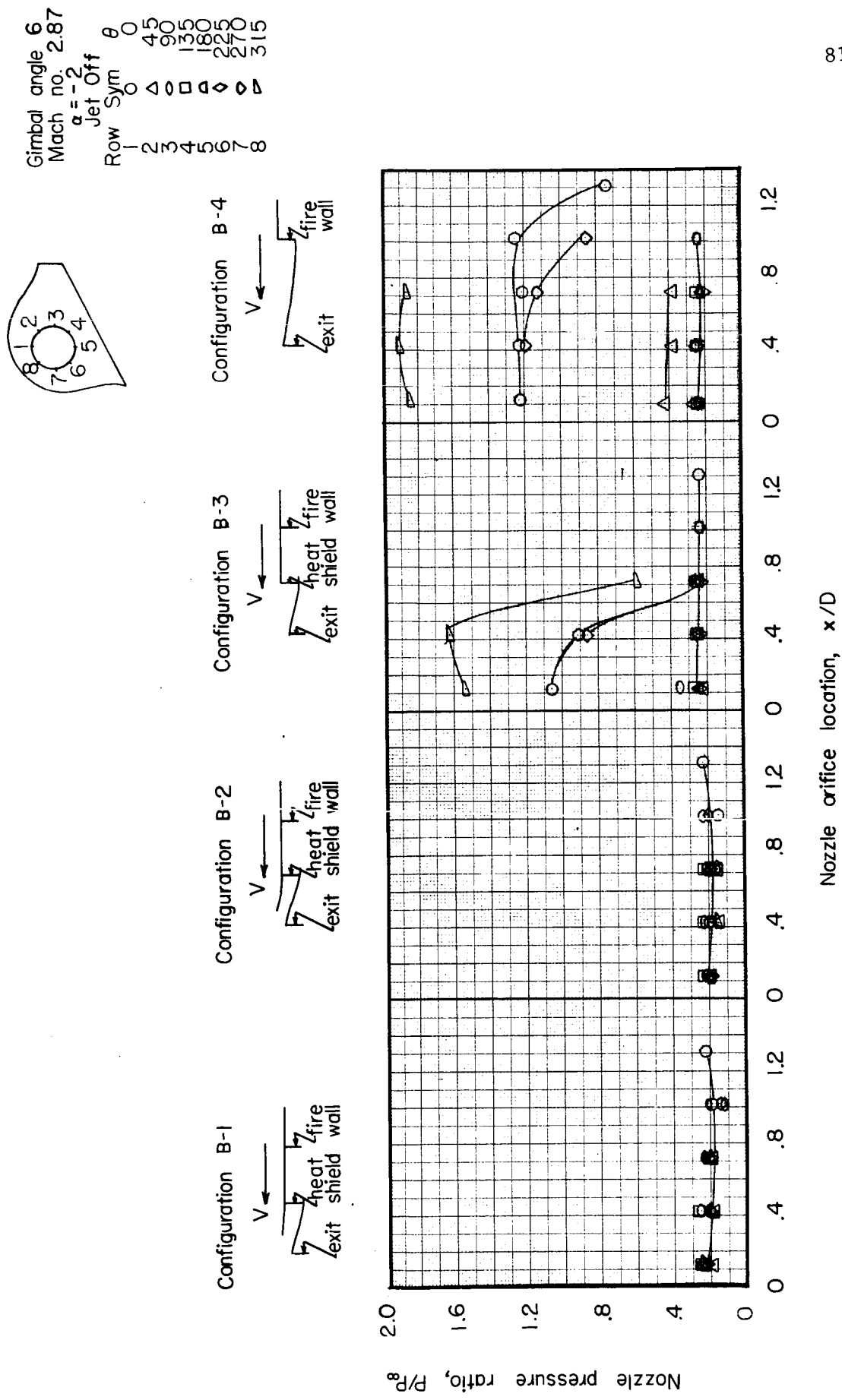


Figure 22b Pressure distribution over the surface of a nozzle with various shroud configurations

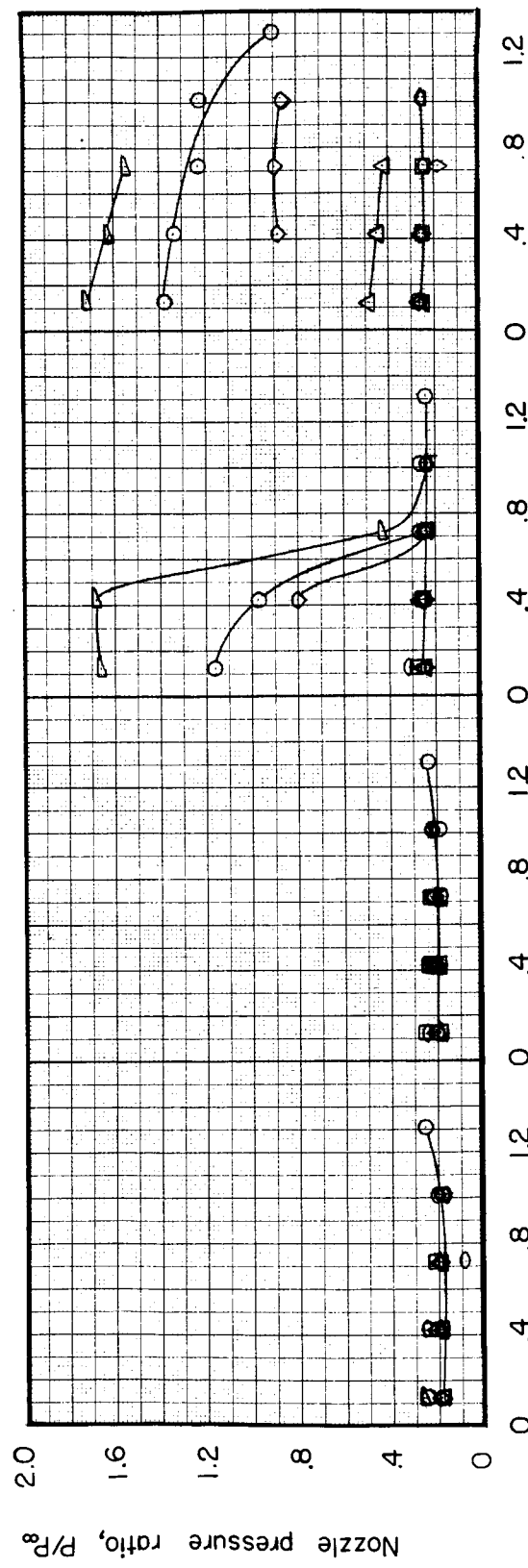
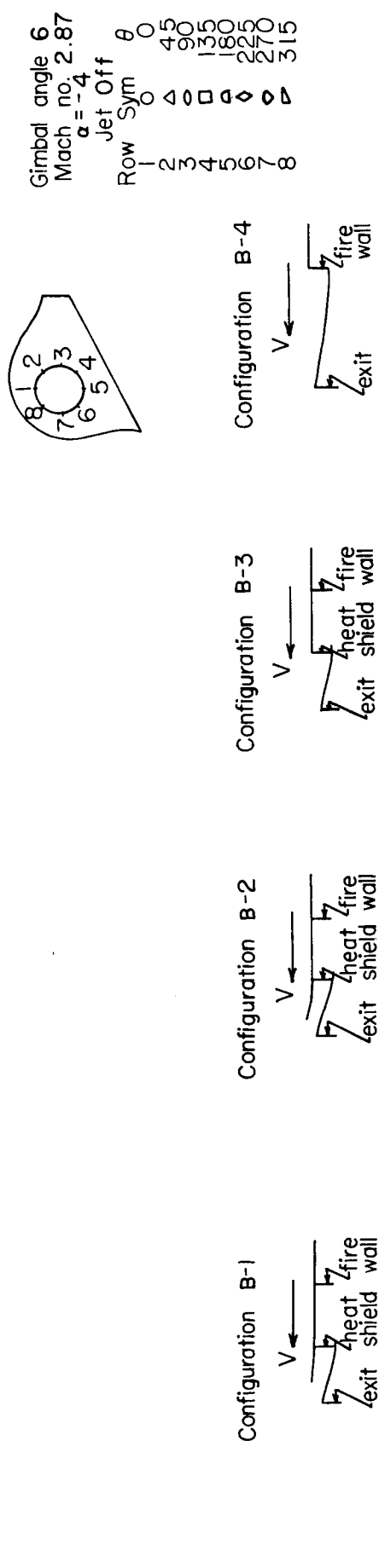


Figure 22c Pressure distribution over the surface of a nozzle with various shroud configurations

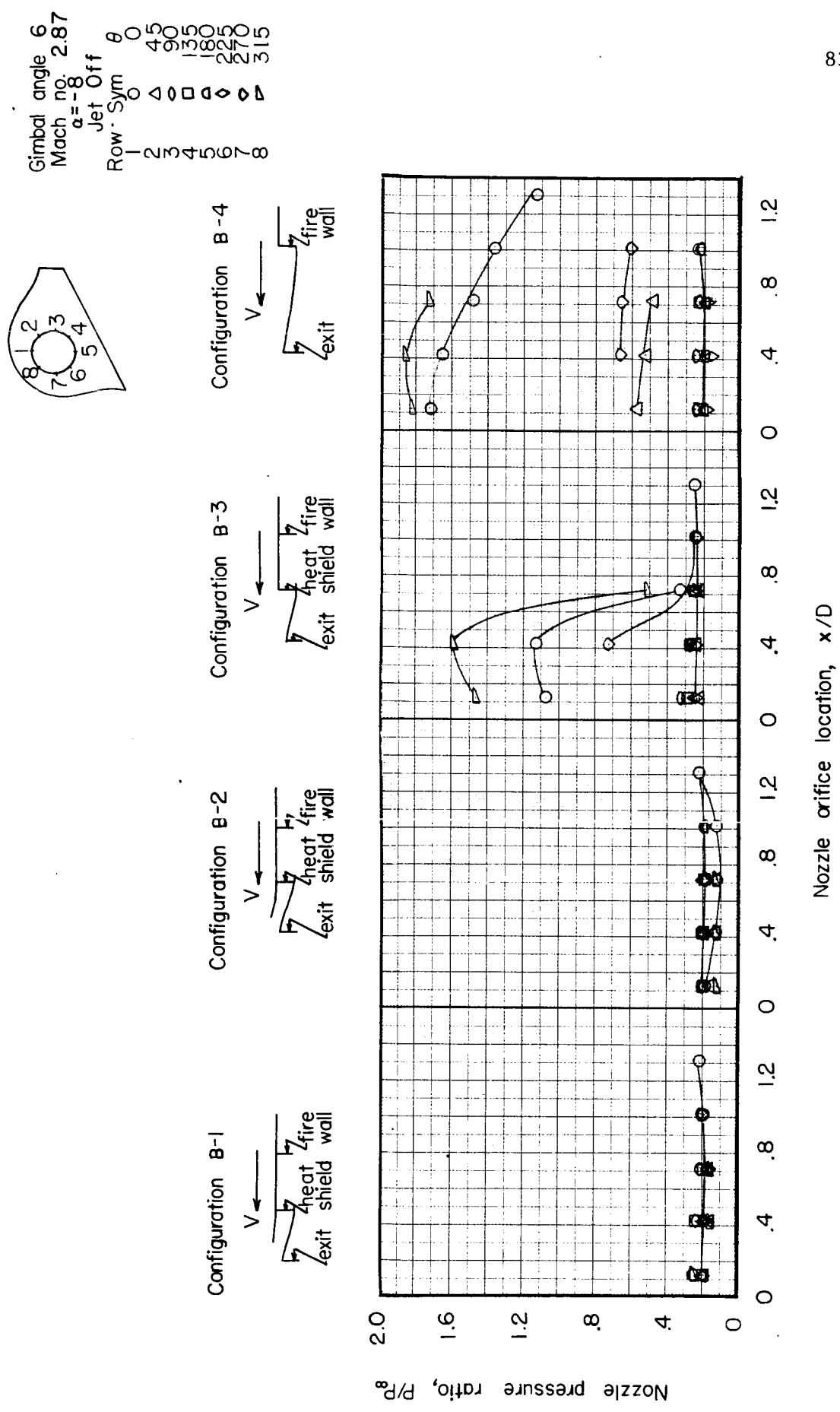


Figure 22d Pressure distribution over the surface of a nozzle with various shroud configurations

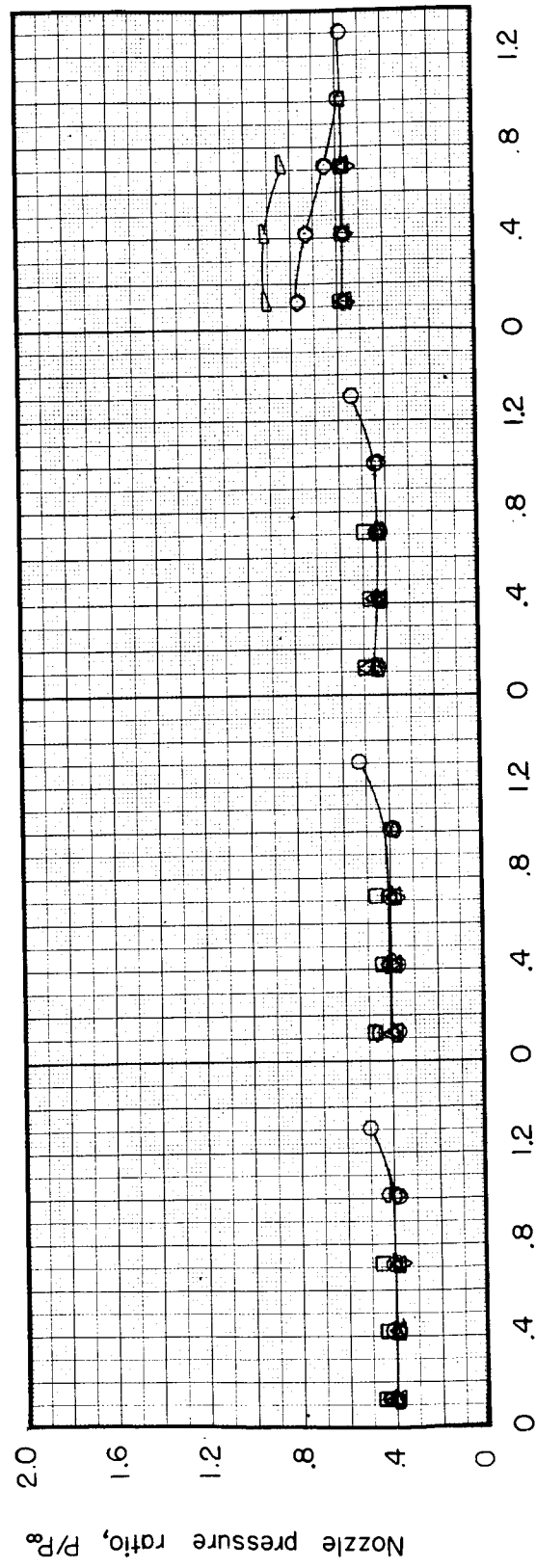
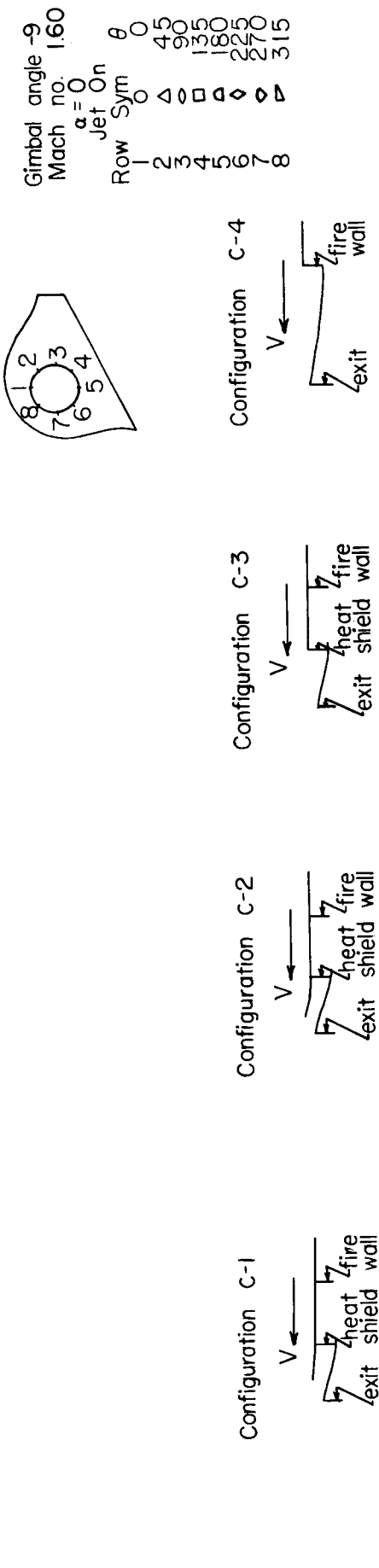


Figure 23a Pressure distribution over the surface of a nozzle with various shroud configurations

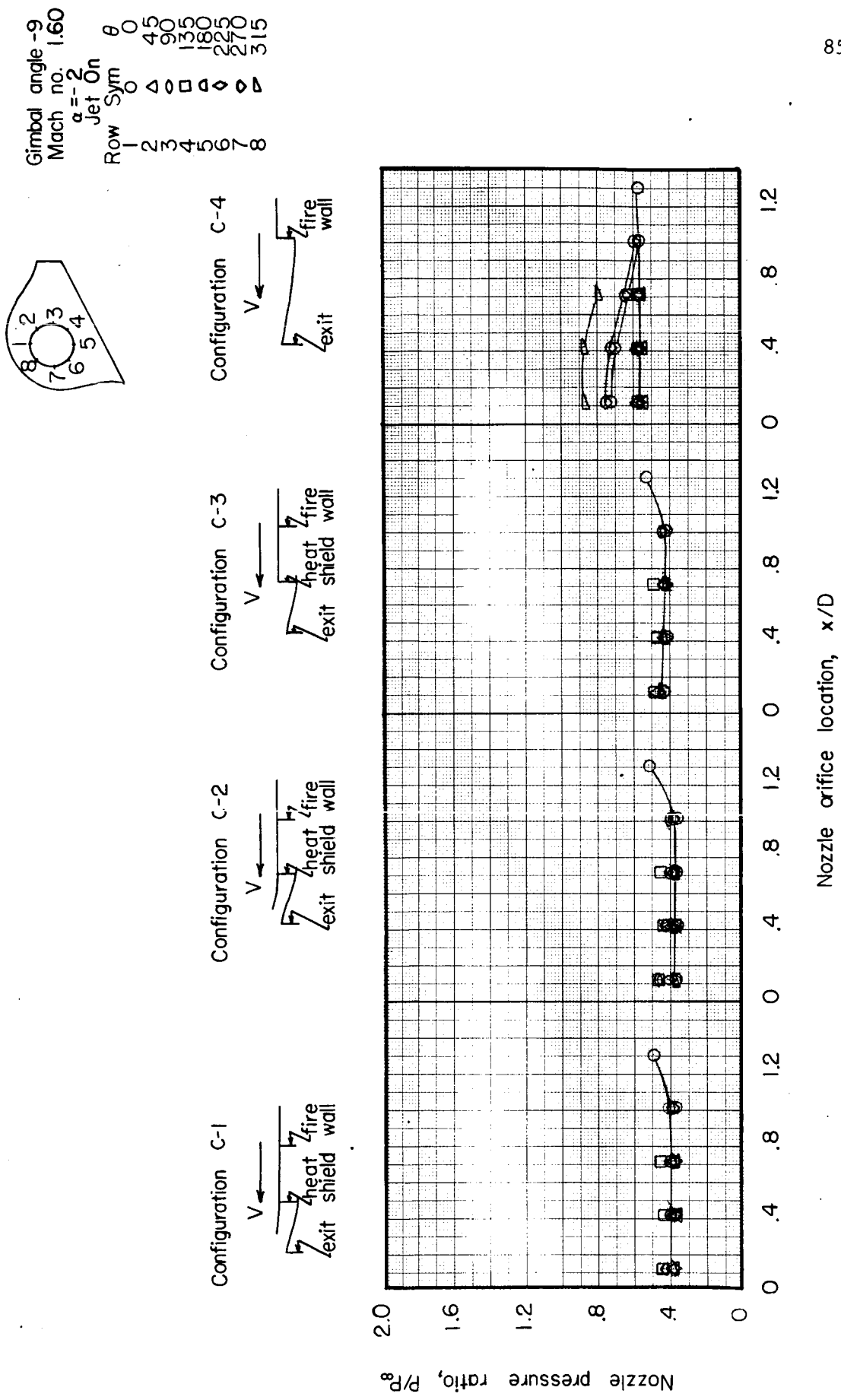


Figure 23b Pressure distribution over the surface of a nozzle with various shroud configurations

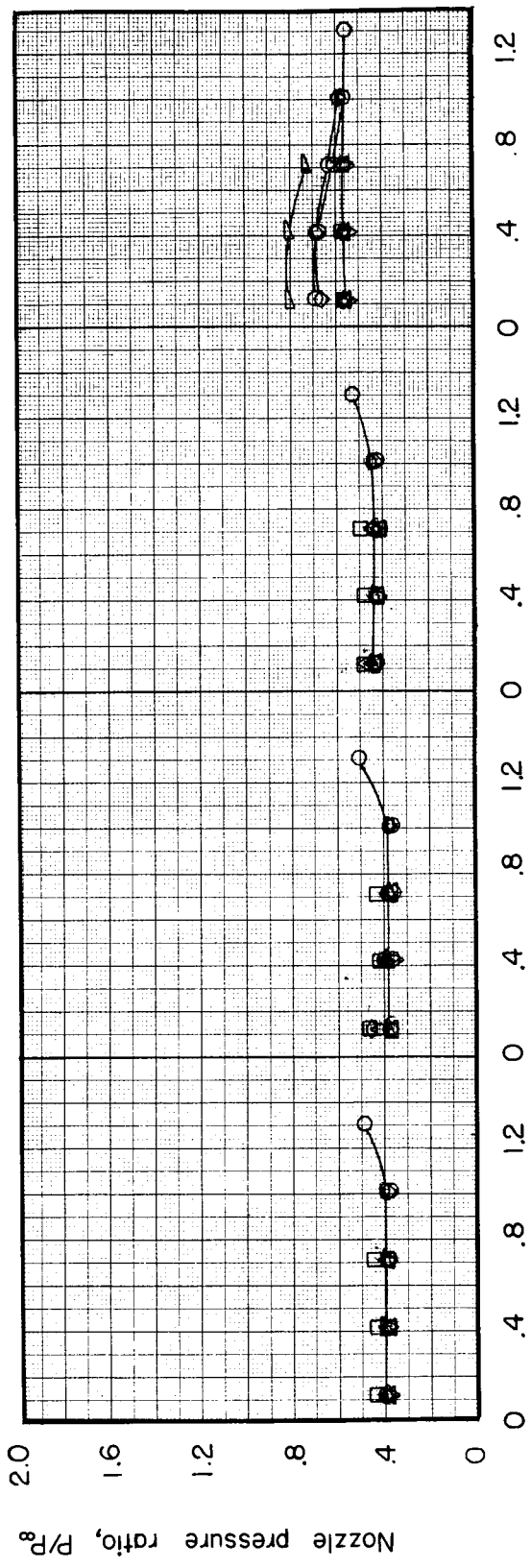
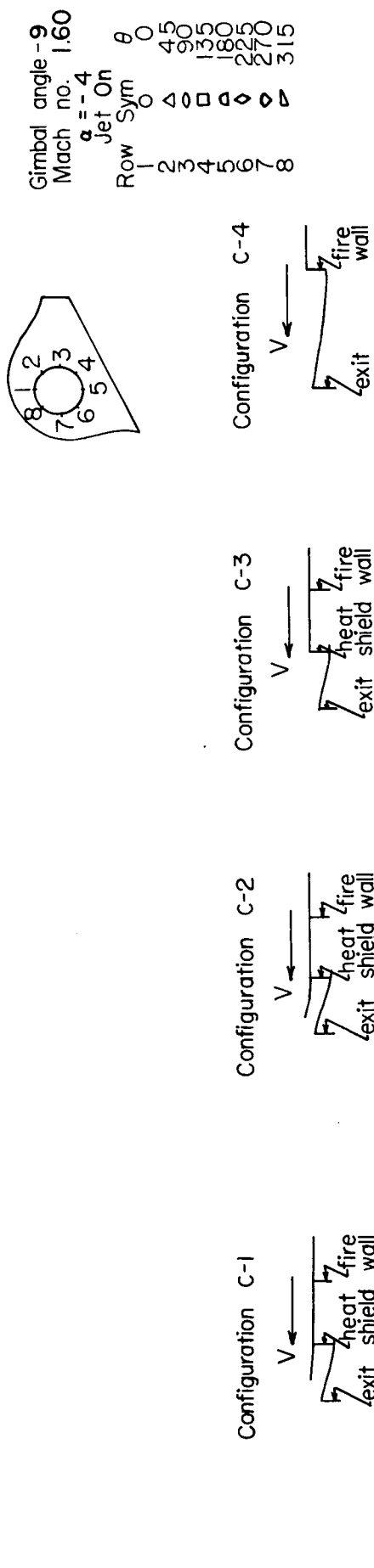


Figure 23c Pressure distribution over the surface of a nozzle with various shroud configurations

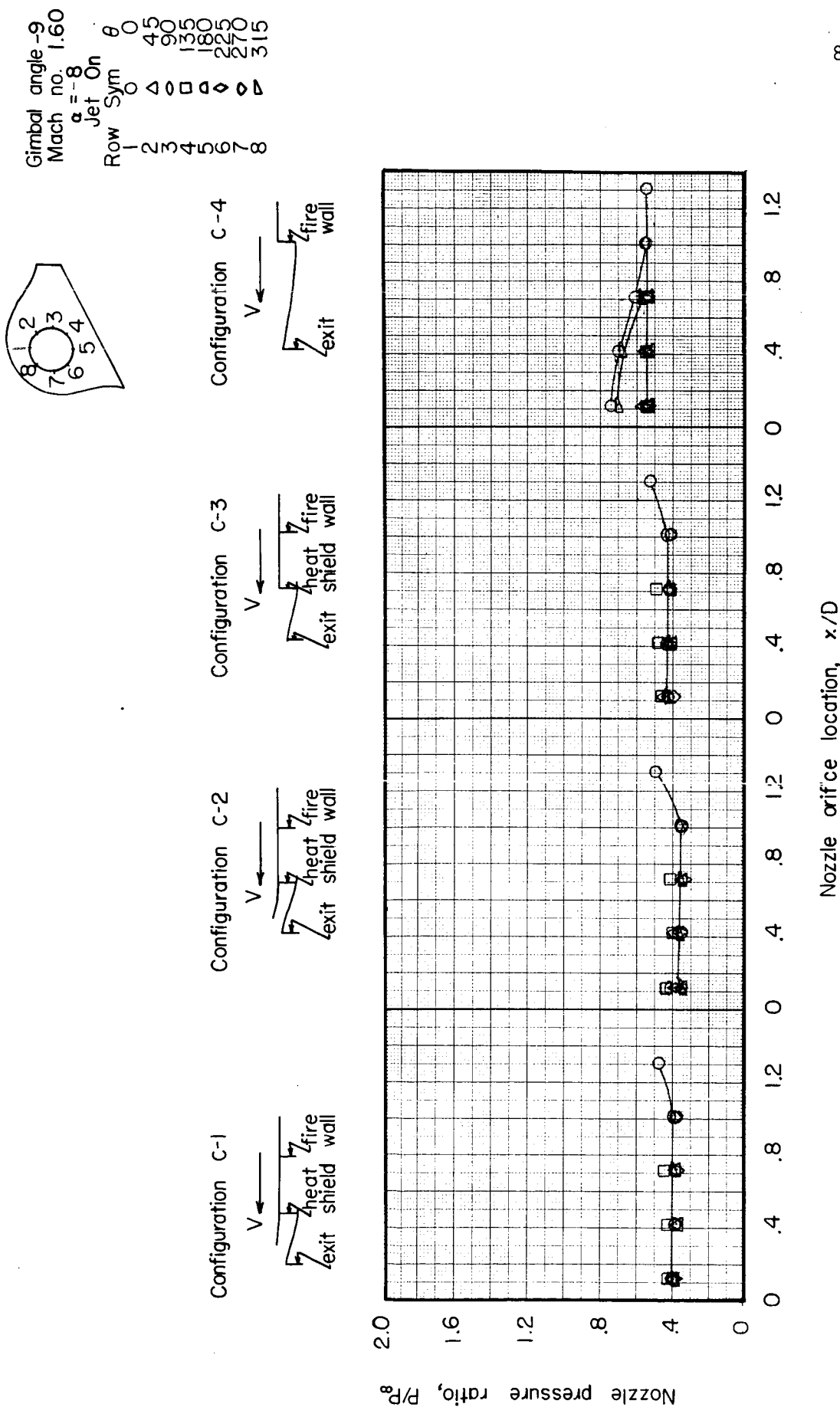


Figure 23d Pressure distribution over the surface of a nozzle with various shroud configurations

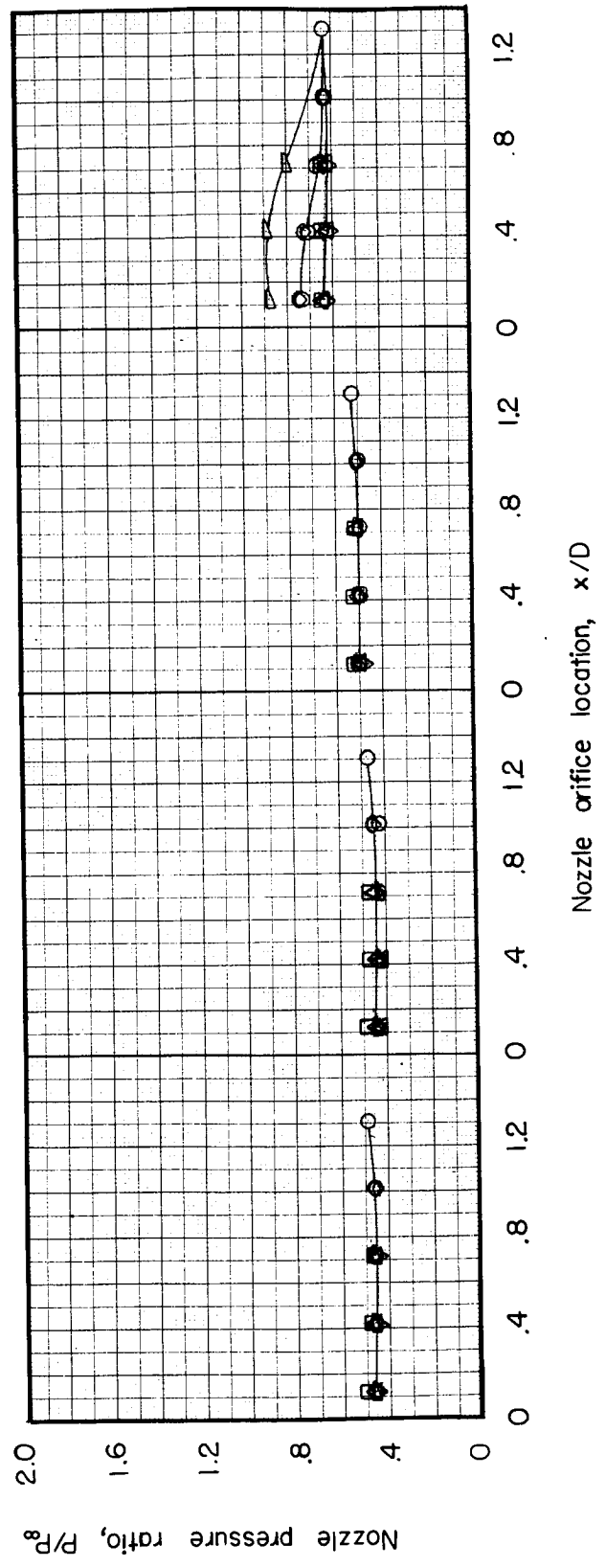
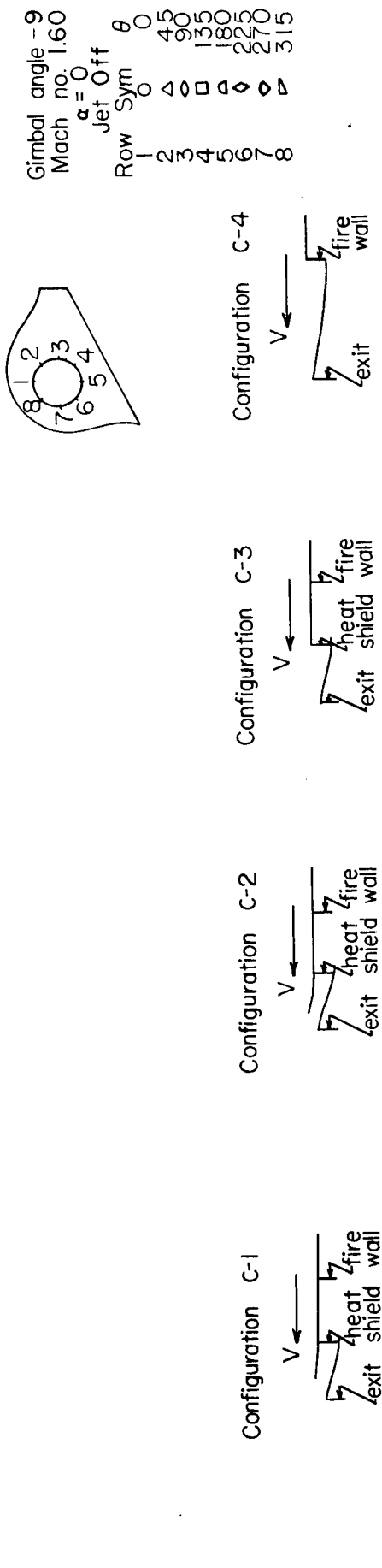


Figure 24a Pressure distribution over the surface of a nozzle with various shroud configurations

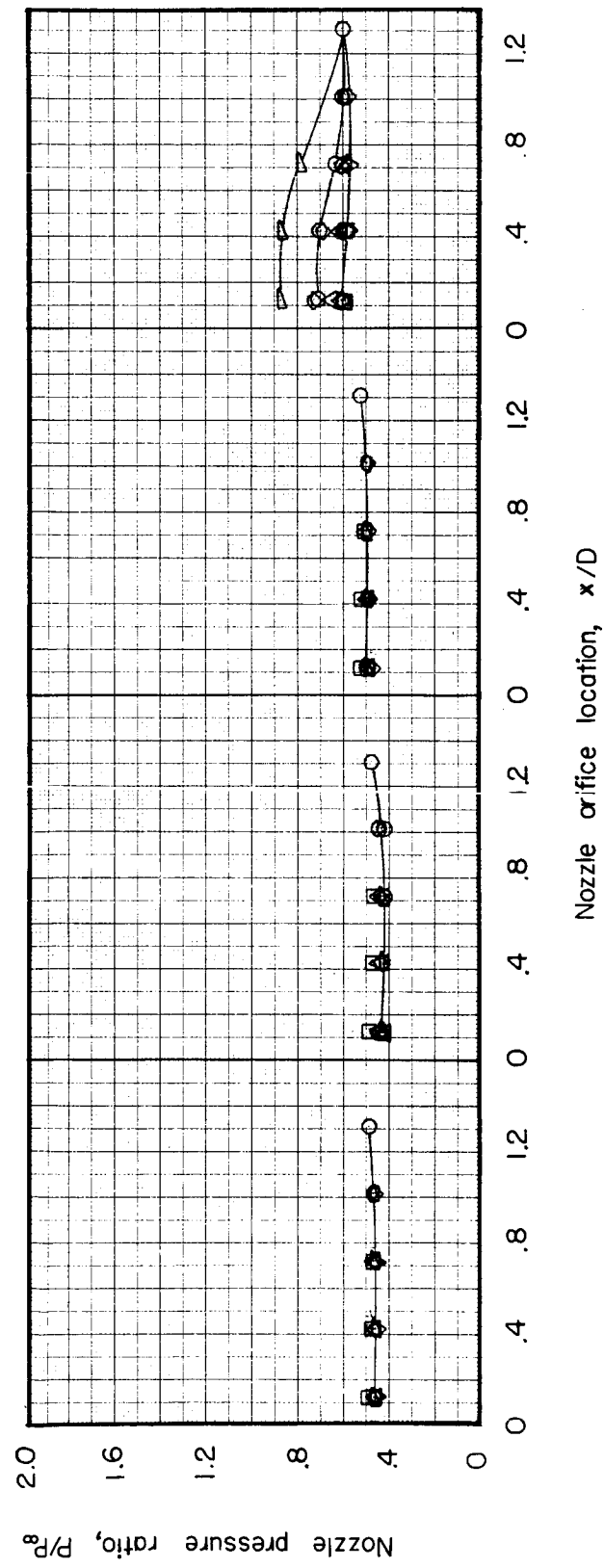
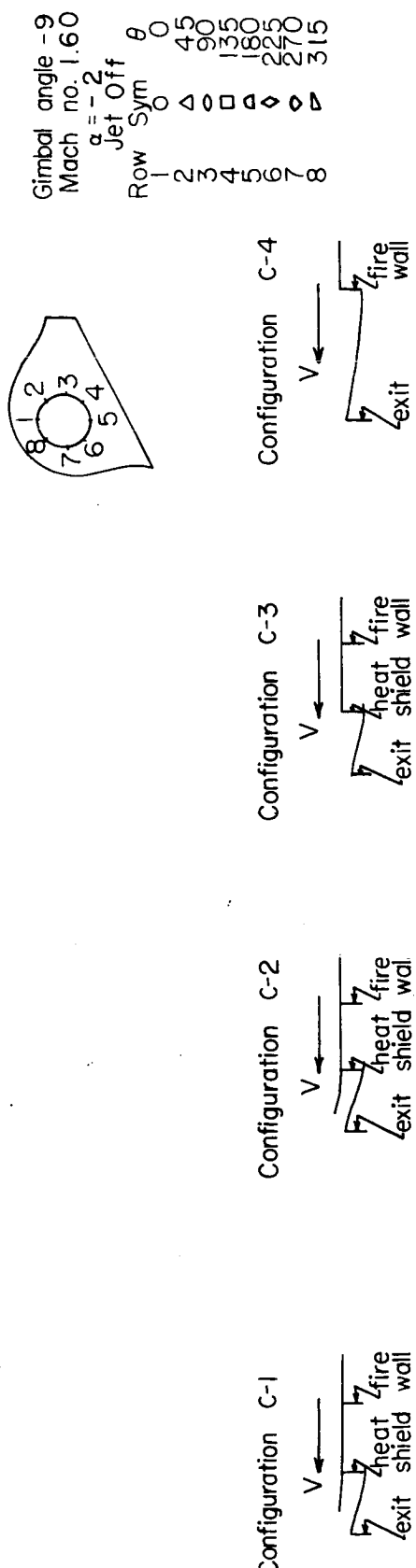


Figure 24b Pressure distribution over the surface of a nozzle with various shroud configurations

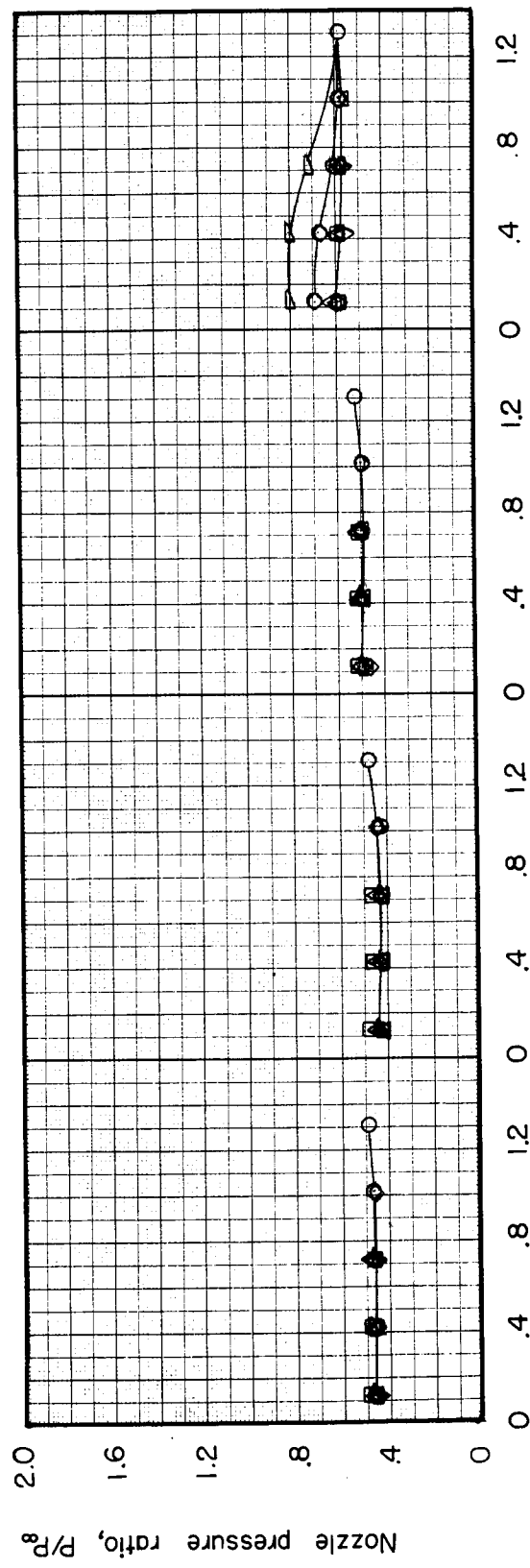
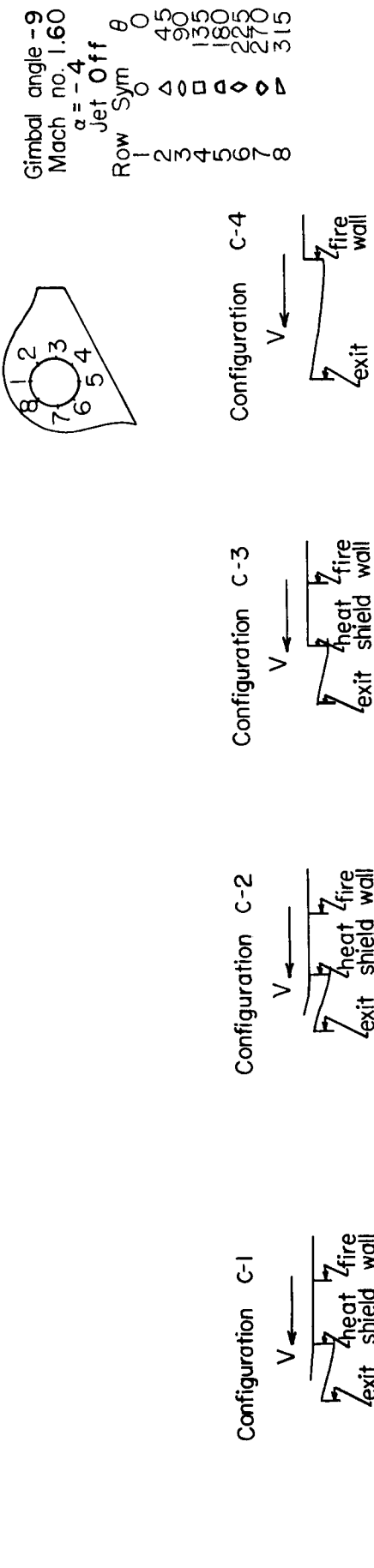


Figure 24c Pressure distribution over the surface of a nozzle with various shroud configurations

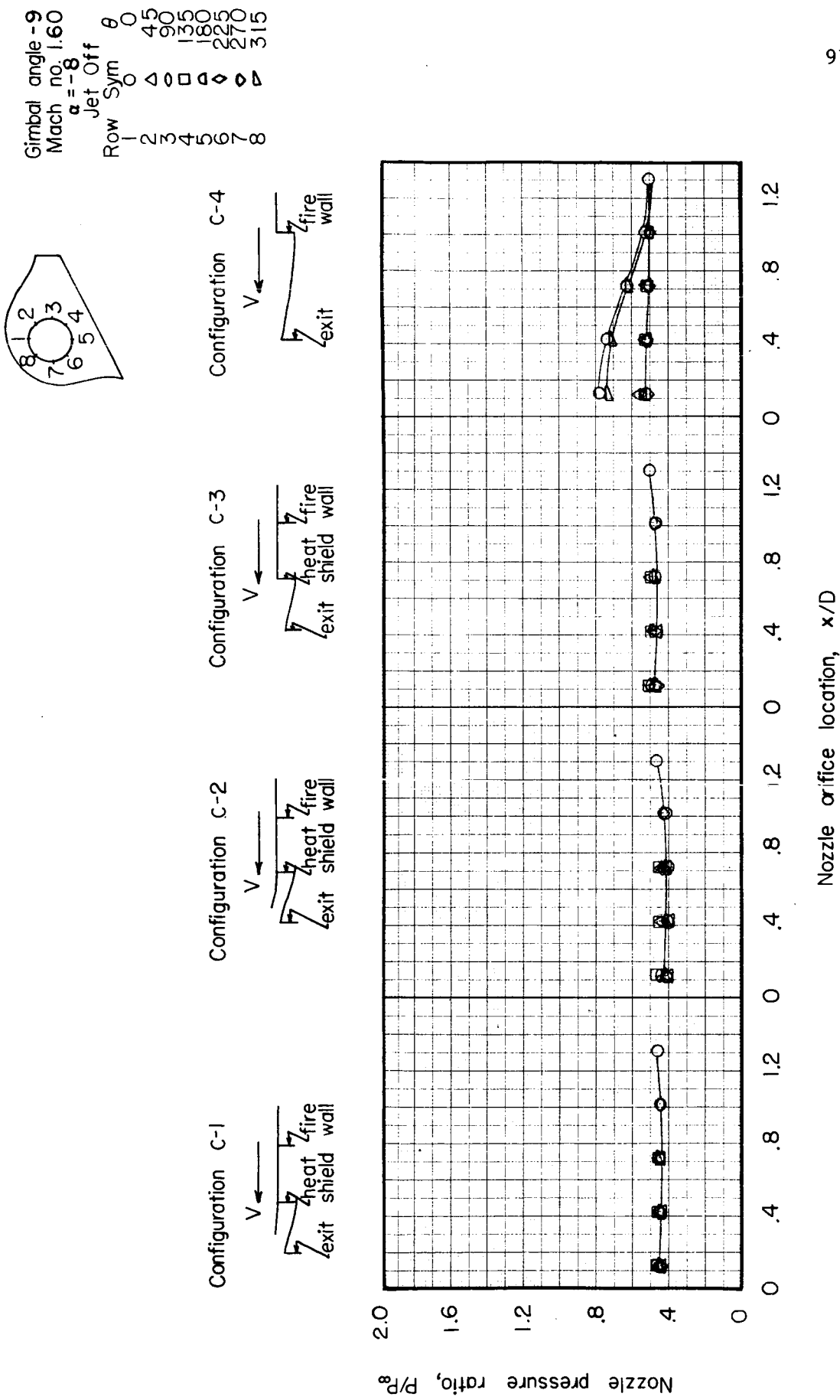


Figure 24d Pressure distribution over the surface of a nozzle with various shroud configurations

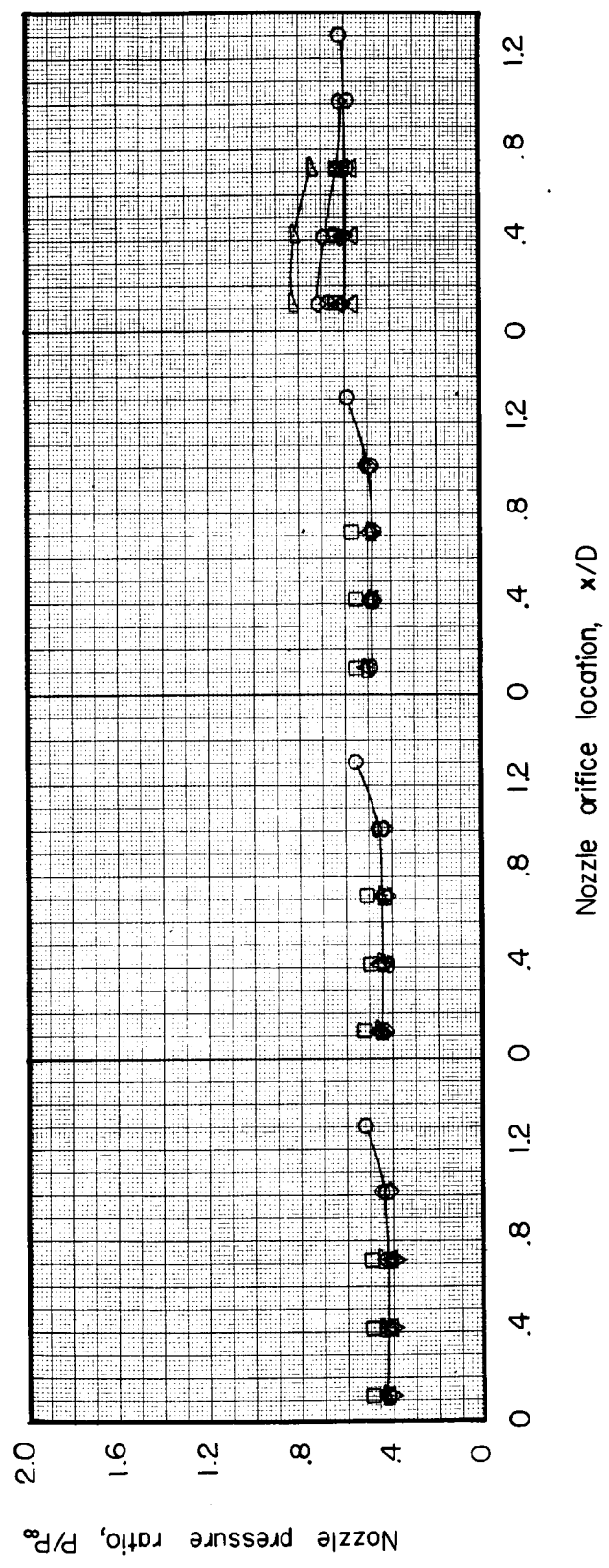
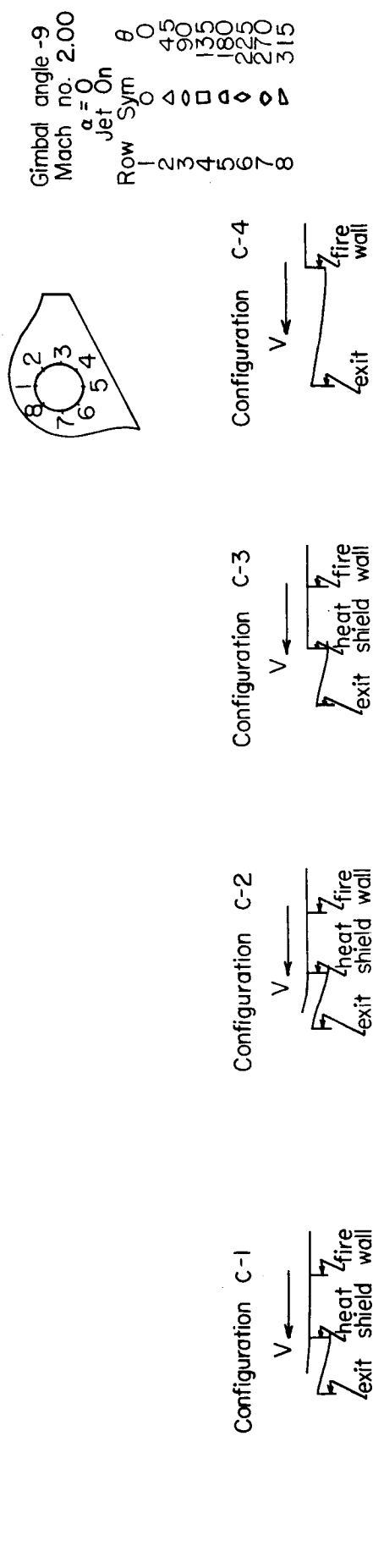


Figure 25a Pressure distribution over the surface of a nozzle with various shroud configurations

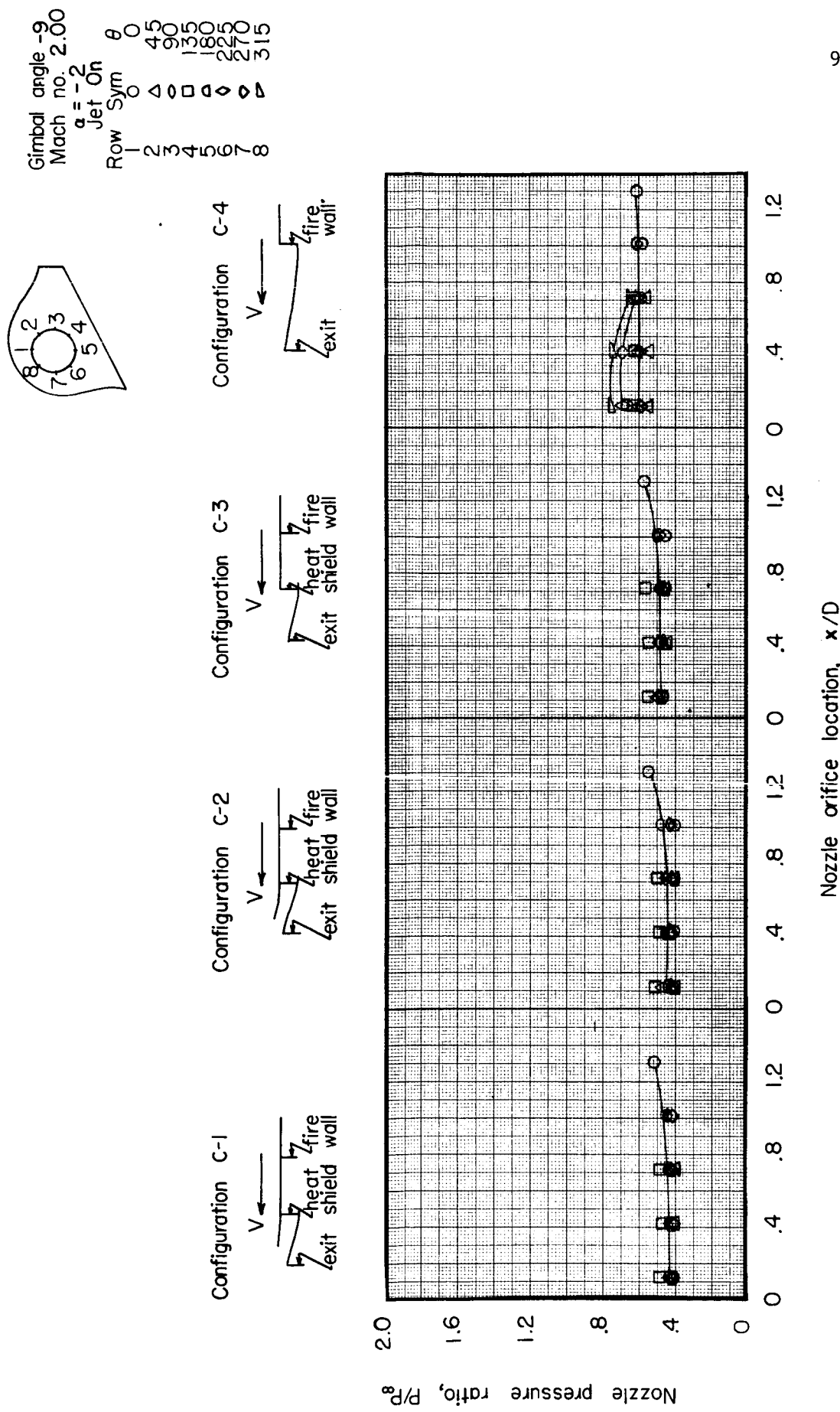


Figure 25b Pressure distribution over the surface of a nozzle with various shroud configurations

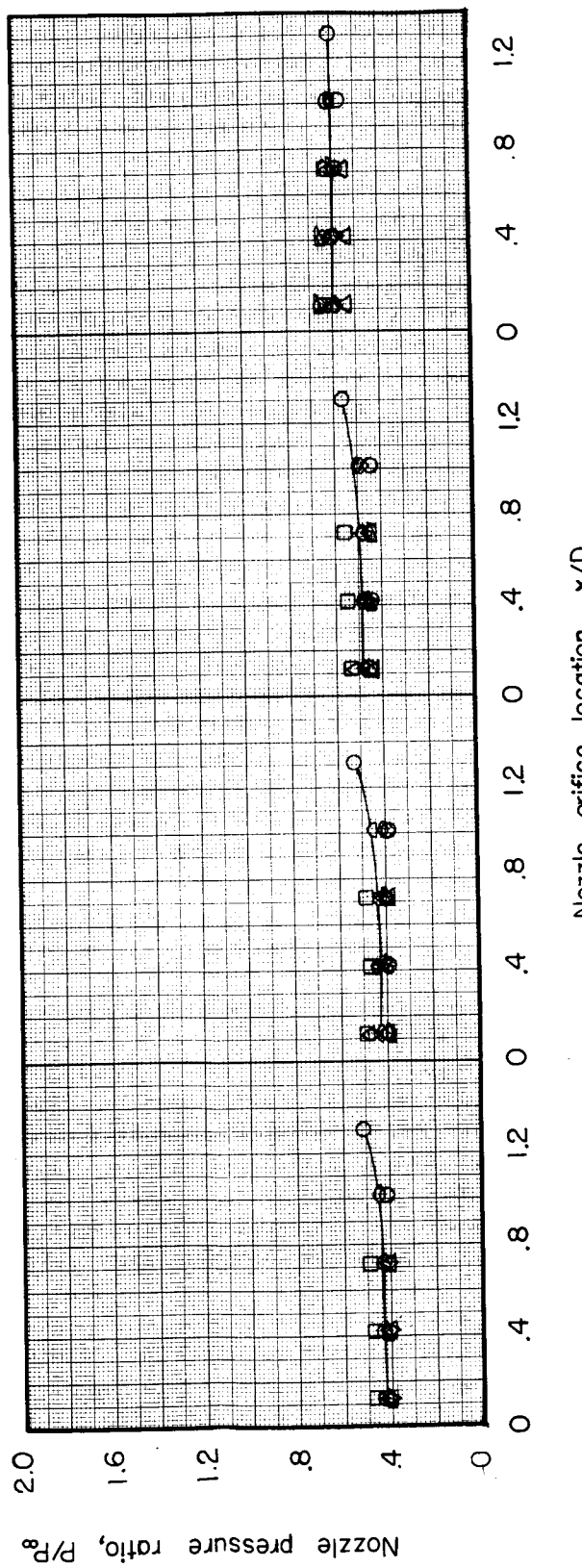
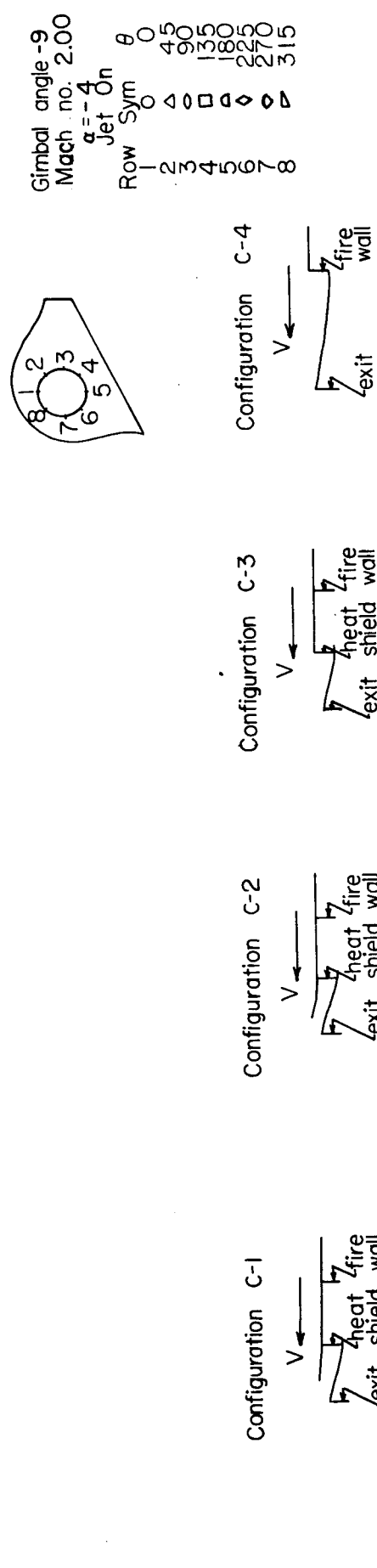
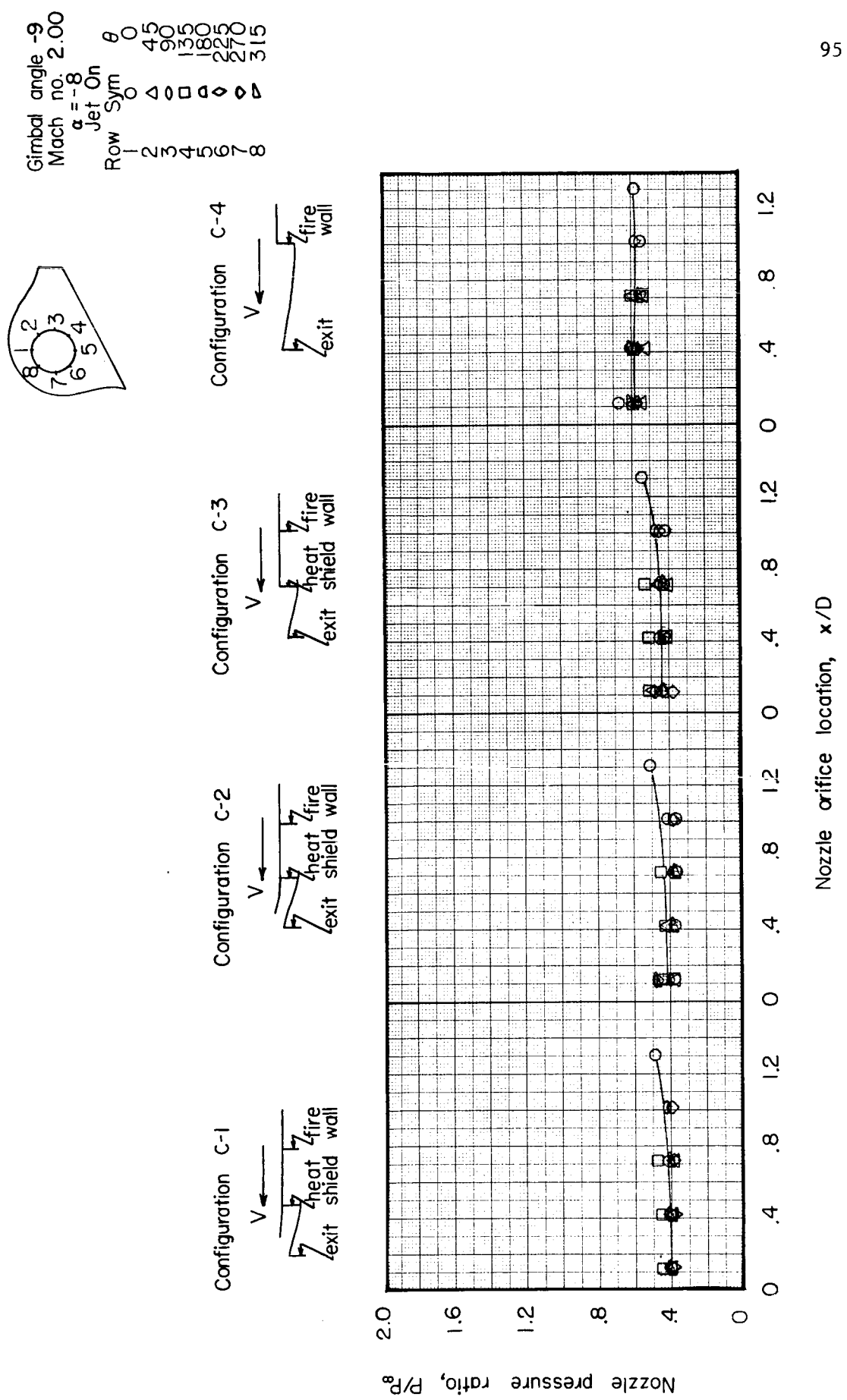


Figure 25c Pressure distribution over the surface of a nozzle with various shroud configurations



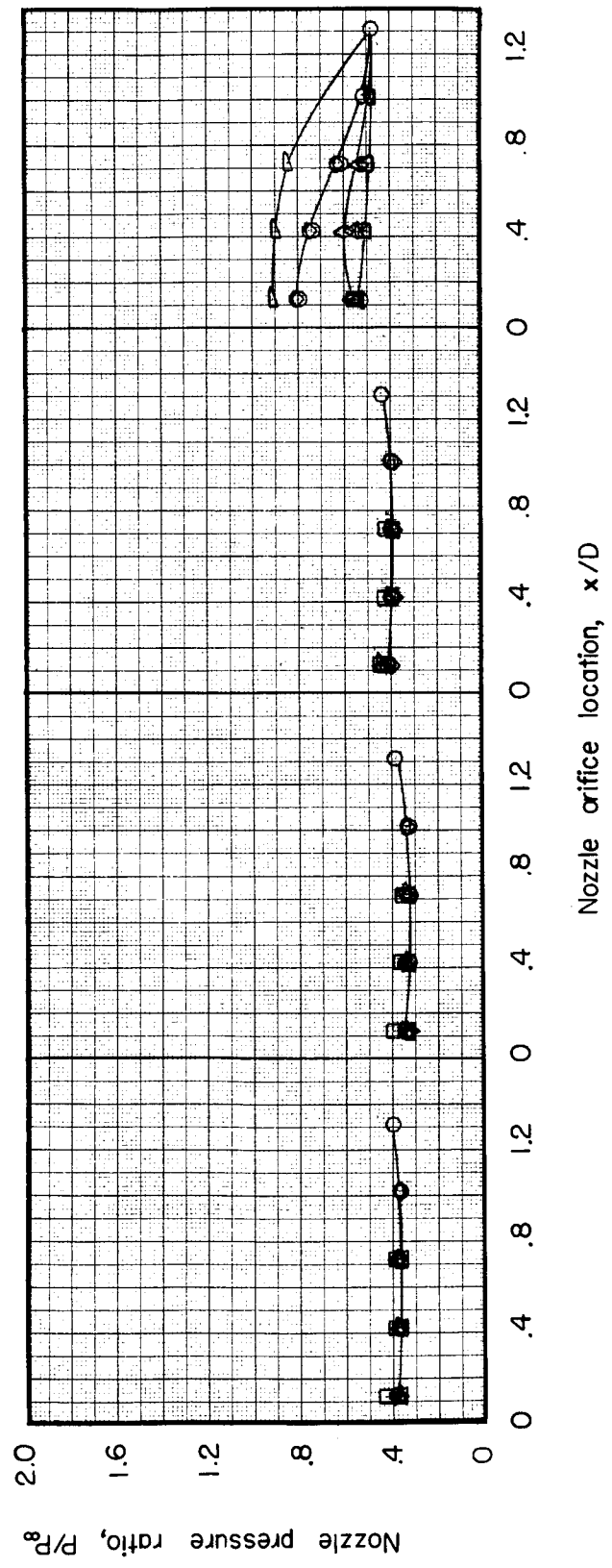
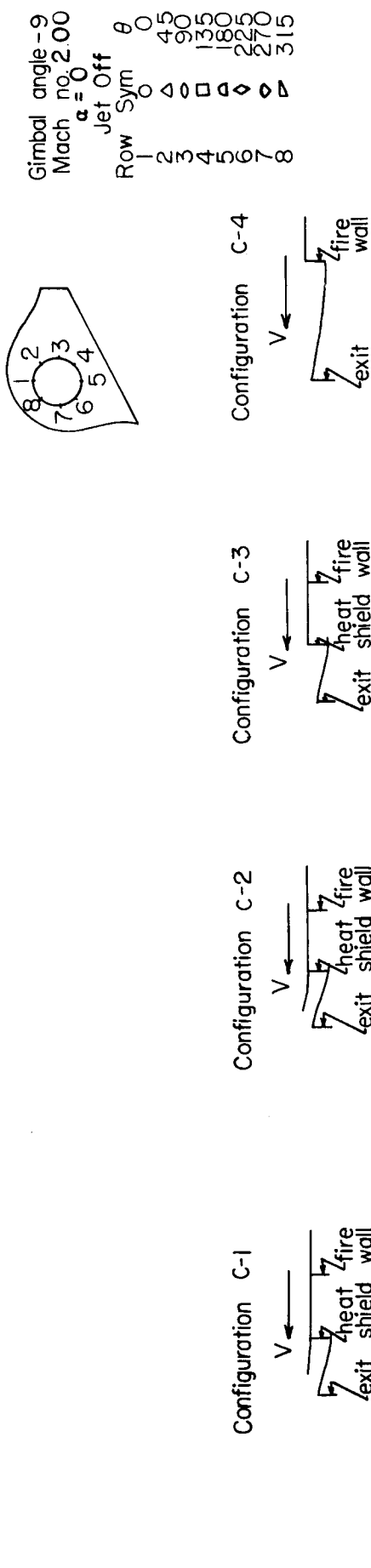


Figure 26a Pressure distribution over the surface of a nozzle with various shroud configurations

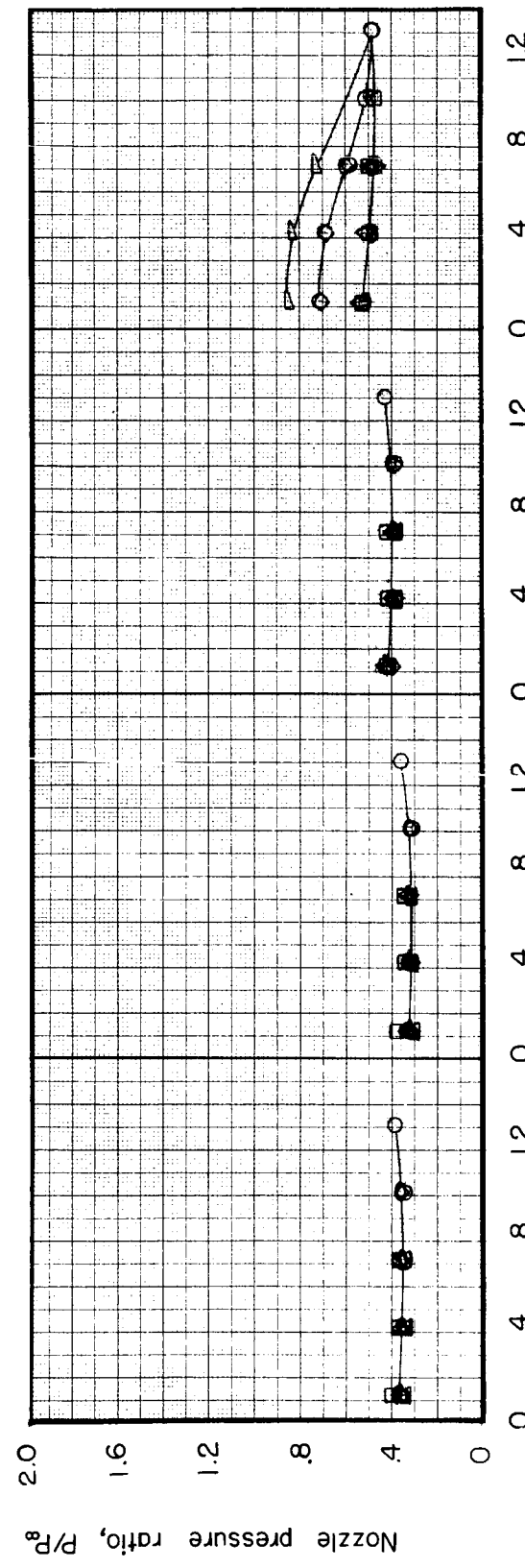
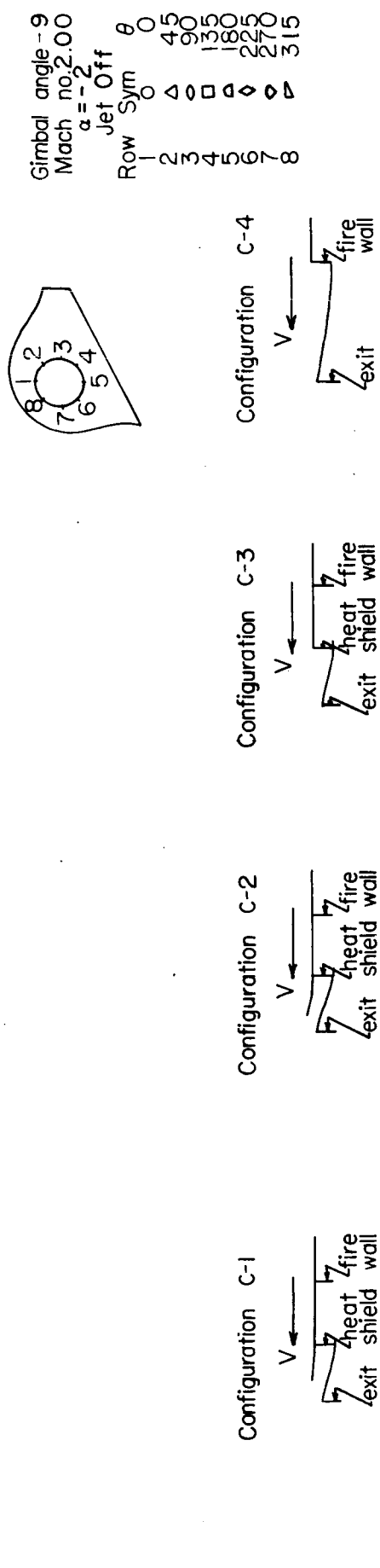


Figure 26b Pressure distribution over the surface of a nozzle with various shroud configurations

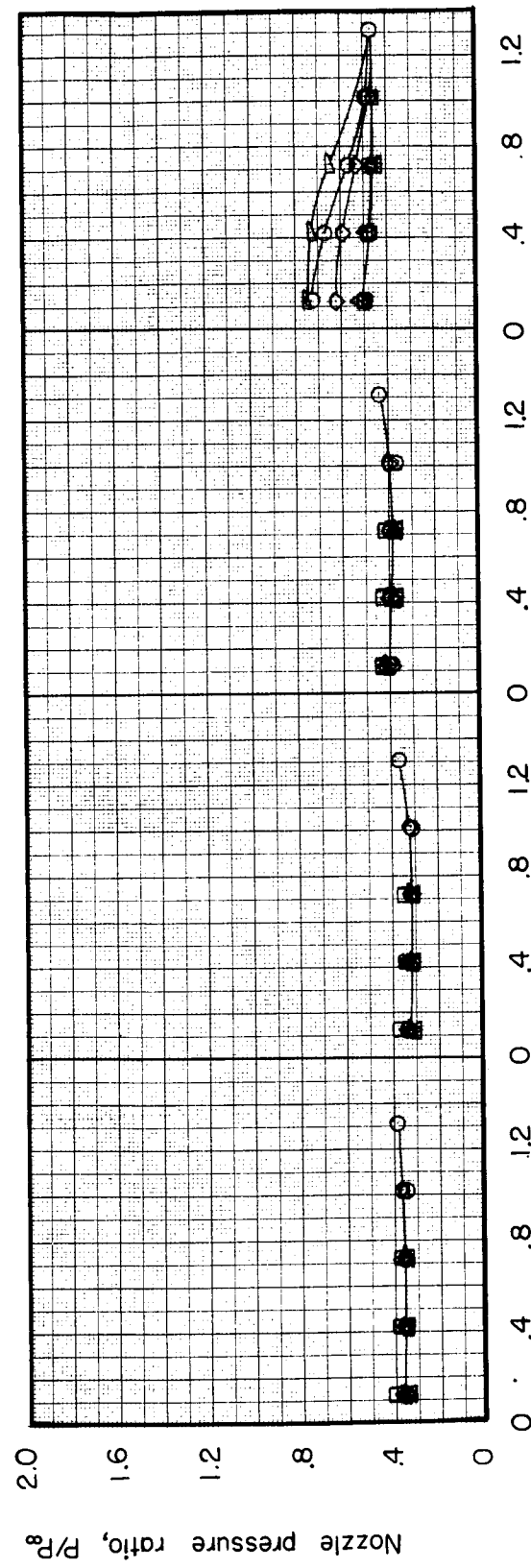
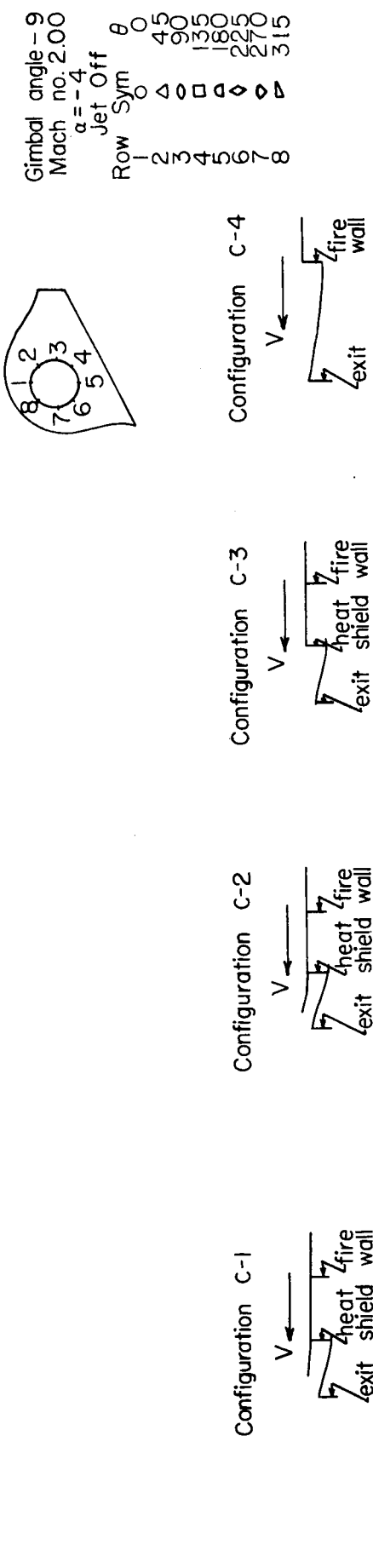


Figure 26c Pressure distribution over the surface of a nozzle with various shroud configurations

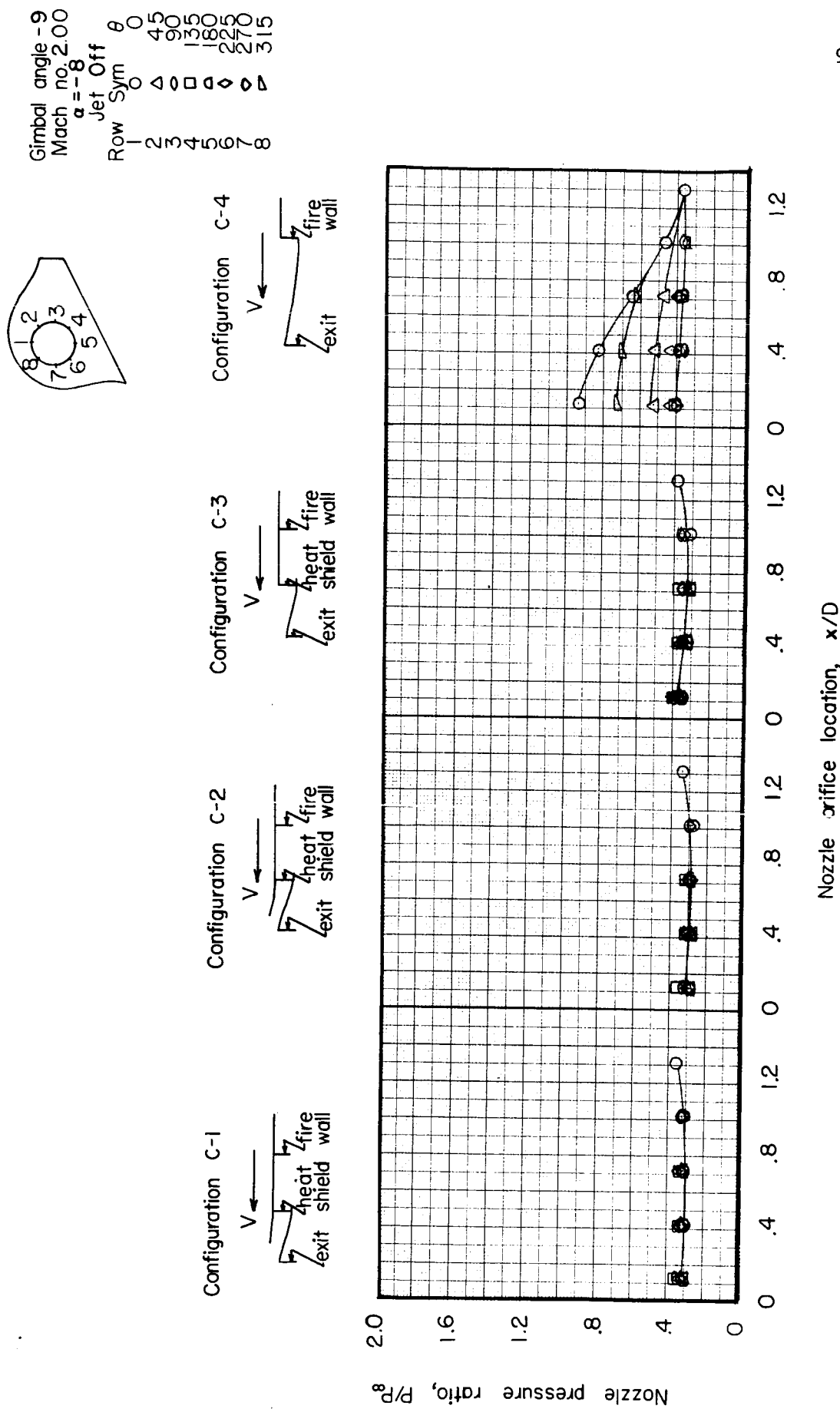


Figure 26d Pressure distribution over the surface of a nozzle with various shroud configurations

100

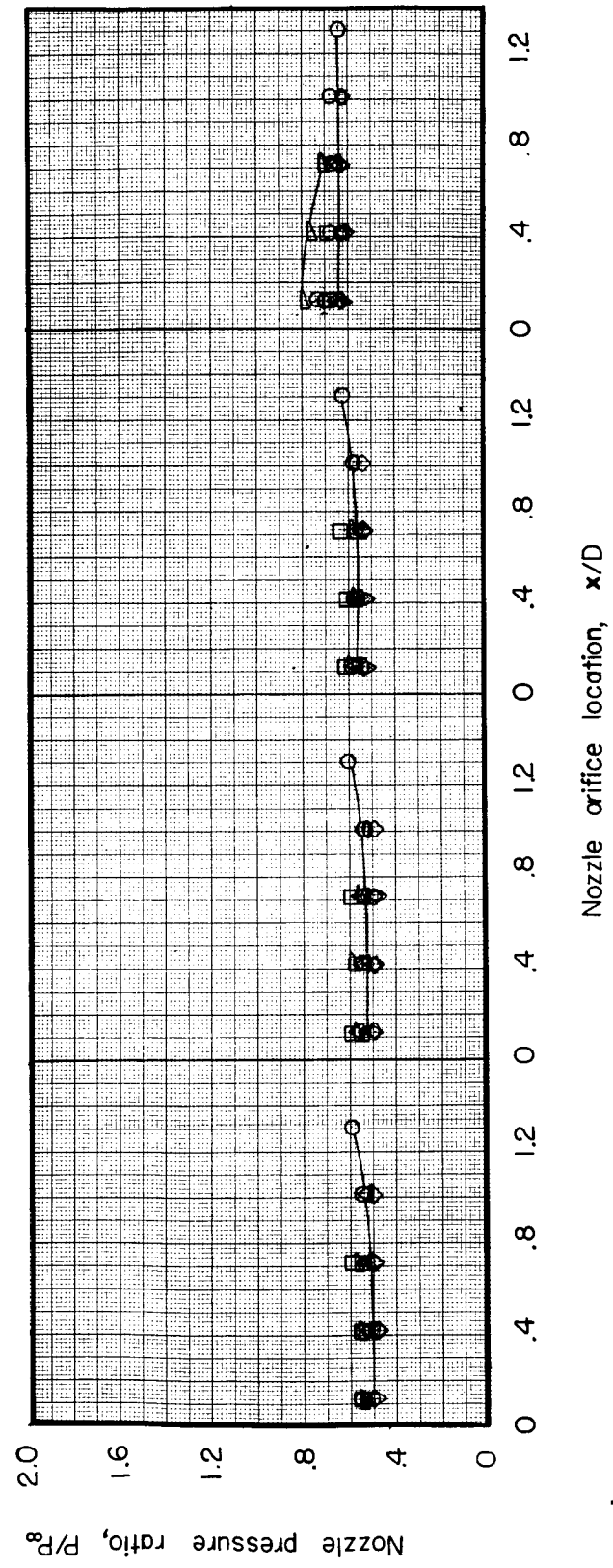
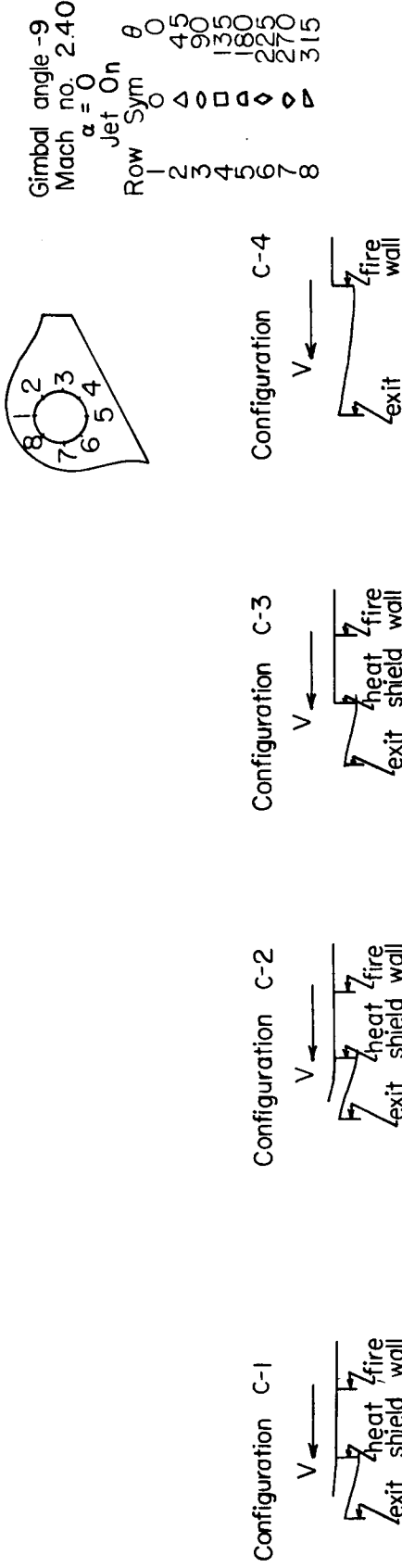


Figure 27a Pressure distribution over the surface of a nozzle with various shroud configurations

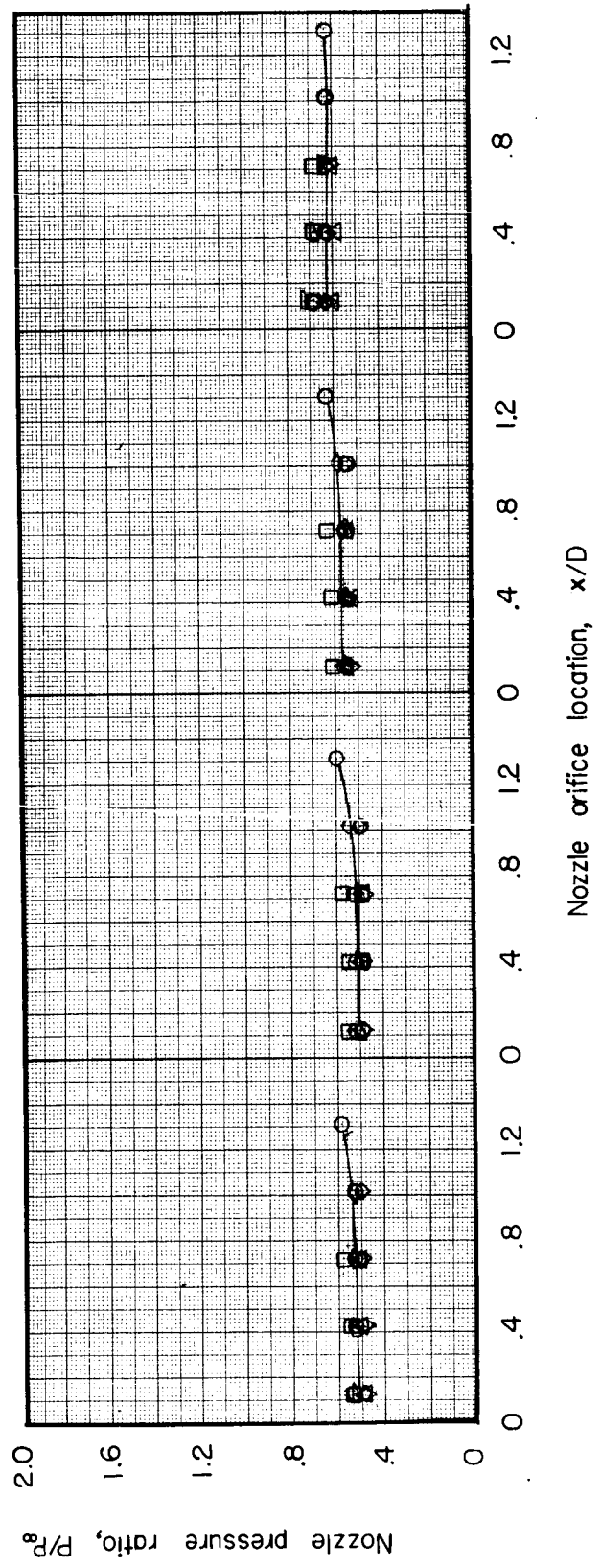
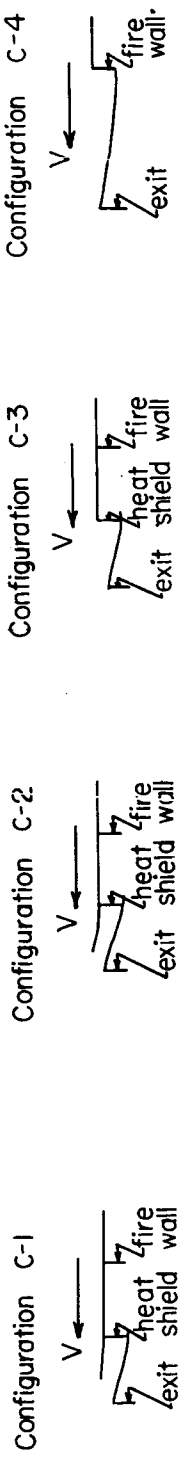
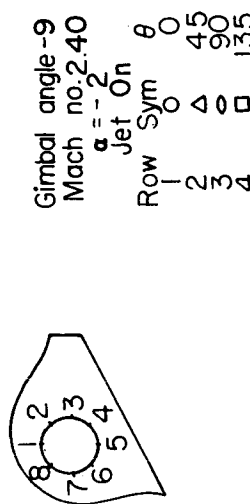


Figure 27b Pressure distribution over the surface of a nozzle with various shroud configurations

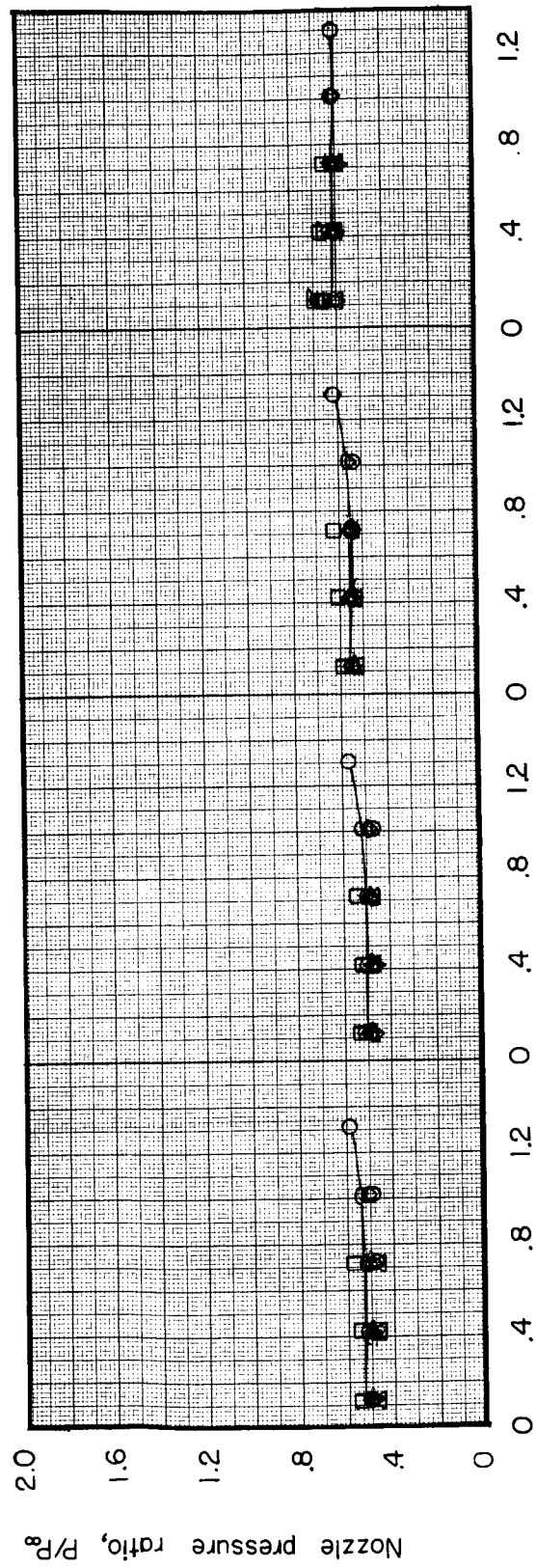
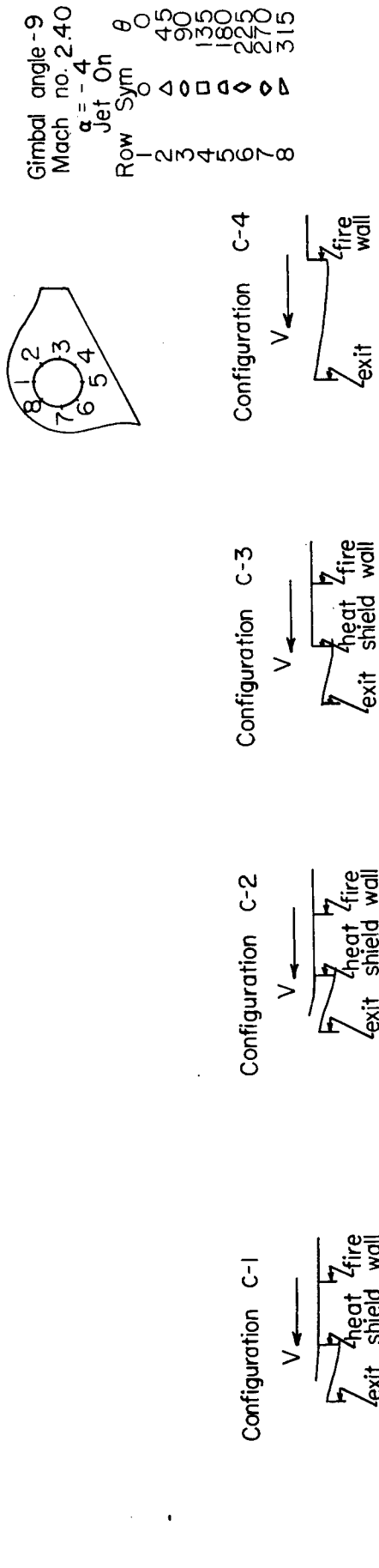


Figure 27c Pressure distribution over the surface of a nozzle with various shroud configurations

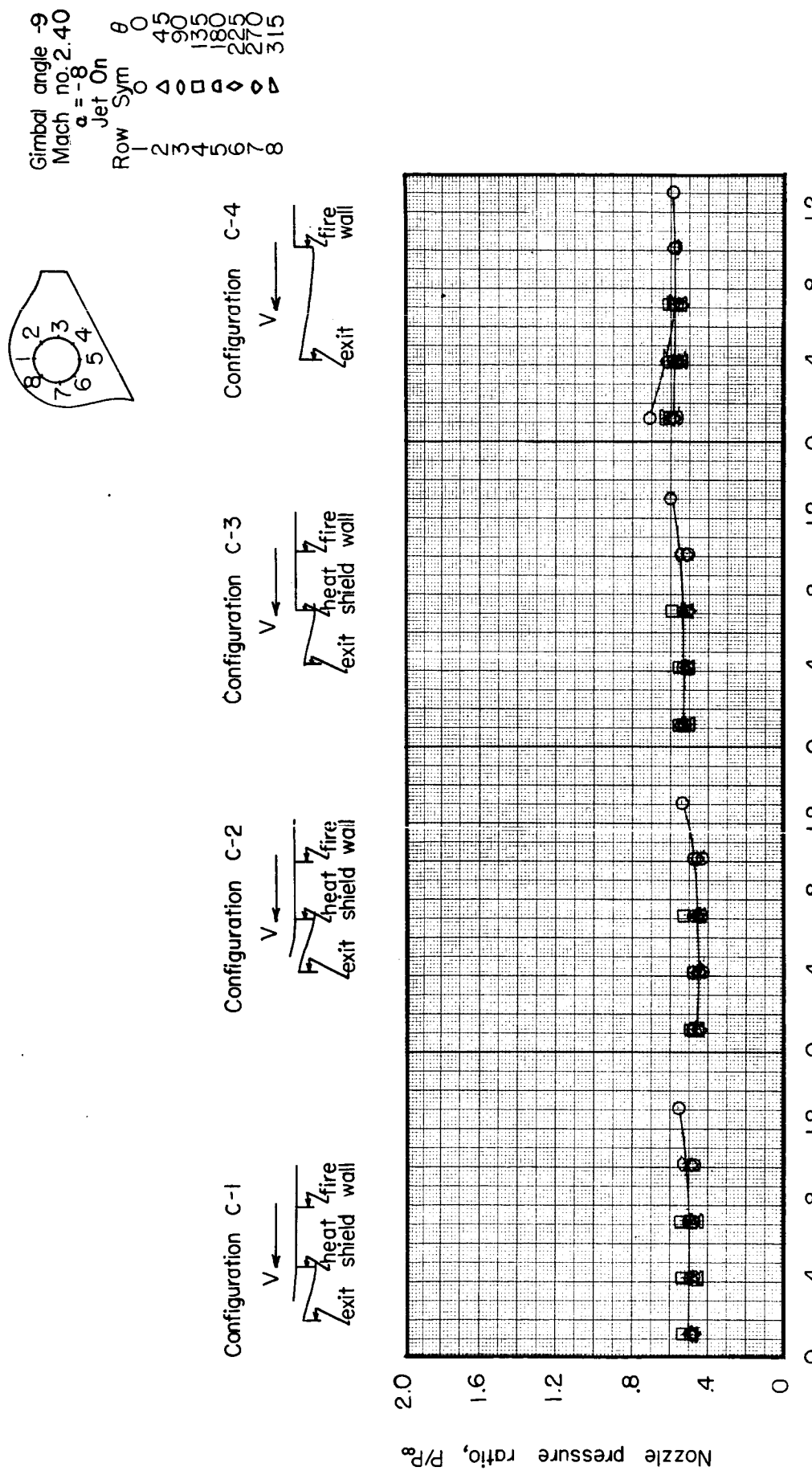


Figure 27d Pressure distribution over the surface of a nozzle with various shroud configurations

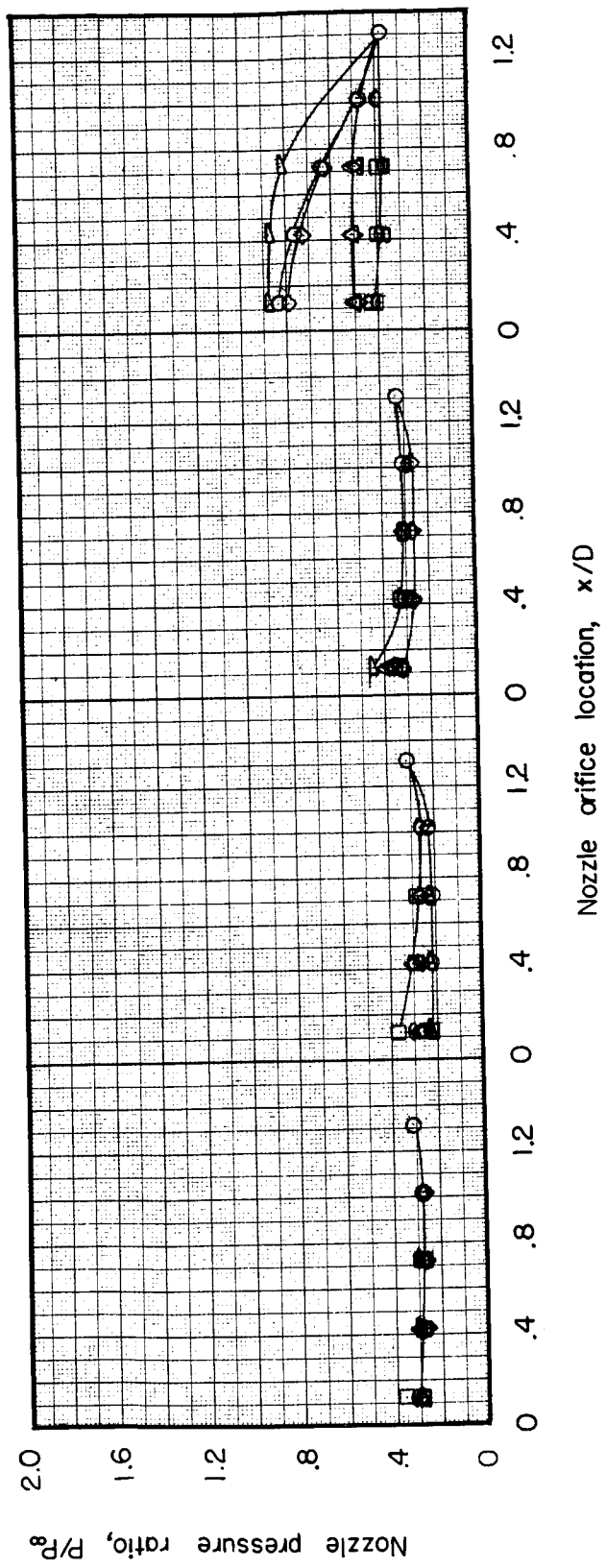
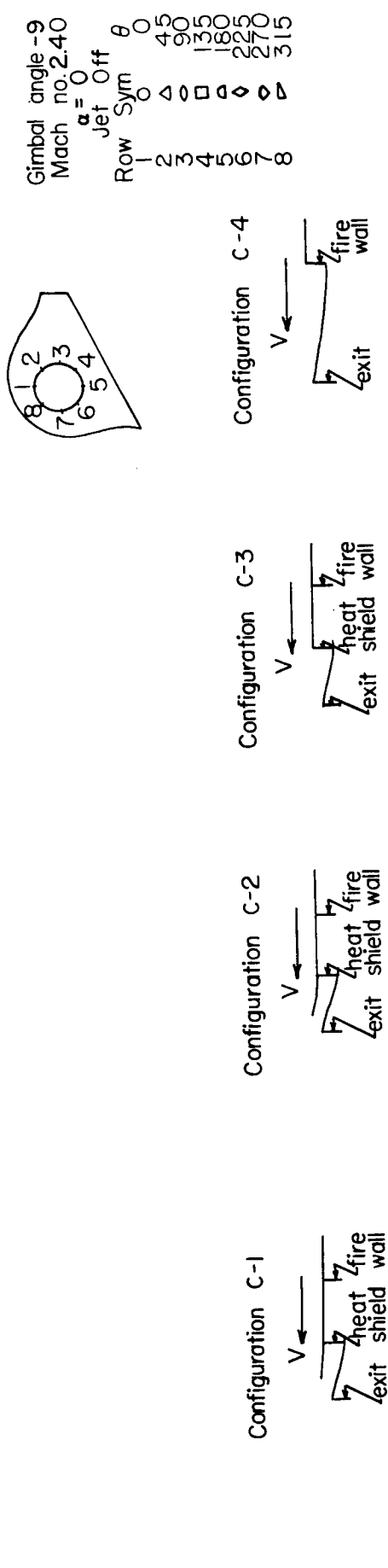
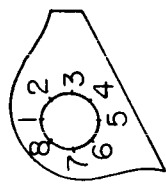


Figure 28a Pressure distribution over the surface of a nozzle with various shroud configurations

Gimbal angle -9  
Mach no. 2.40  
 $\alpha = -2^\circ$   
Jet off

Row	Sym	$\theta$
1	0	0
2	△	45
3	□	90
4	◊	135
5	◊	180
6	◊	225
7	◊	270
8	◊	315



Configuration C-1      Configuration C-2      Configuration C-3      Configuration C-4

V ←                          V ←                          V ←                          V ←

exit      heat shield wall      exit      heat shield wall      exit      heat shield wall      exit      heat shield wall

$Z_{fire}$  wall

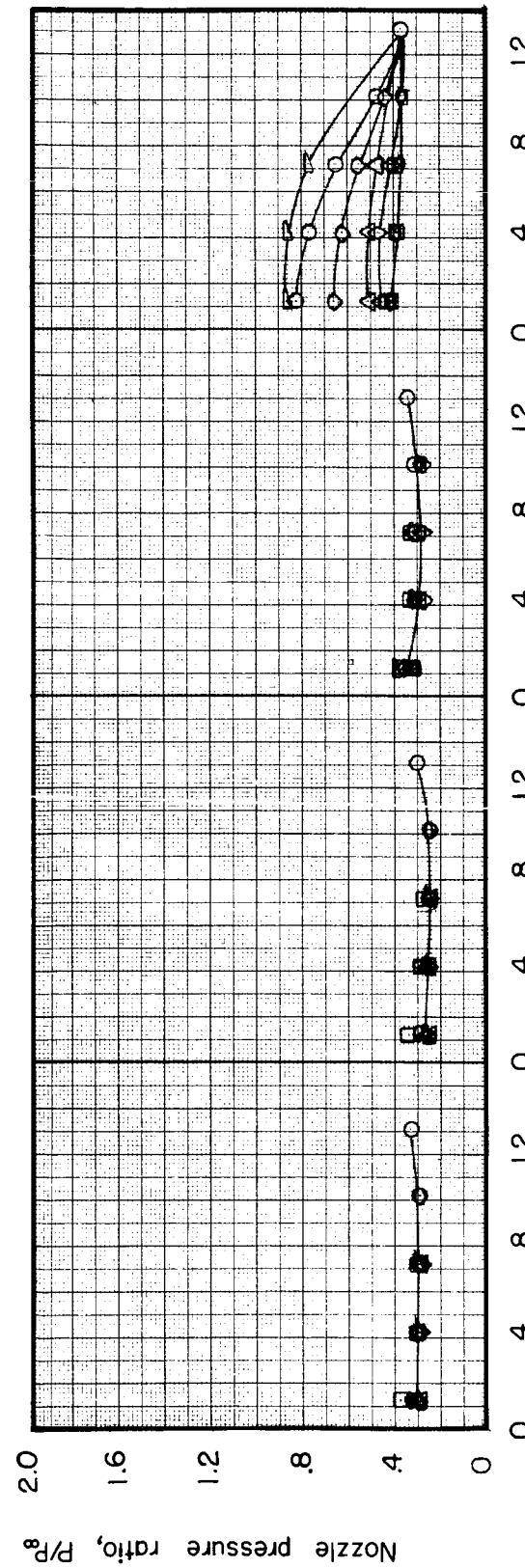


Figure 28b Pressure distribution over the surface of a nozzle with various shroud configurations

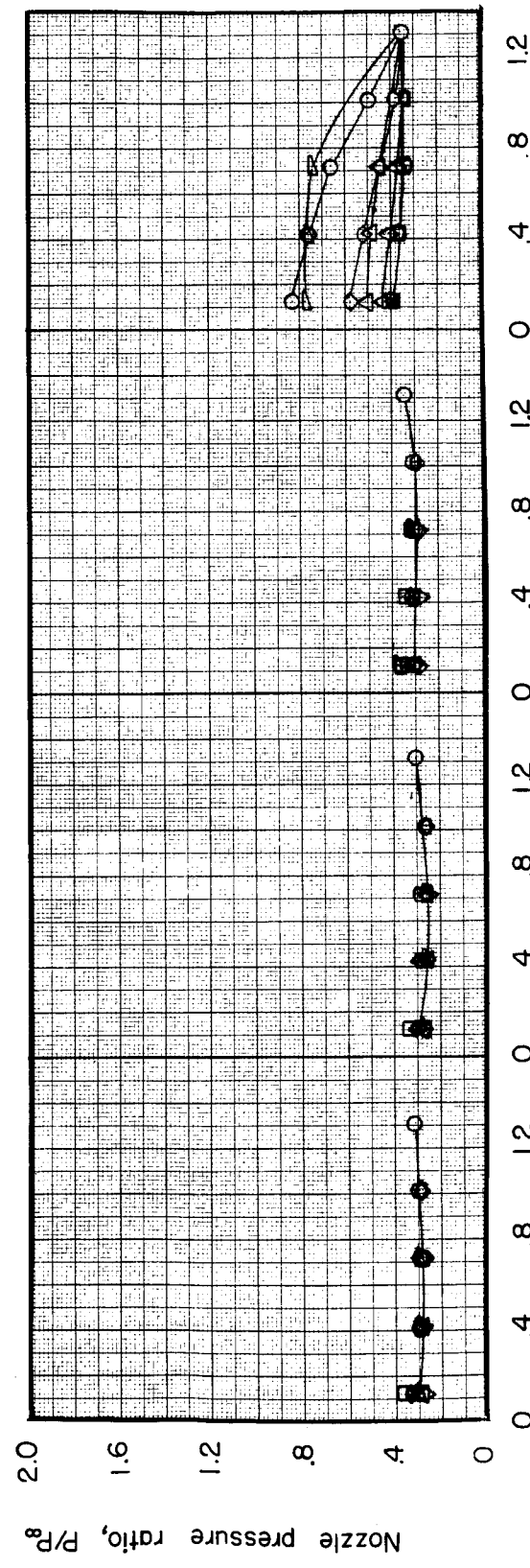
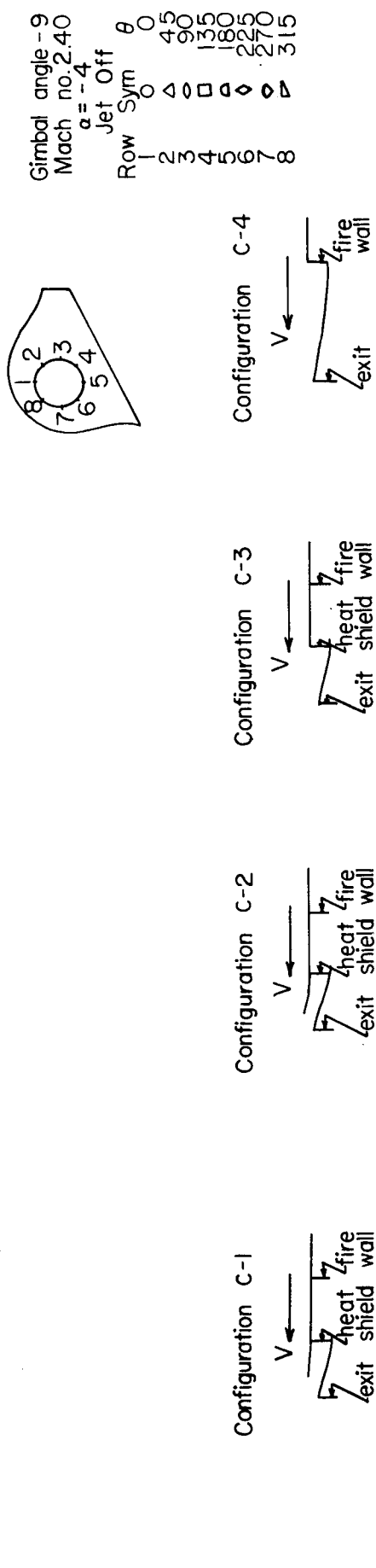


Figure 28c Pressure distribution over the surface of a nozzle with various shroud configurations

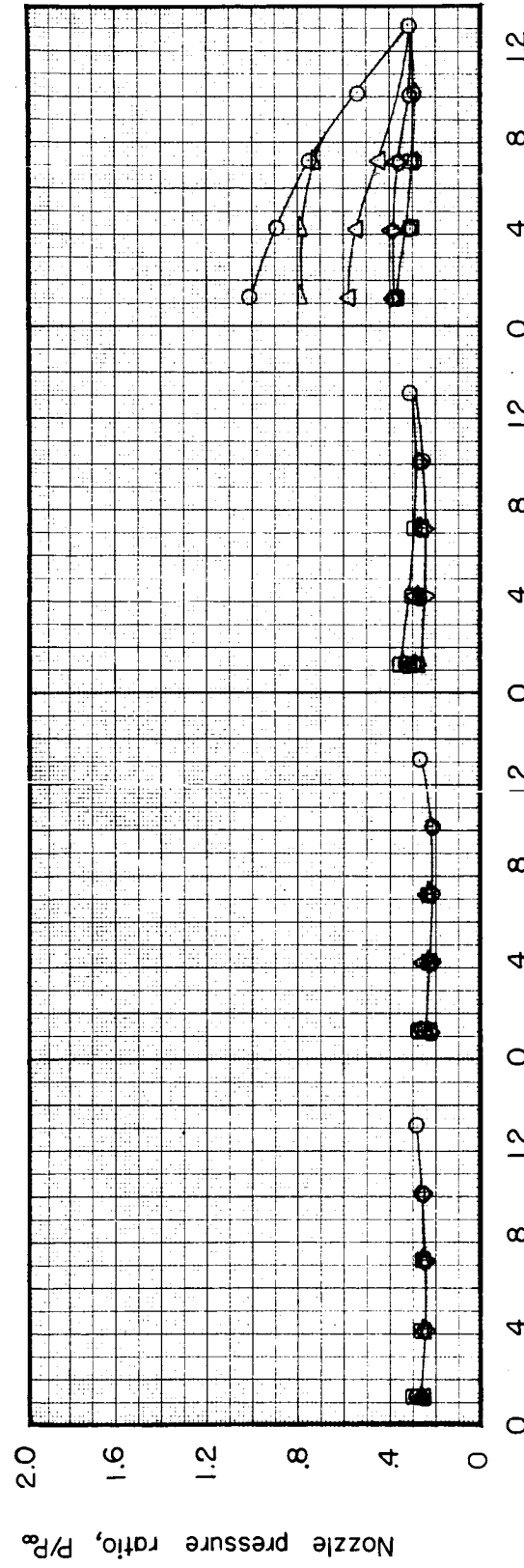
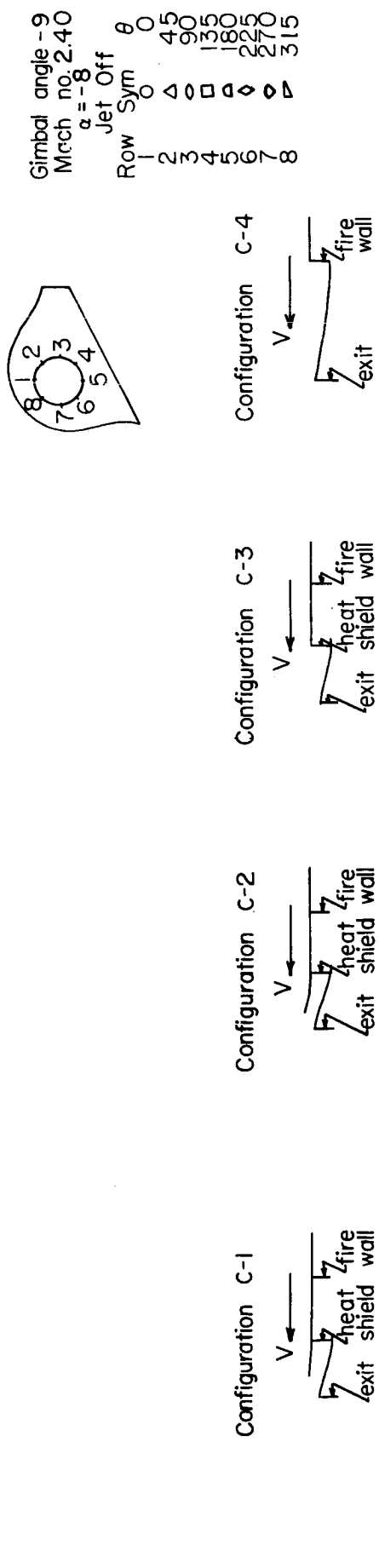


Figure 28d Pressure distribution over the surface of a nozzle with various shroud configurations

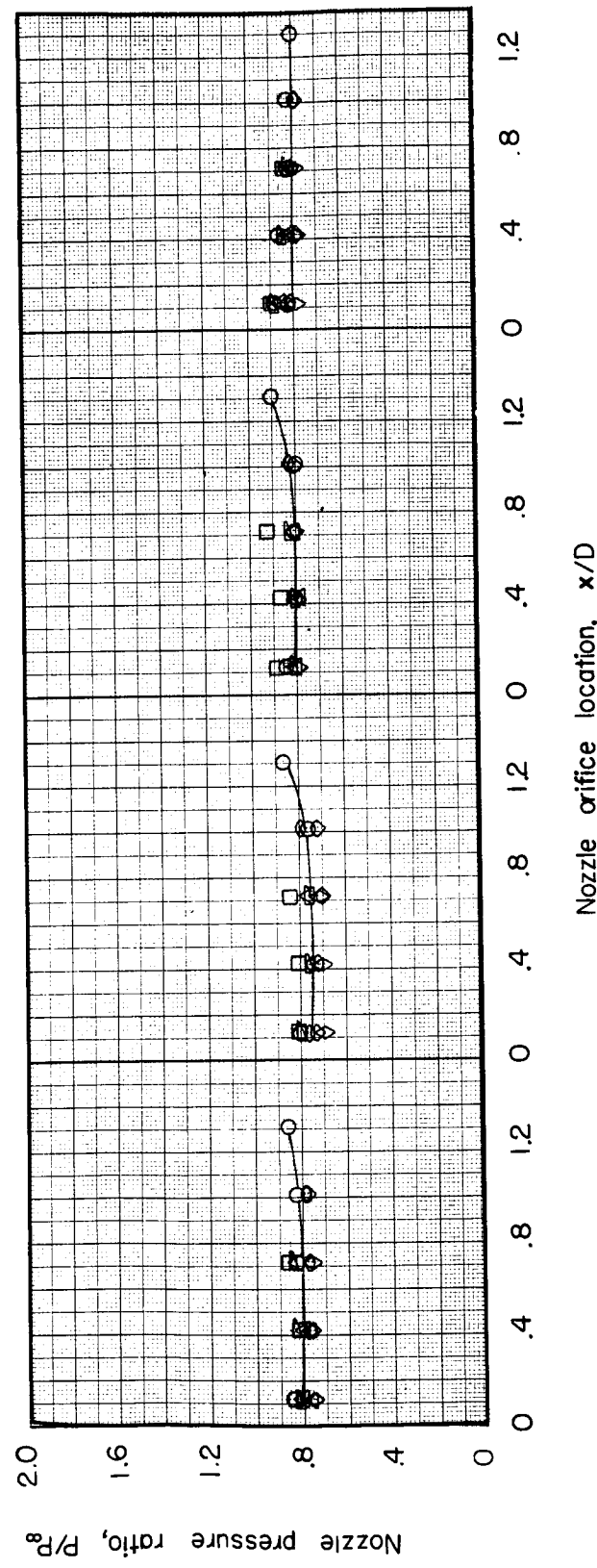
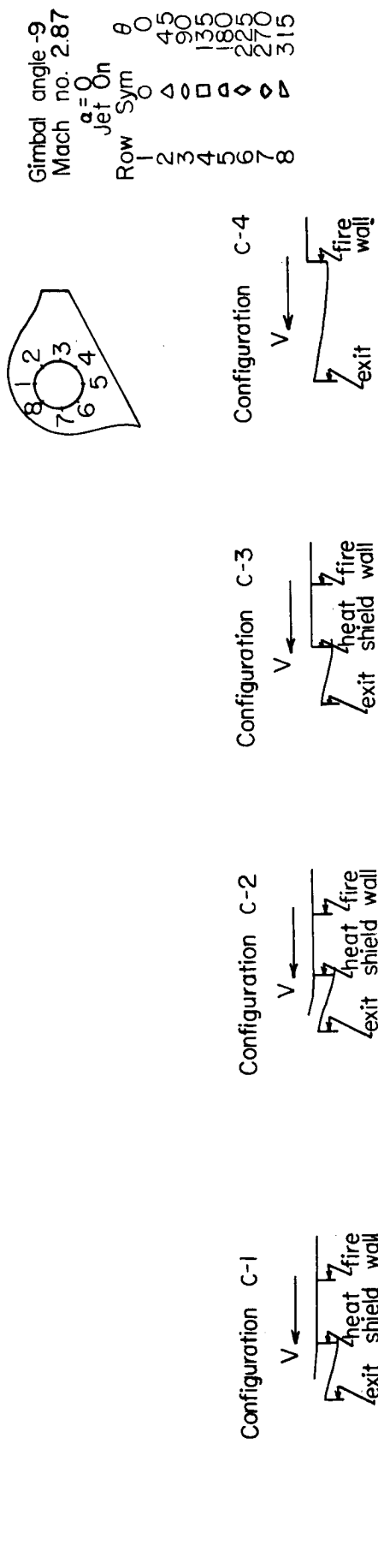


Figure 29a Pressure distribution over the surface of a nozzle with various shroud configurations

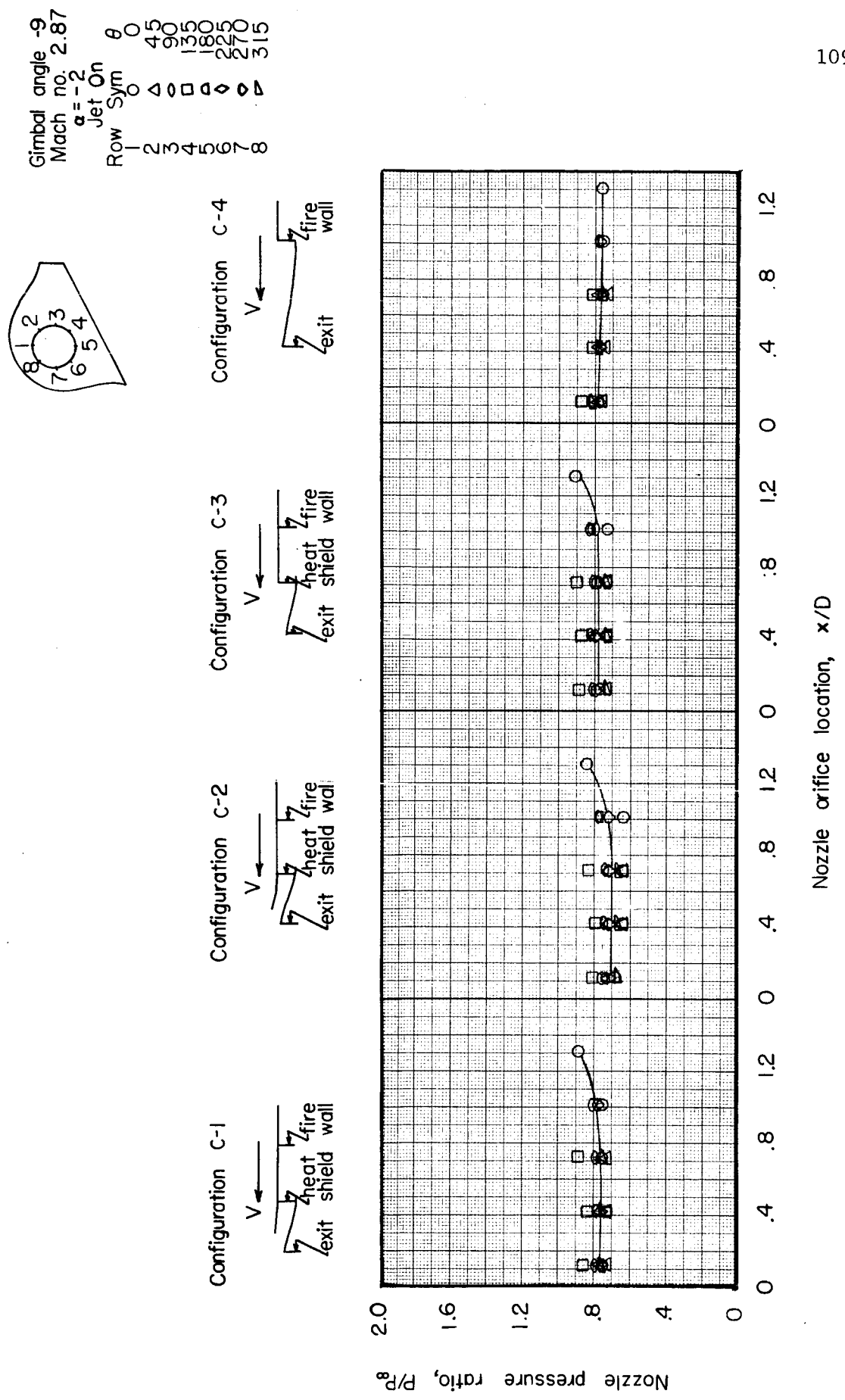


Figure 29b Pressure distribution over the surface of a nozzle with various shroud configurations.

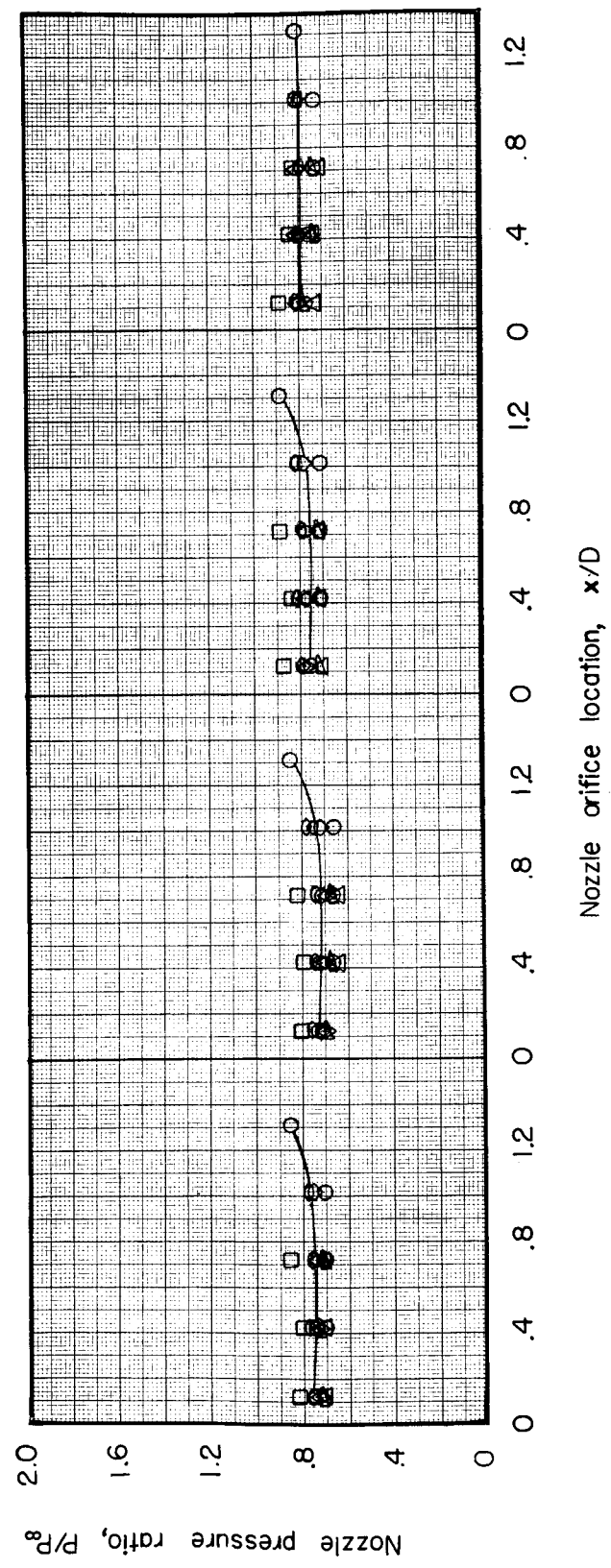
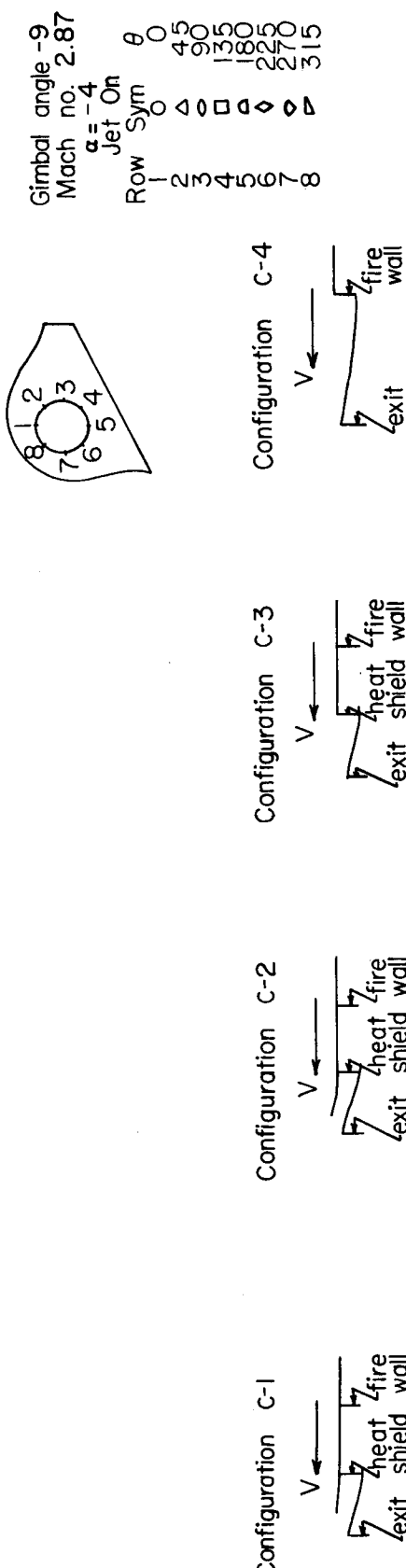


Figure 29c Pressure distribution over the surface of a nozzle with various shroud configurations

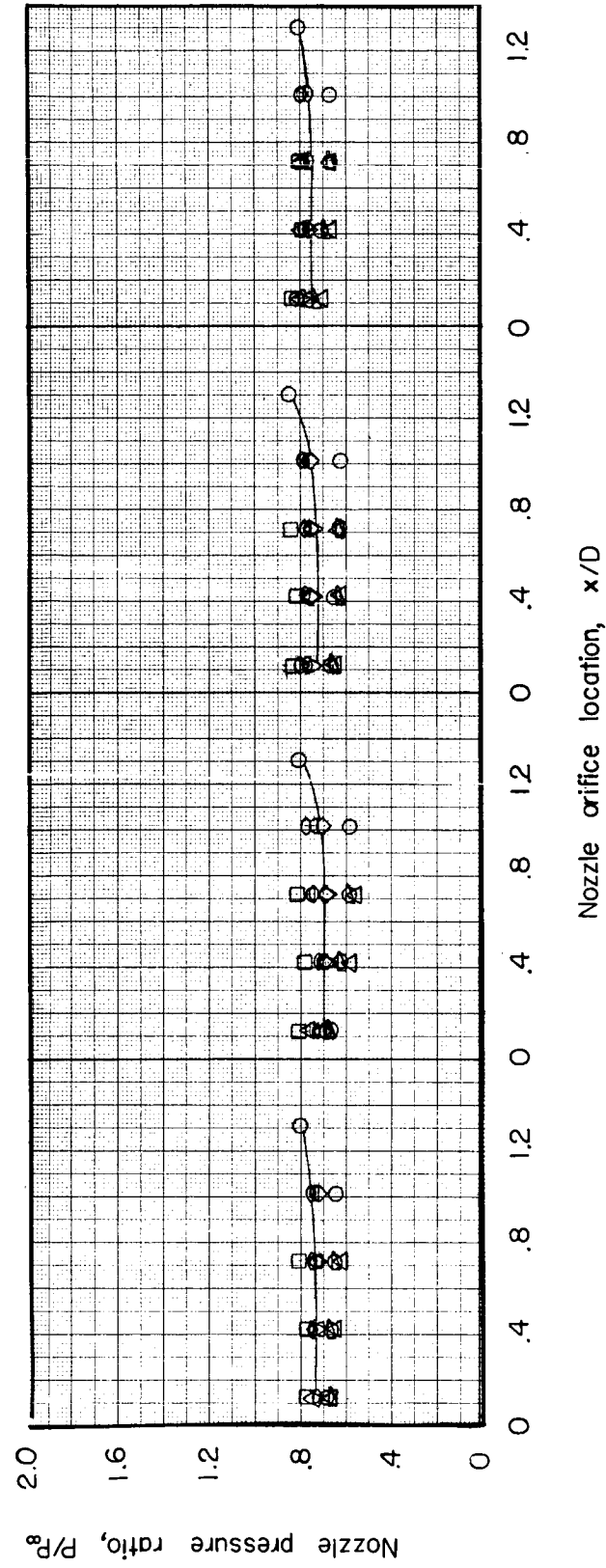
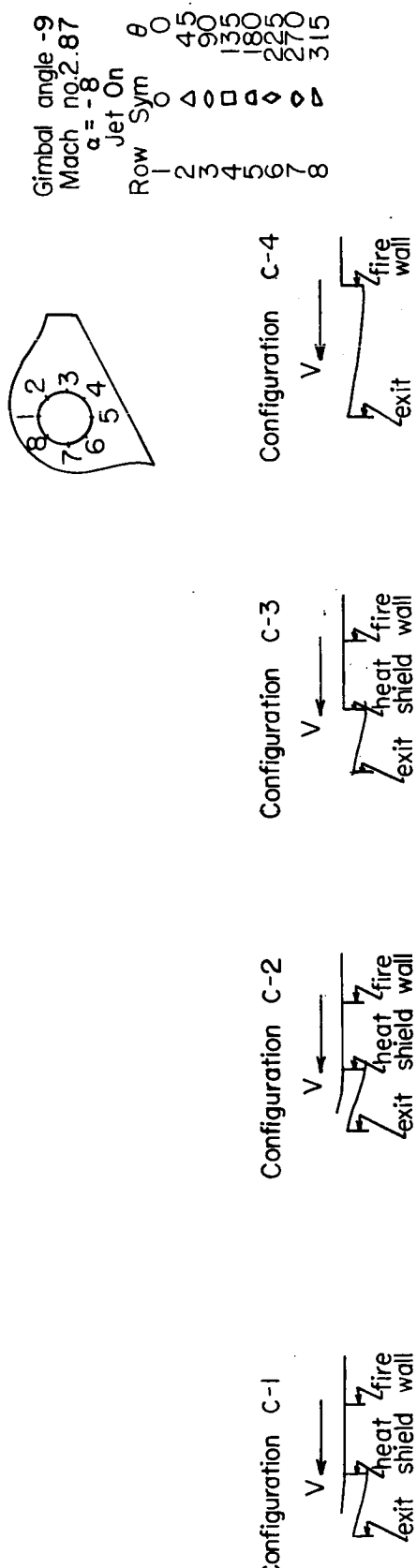


Figure 29d Pressure distribution over the surface of a nozzle with various shroud configurations

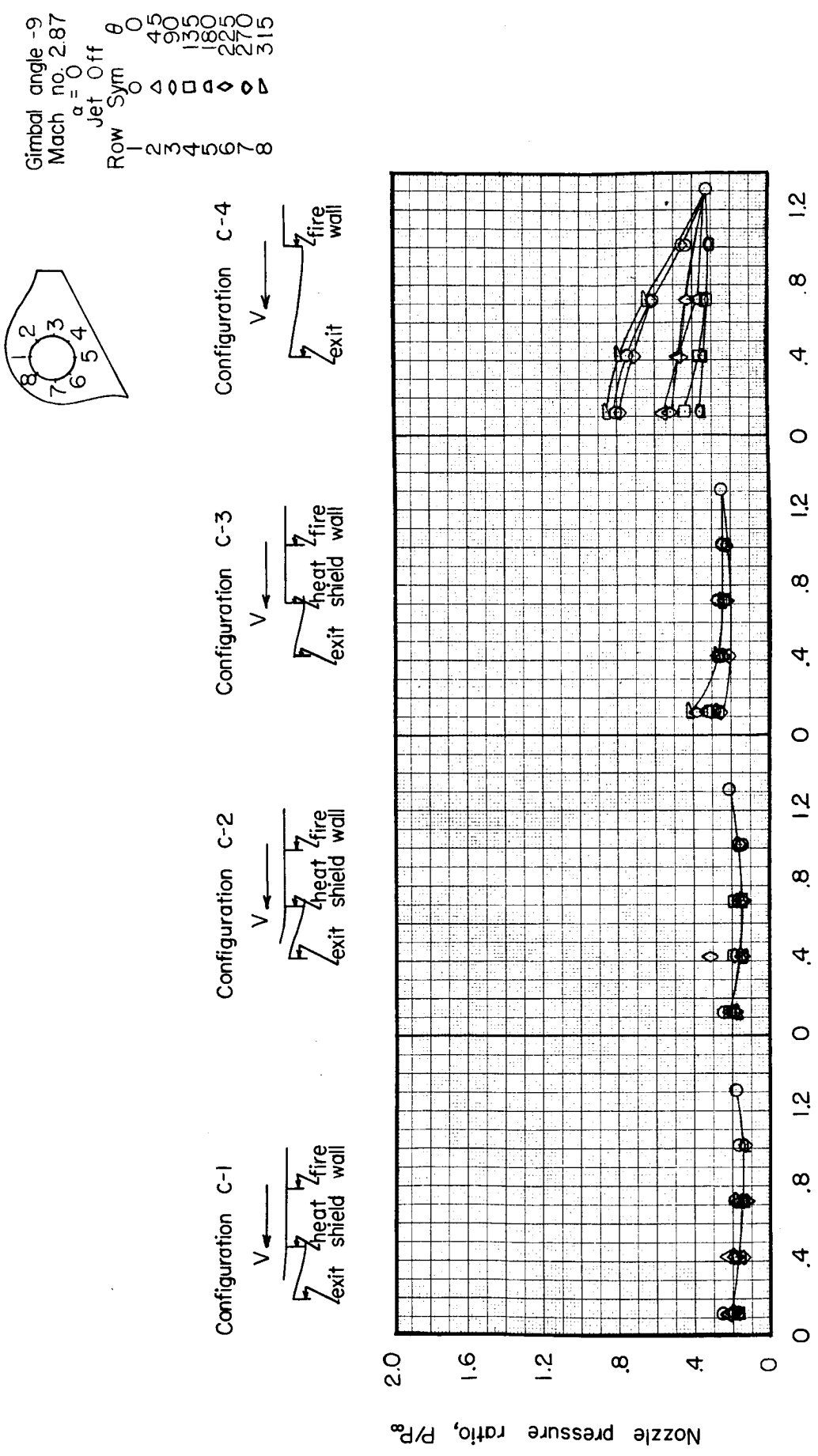


Figure 30a Pressure distribution over the surface of a nozzle with various shroud configurations

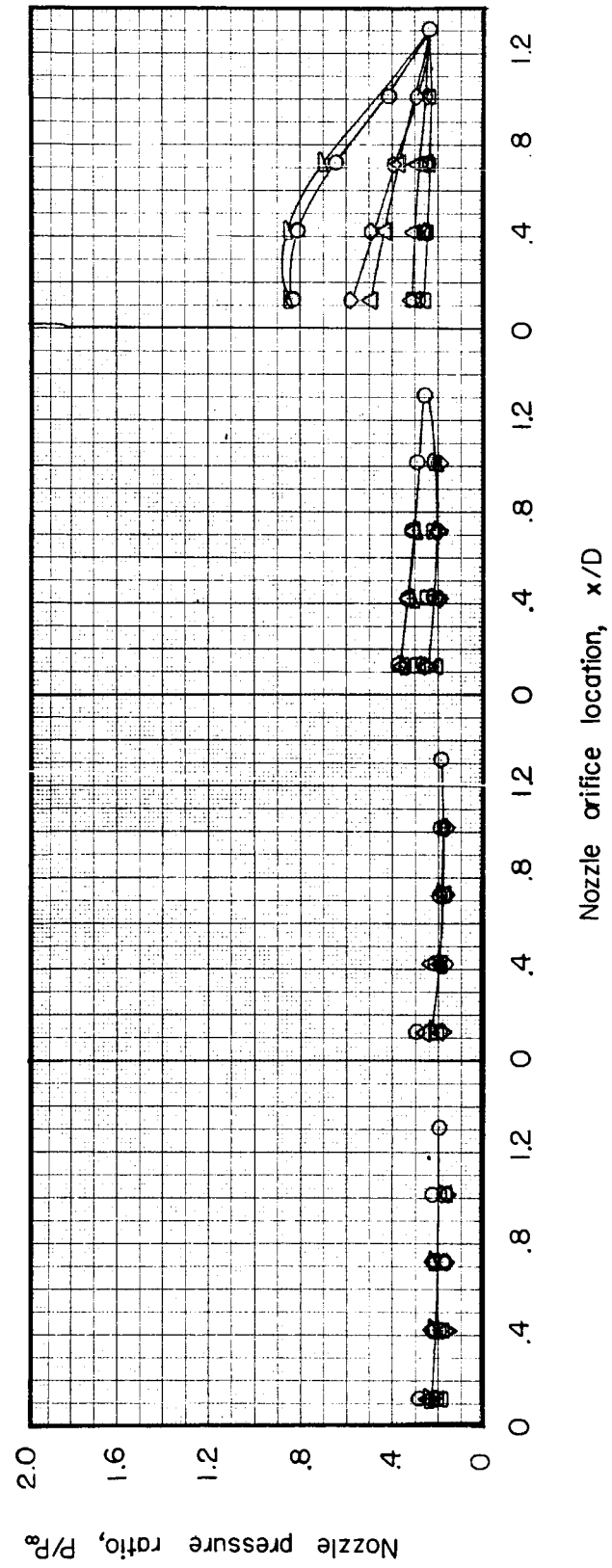
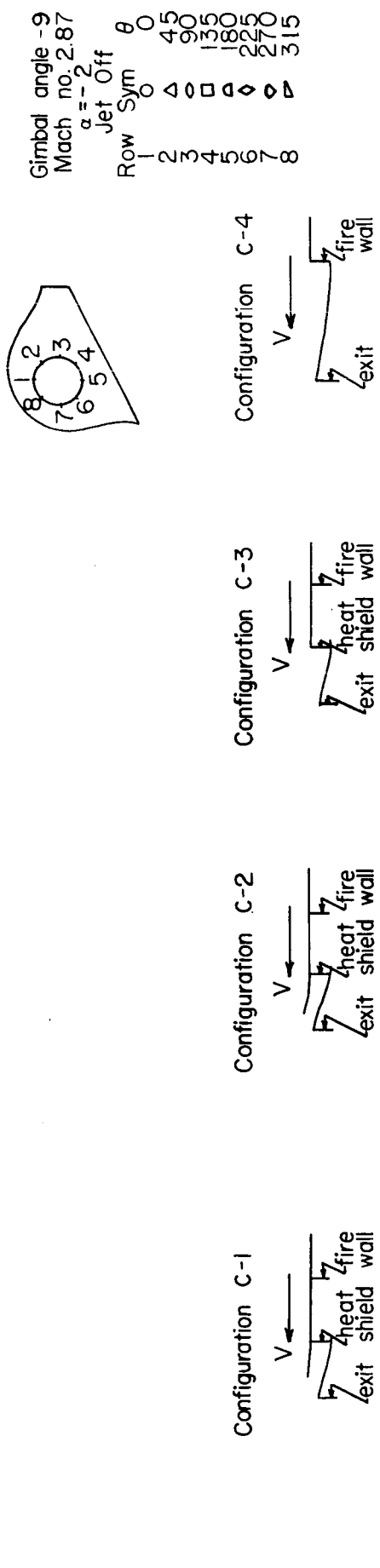


Figure 30b Pressure distribution over the surface of a nozzle with various shroud configurations

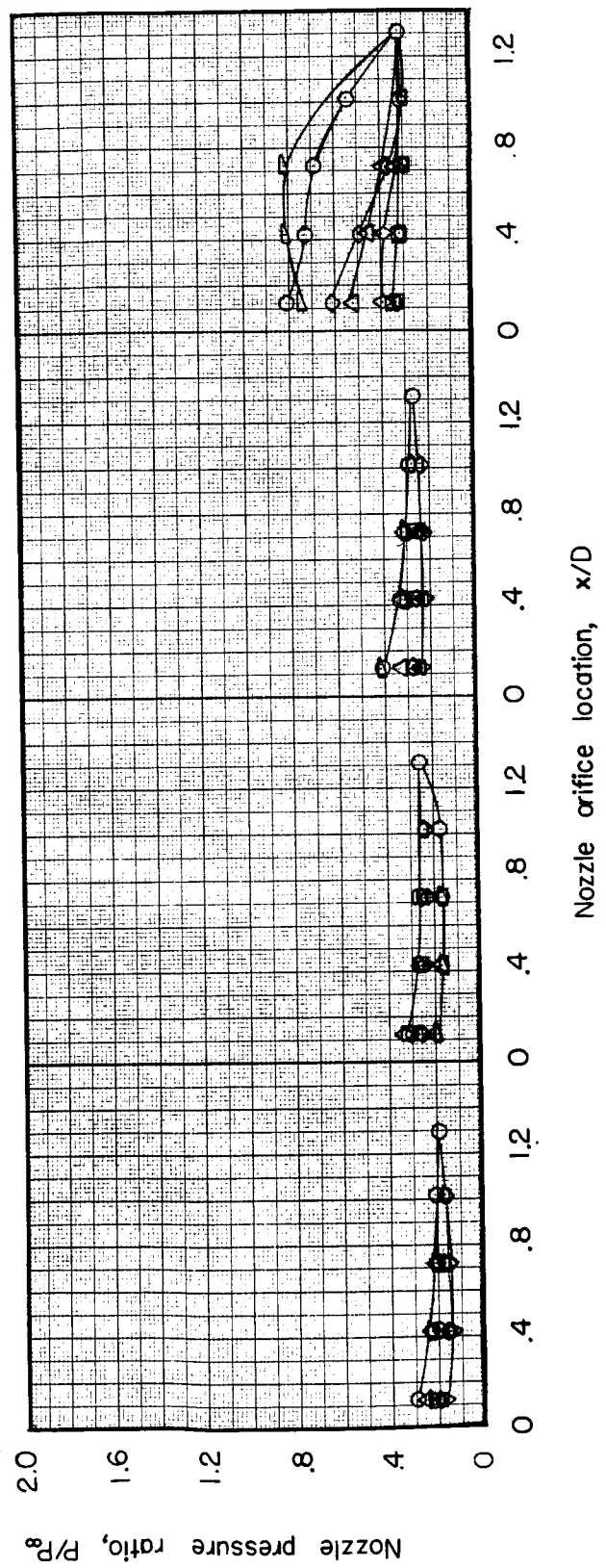
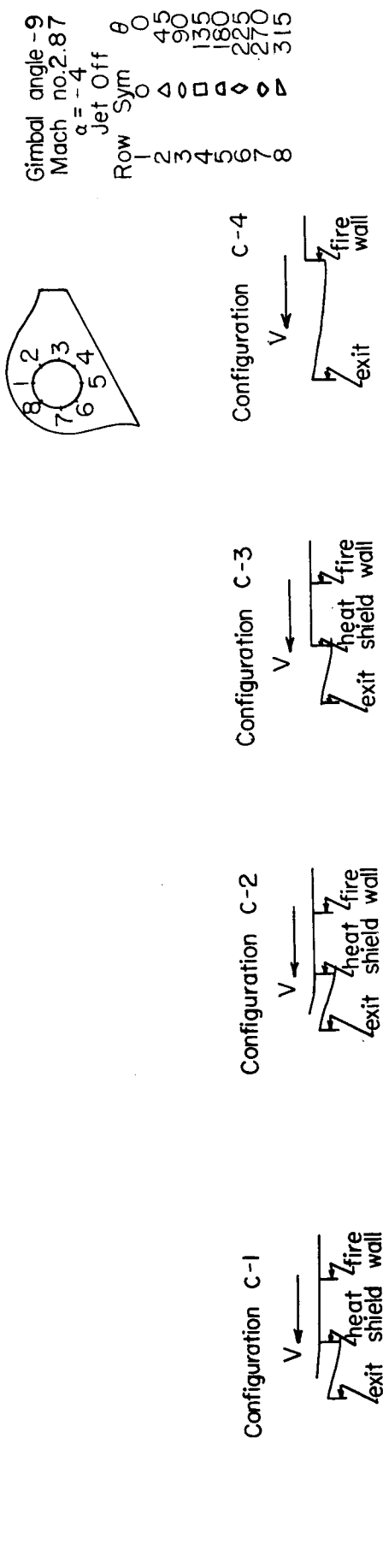
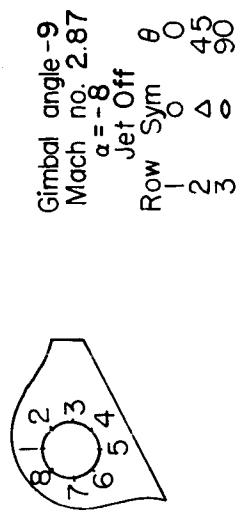


Figure 30c Pressure distribution over the surface of a nozzle with various shroud configurations



Configuration C-1      Configuration C-2      Configuration C-3      Configuration C-4

Configuration C-1: Shows the nozzle exit at the bottom left, a fire wall at the top right, and a heat shield wall extending from the fire wall towards the exit. Flow direction is indicated by an arrow labeled  $V \leftarrow$ .

Configuration C-2: Similar to C-1, but the heat shield wall is shorter and positioned closer to the nozzle exit.

Configuration C-3: The heat shield wall is longer and extends further towards the nozzle exit.

Configuration C-4: The heat shield wall is very long, nearly reaching the nozzle exit.

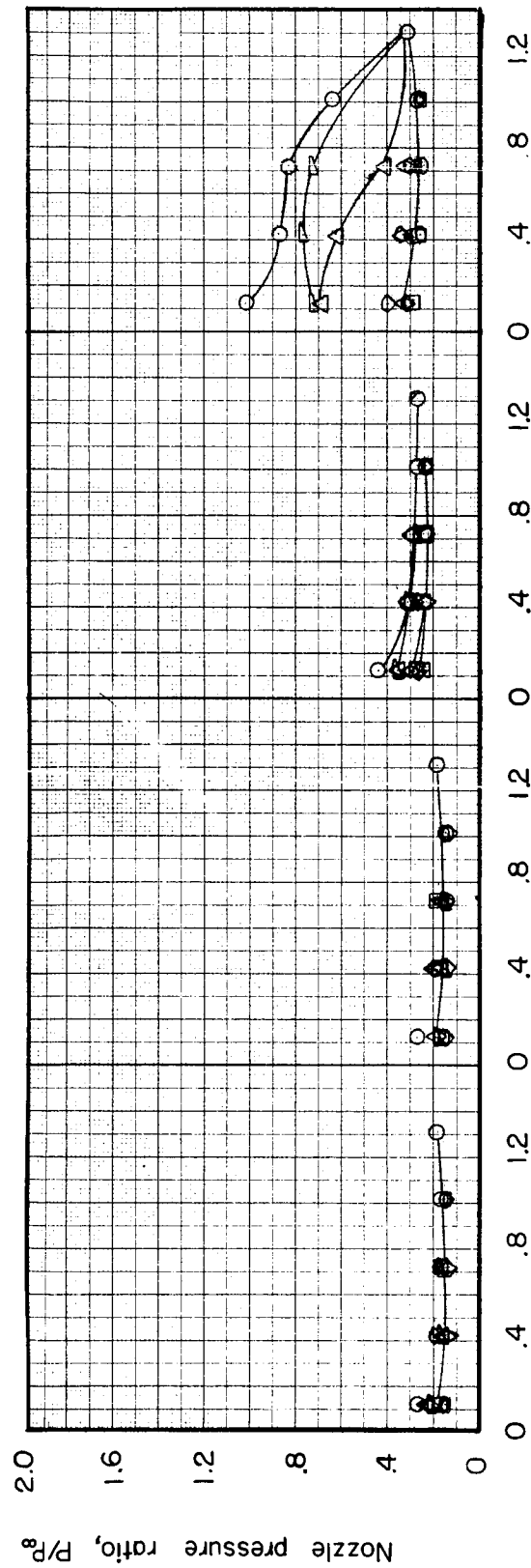


Figure 30d Pressure distribution over the surface of a nozzle with various shroud configurations

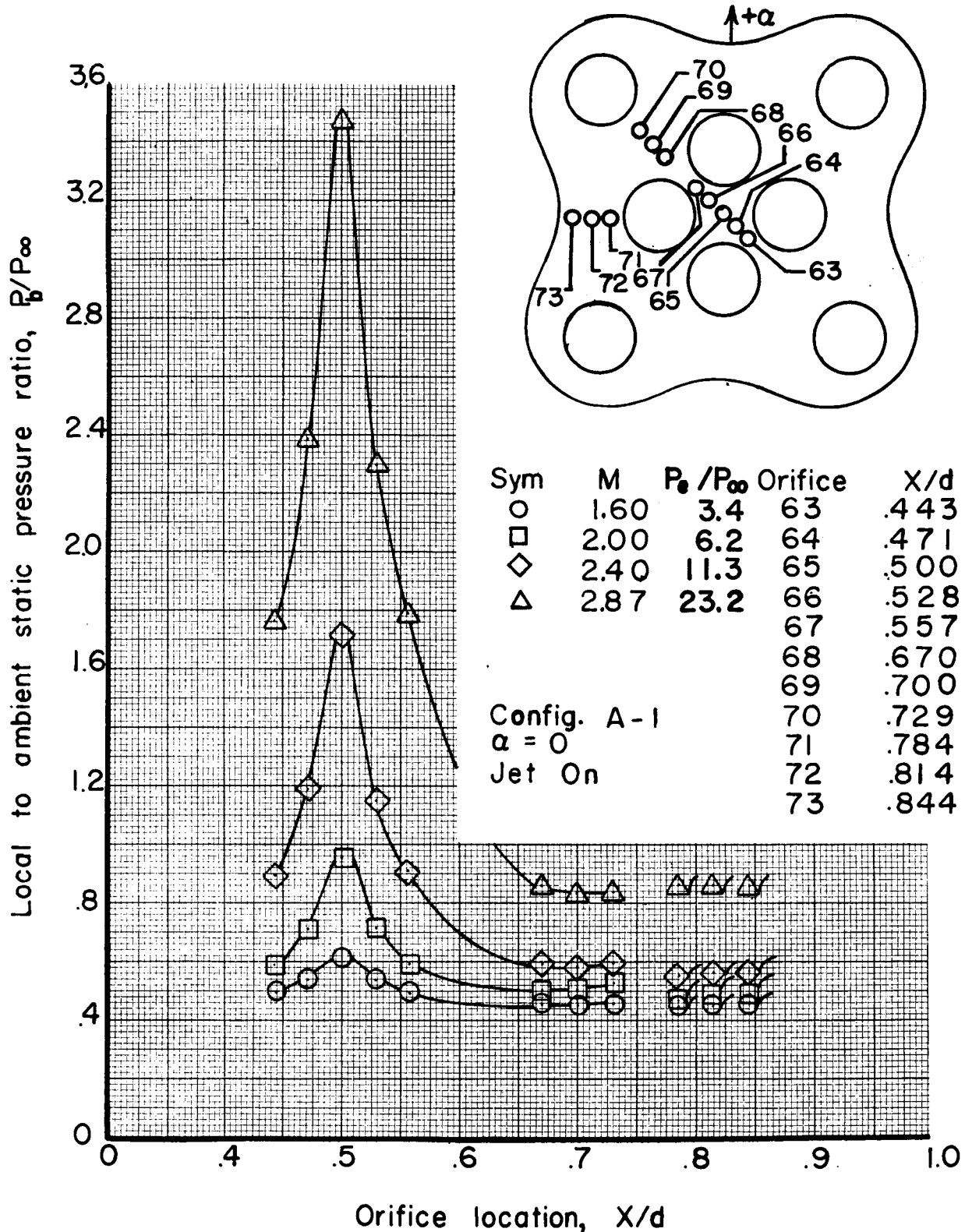


Figure 31a Effect of Mach number on star and base pressure ratios at various  $X/d$ 's

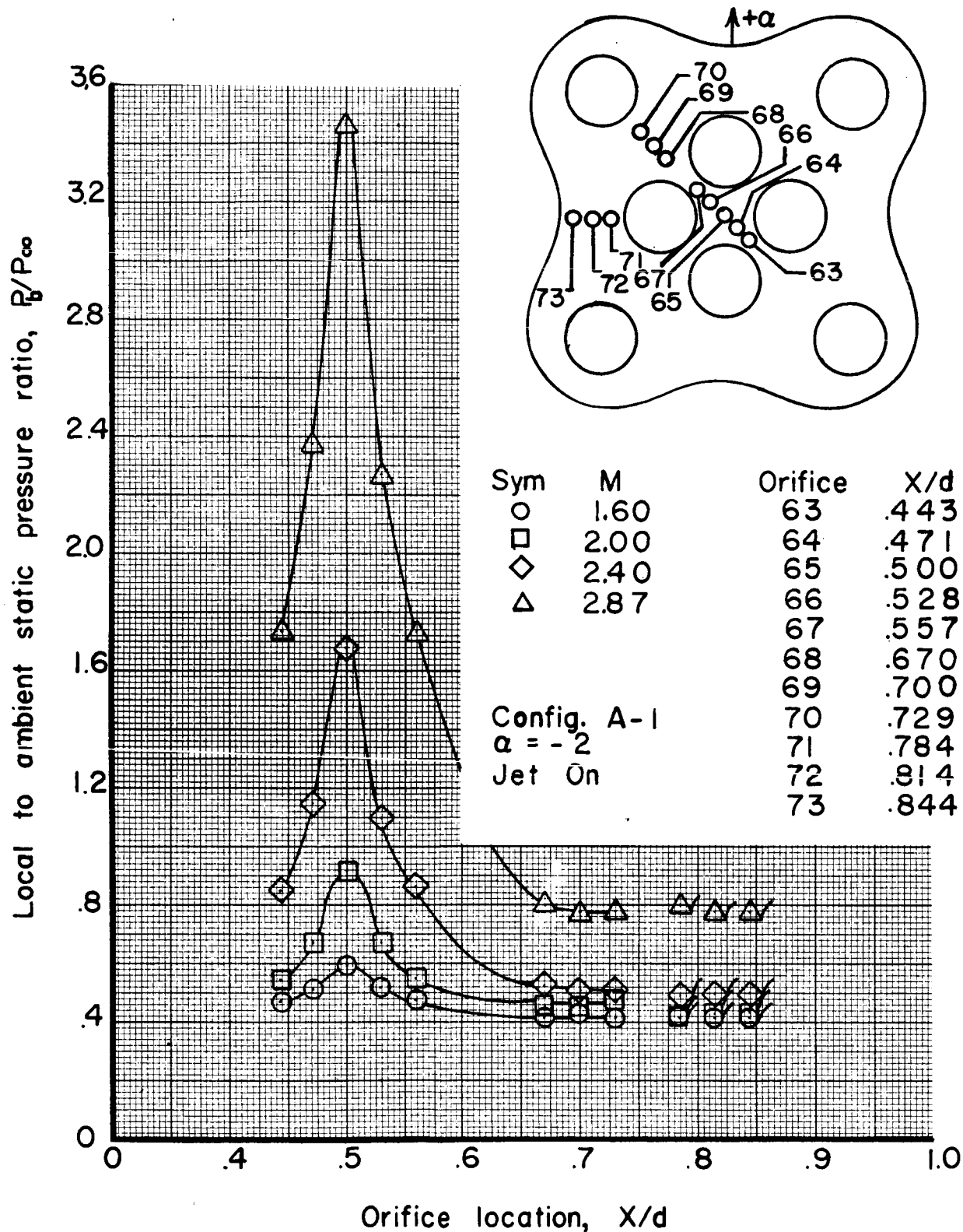


Figure 31b Effect of Mach number on star and base pressure ratios at various  $X/d$ 's

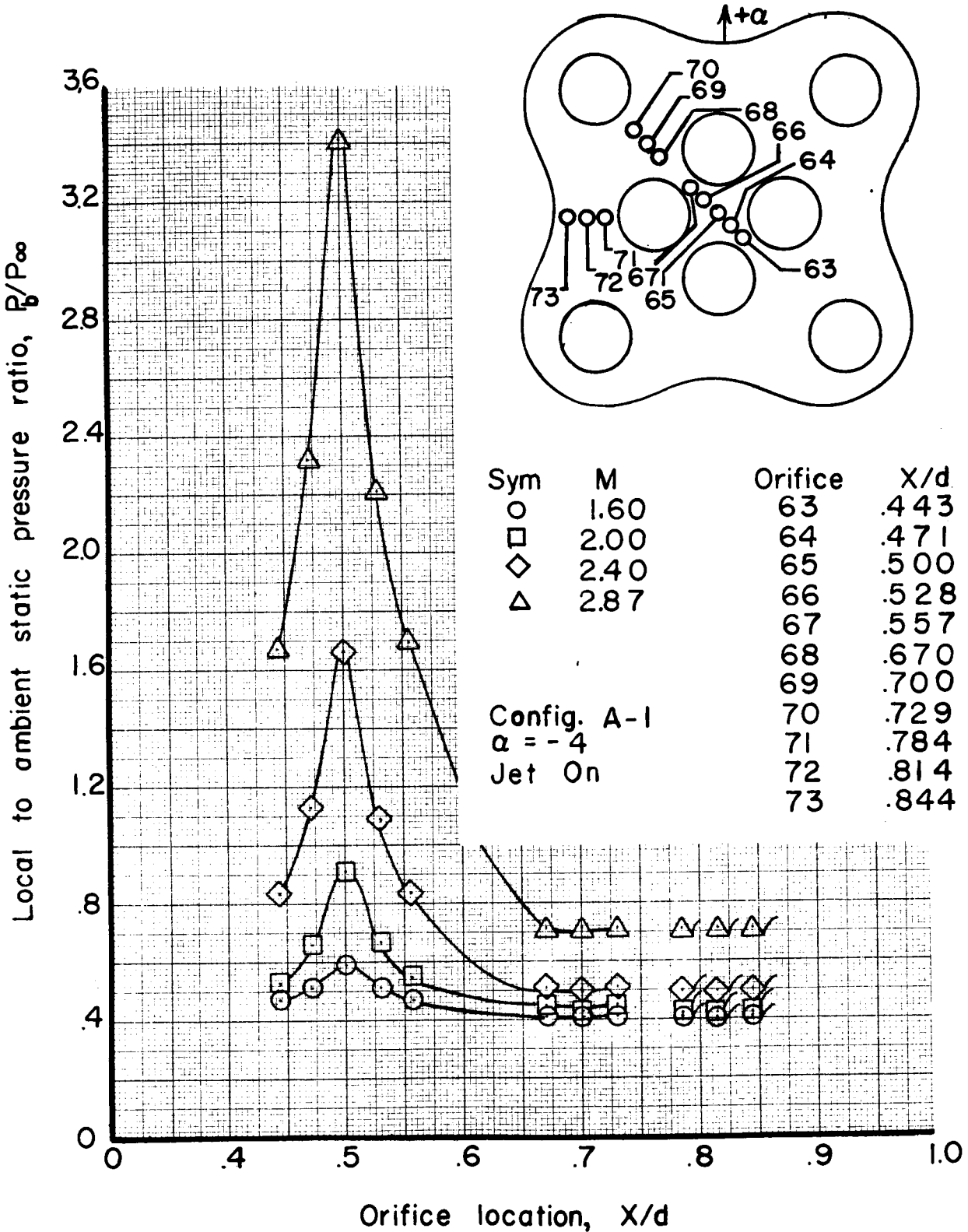


Figure 31c Effect of Mach number on star and base pressure ratios at various  $X/d$ 's

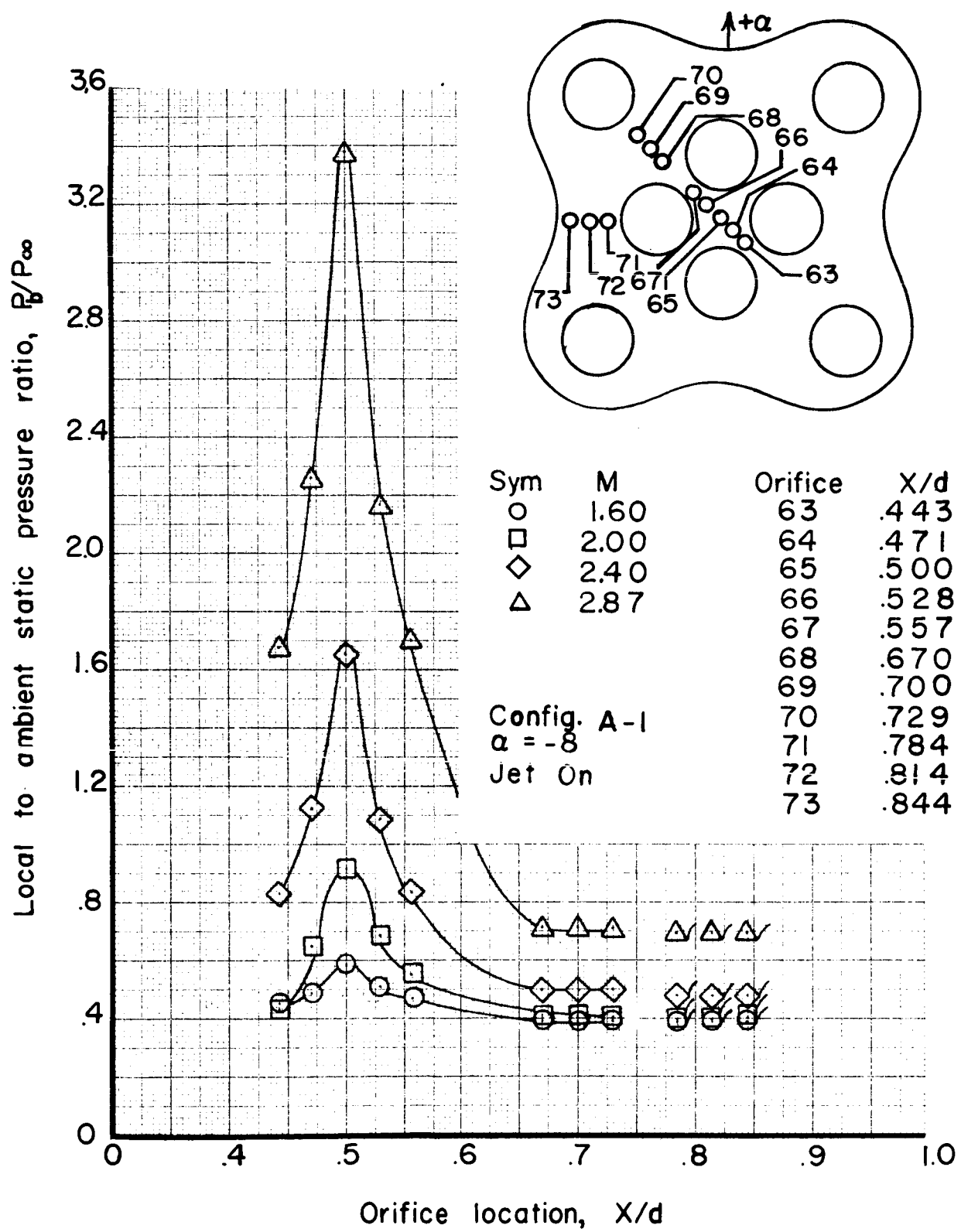


Figure 31d Effect of Mach number on star and base pressure ratios at various  $X/d$ 's

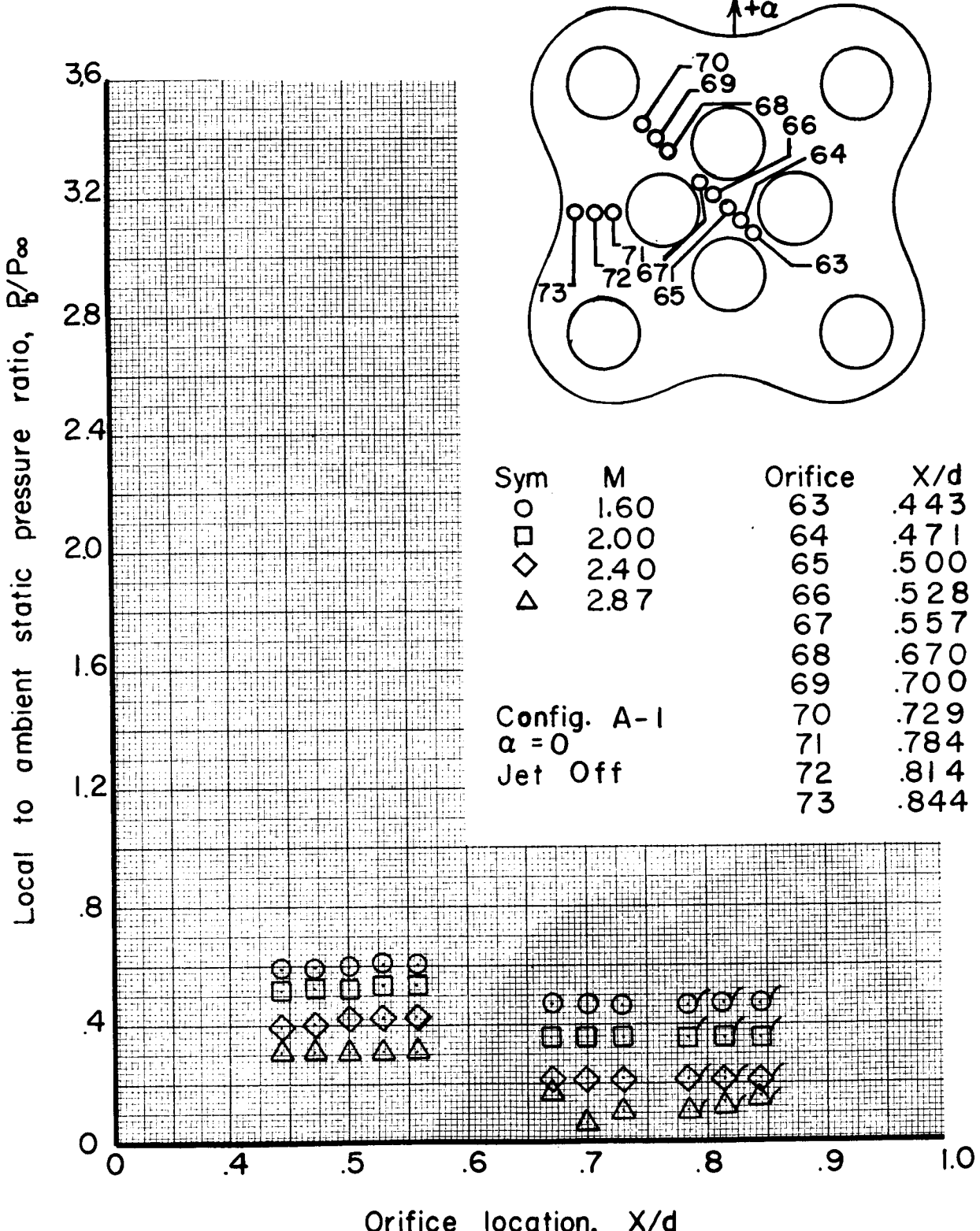


Figure 32a Effect of Mach number on star and base pressure ratios at various  $X/d$ 's

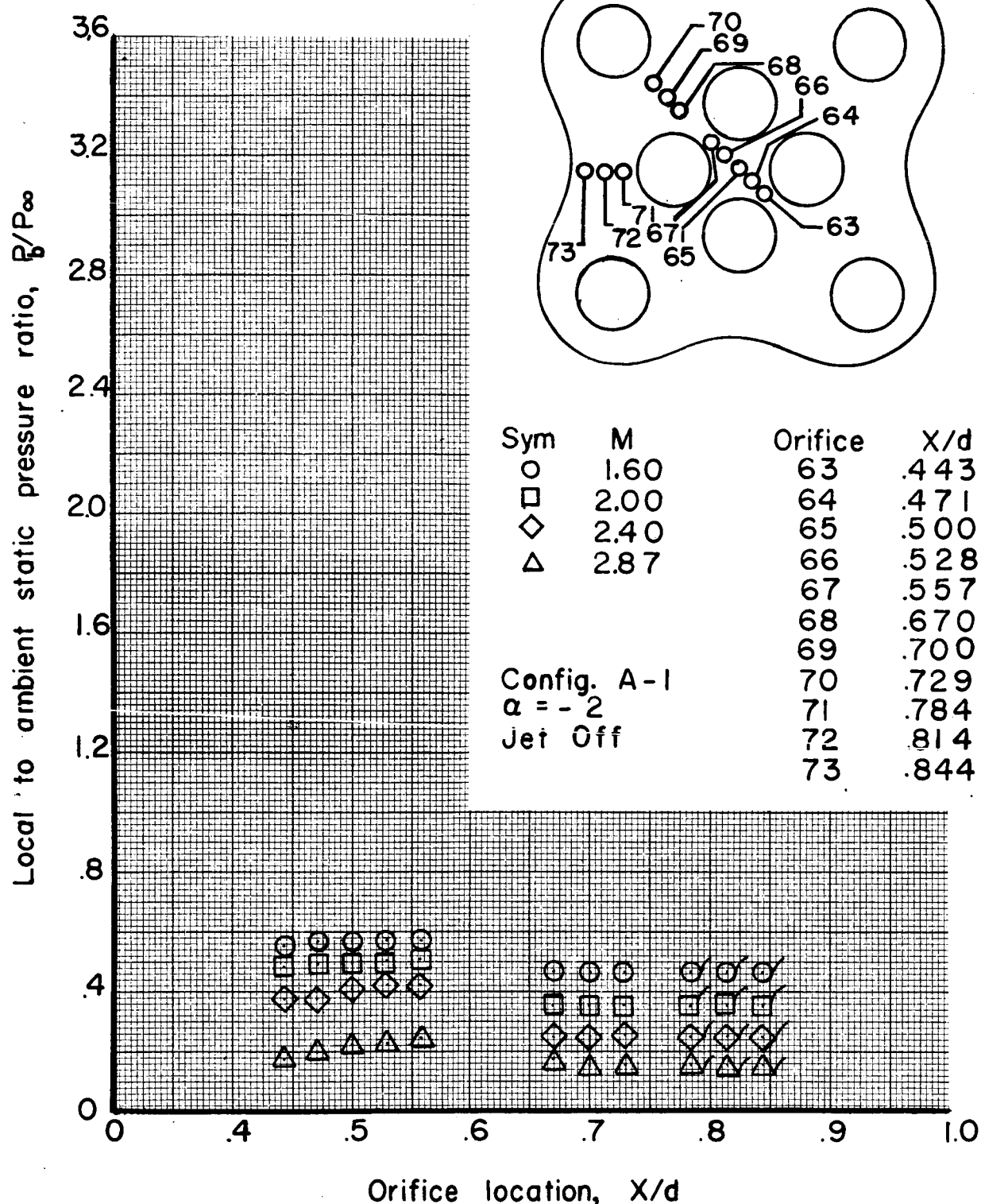


Figure 32b Effect of Mach number on star and base pressure ratios at various  $X/d$ 's

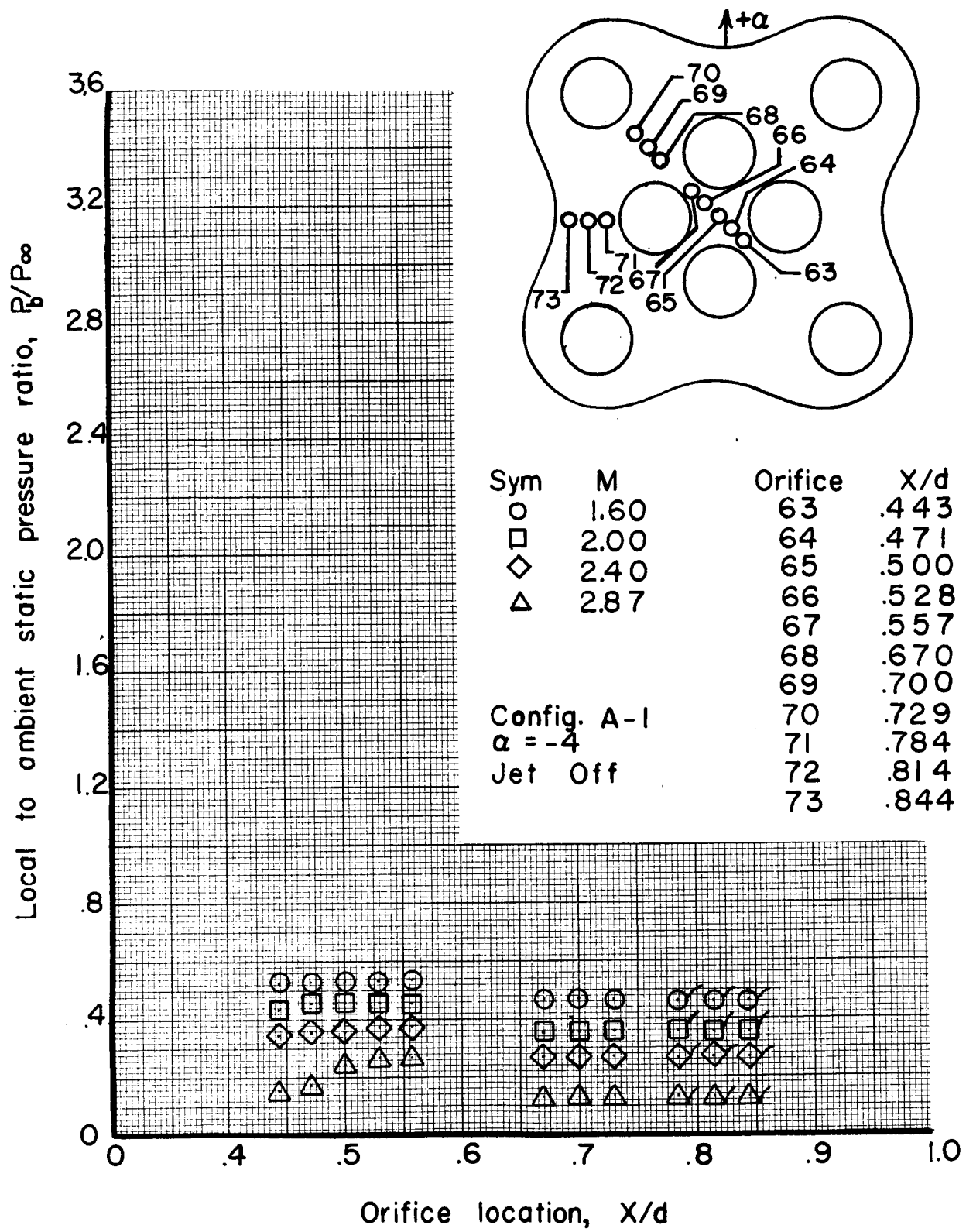


Figure 32c Effect of Mach number on star and base pressure ratios at various  $X/d$ 's

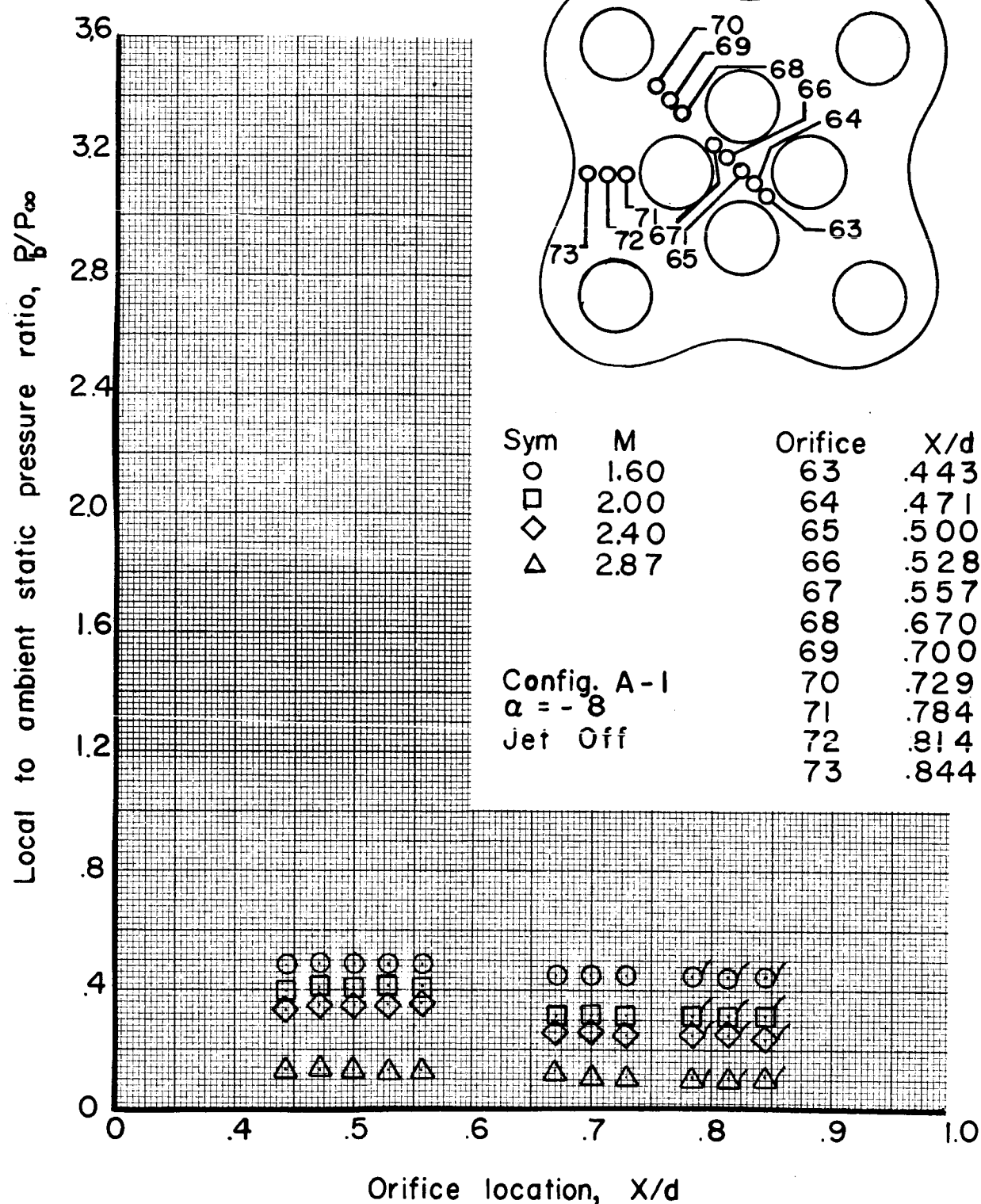


Figure 32d Effect of Mach number on star and base pressure ratios at various  $X/d$ 's

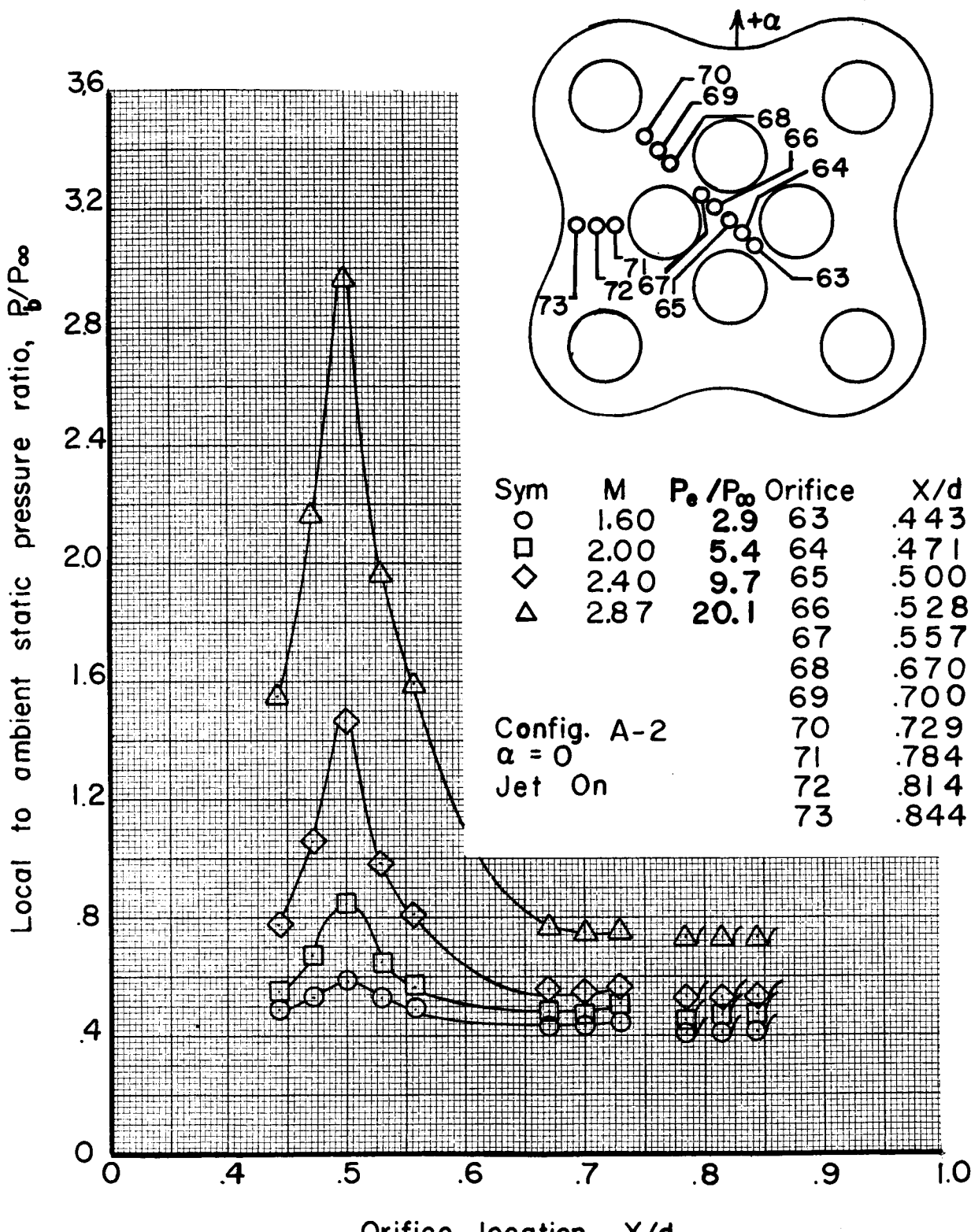


Figure 33a Effect of Mach number on star and base pressure ratios at various  $X/d$ 's

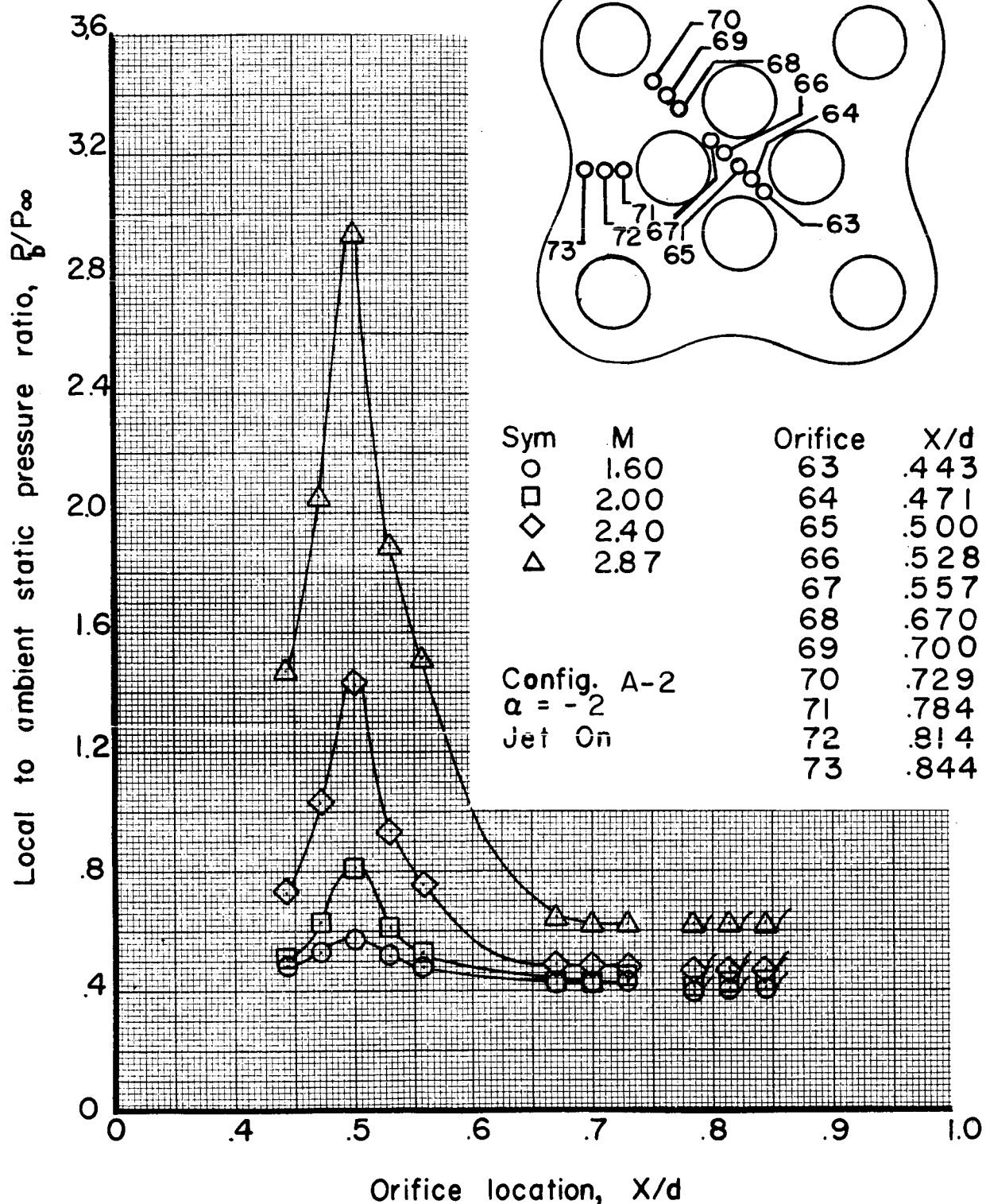


Figure 33b Effect of Mach number on star and base pressure ratios at various  $X/d$ 's

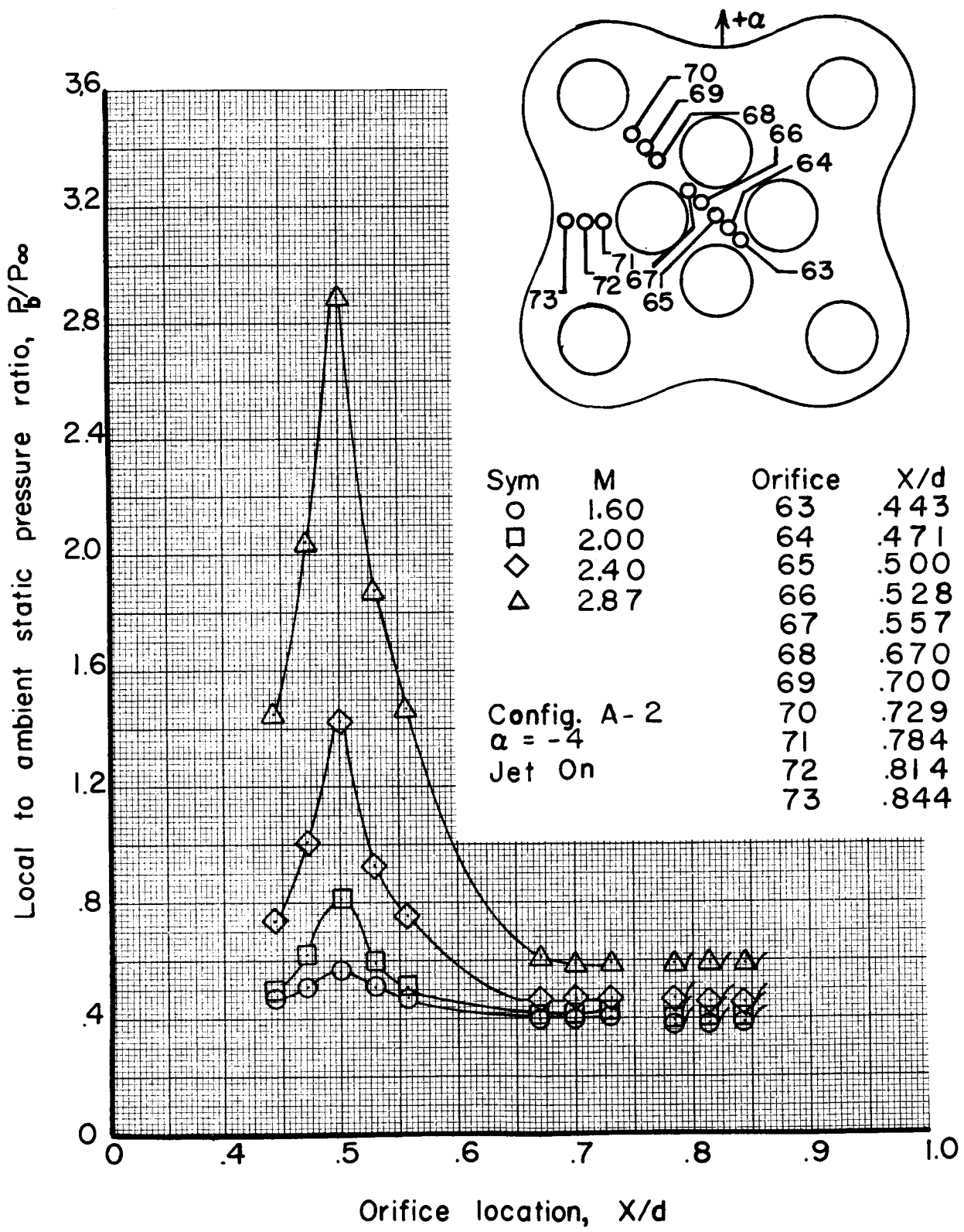


Figure 33c Effect of Mach number on star and base pressure ratios at various  $X/d$ 's

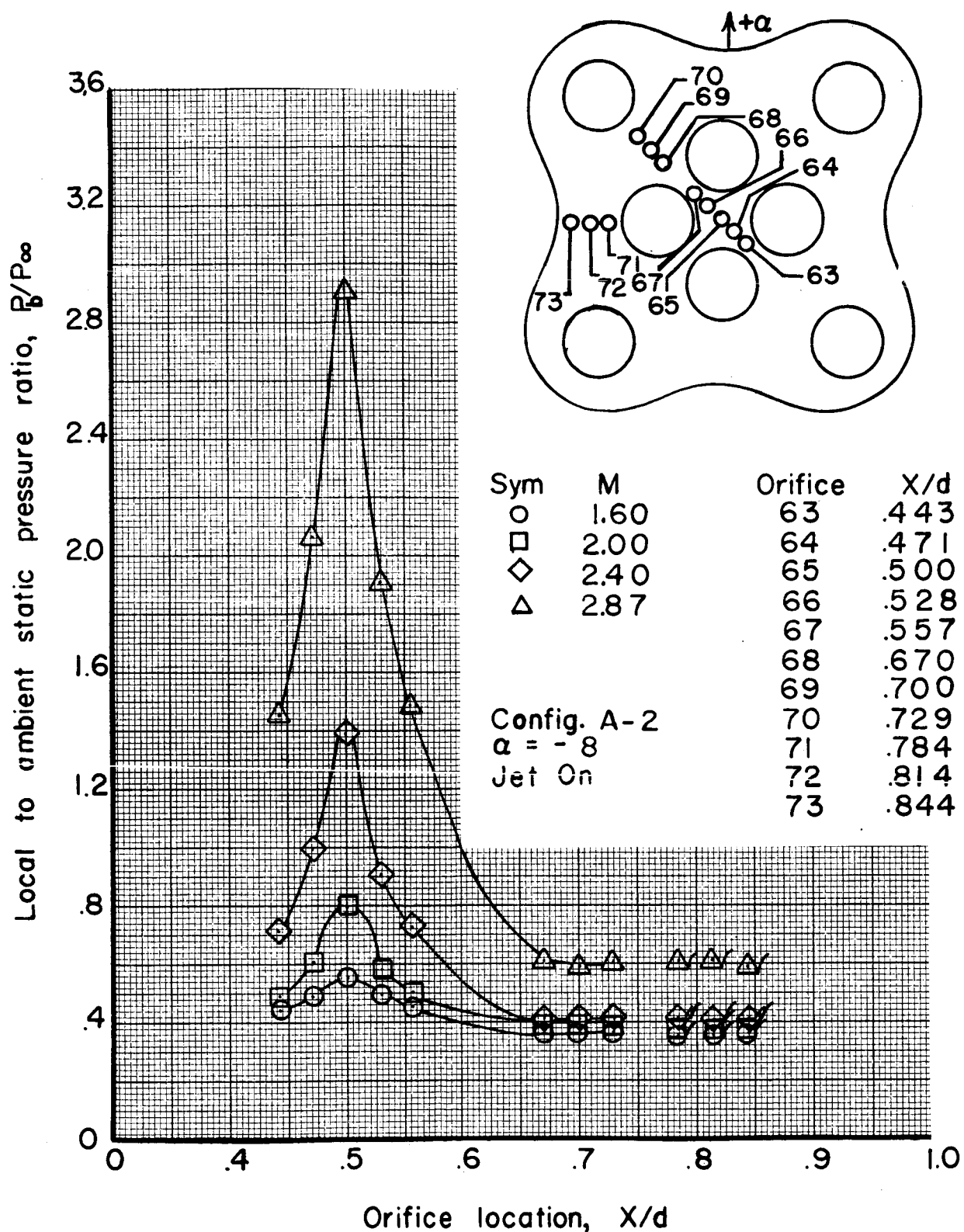


Figure 33d Effect of Mach number on star and base pressure ratios at various  $X/d$ 's

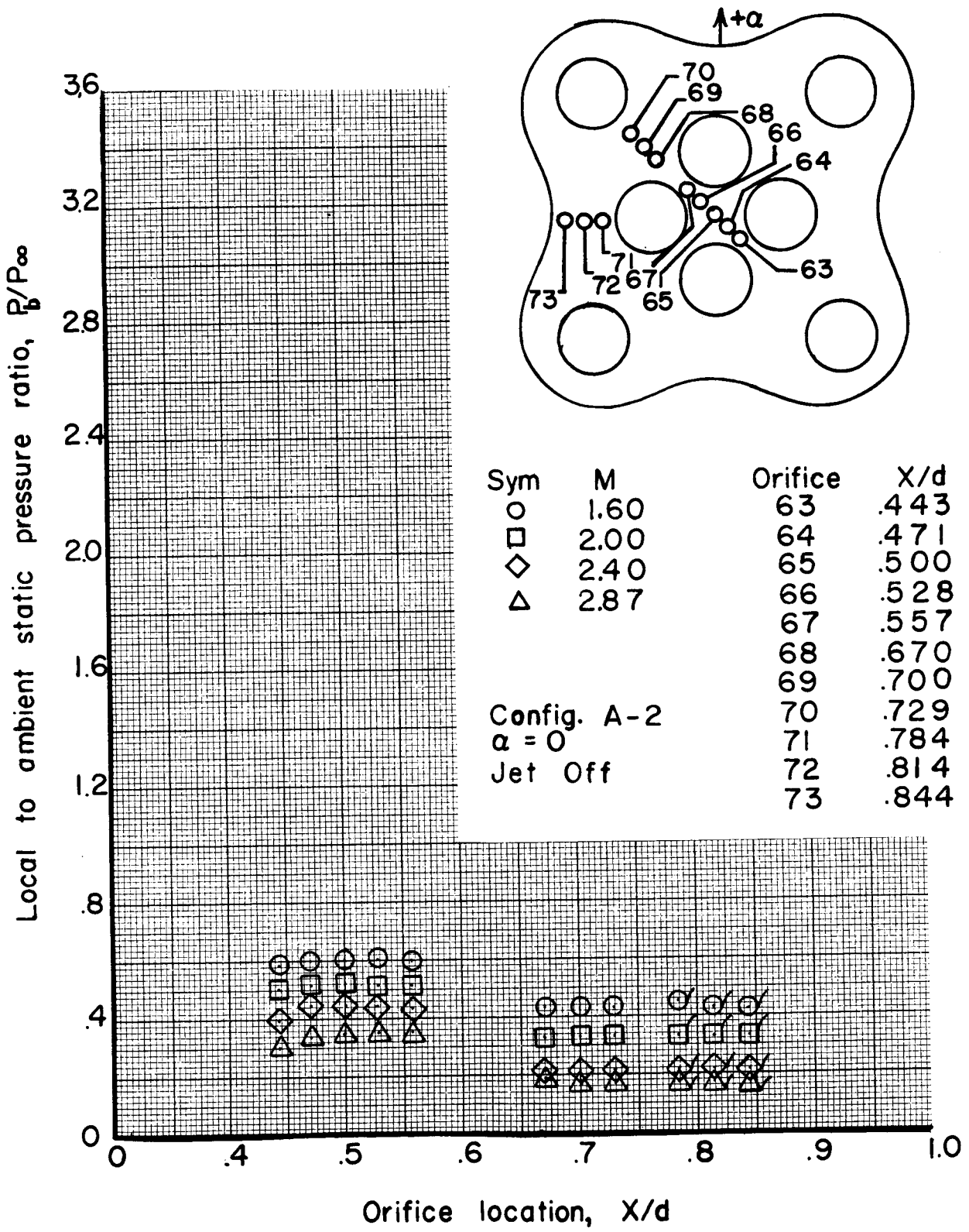


Figure 34a Effect of Mach number on star and base pressure ratios at various  $X/d$ 's

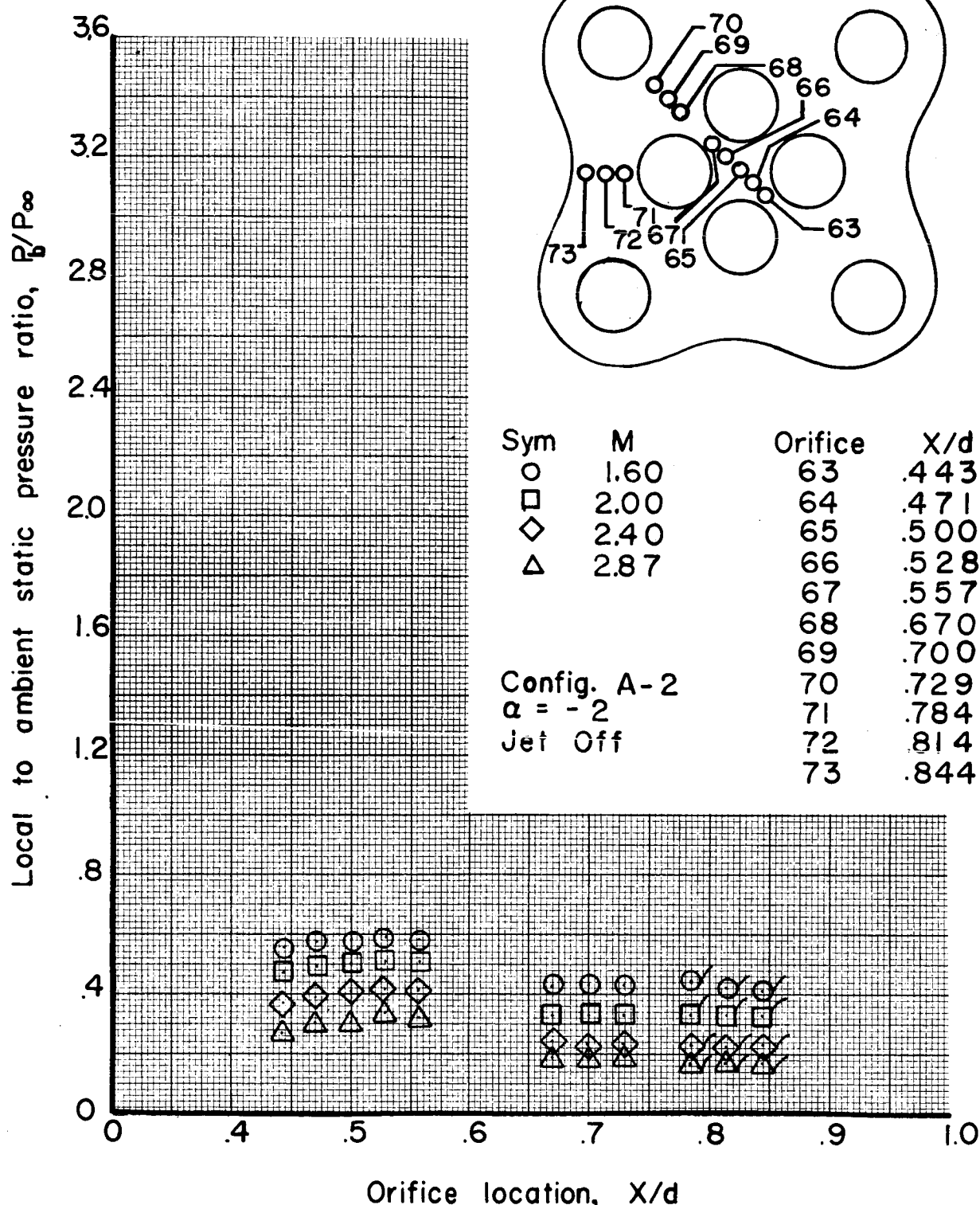


Figure 34b Effect of Mach number on star and base  
pressure ratios at various  $X/d$ 's

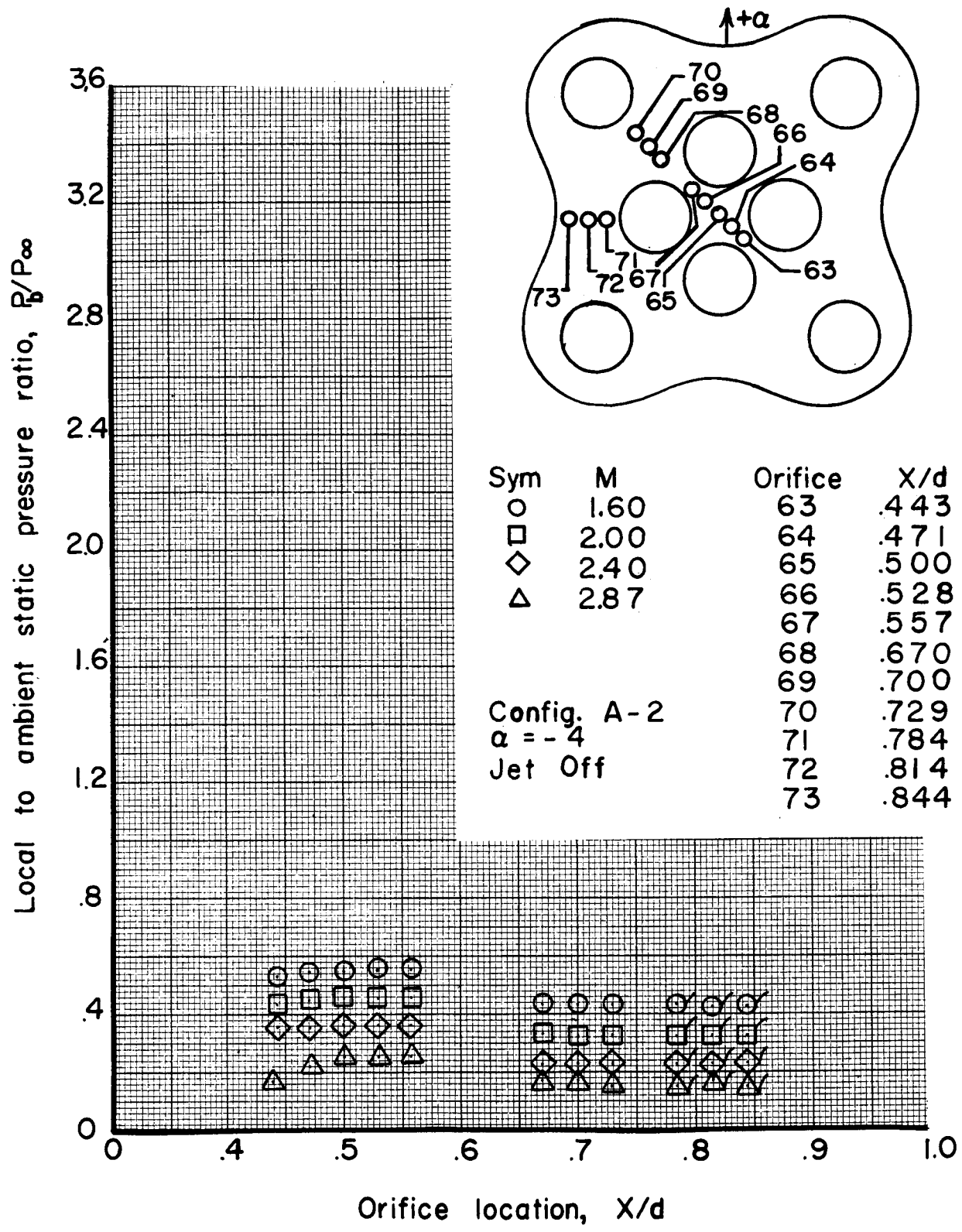


Figure 34c Effect of Mach number on star and base pressure ratios at various  $X/d$ 's

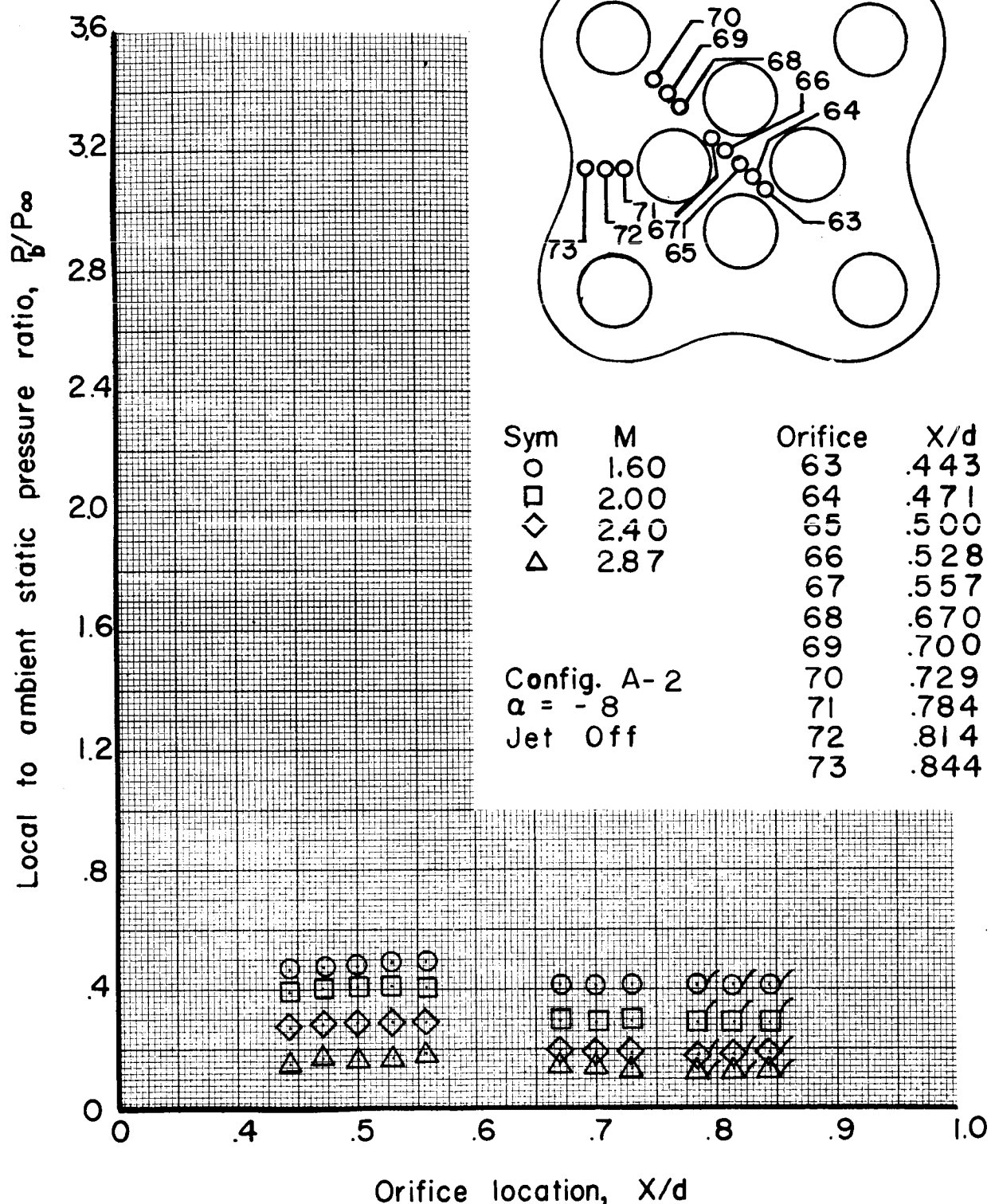


Figure 34d Effect of Mach number on star and base pressure ratios at various  $X/d$ 's

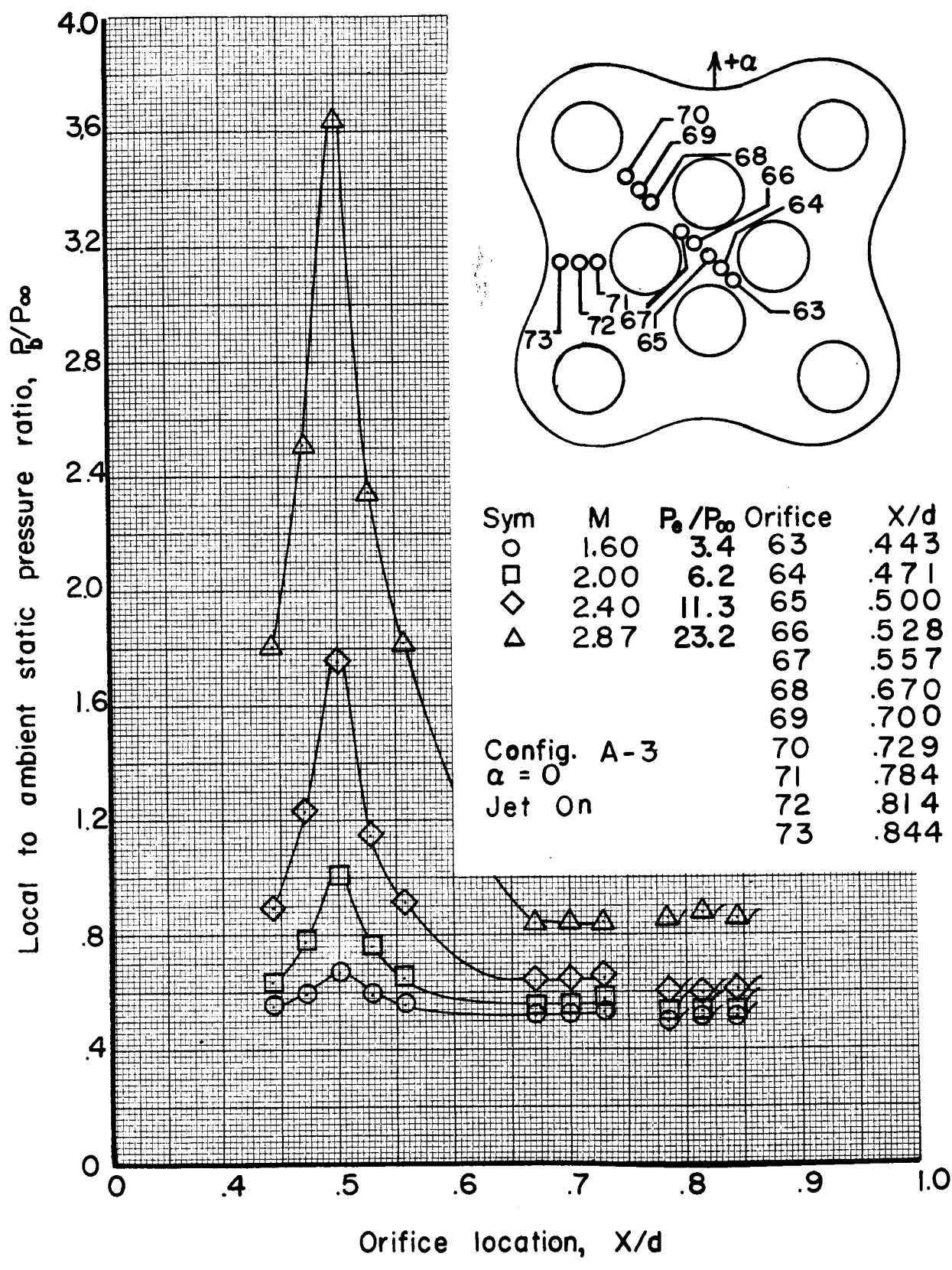


Figure 35a Effect of Mach number on star and base pressure ratios at various  $X/d$ 's

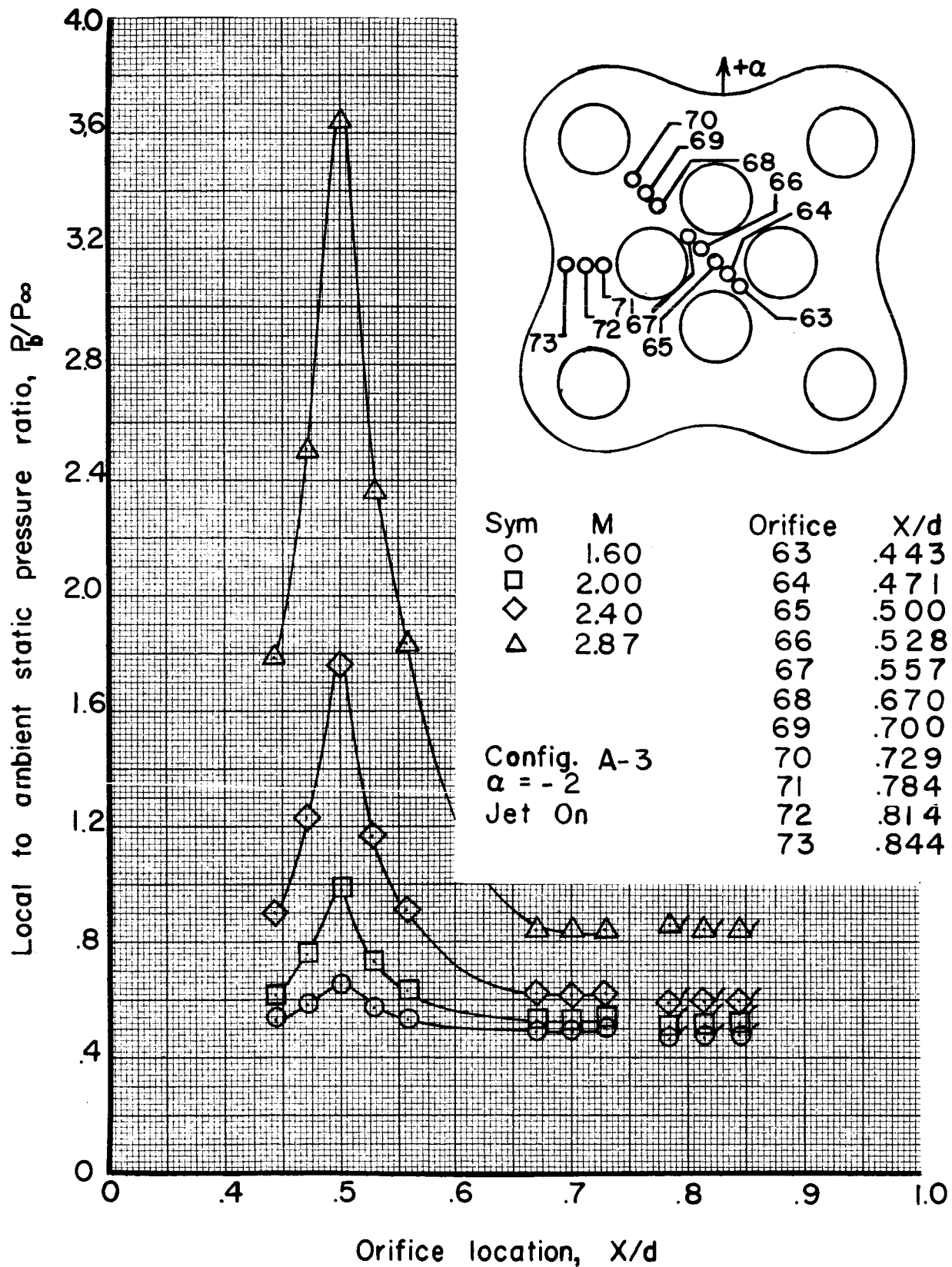


Figure 35b Effect of Mach number on star and base pressure ratios at various  $X/d$ 's

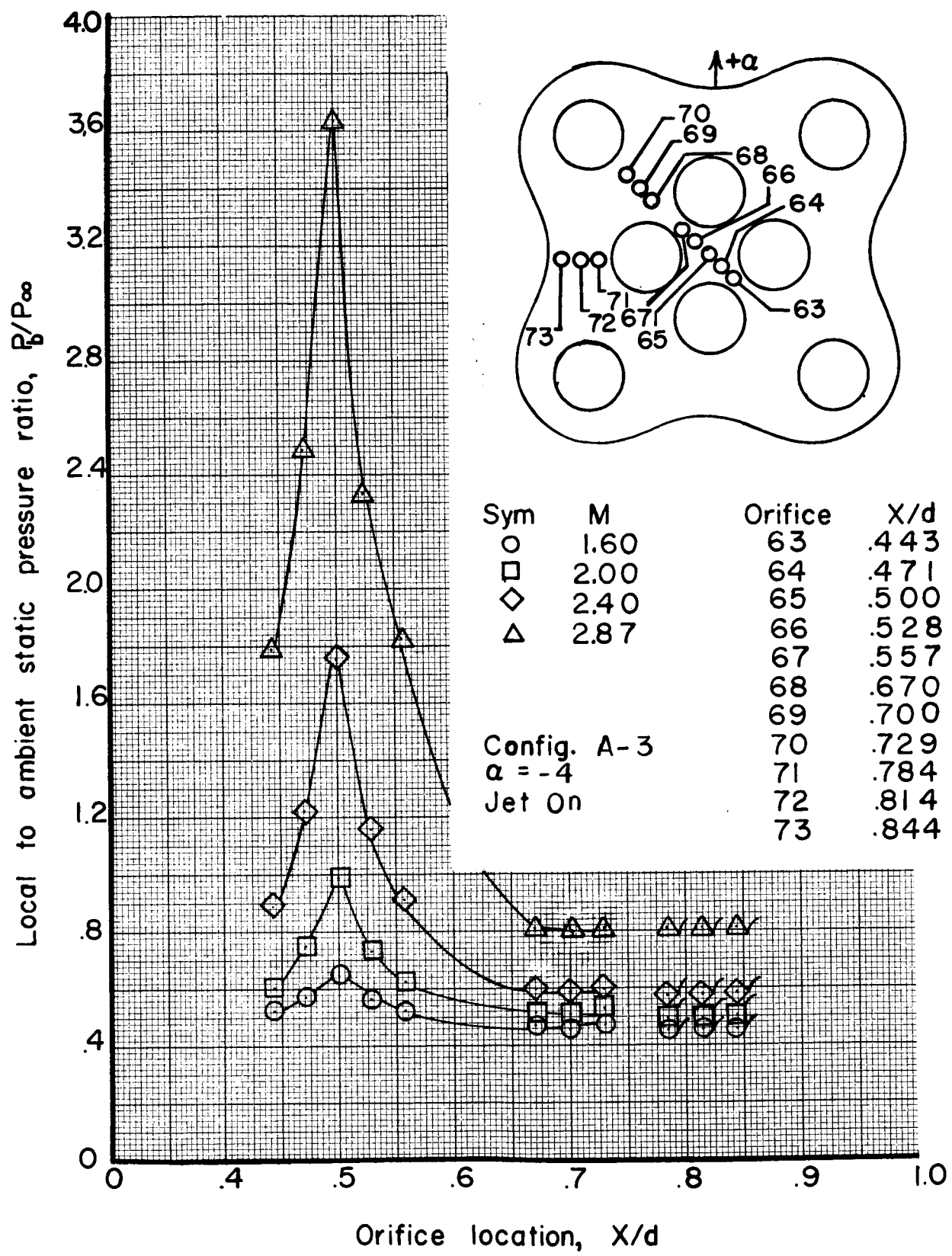


Figure 35c Effect of Mach number on star and base pressure ratios at various  $X/d$ 's

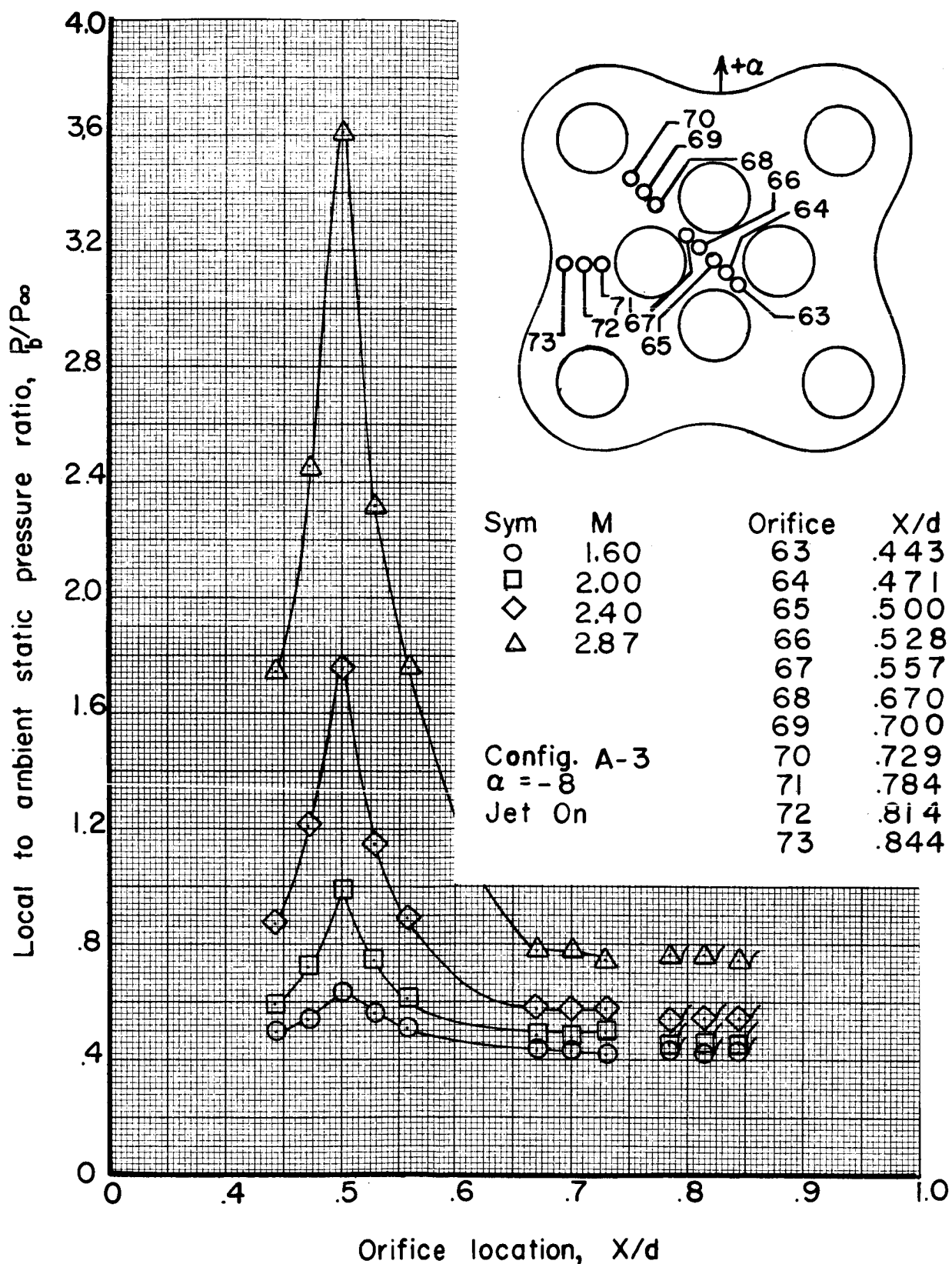


Figure 35d Effect of Mach number on star and base pressure ratios at various  $X/d$ 's

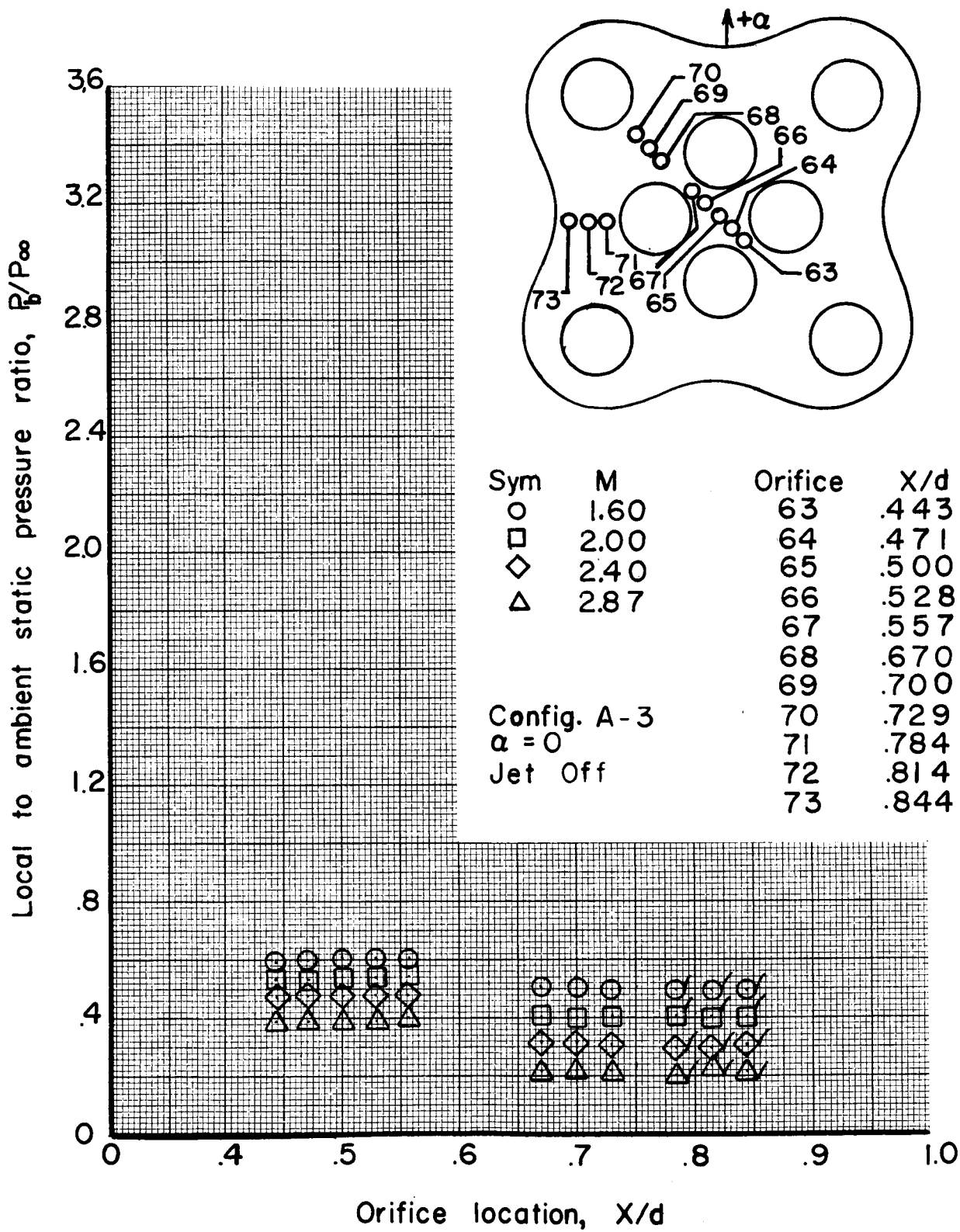


Figure 36a Effect of Mach number on star and base  
pressure ratios at various  $X/d$ 's

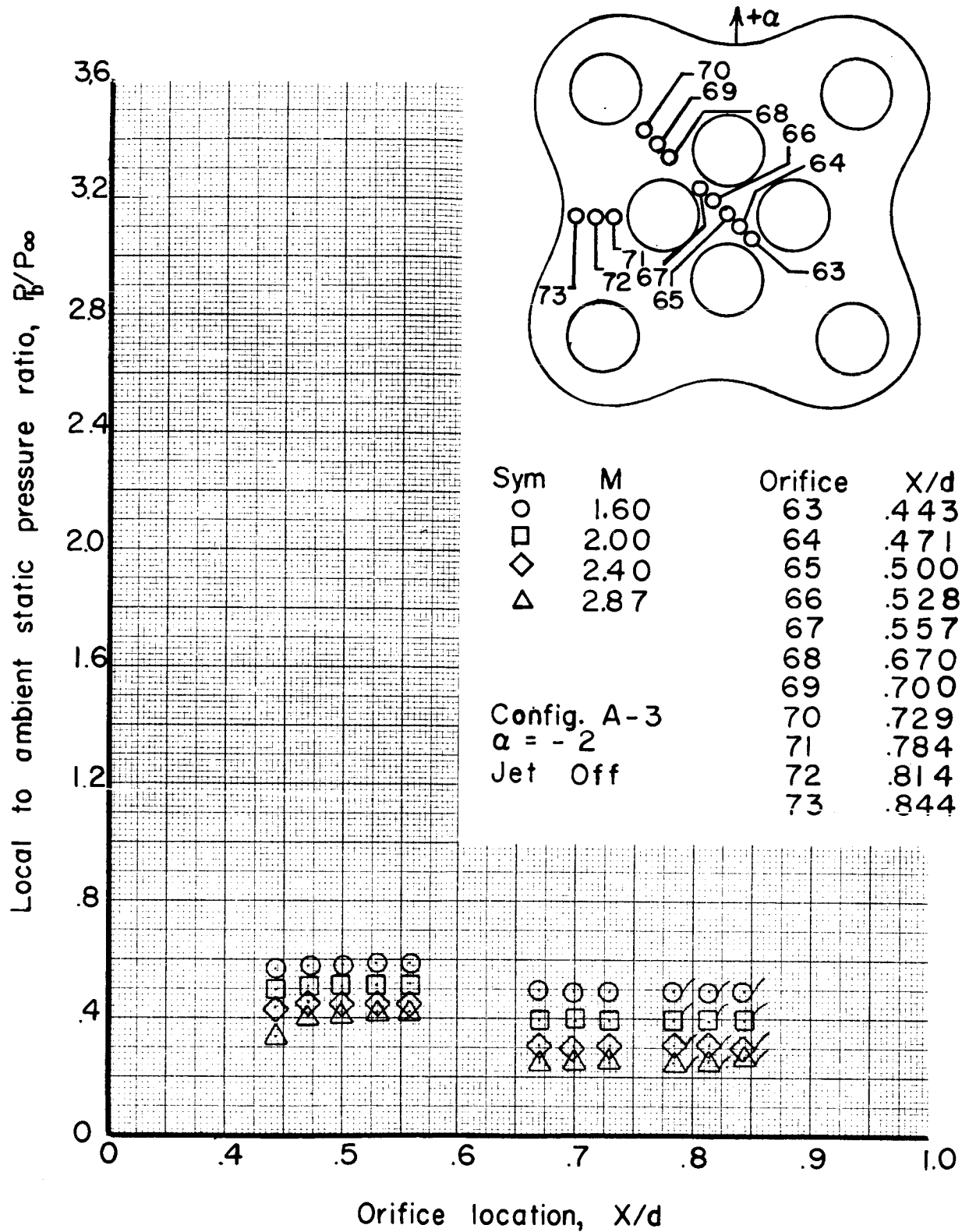


Figure 36b Effect of Mach number on star and base pressure ratios at various  $X/d$ 's

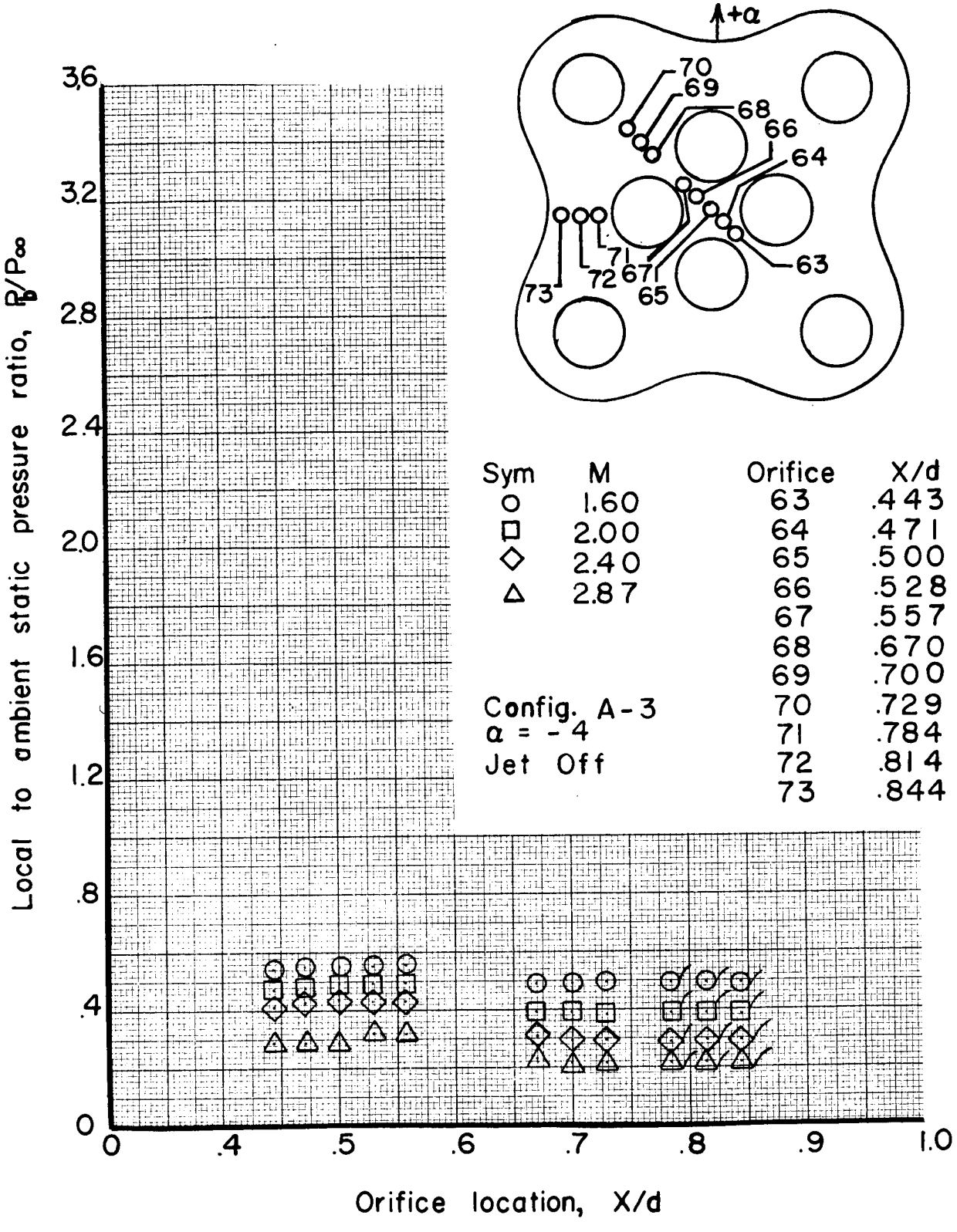


Figure 36c Effect of Mach number on star and base pressure ratios at various  $X/d$ 's

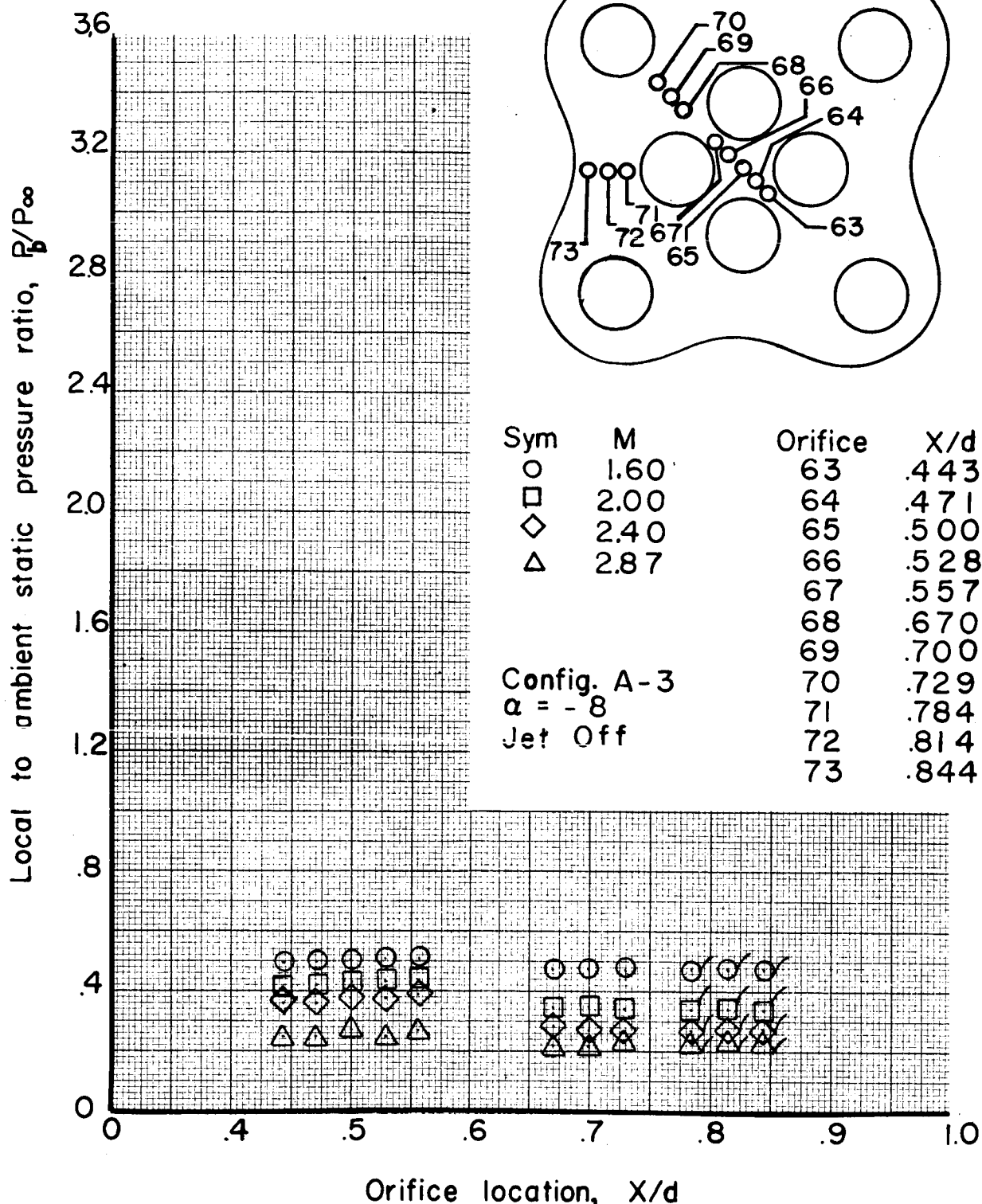


Figure 36d Effect of Mach number on star and base pressure ratios at various  $X/d$ 's

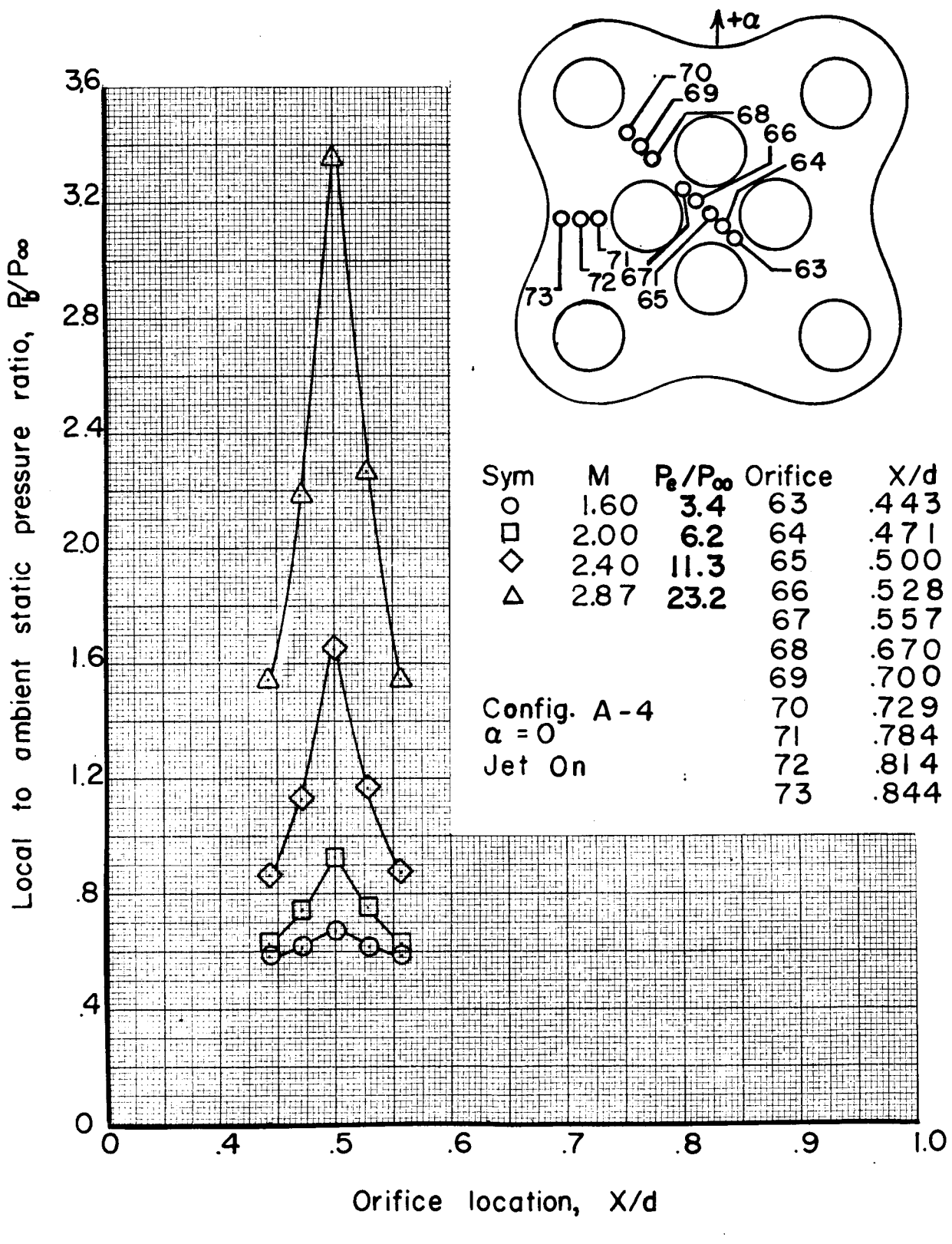


Figure 37a Effect of Mach number on star and base pressure ratios at various  $X/d$ 's

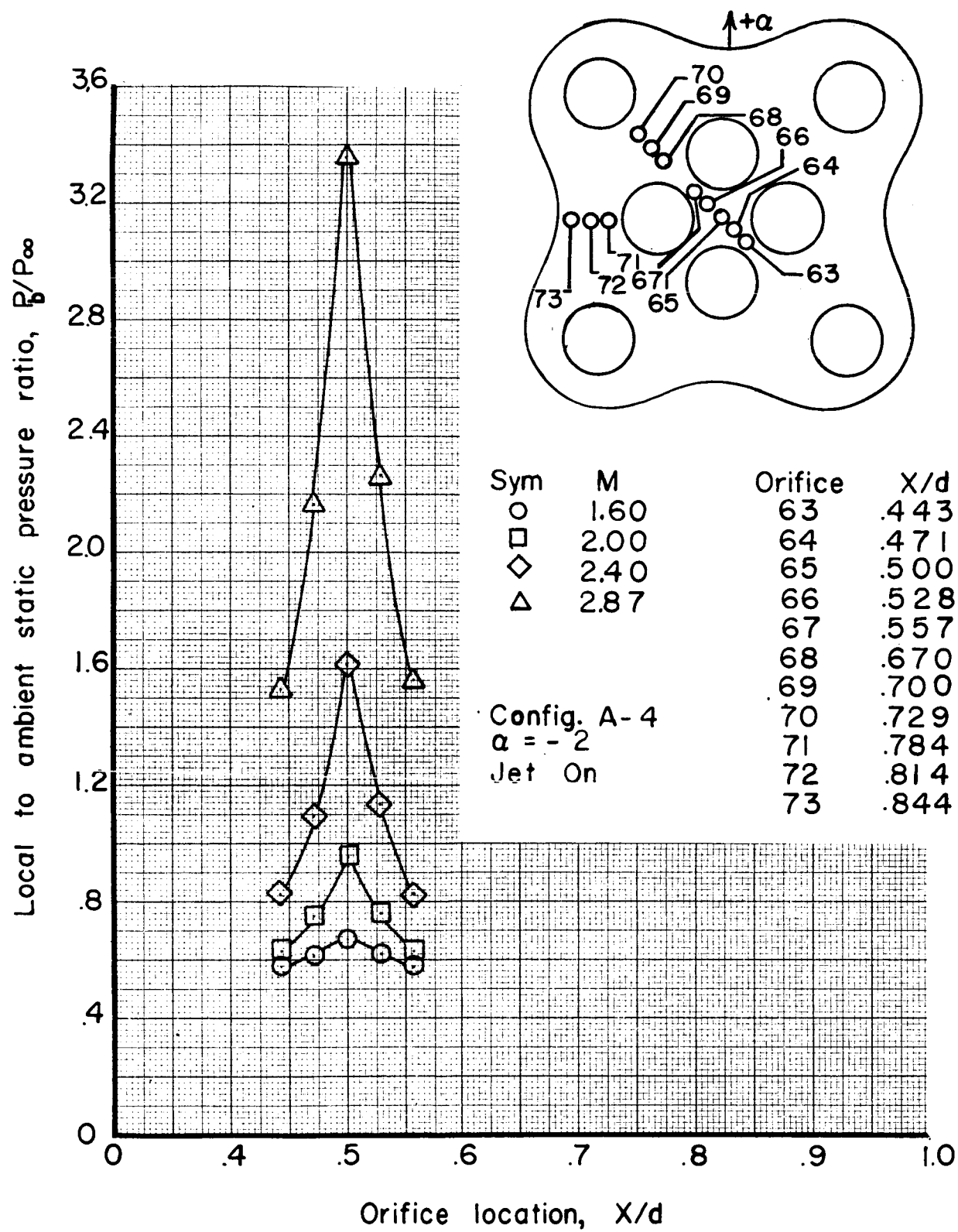


Figure 37b Effect of Mach number on star and base pressure ratios at various  $X/d$ 's

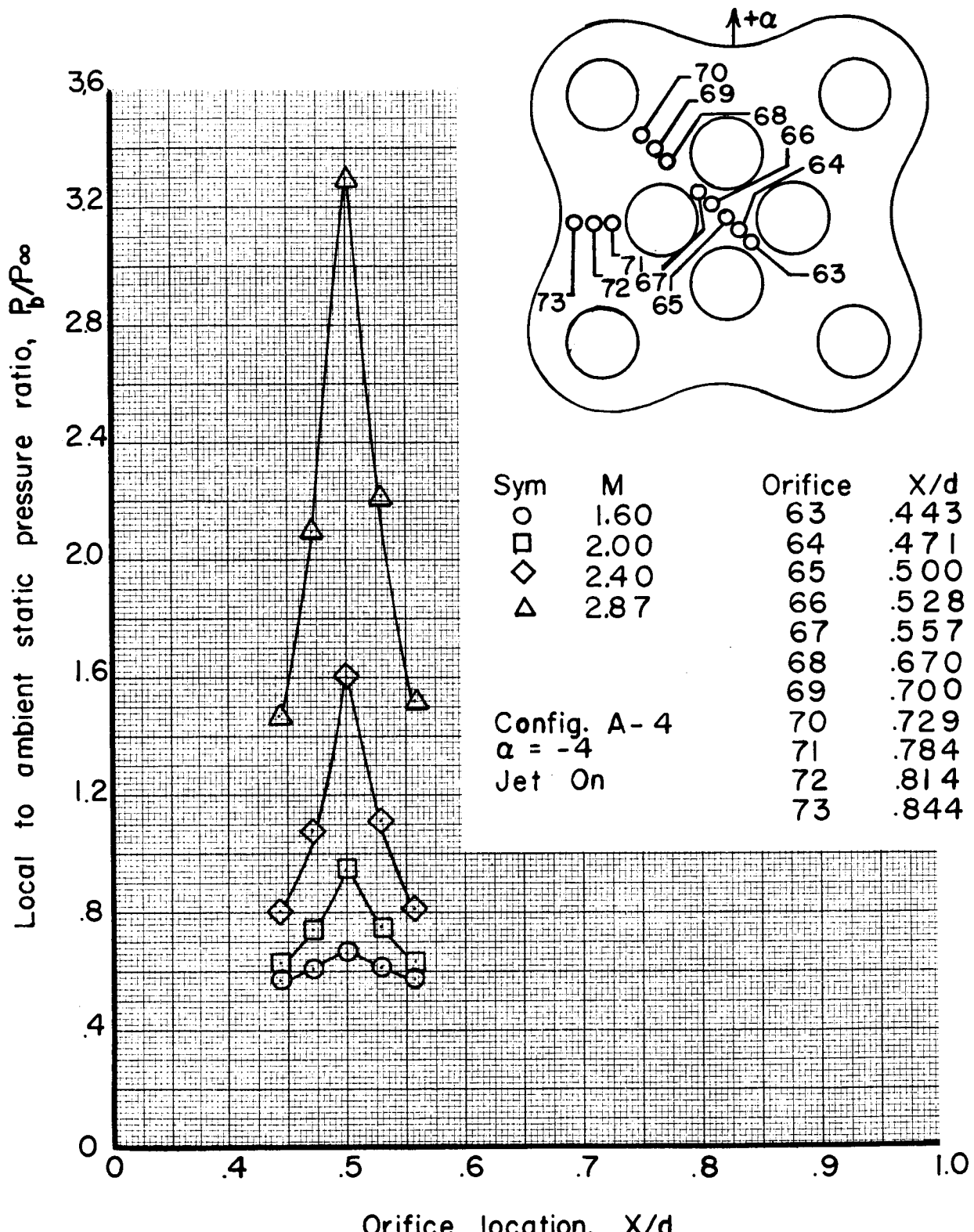


Figure 37c Effect of Mach number on star and base pressure ratios at various  $X/d$ 's

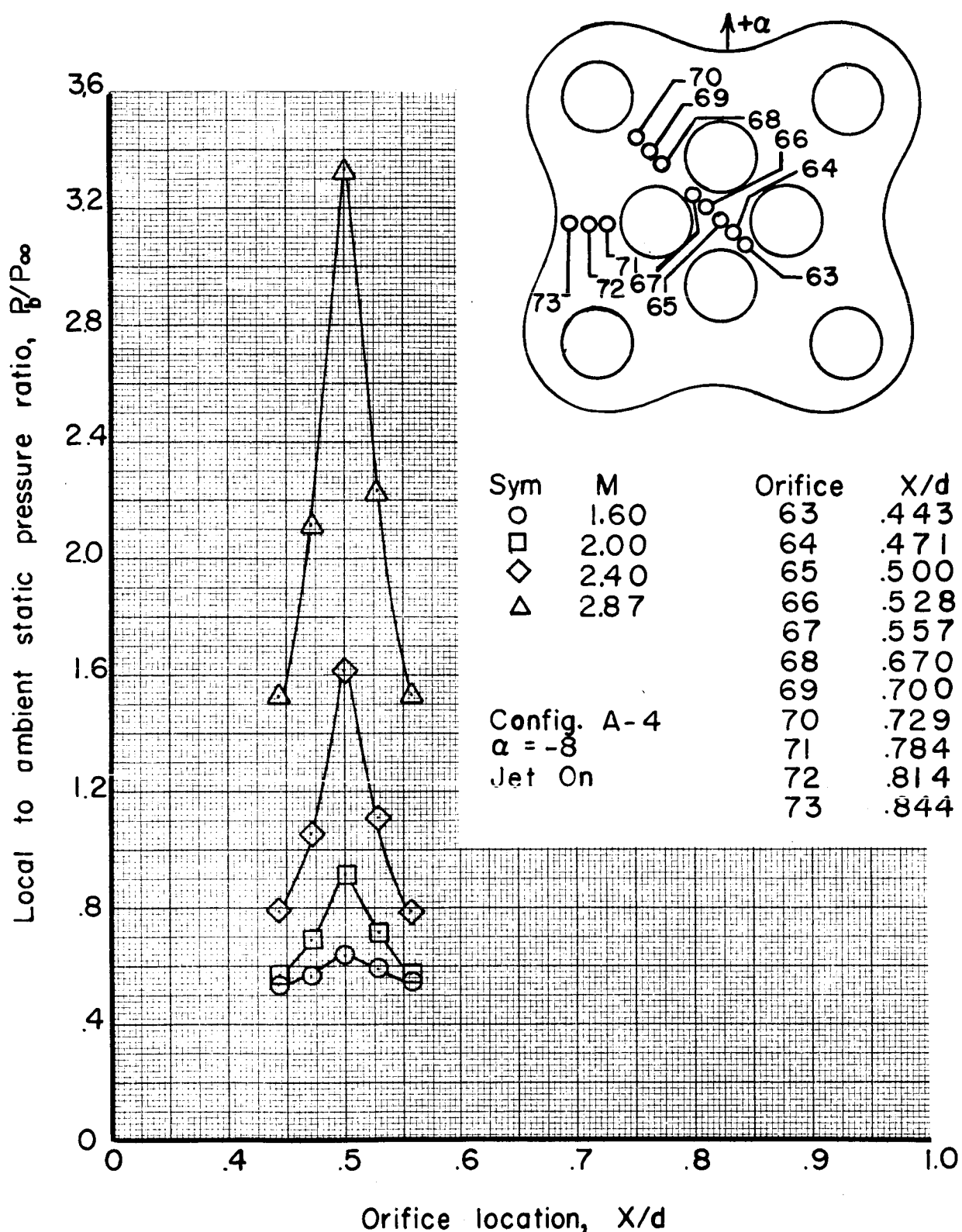


Figure 37d Effect of Mach number on star and base pressure ratios at various  $X/d$ 's

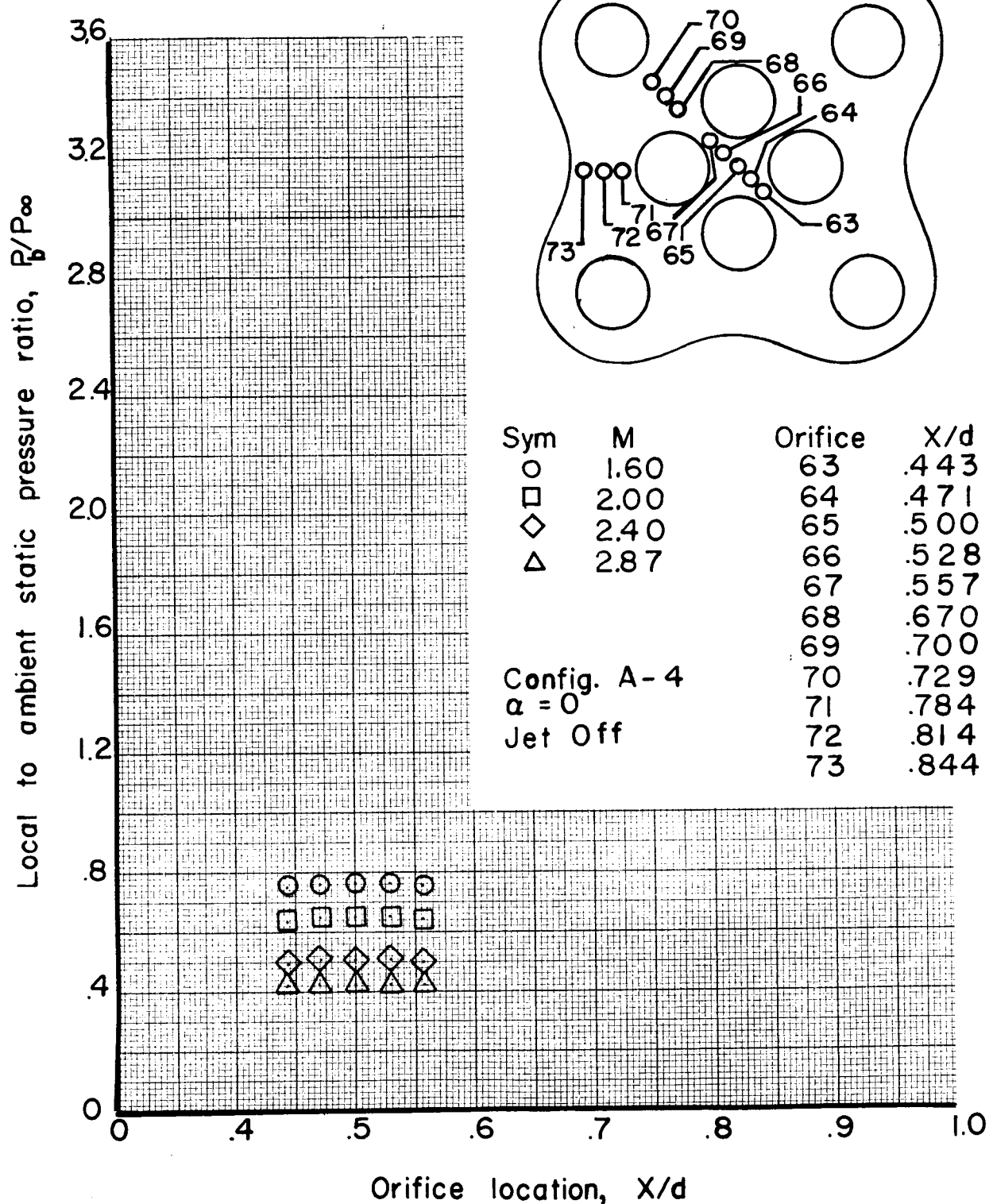


Figure 38a Effect of Mach number on star and base pressure ratios at various  $X/d$ 's

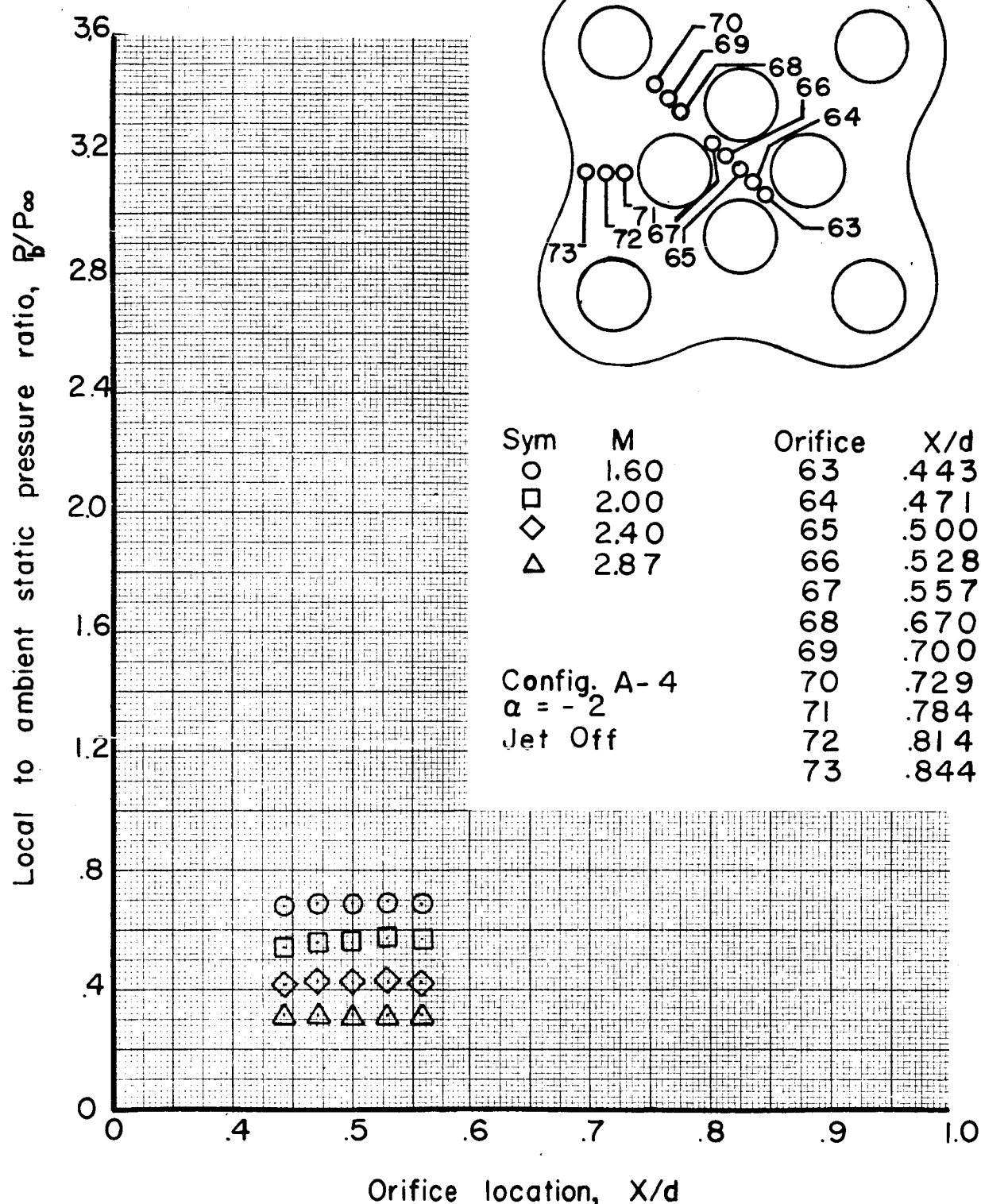


Figure 38 b Effect of Mach number on star and base pressure ratios at various  $X/d$ 's

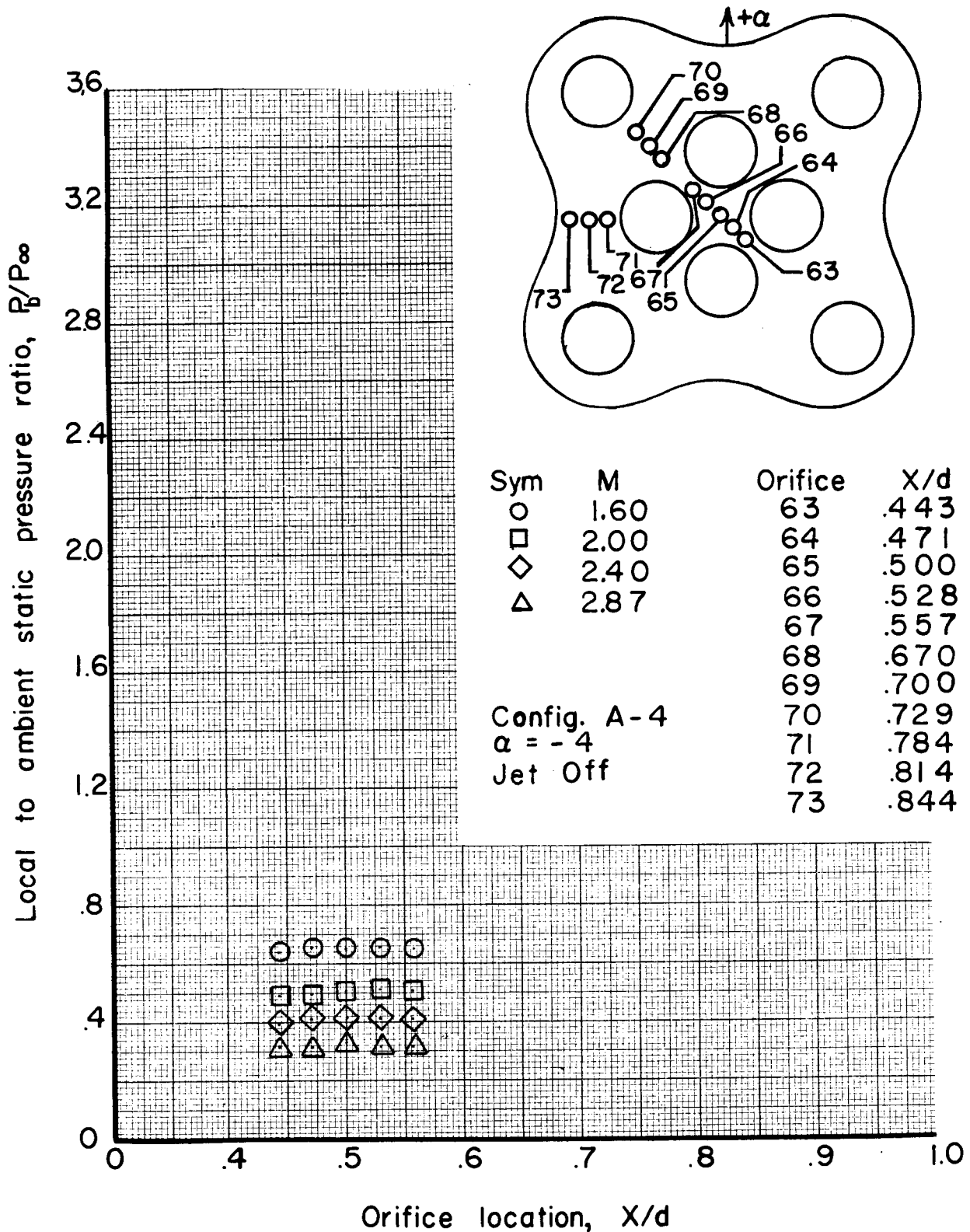


Figure 38c Effect of Mach number on star and base pressure ratios at various  $X/d$ 's

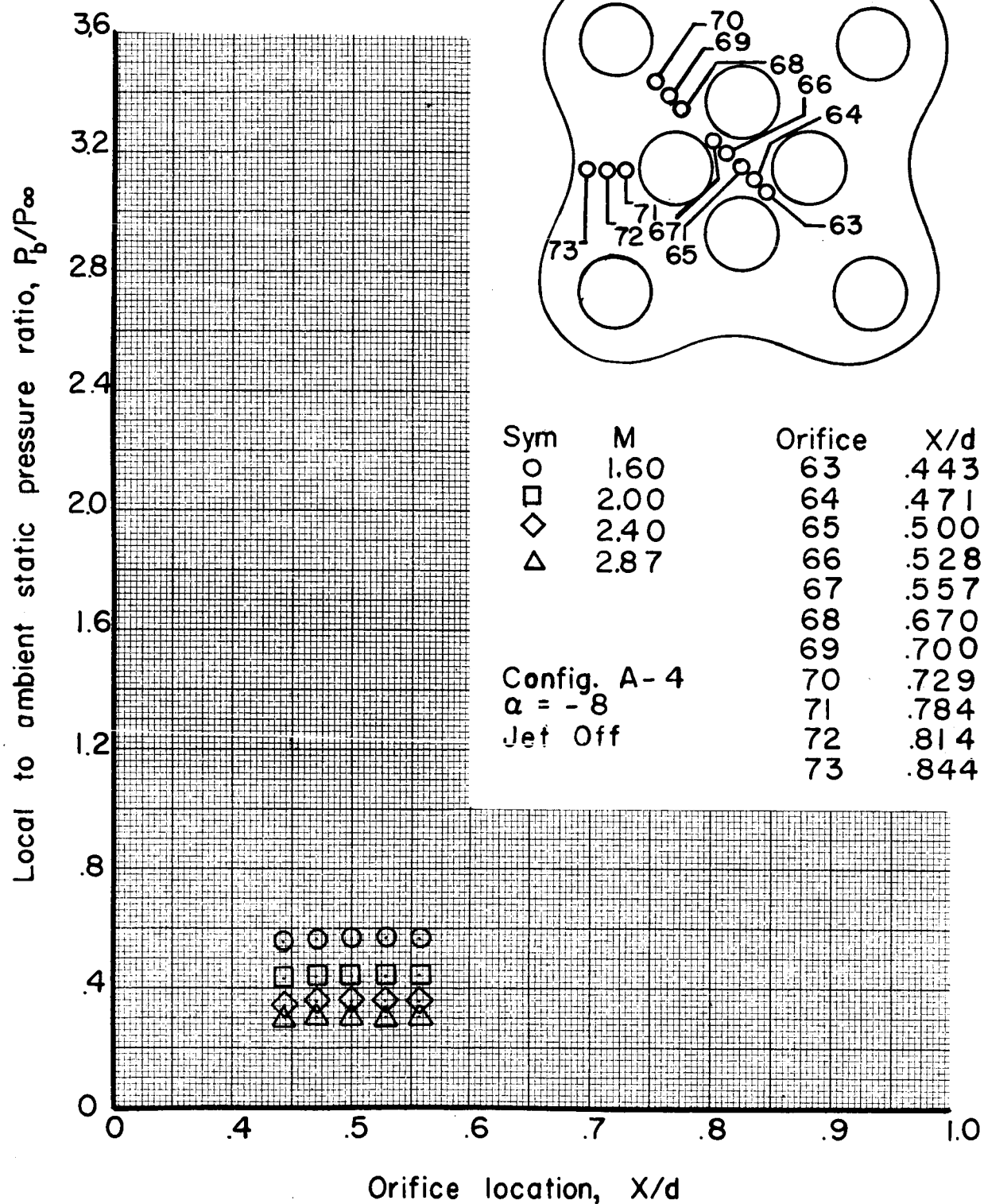
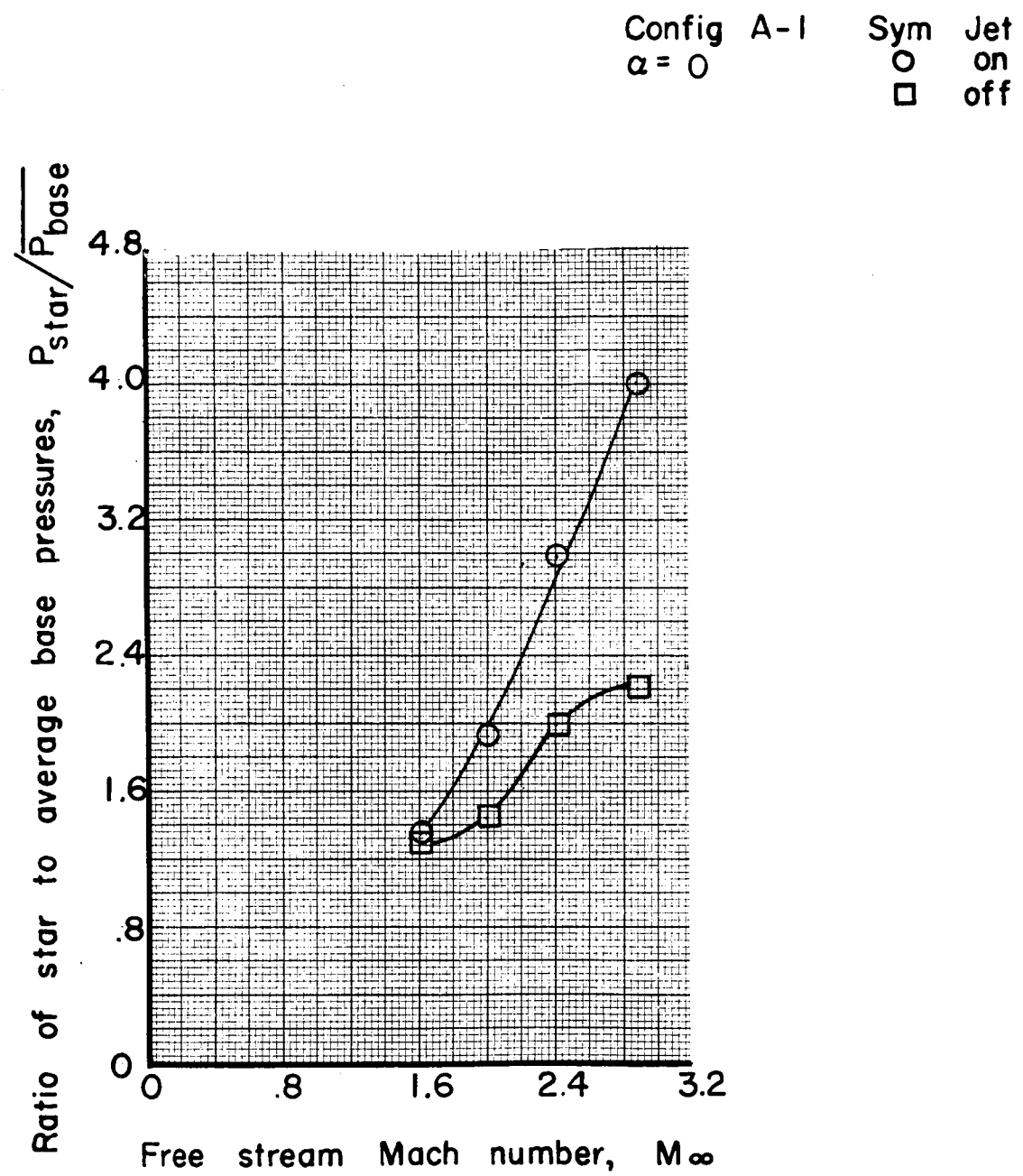


Figure 38d Effect of Mach number on star and base pressure ratios at various  $X/d$ 's



**Figure 39a** Variation of ratio of center star to base pressure with Mach number

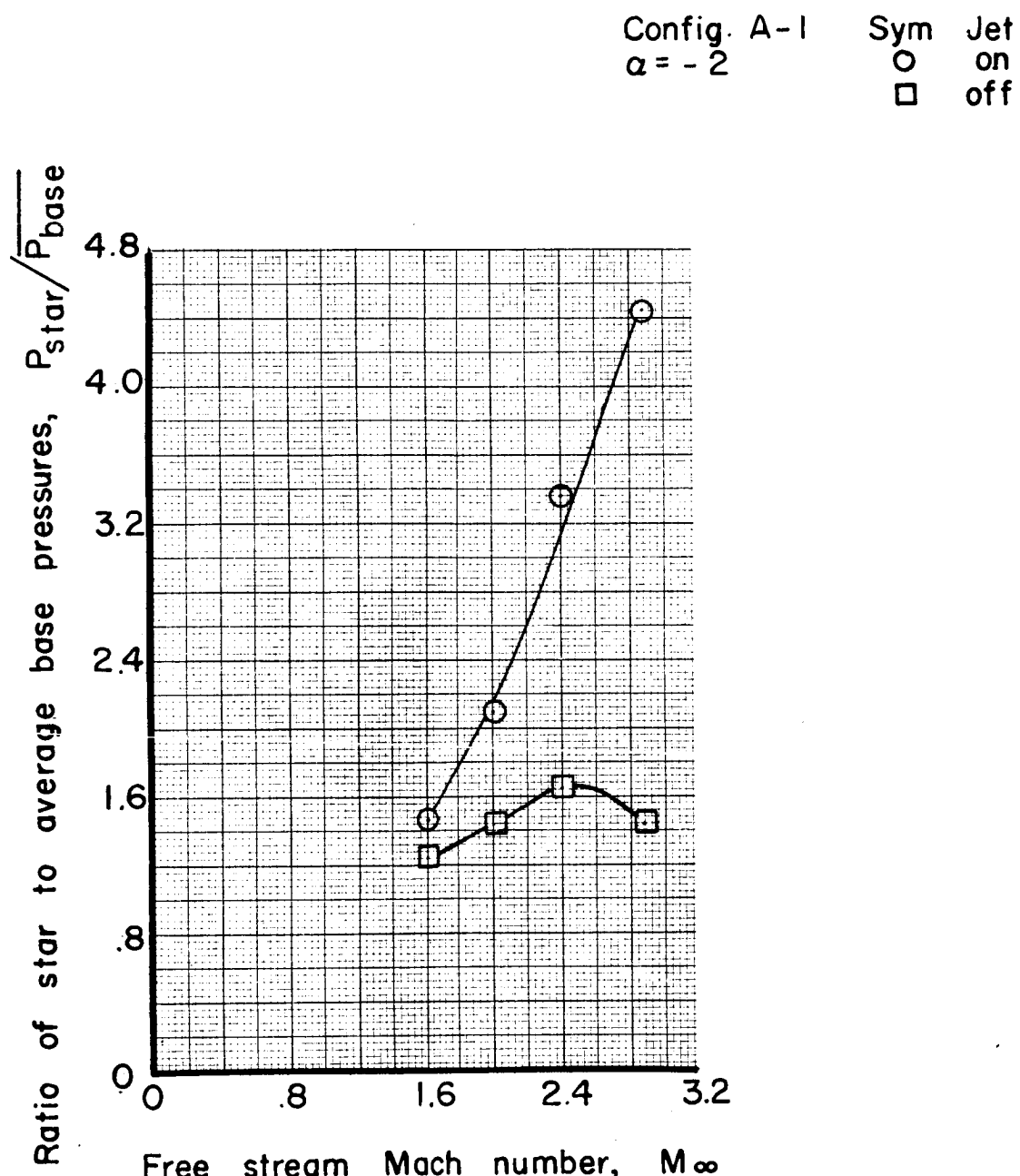


Figure 39b Variation of ratio of center star to base pressure with Mach number

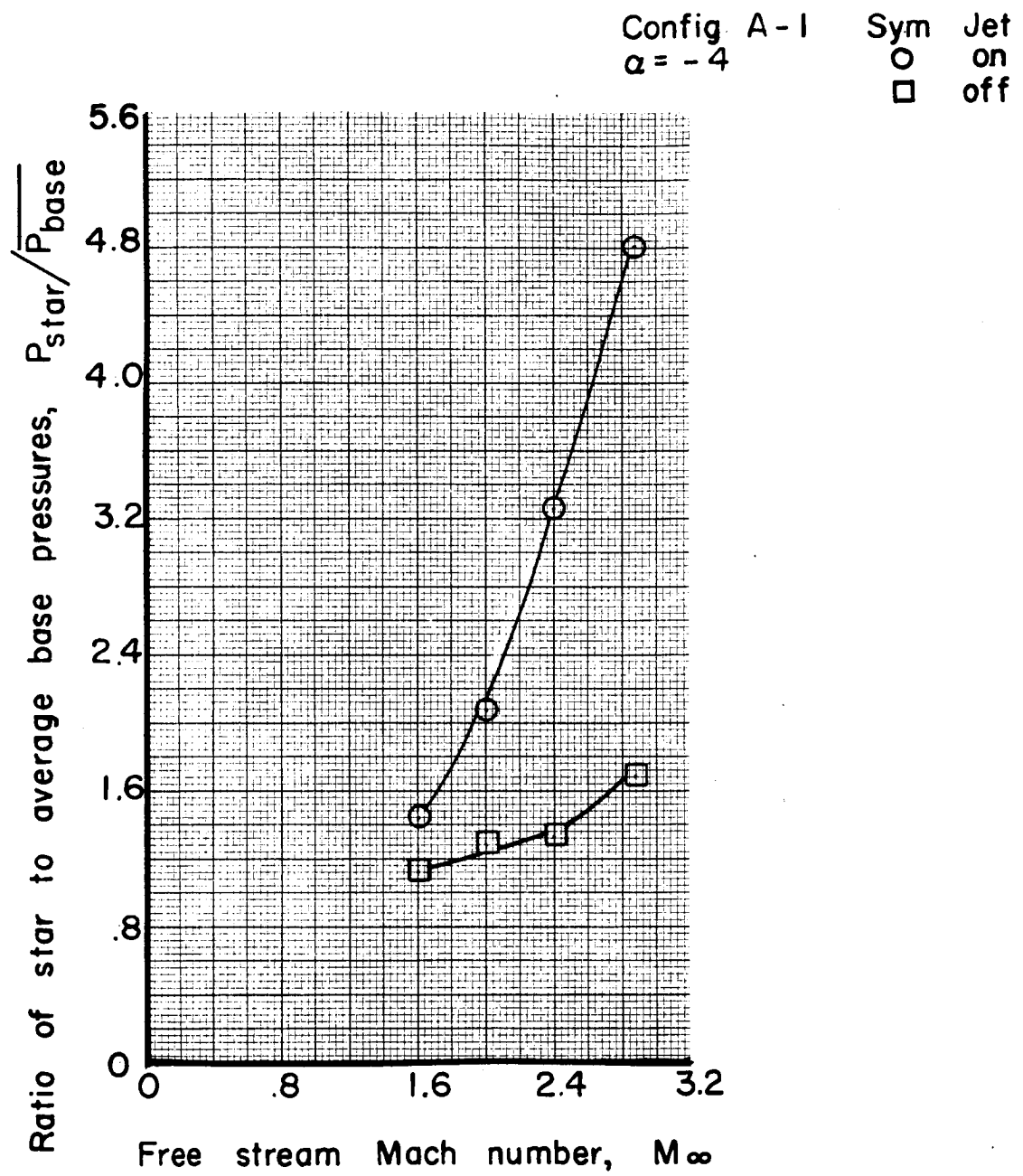


Figure 39c Variation of ratio of center star to base pressure with Mach number

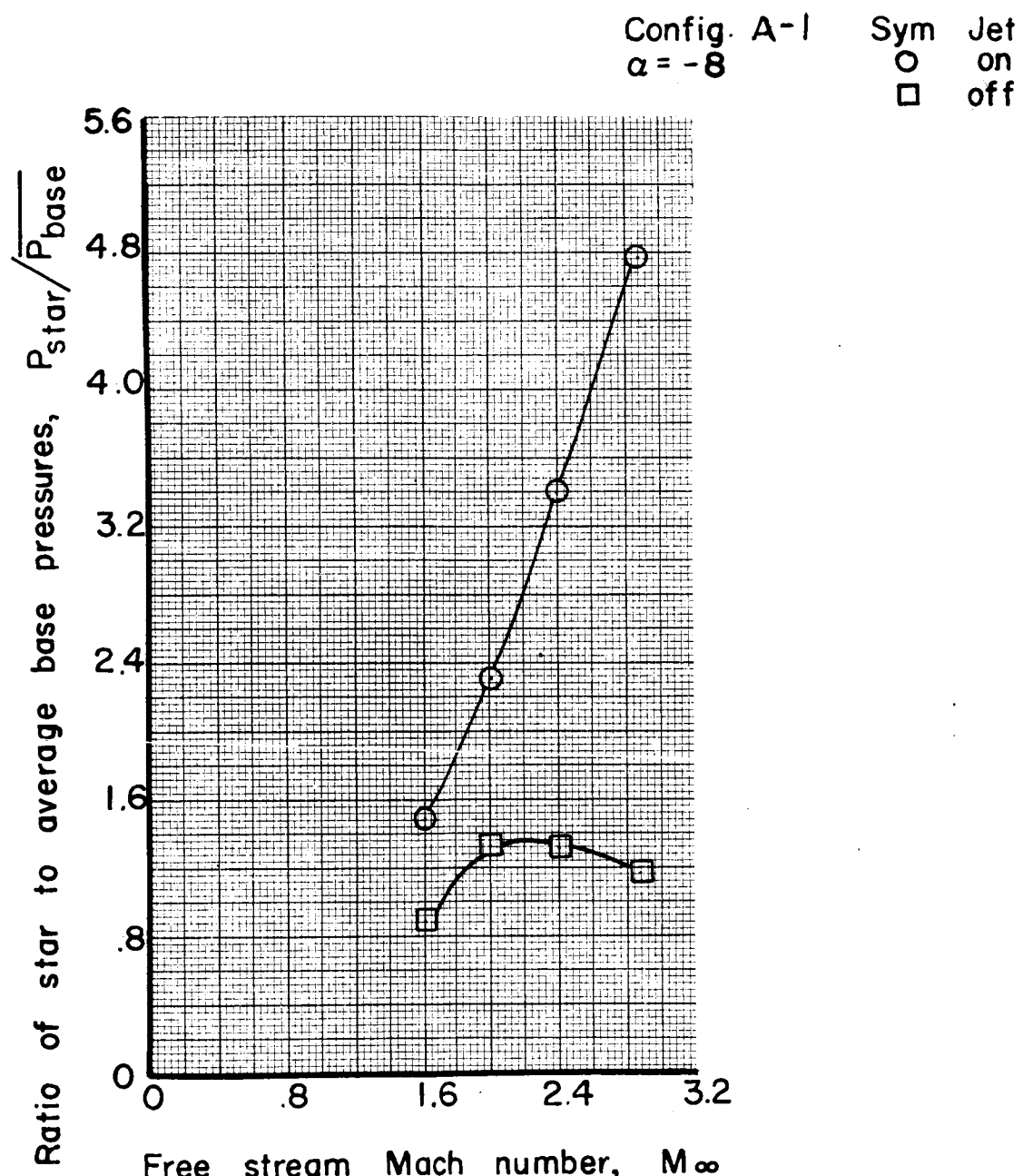


Figure 39d Variation of ratio of center star to base pressure with Mach number

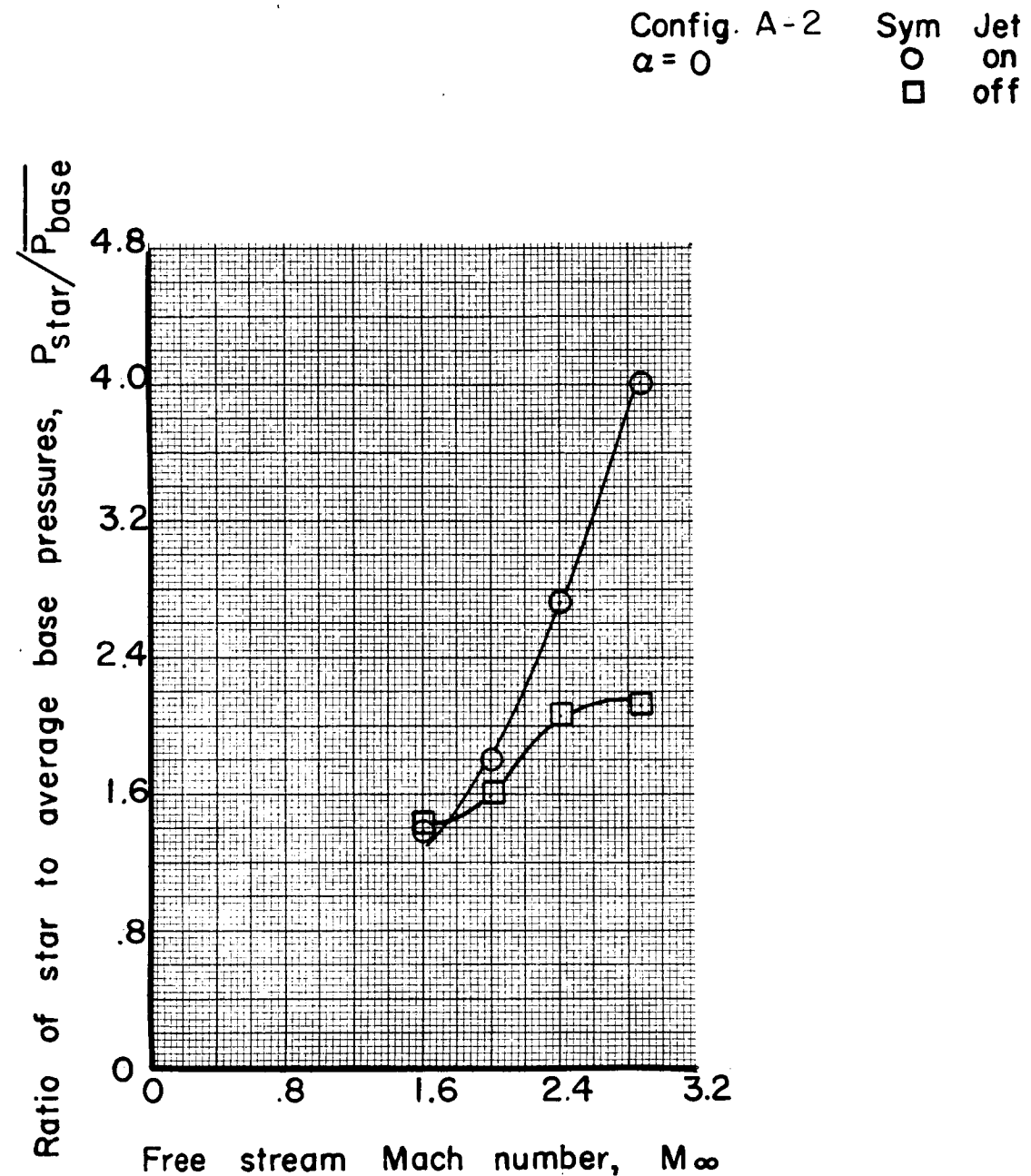


Figure 40a Variation of ratio of center star to base pressure with Mach number

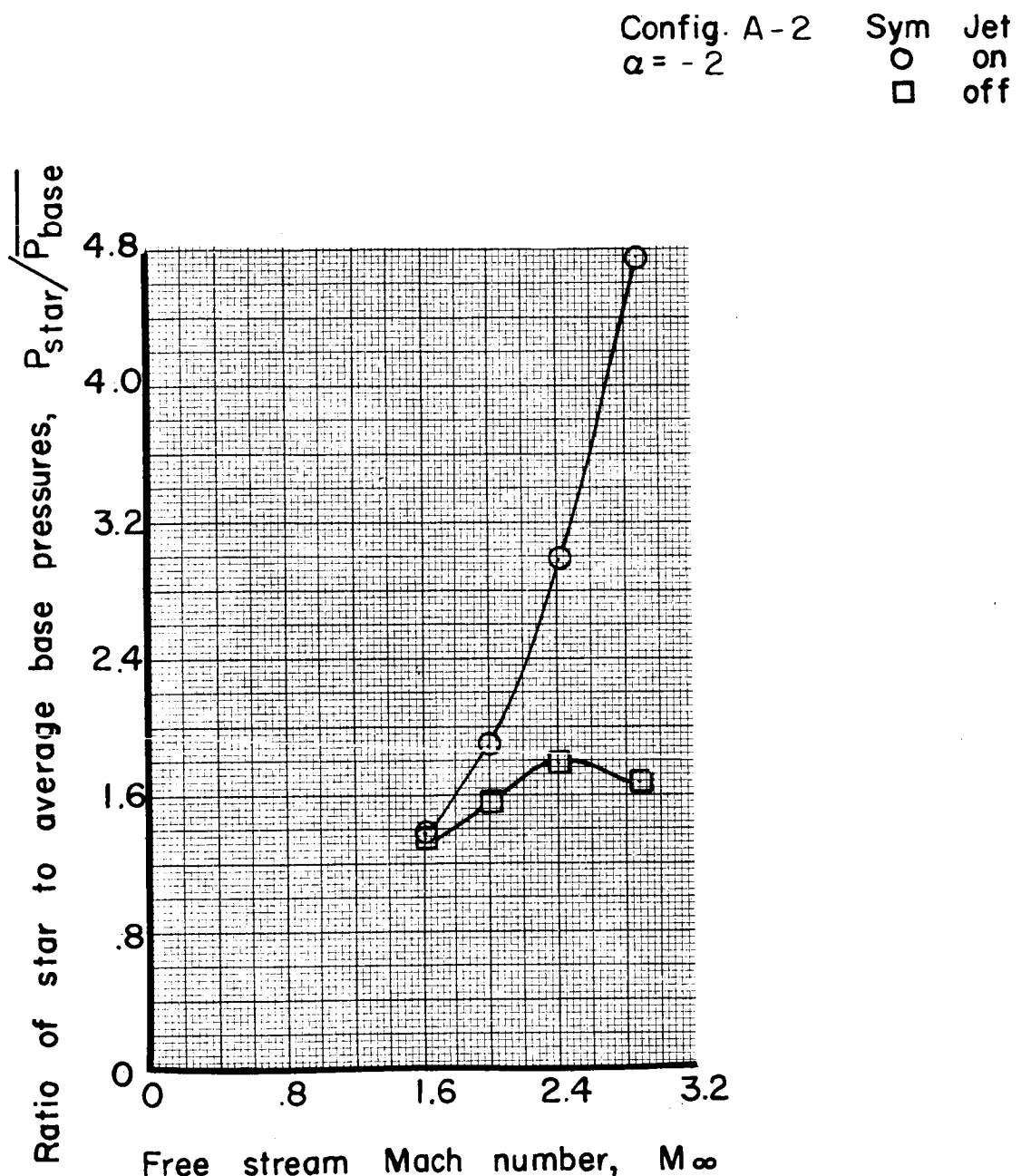


Figure 40b Variation of ratio of center star to base pressure with Mach number

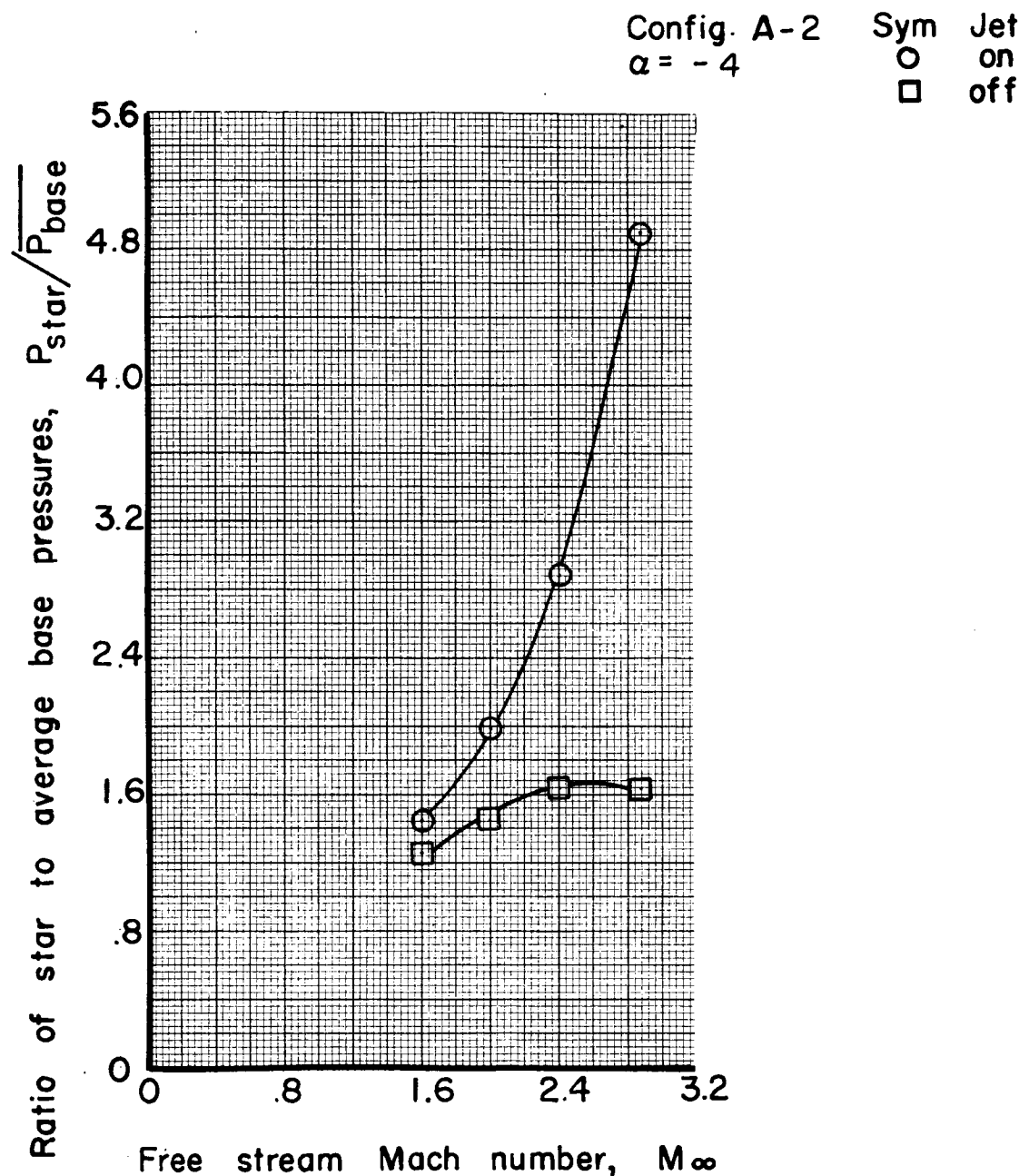


Figure 40c Variation of ratio of center star to base pressure with Mach number

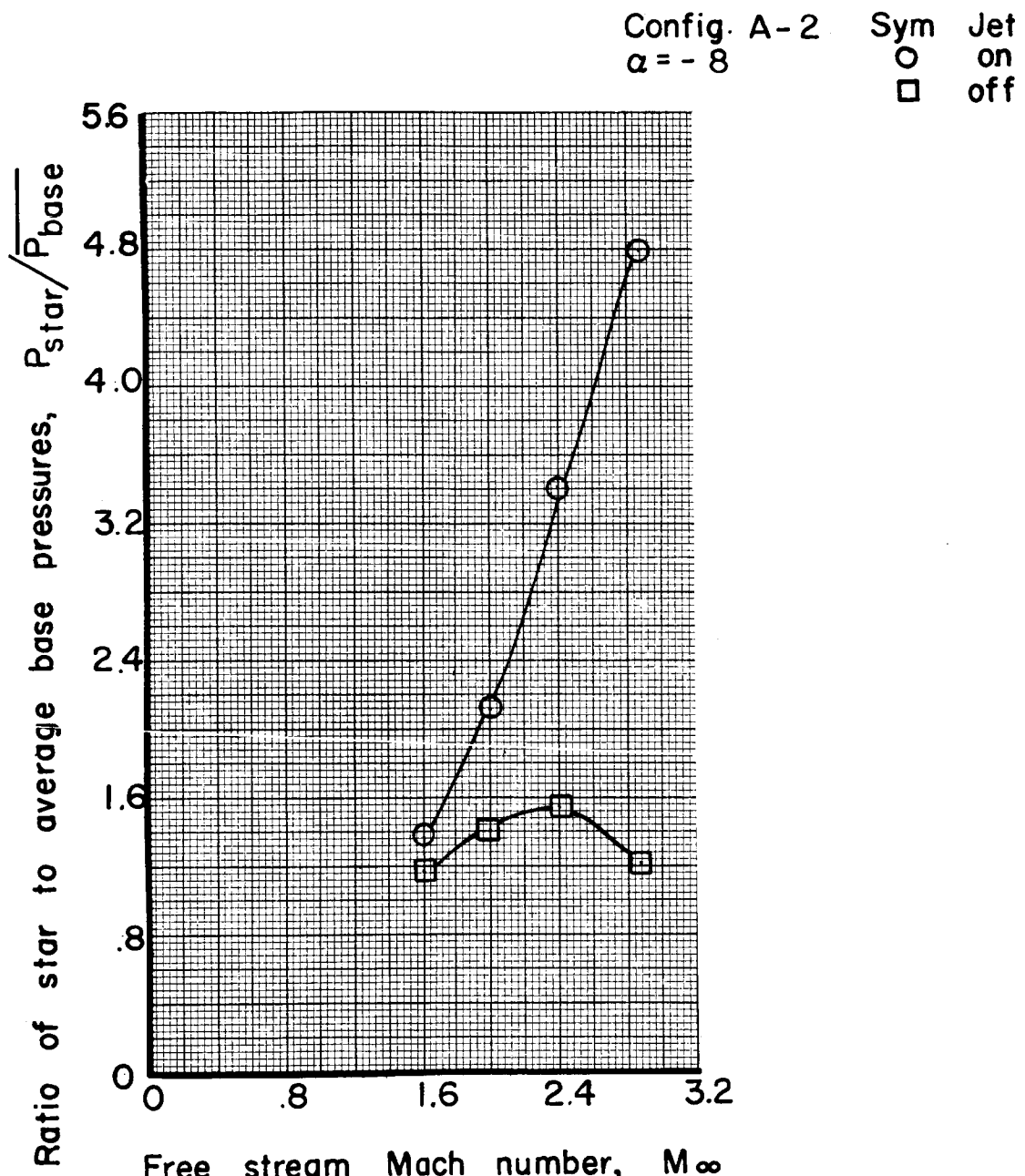


Figure 40d Variation of ratio of center star to base pressure with Mach number

Config. A-3      Sym      Jet  
 $\alpha = 0$                $\square$   $\circ$       on  
                        off

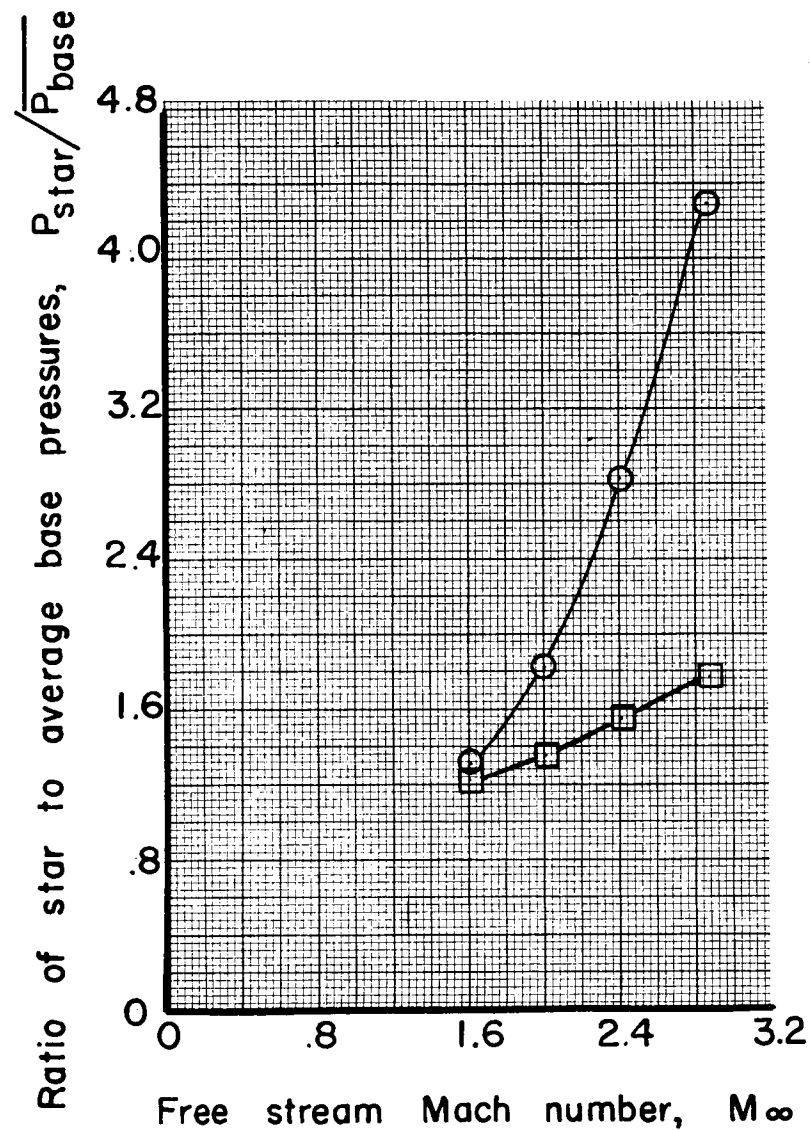


Figure 41a Variation of ratio of center star to base pressure with Mach number

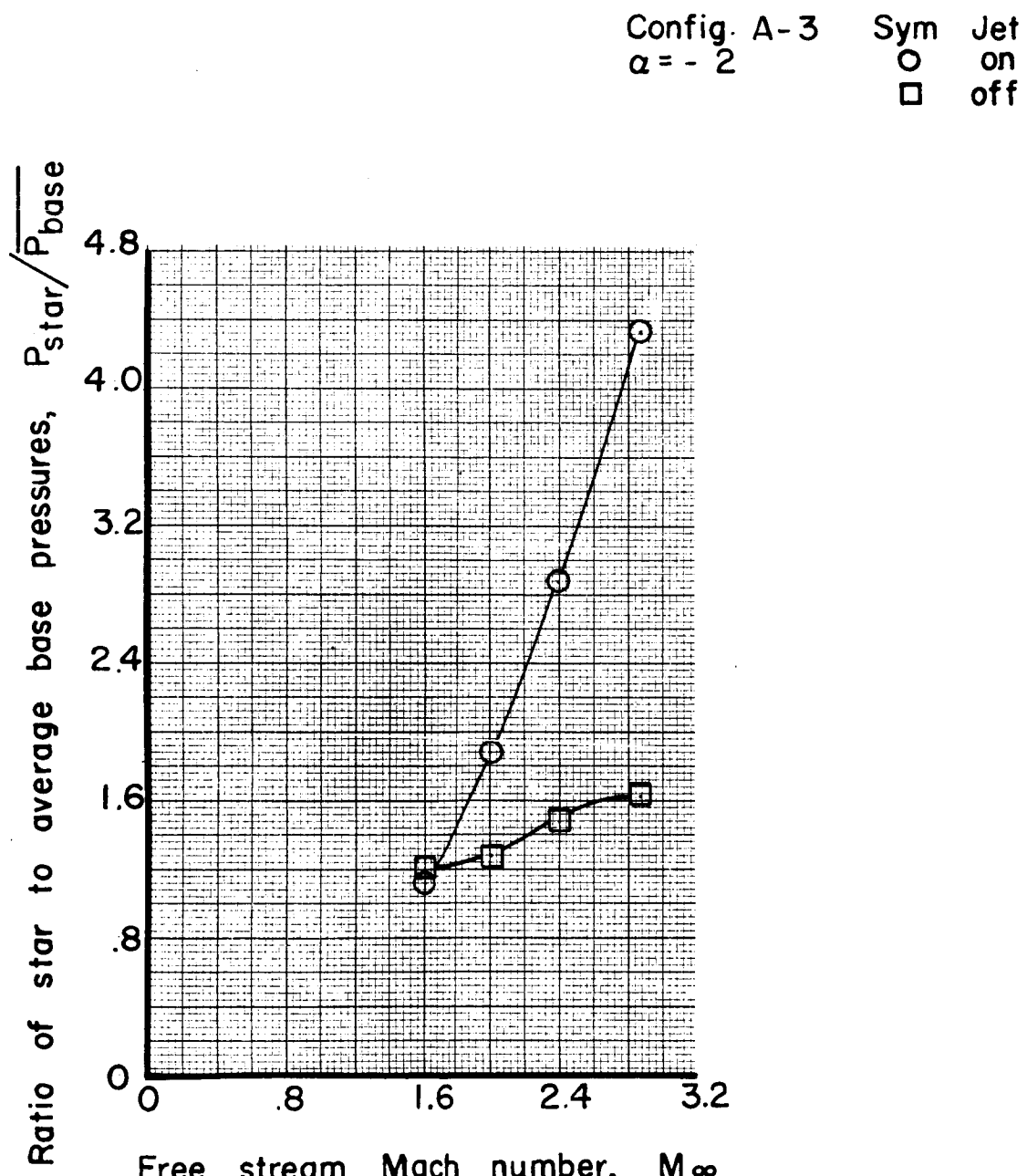


Figure 41b Variation of ratio of center star to base pressure with Mach number

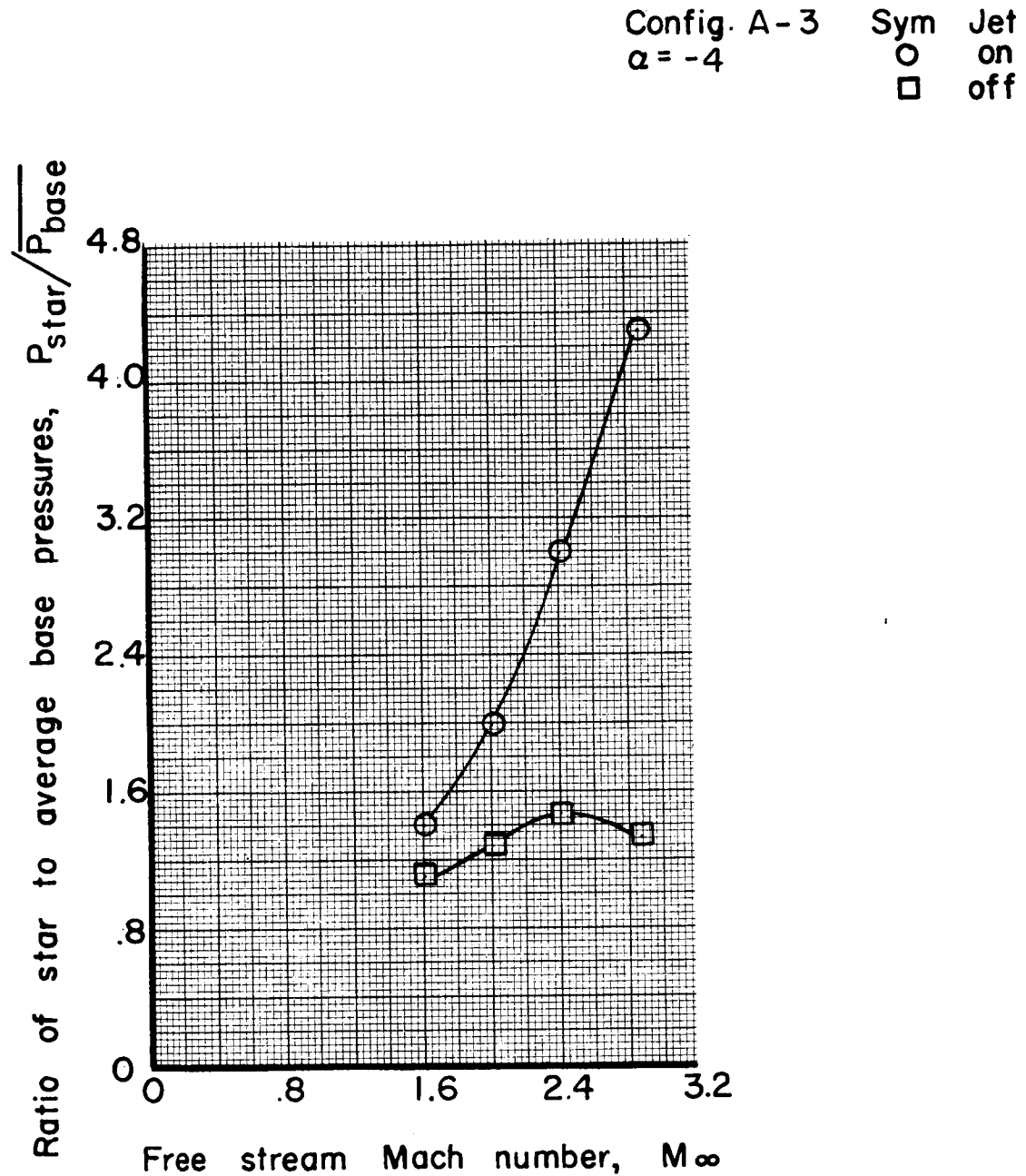


Figure 4|c Variation of ratio of center star to base pressure with Mach number

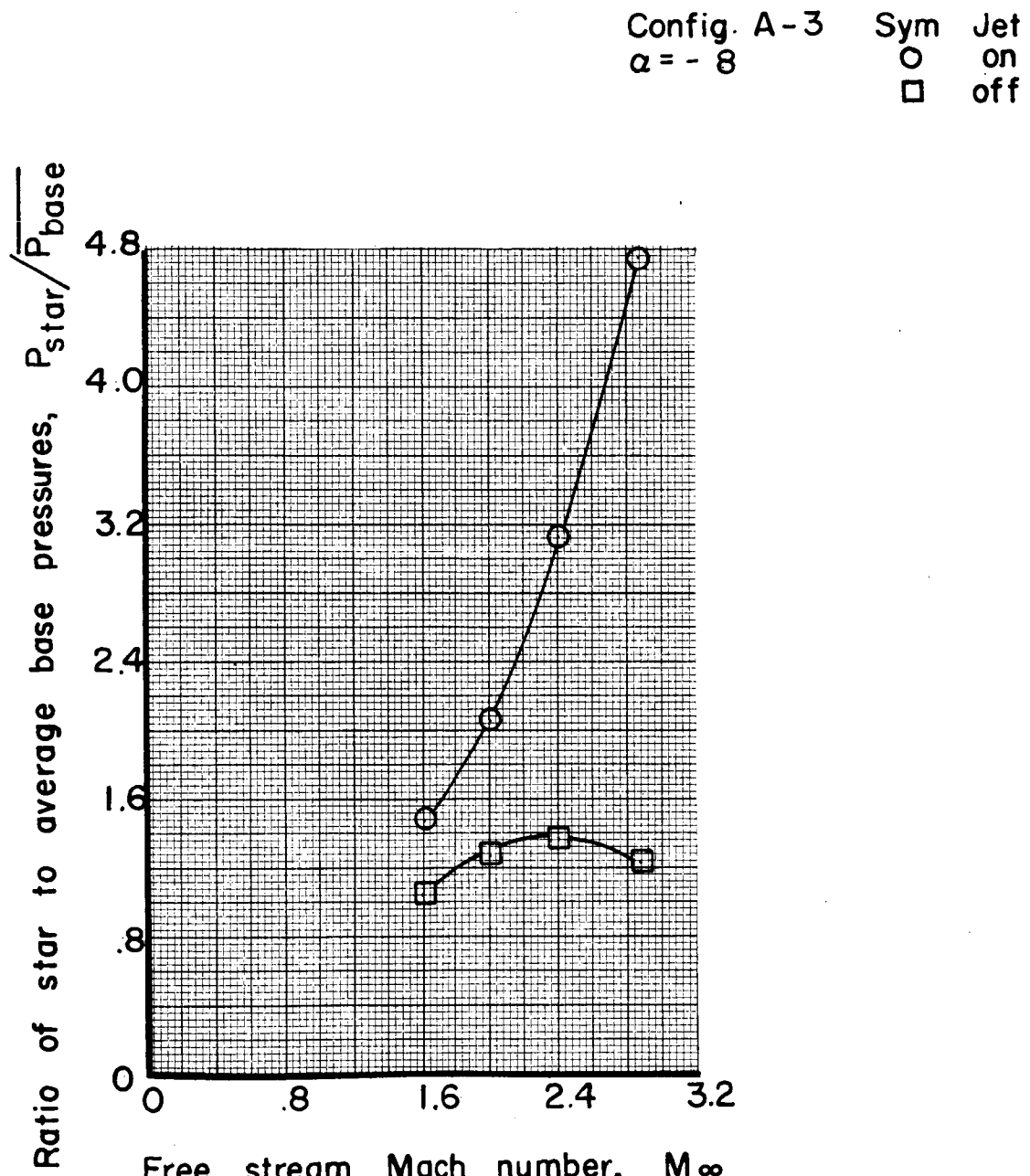


Figure 4Id Variation of ratio of center star to base pressure with Mach number

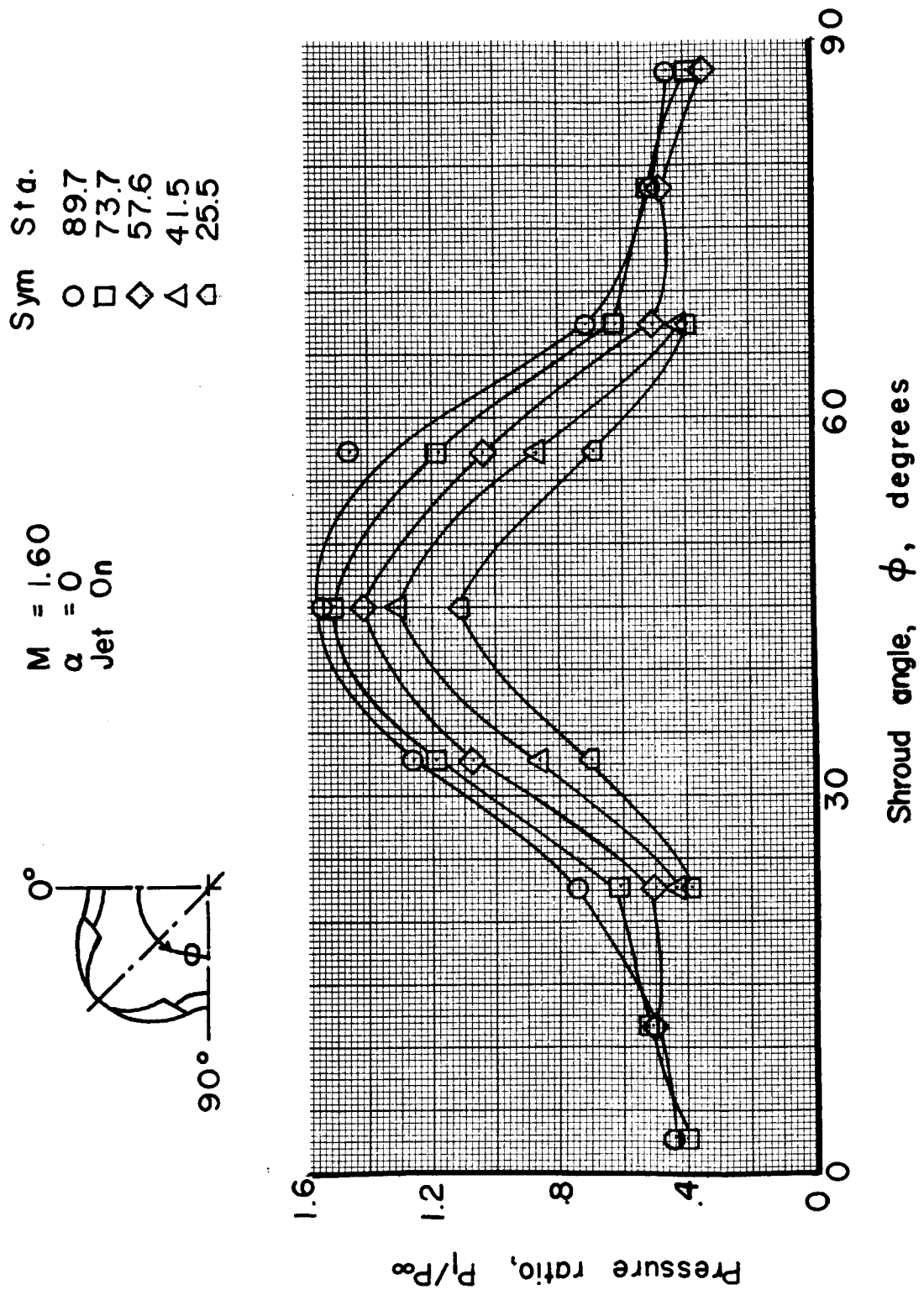


Figure 42d Results of wind tunnel tests showing variation of shroud pressures

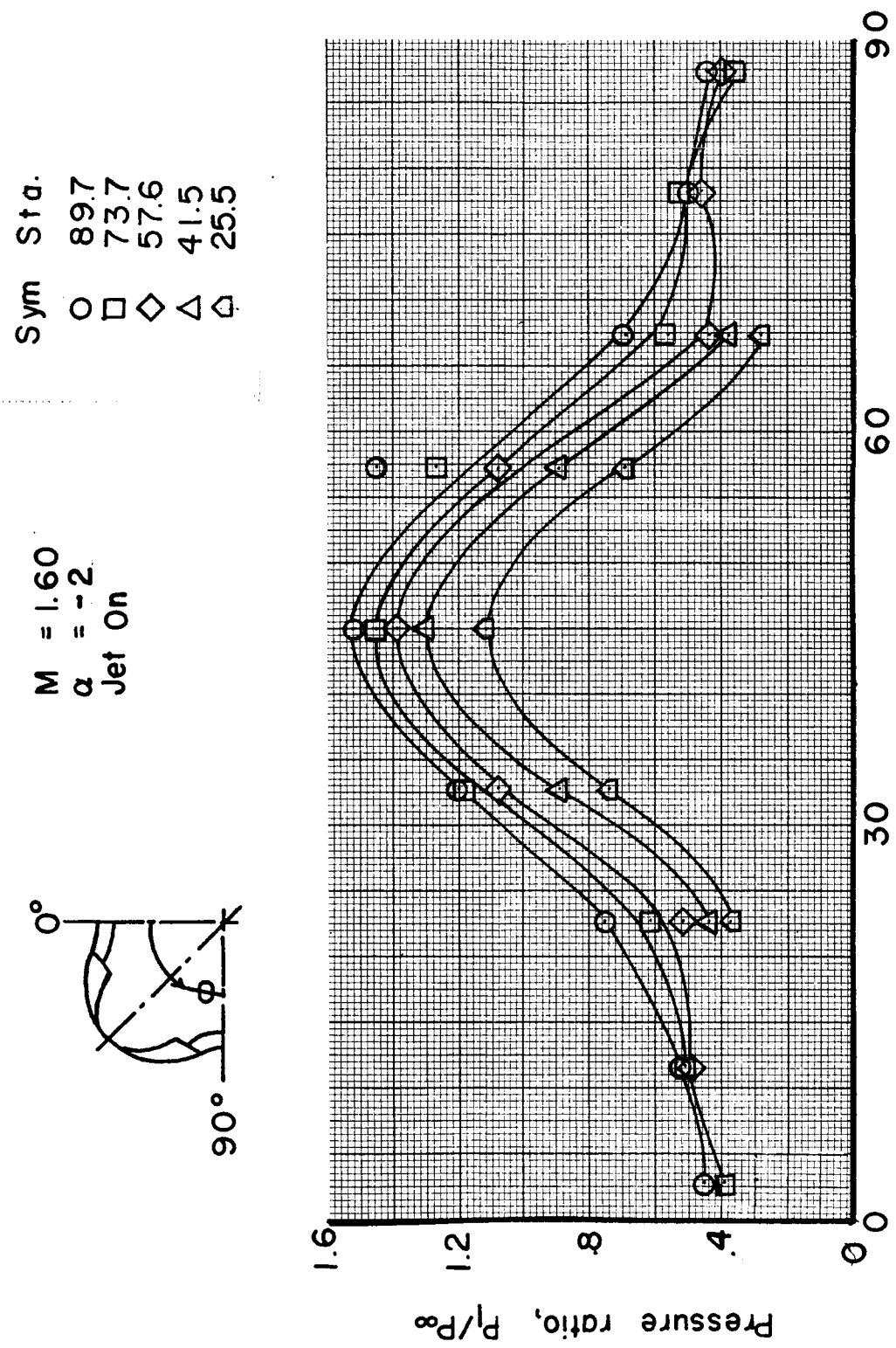


Figure 42b Results of wind tunnel tests showing variation of shroud pressures

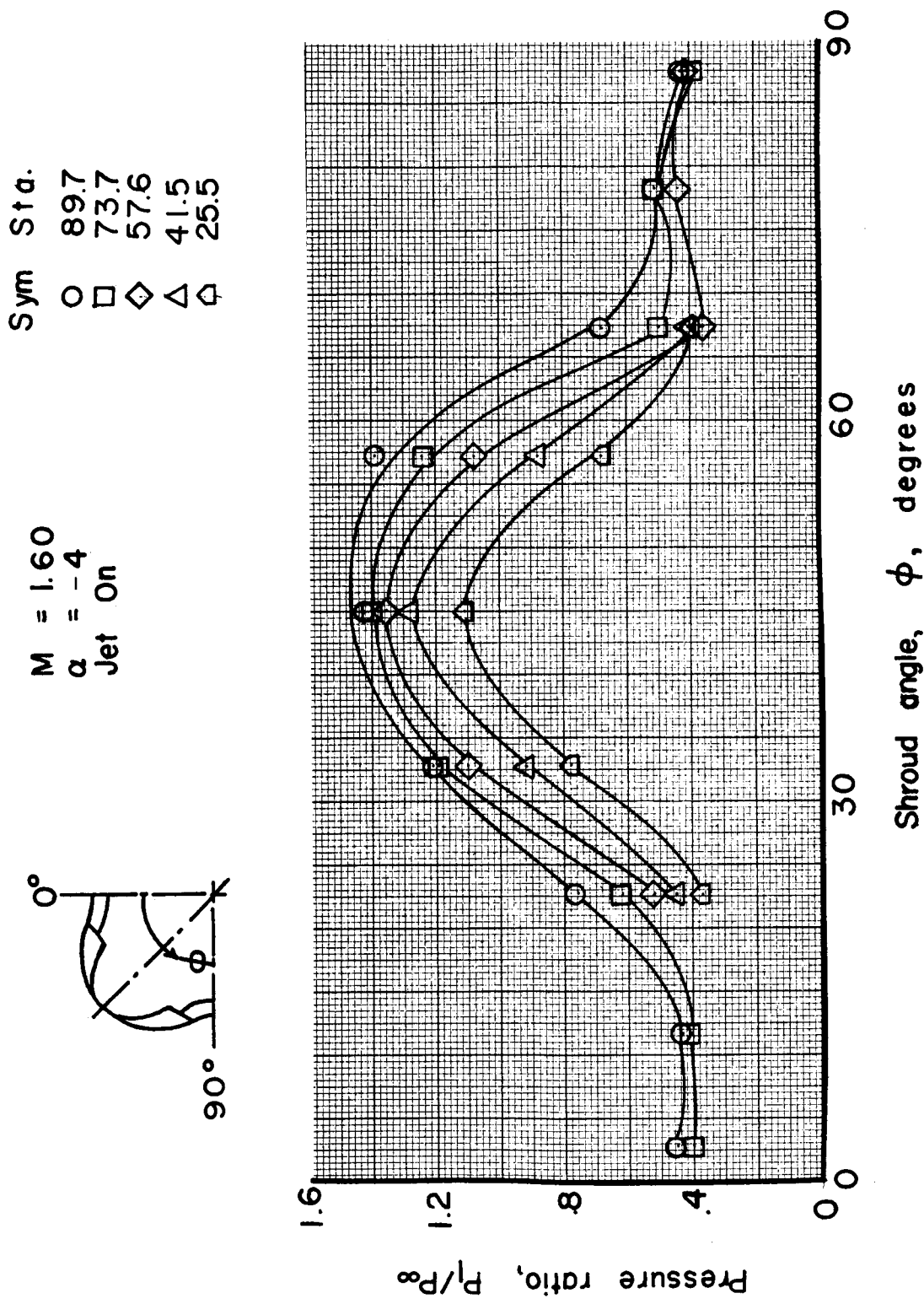


Figure 42c Results of wind tunnel tests showing variation of shroud pressures

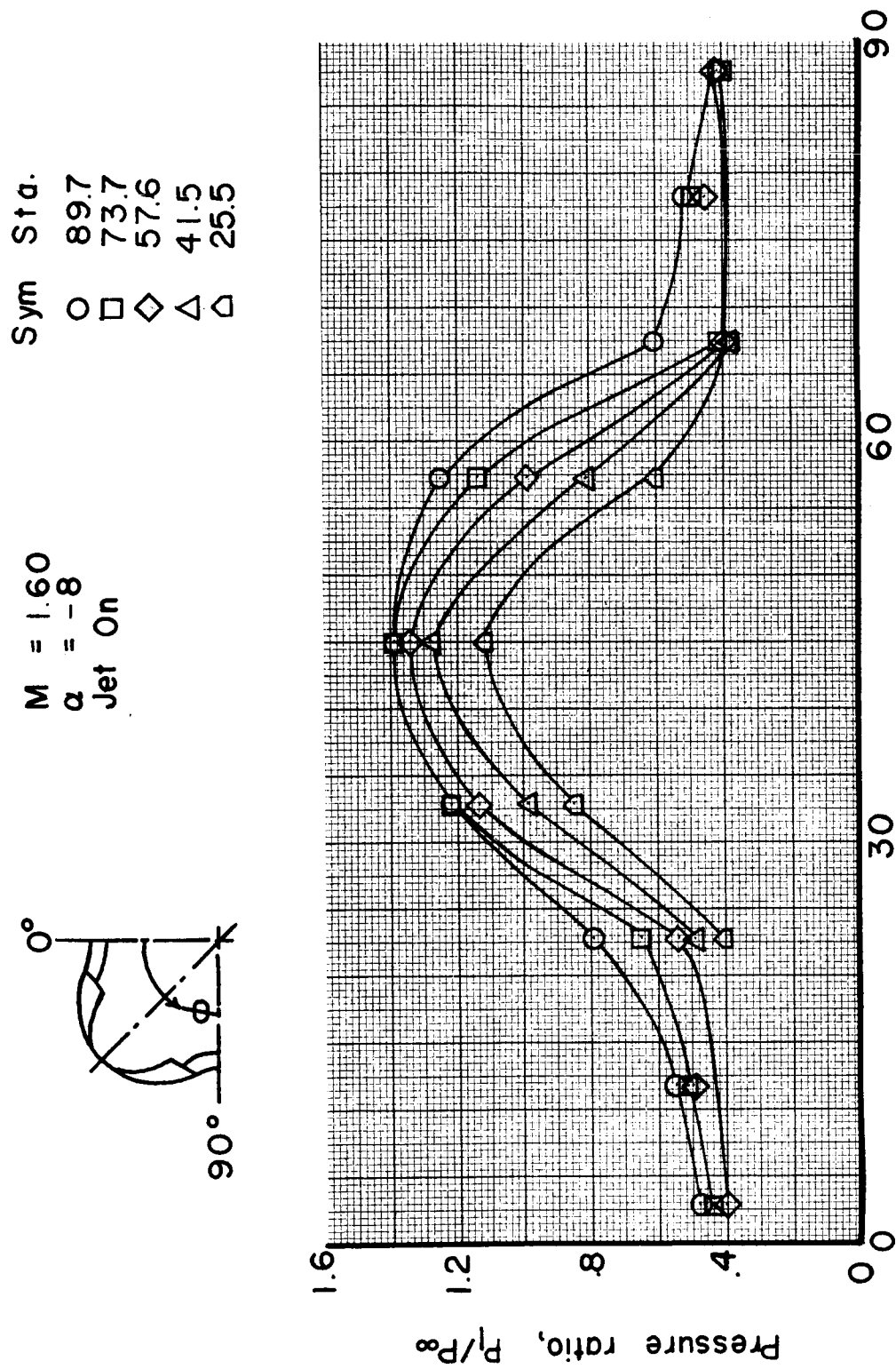


Figure 42d Results of wind tunnel tests showing variation of shroud pressures

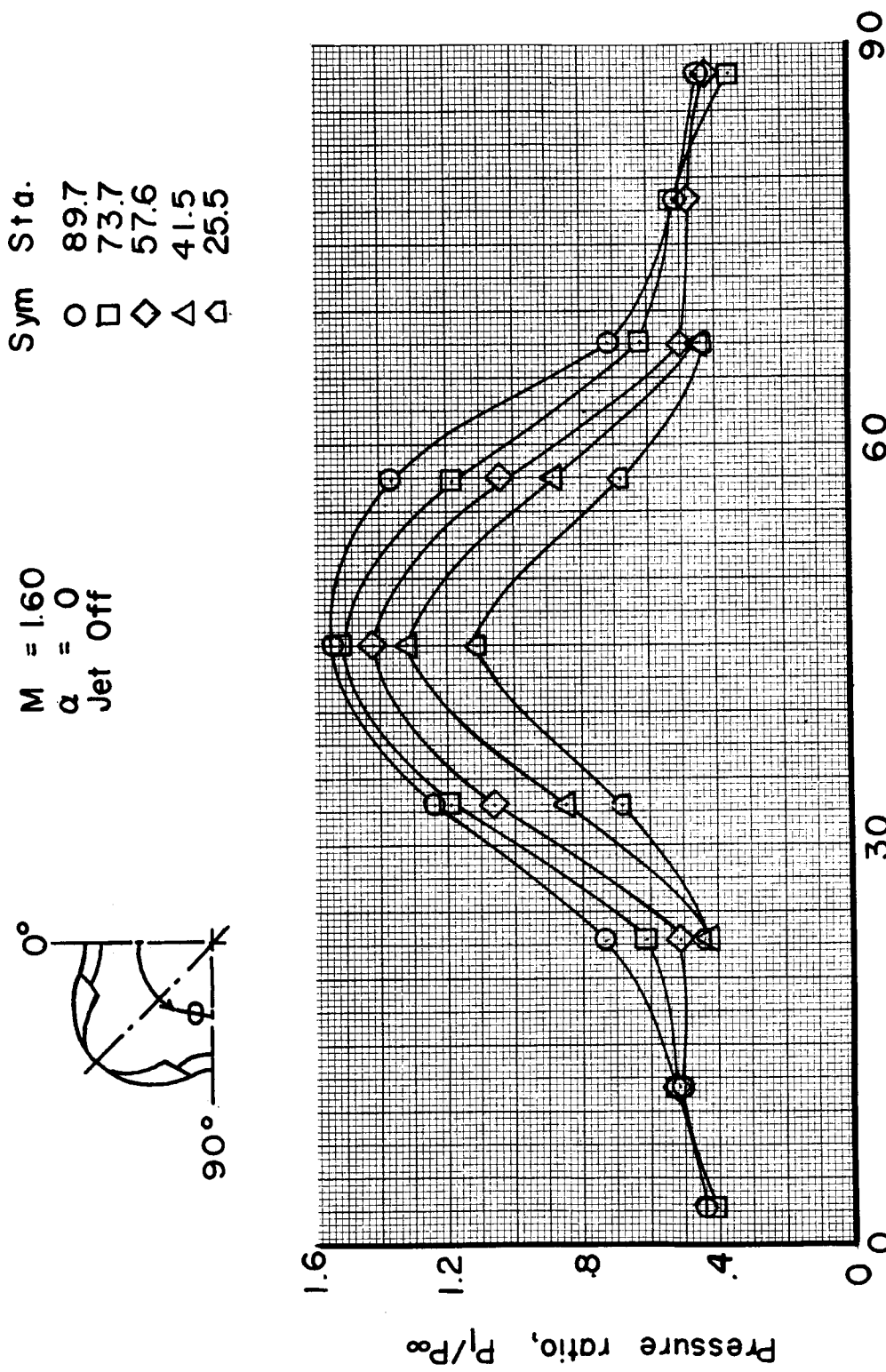


Figure 43a Results of wind tunnel tests showing variation of shroud pressures

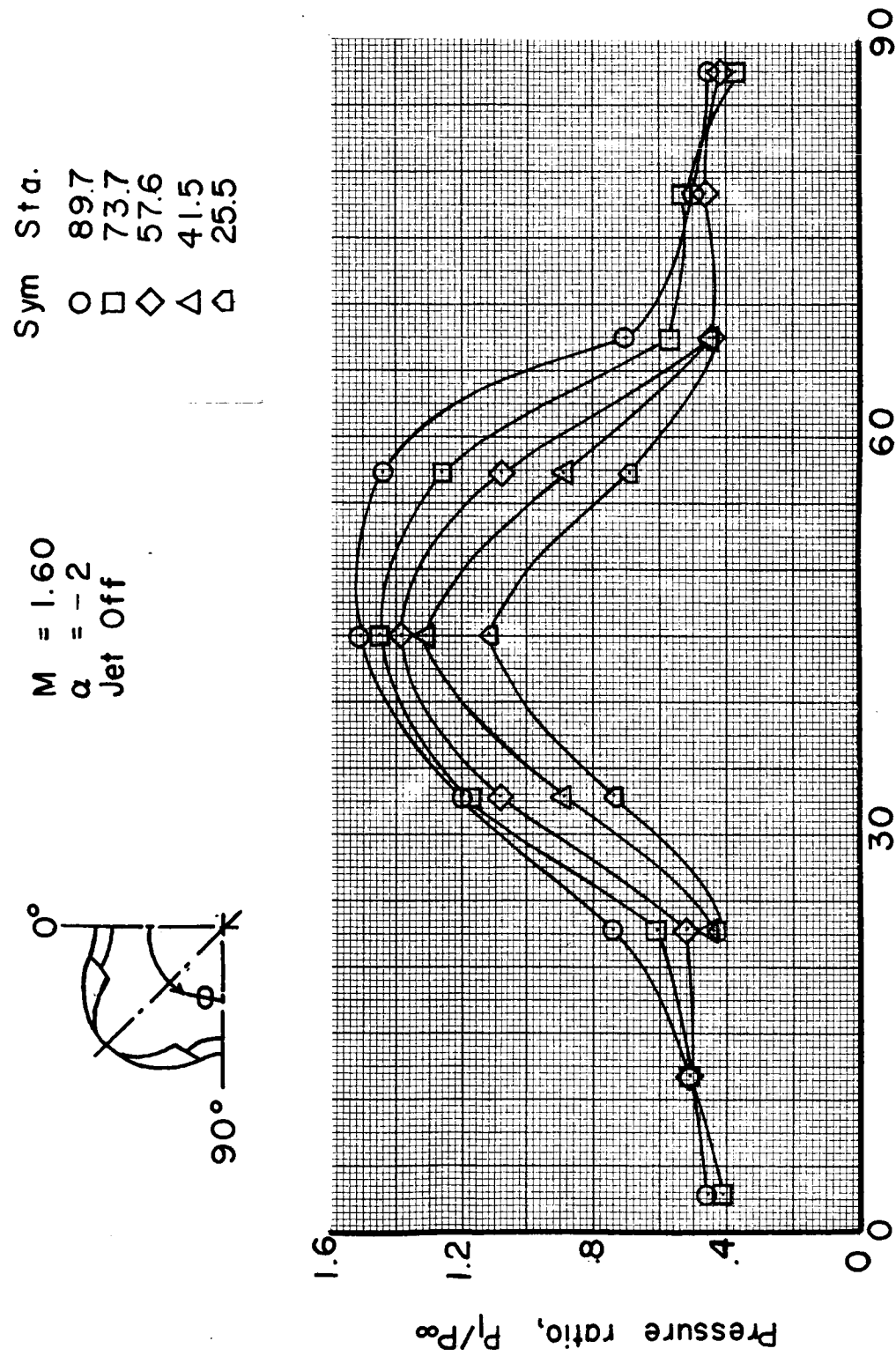


Figure 43b Results of wind tunnel tests showing variation of shroud pressures

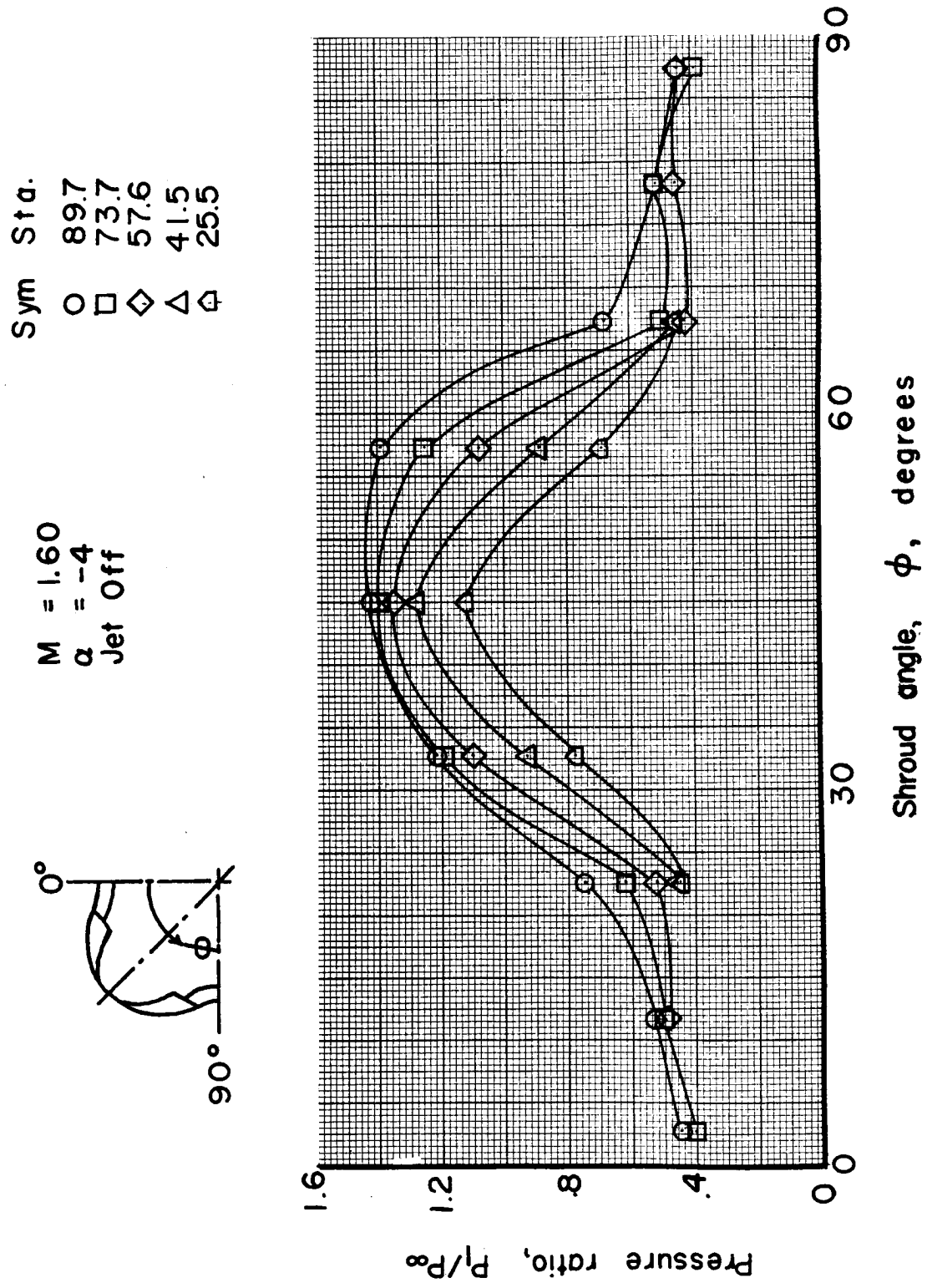


Figure 43c Results of wind tunnel tests showing variation of shroud pressures

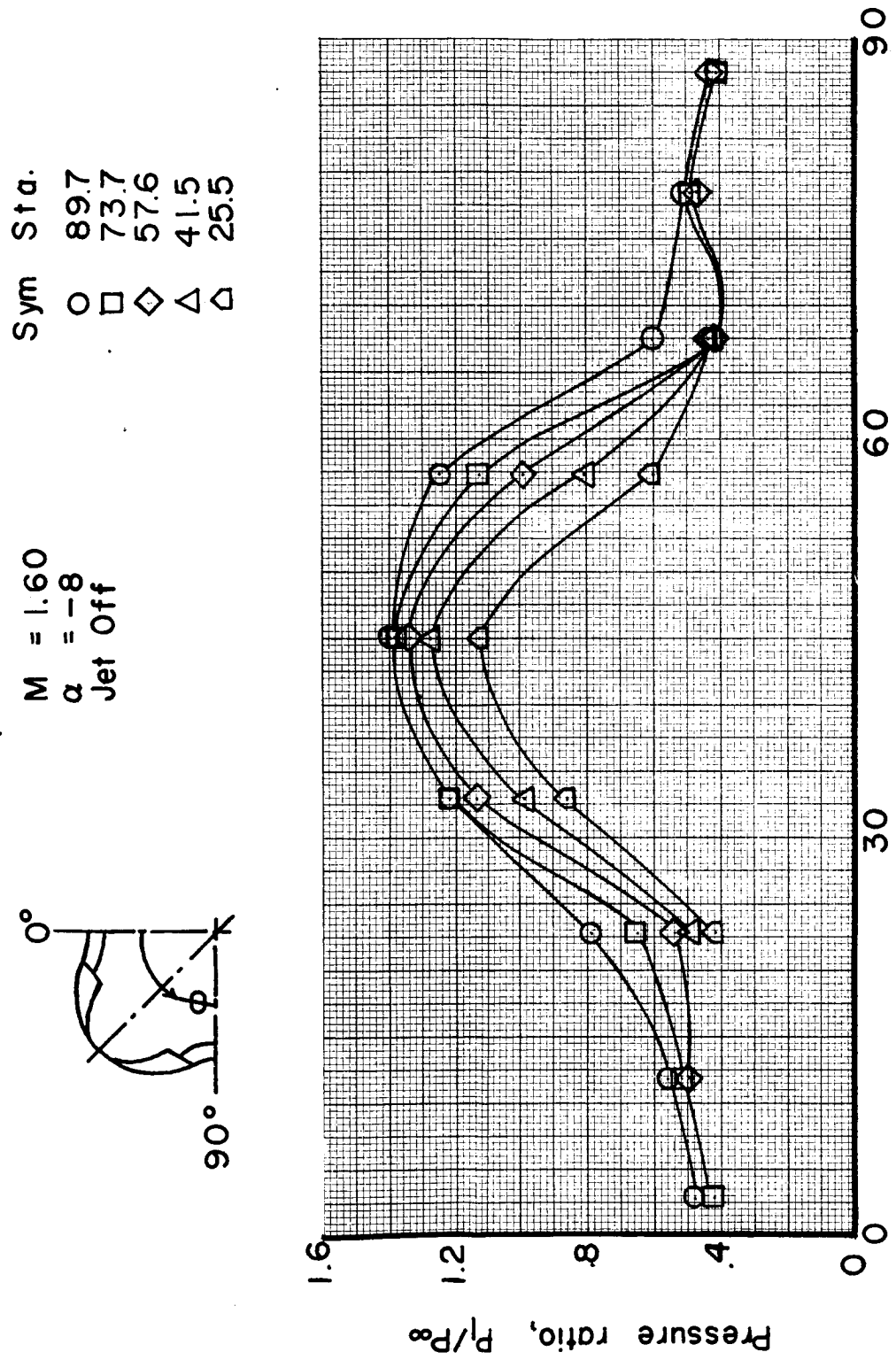


Figure 43d Results of wind tunnel tests showing variation of shroud pressures

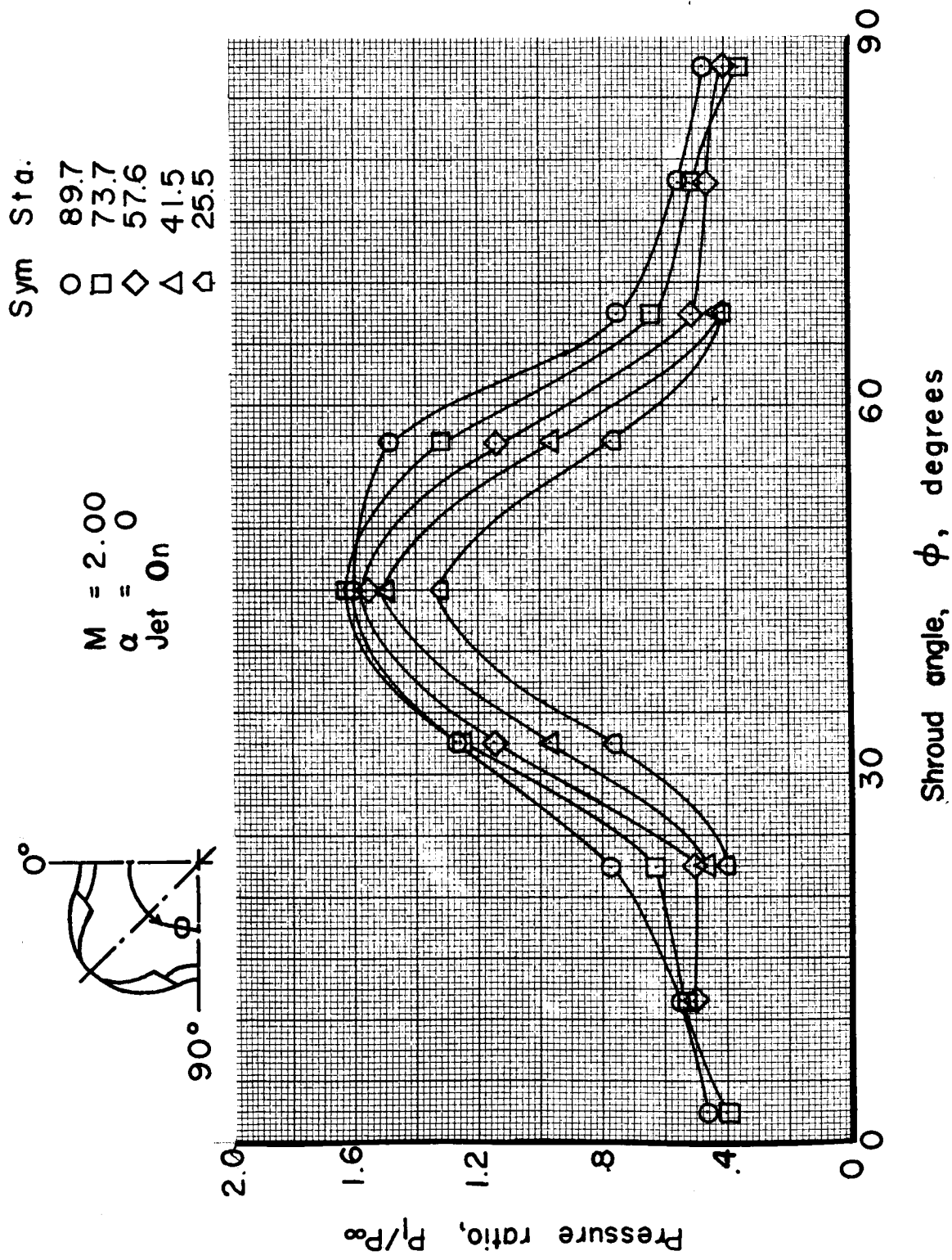


Figure 44a Results of wind tunnel tests showing variation of shroud pressures

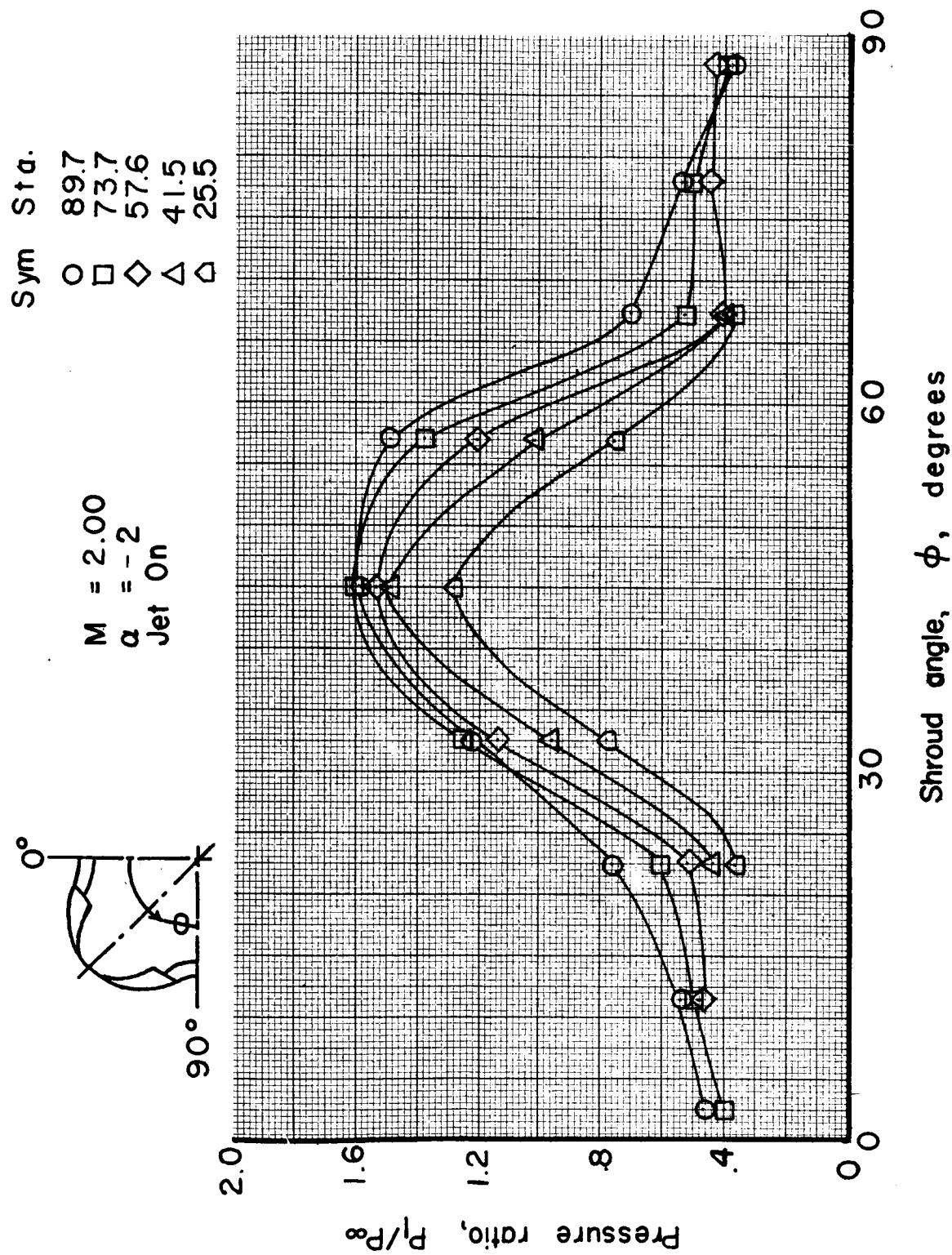


Figure 44b Results of wind tunnel tests showing variation of shroud pressures

$M = 2.00$   
 $\alpha = -4$   
 Jet On  
  
 Sym Sta.  
 ○ 89.7  
 □ 73.7  
 ◇ 57.6  
 △ 41.5  
 ▽ 25.5

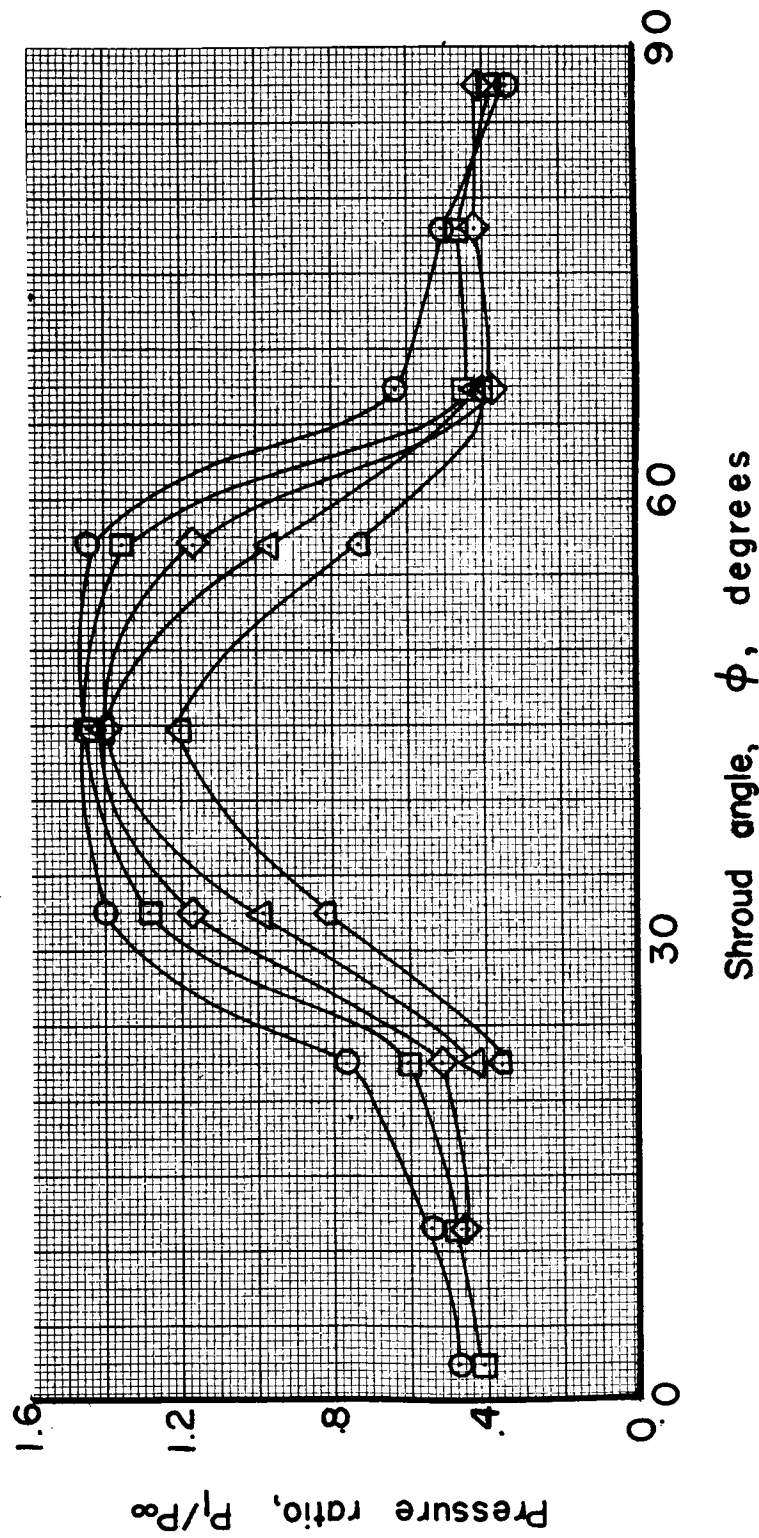


Figure 44c Results of wind tunnel tests showing variation of shroud pressures

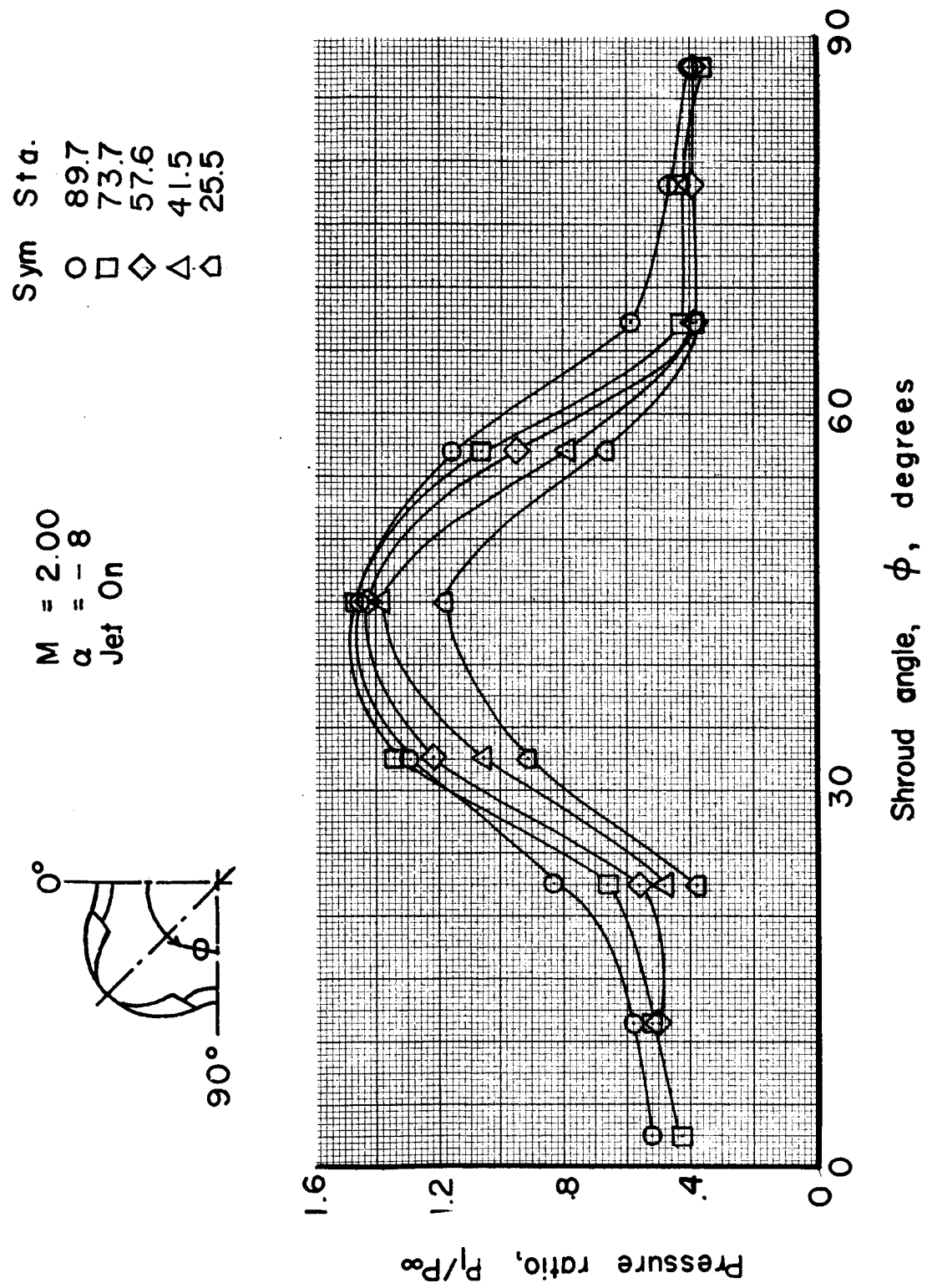


Figure 44-d Results of wind tunnel tests showing variation of shroud pressures

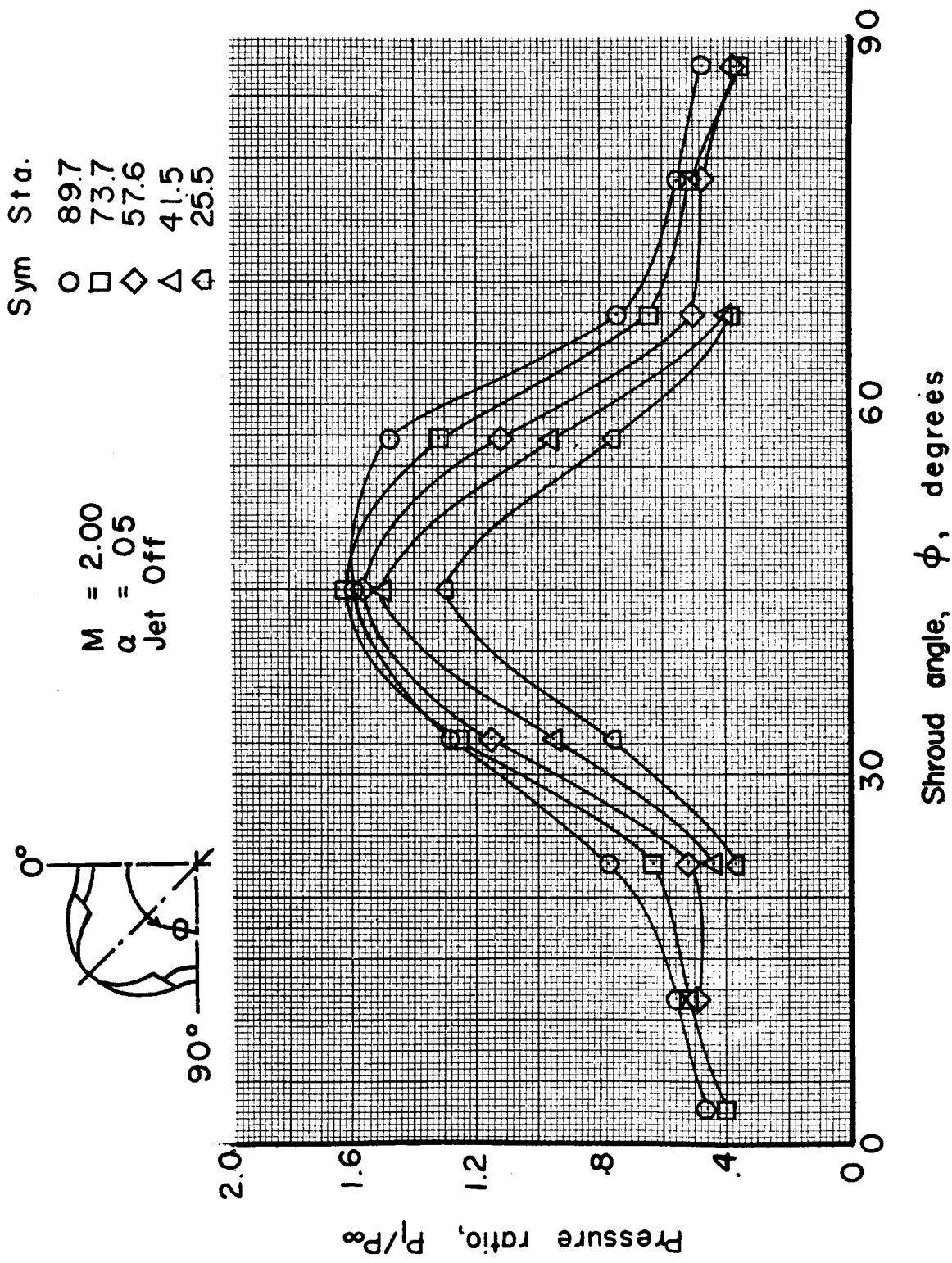


Figure 45d Results of wind tunnel tests showing variation of shroud pressures

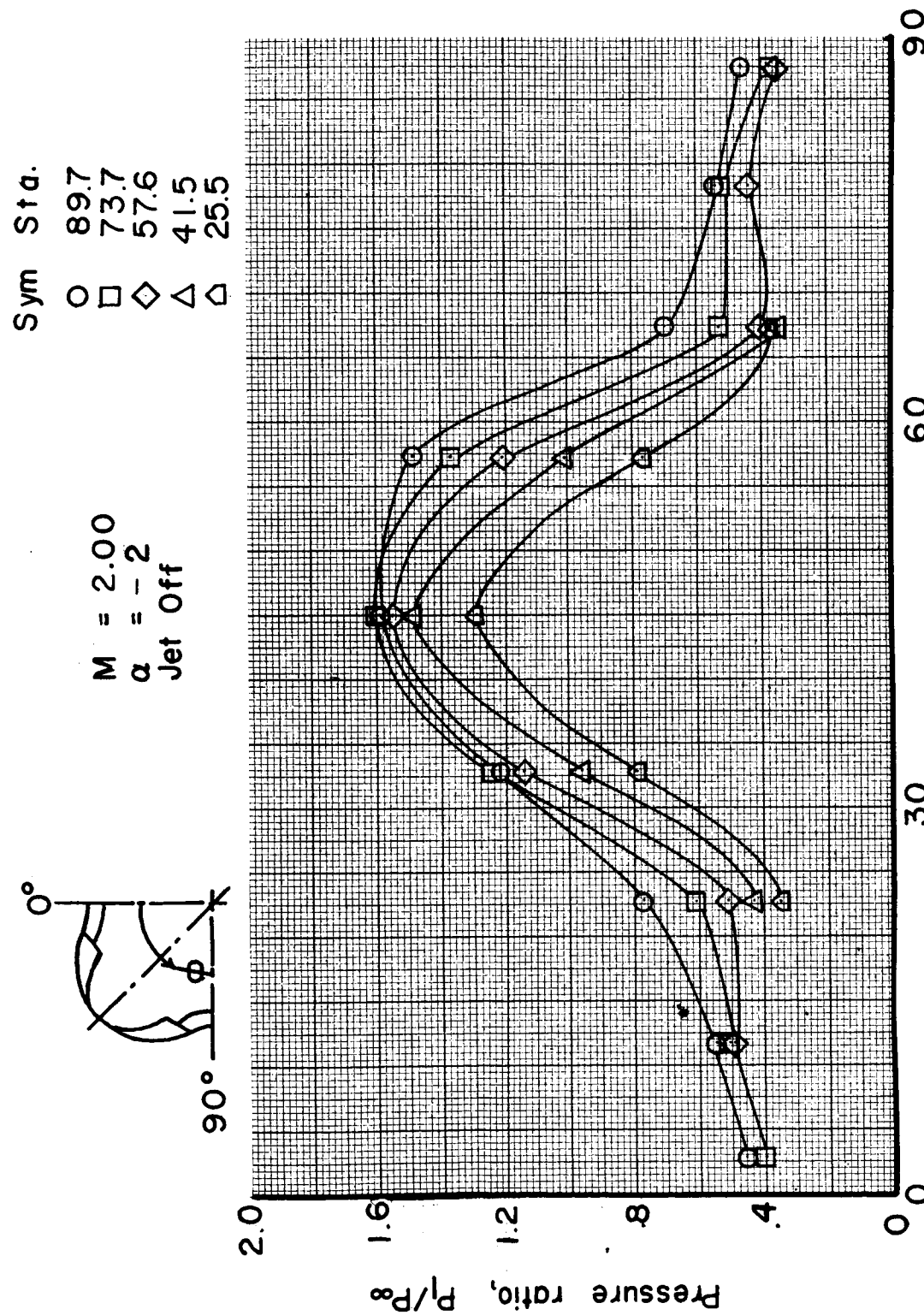


Figure 45b Results of wind tunnel tests showing variation of shroud pressures

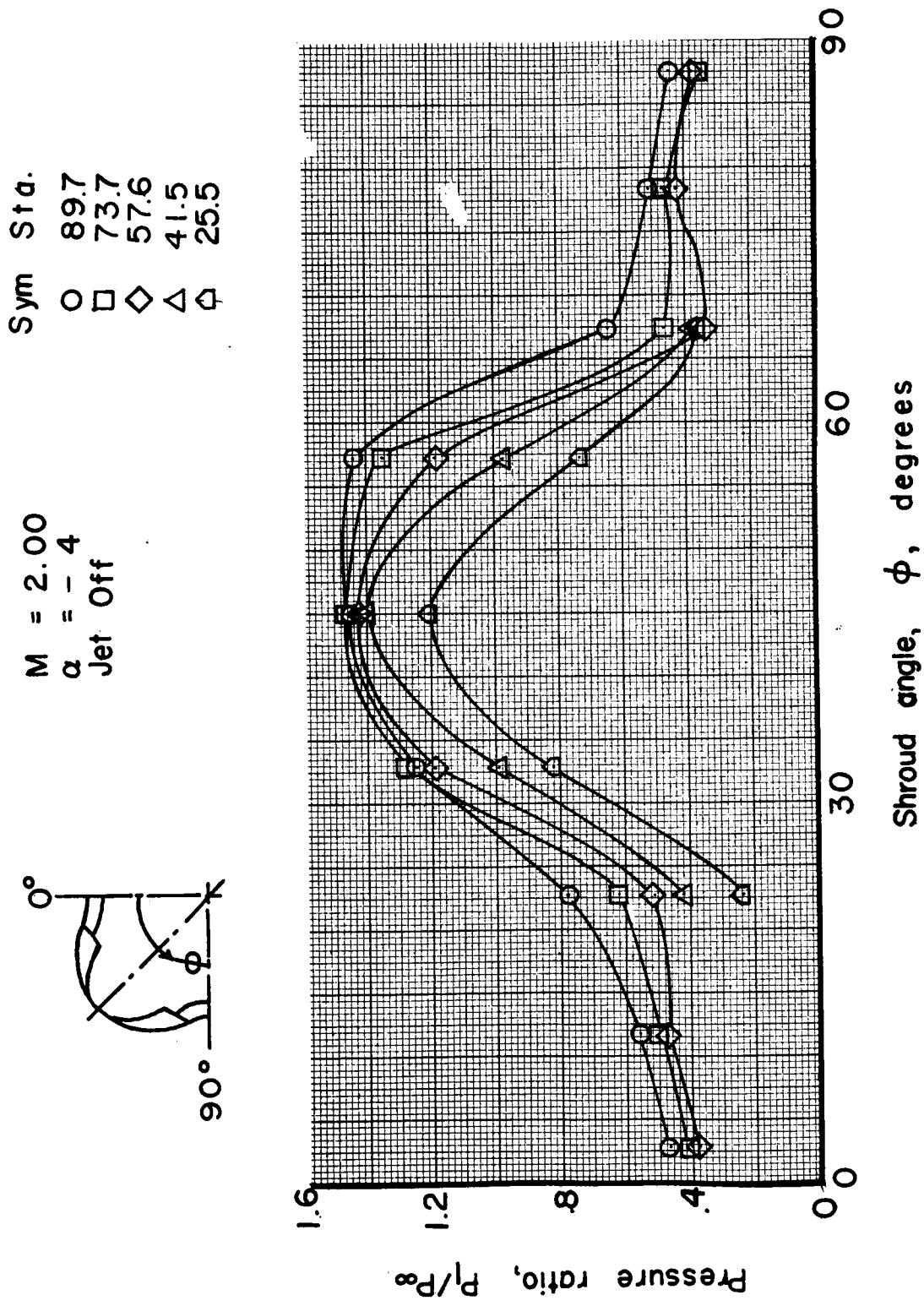


Figure 45c Results of wind tunnel tests showing variation of shroud pressures

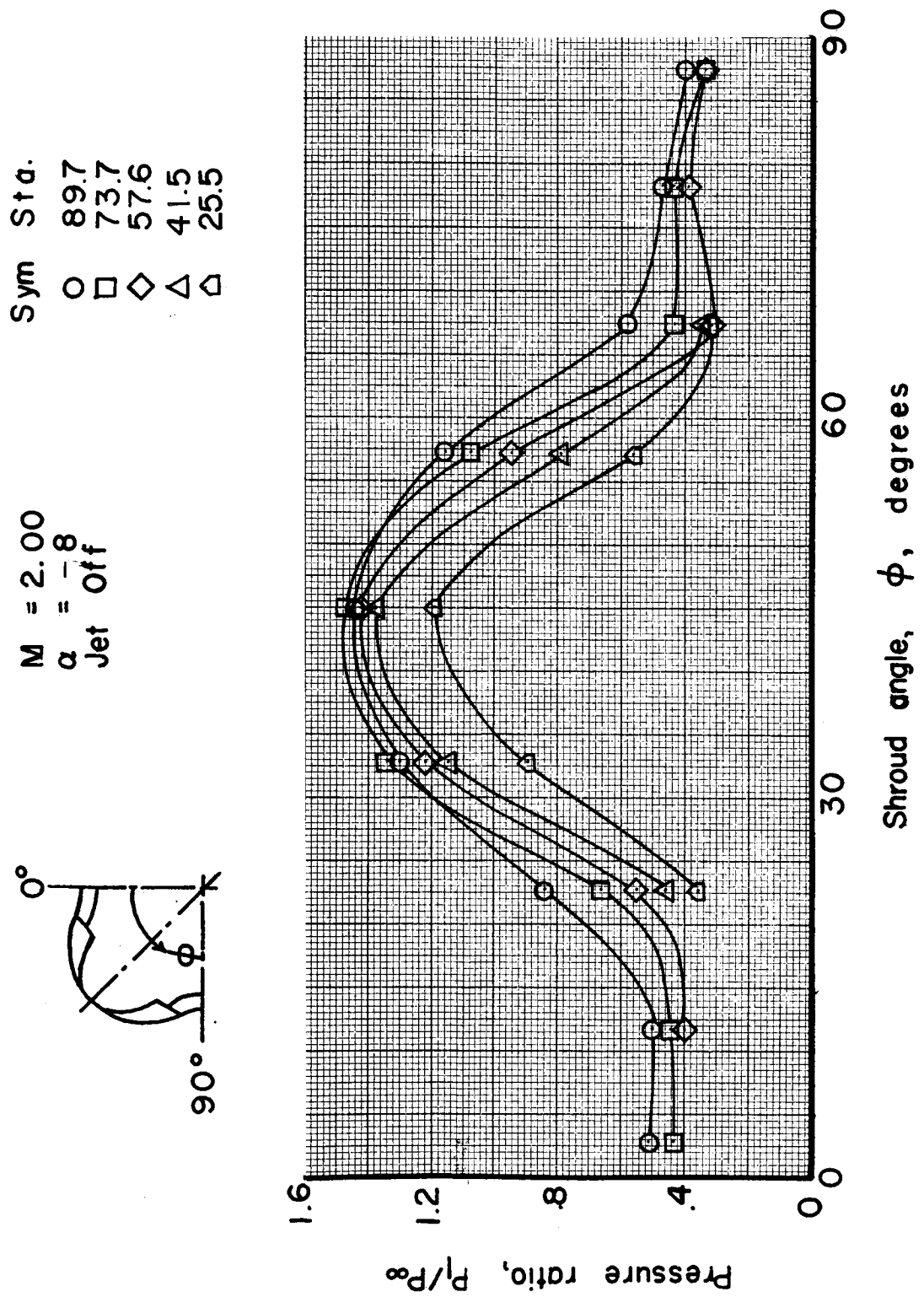


Figure 45d Results of wind tunnel tests showing variation of shroud pressures

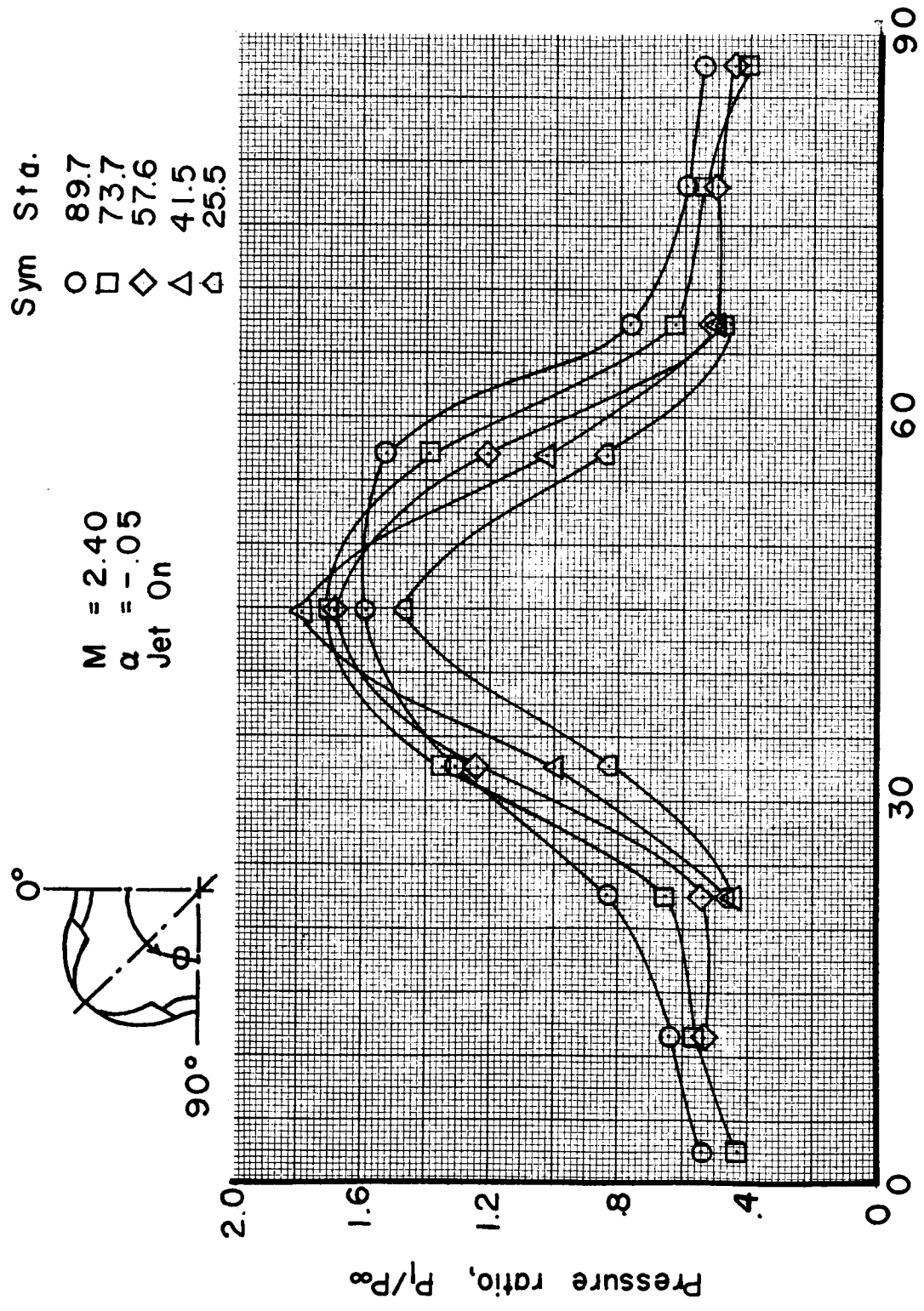


Figure 46a Results of wind tunnel tests showing variation of shroud pressures

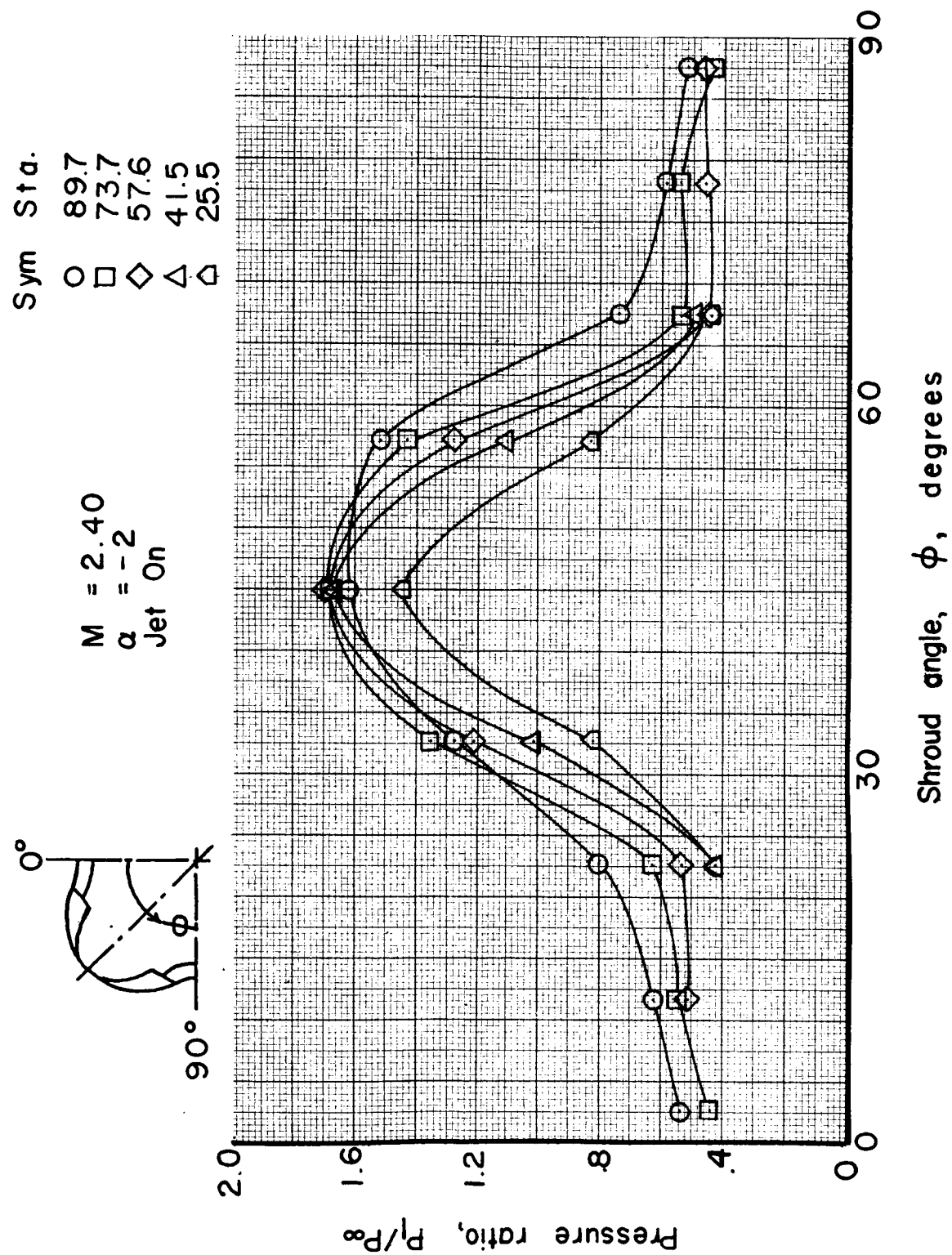


Figure 46b Results of wind tunnel tests showing variation of shroud pressures

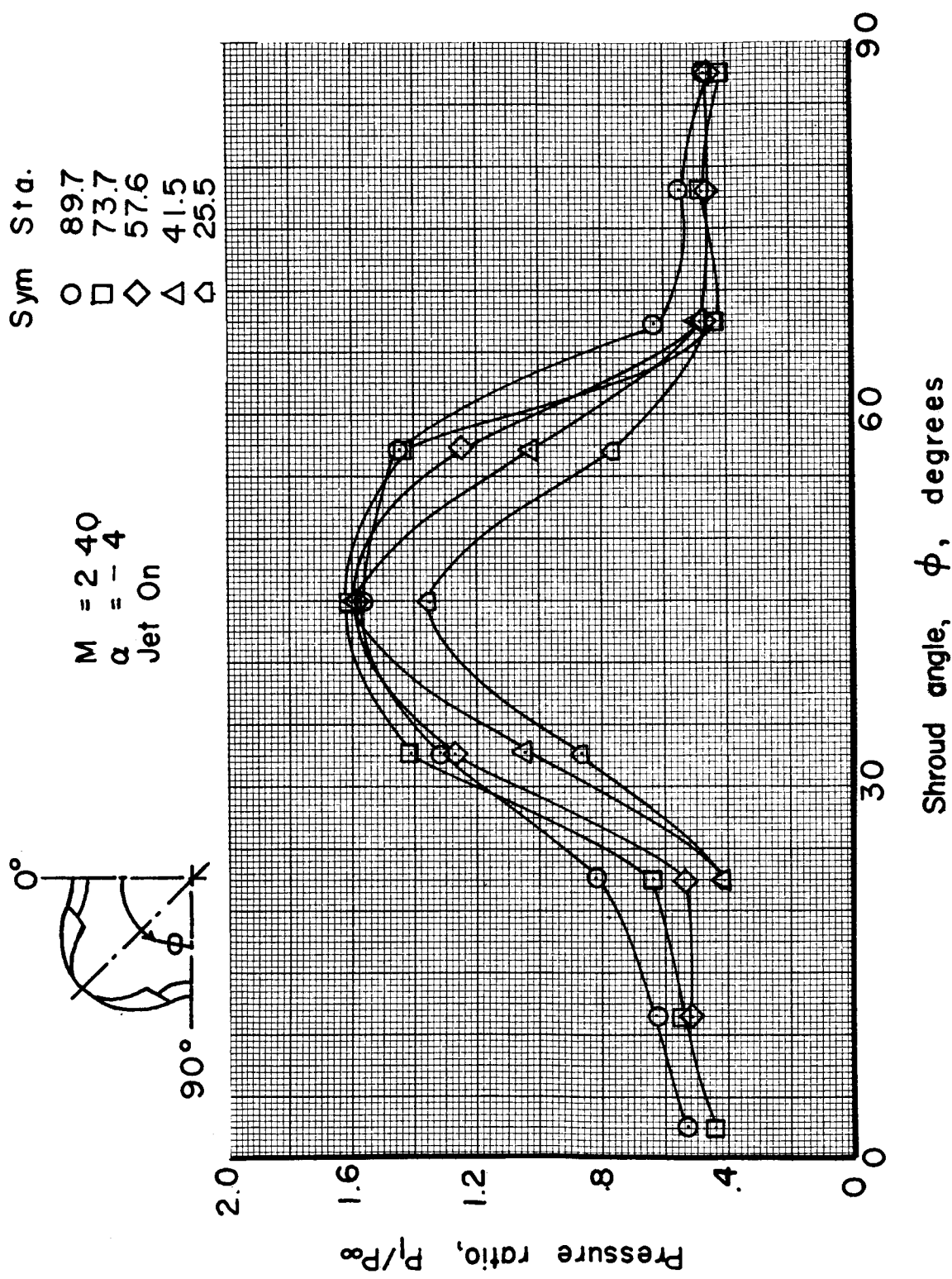


Figure 46c Results of wind tunnel tests showing variation of shroud pressures

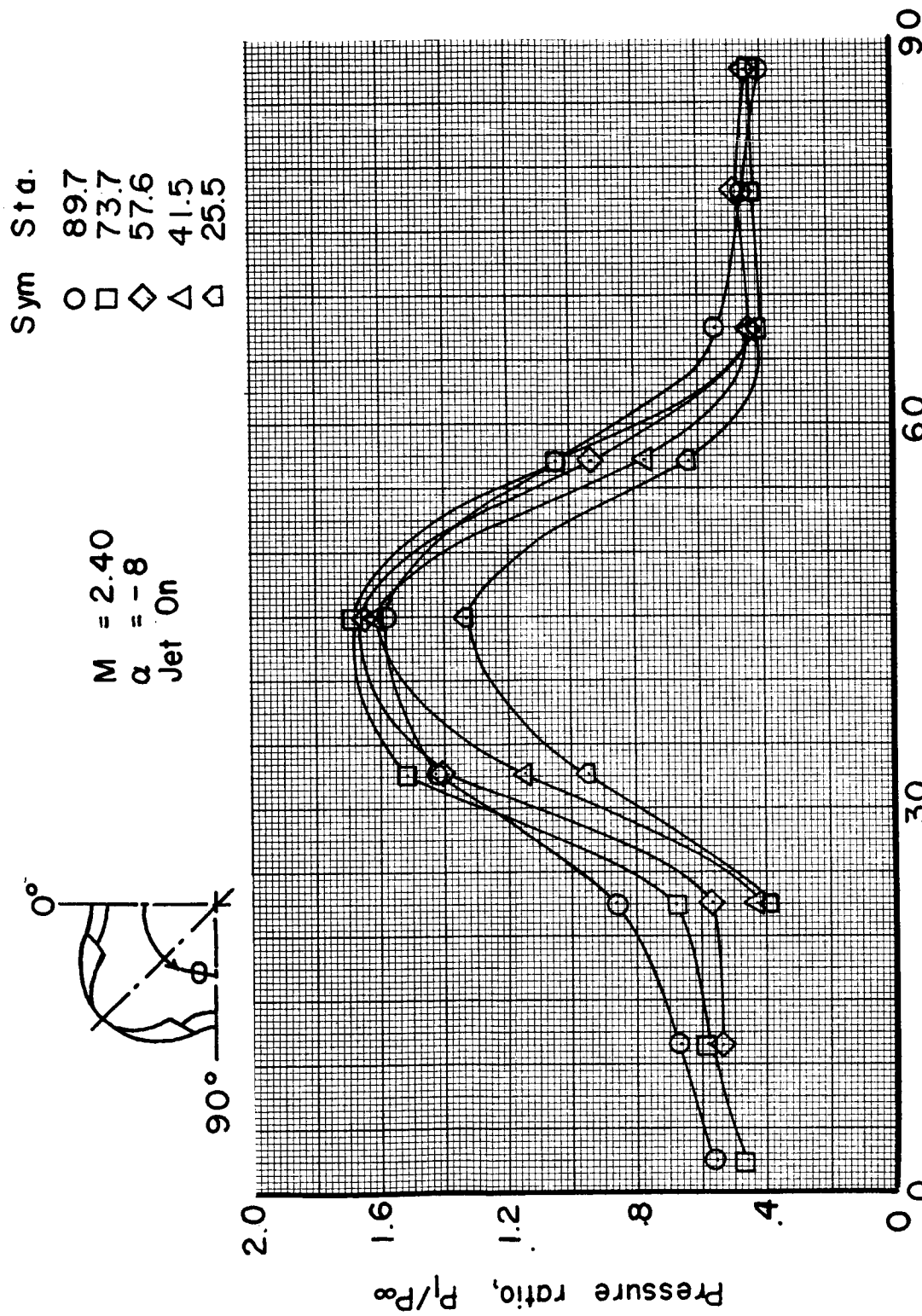


Figure 46d Results of wind tunnel tests showing variation of shroud pressures

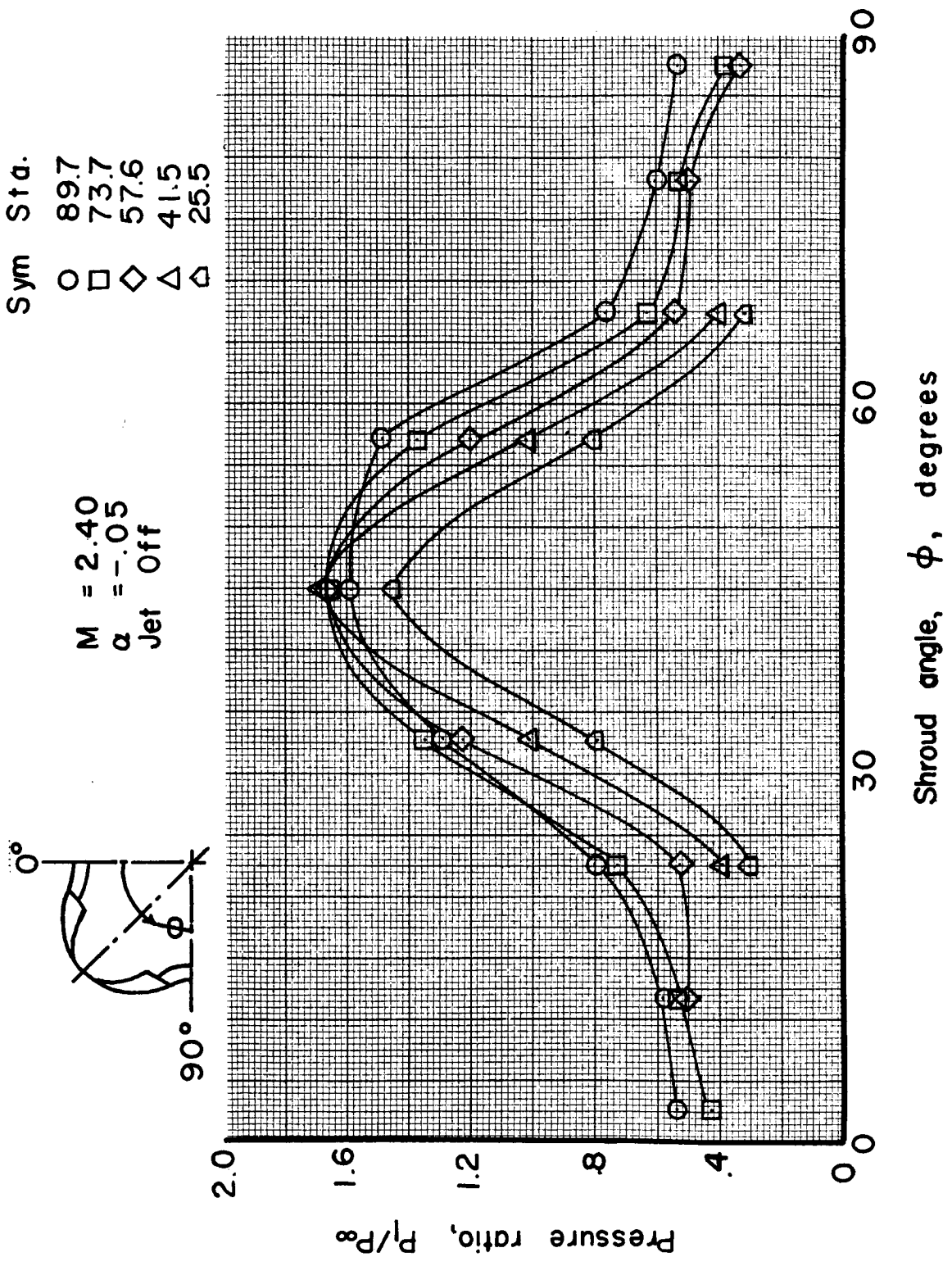


Figure 47a Results of wind tunnel tests showing variation of shroud pressures

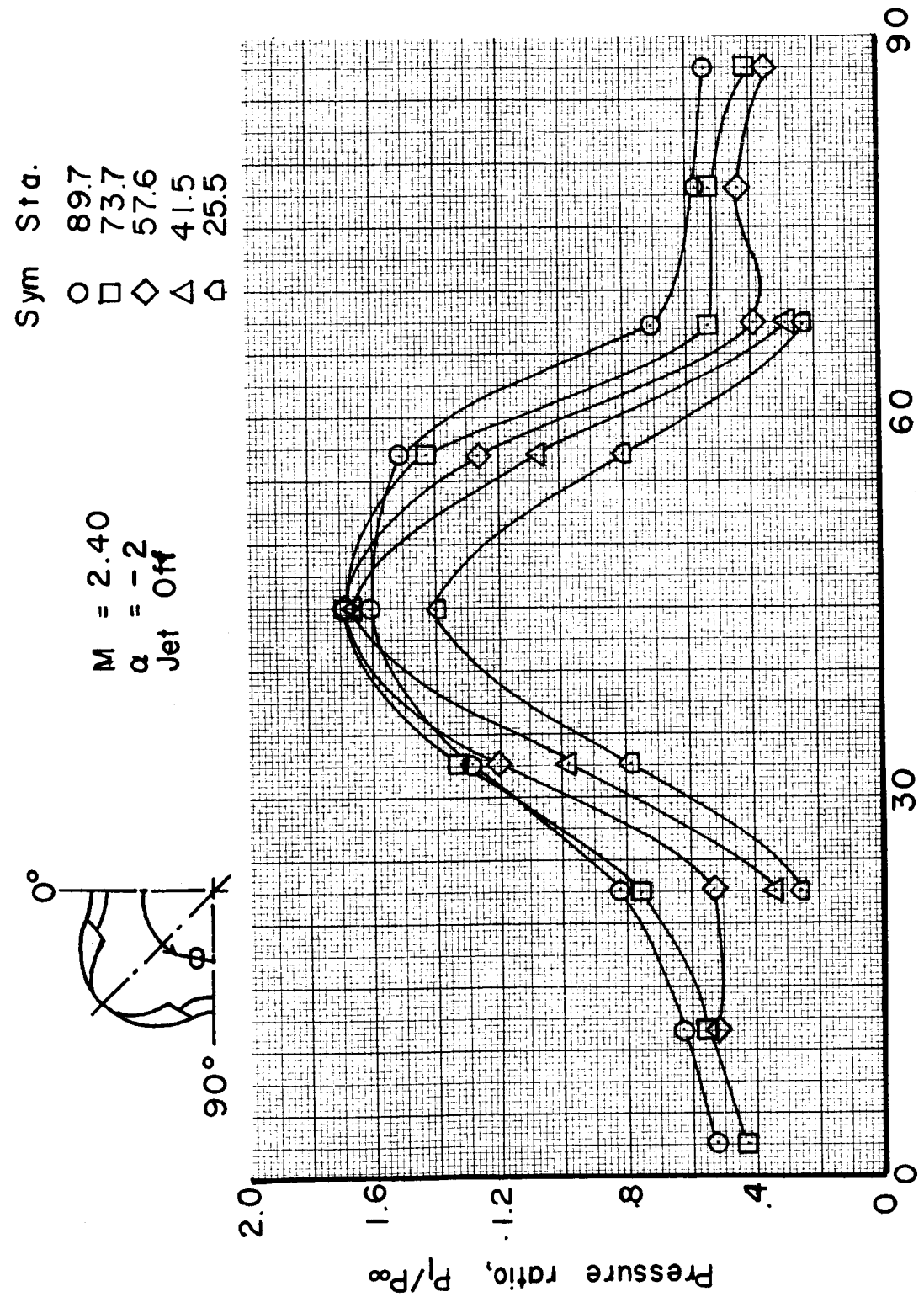


Figure 47b Results of wind tunnel tests showing variation of shroud pressures

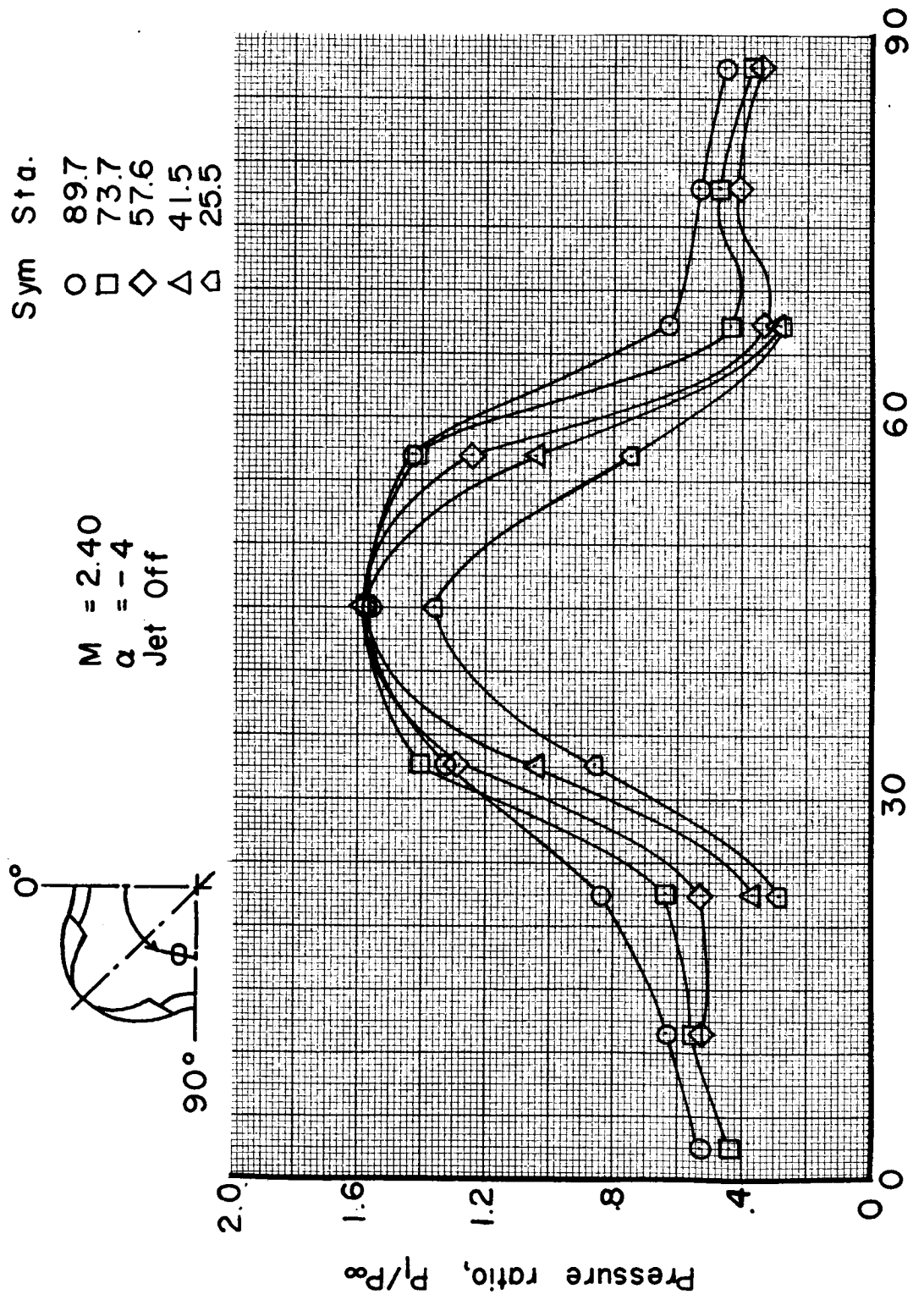


Figure 47c Results of wind tunnel tests showing variation of shroud pressures

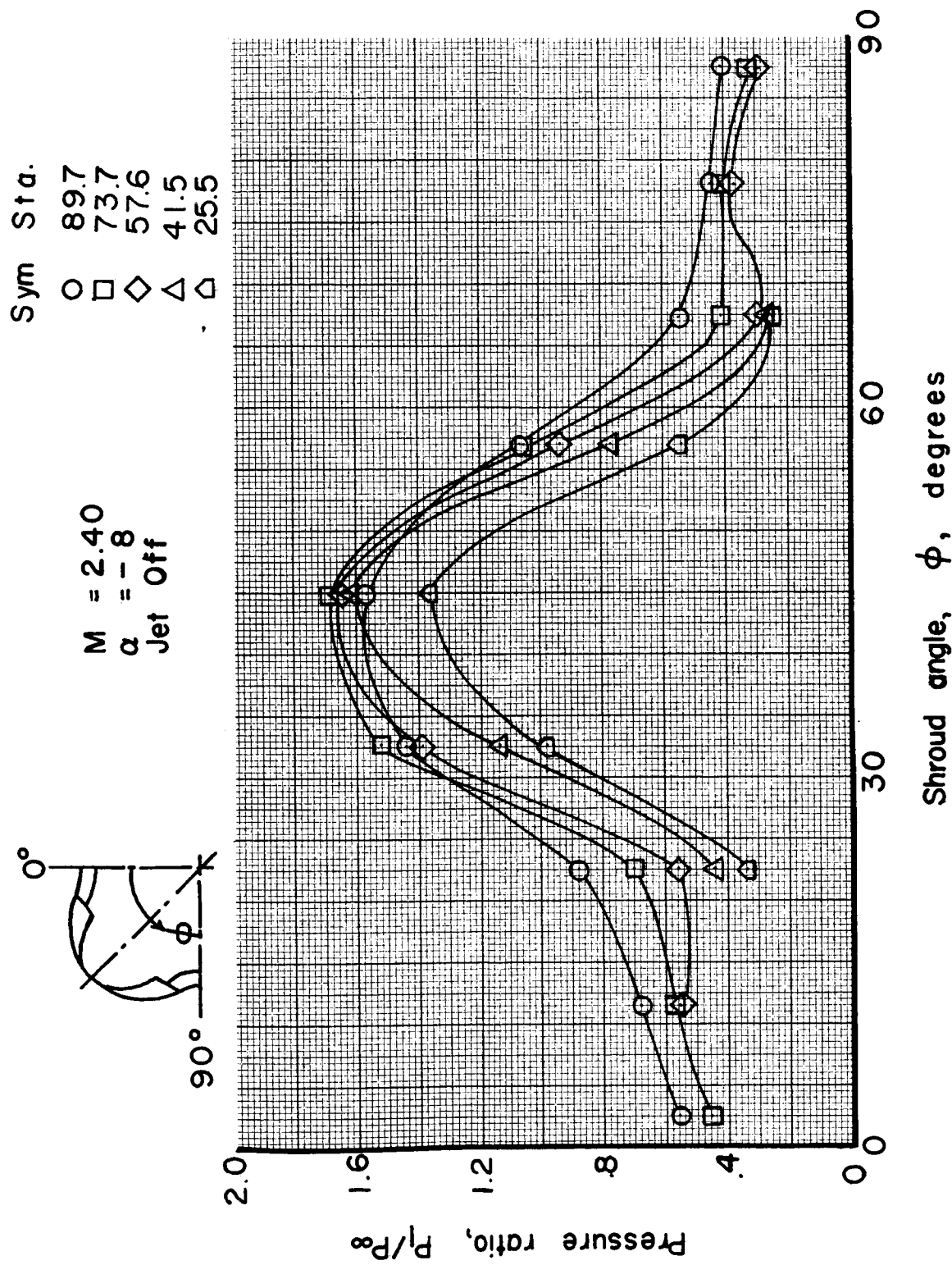


Figure 47d Results of wind tunnel tests showing variation of shroud pressures

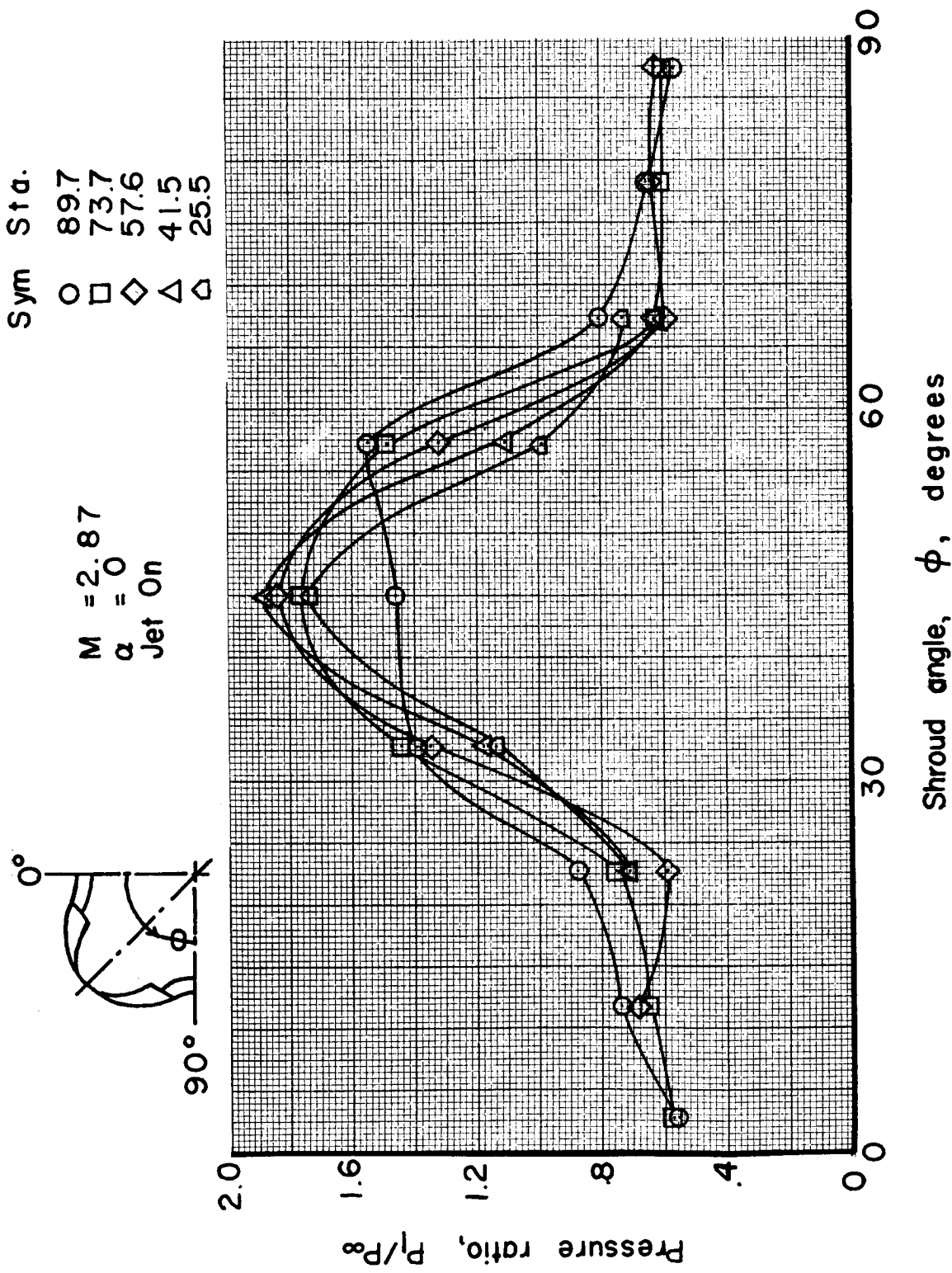


Figure 48a Results of wind tunnel tests showing variation of shroud pressures

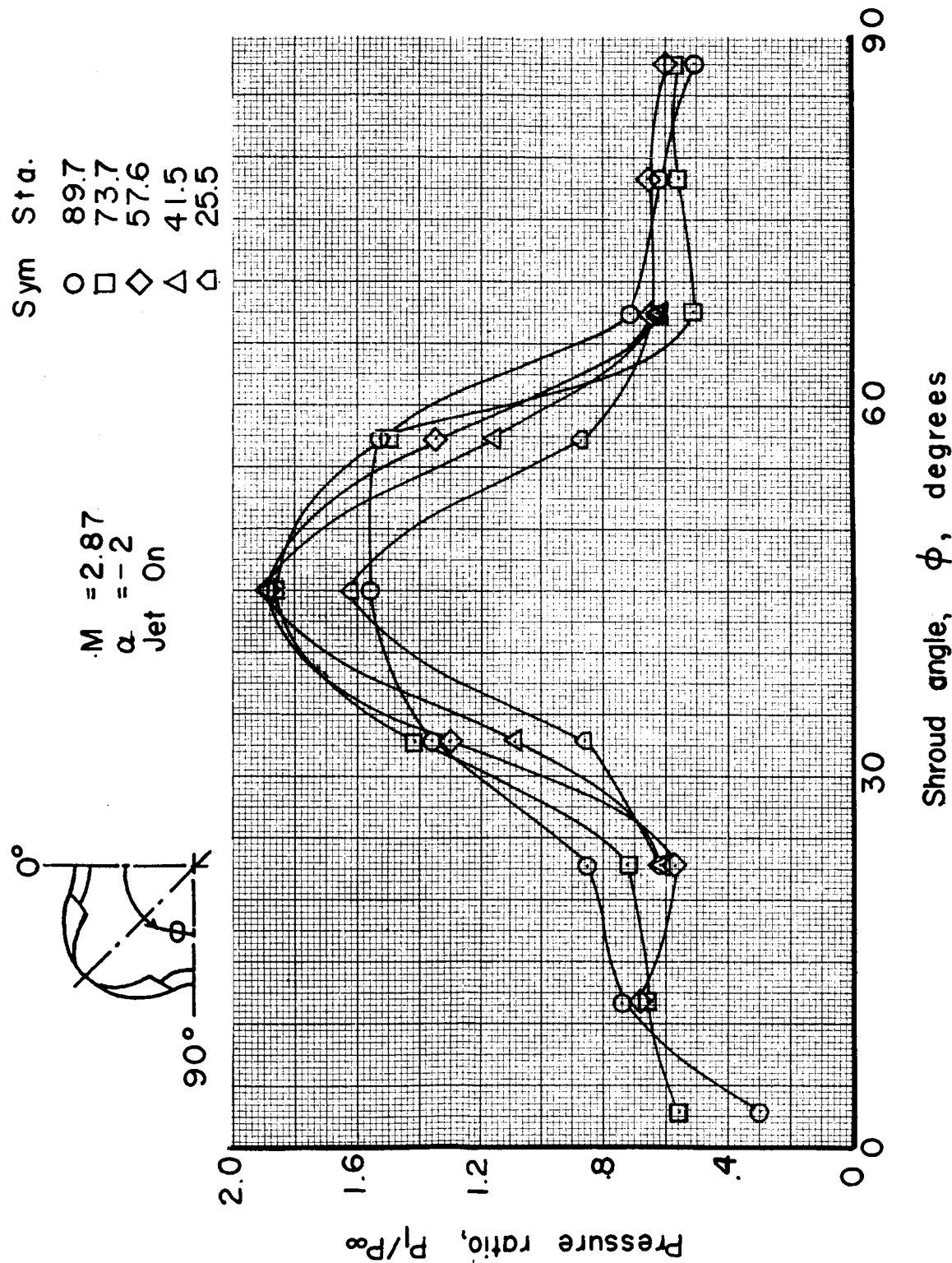


Figure 48b Results of wind tunnel tests showing variation of shroud pressures

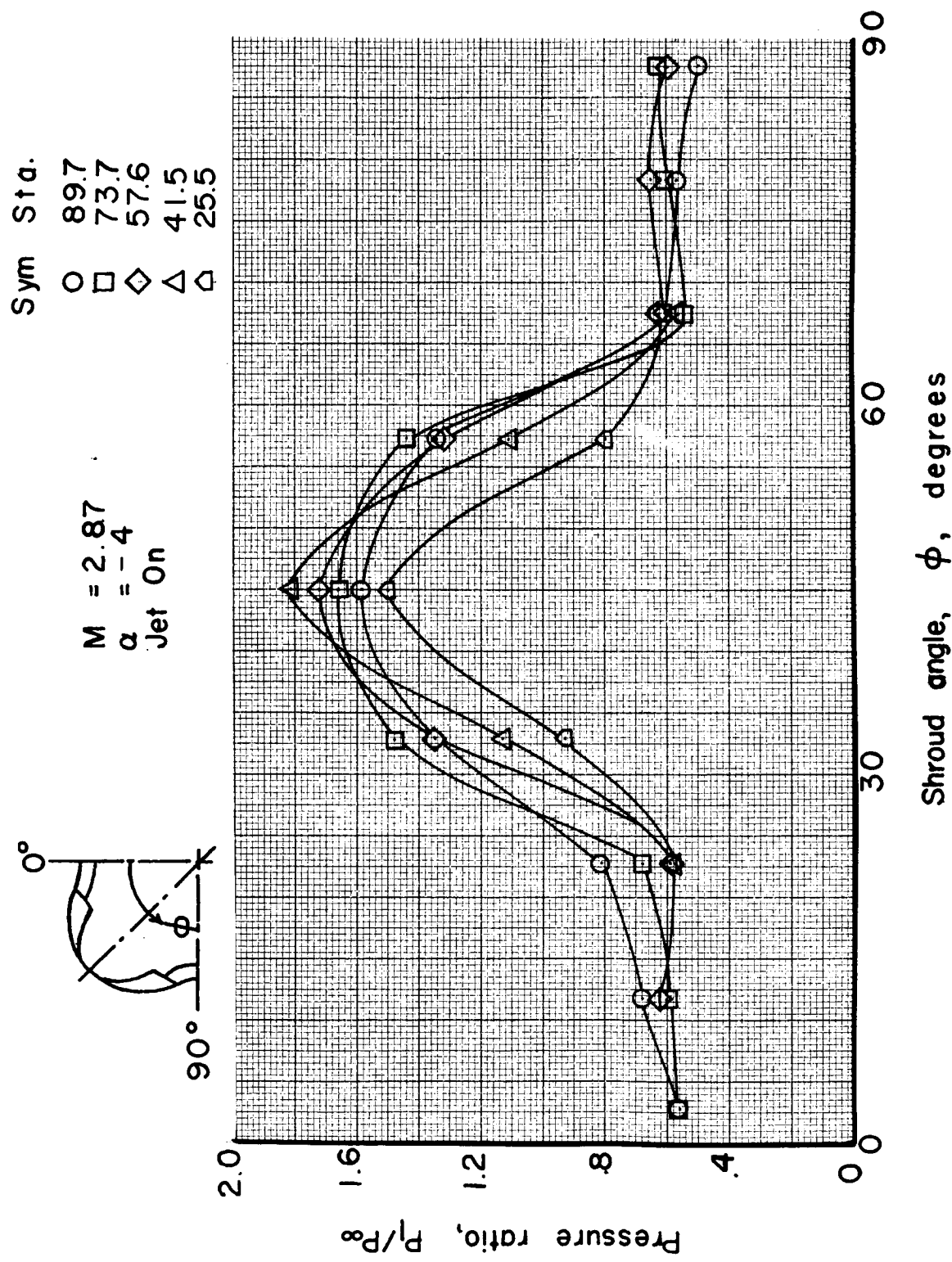


Figure 48c Results of wind tunnel tests showing variation of shroud pressures

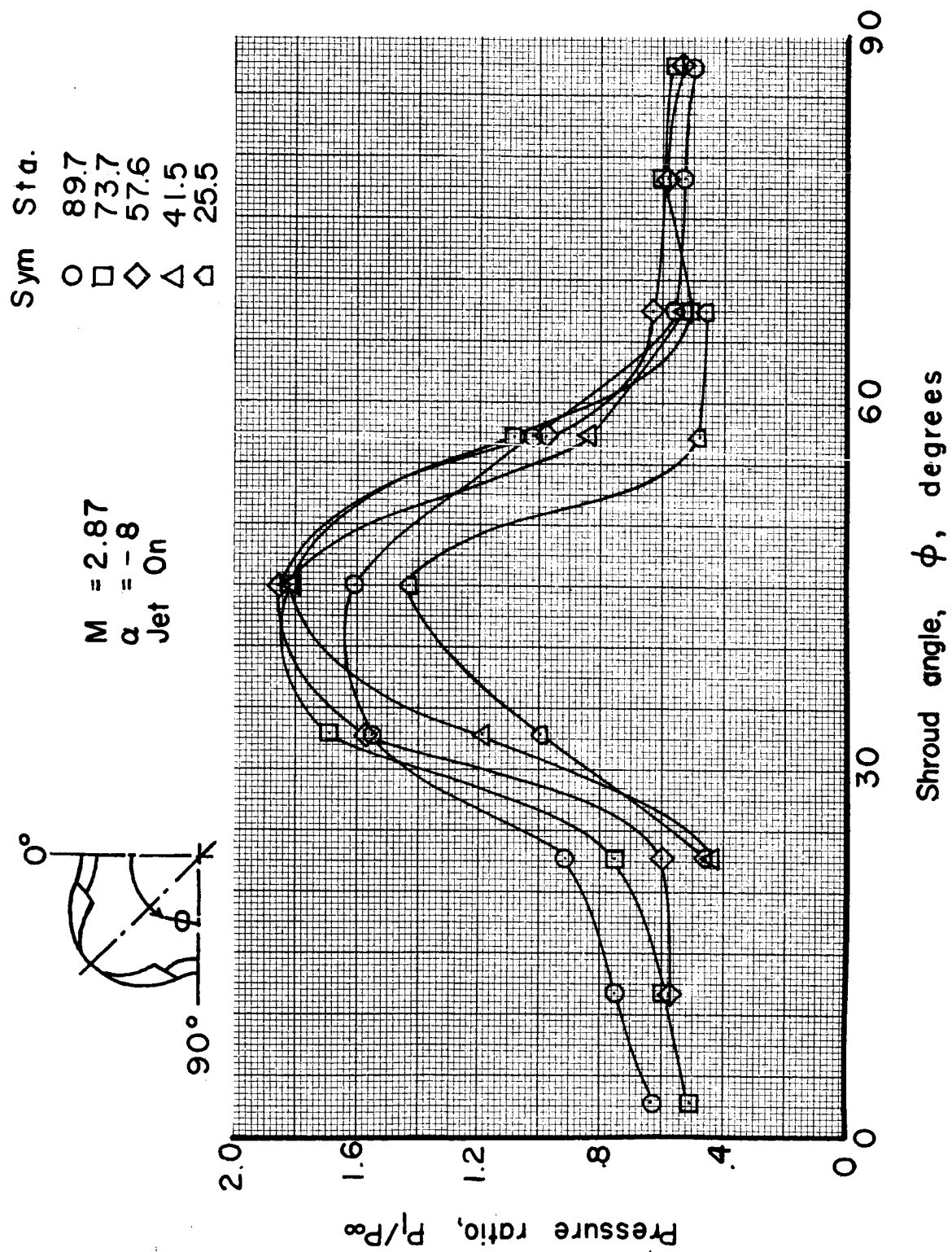


Figure 48d Results of wind tunnel tests showing variation of shroud pressures

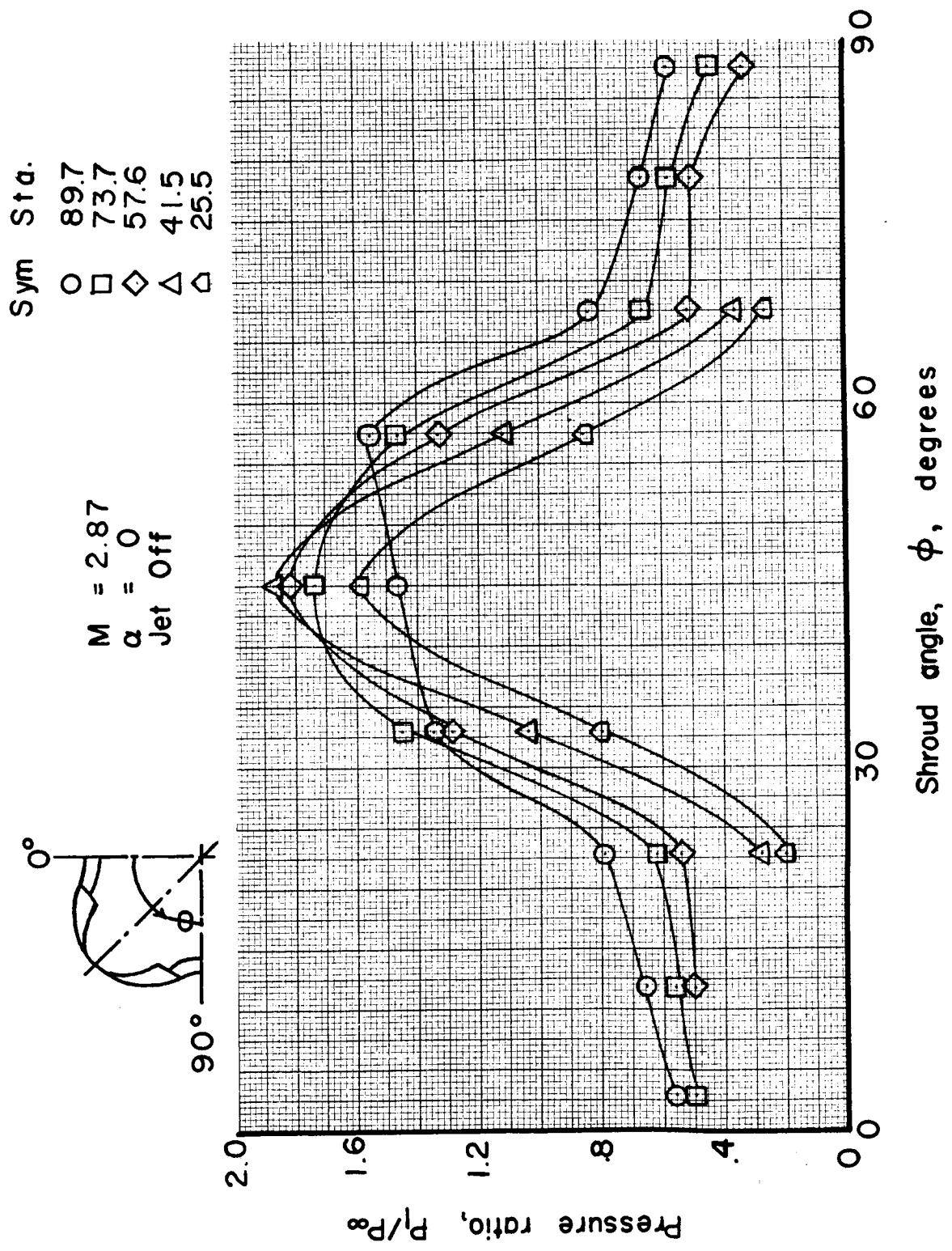


Figure 49q Results of wind tunnel tests showing variation of shroud pressures

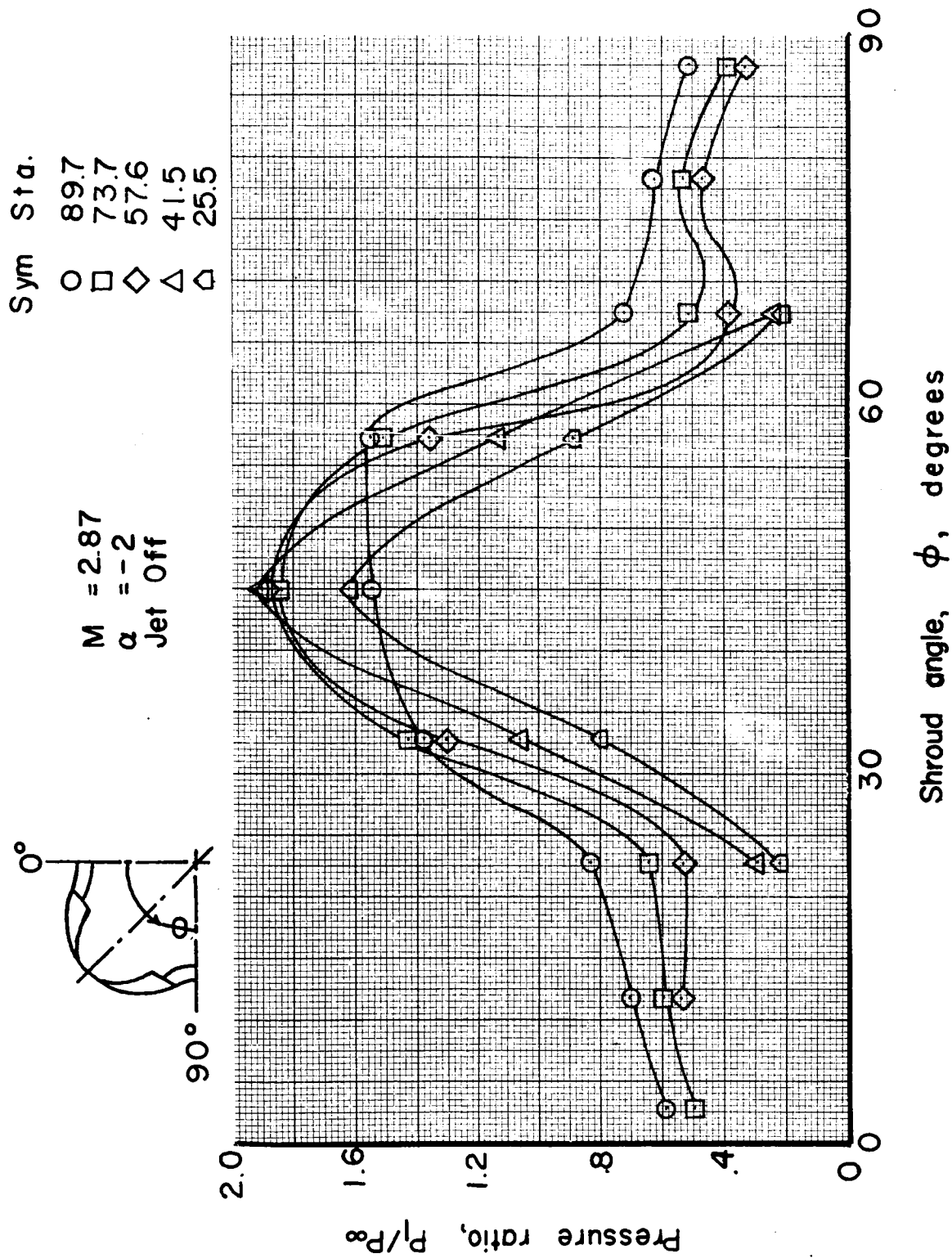


Figure 49b Results of wind tunnel tests showing variation of shroud pressures

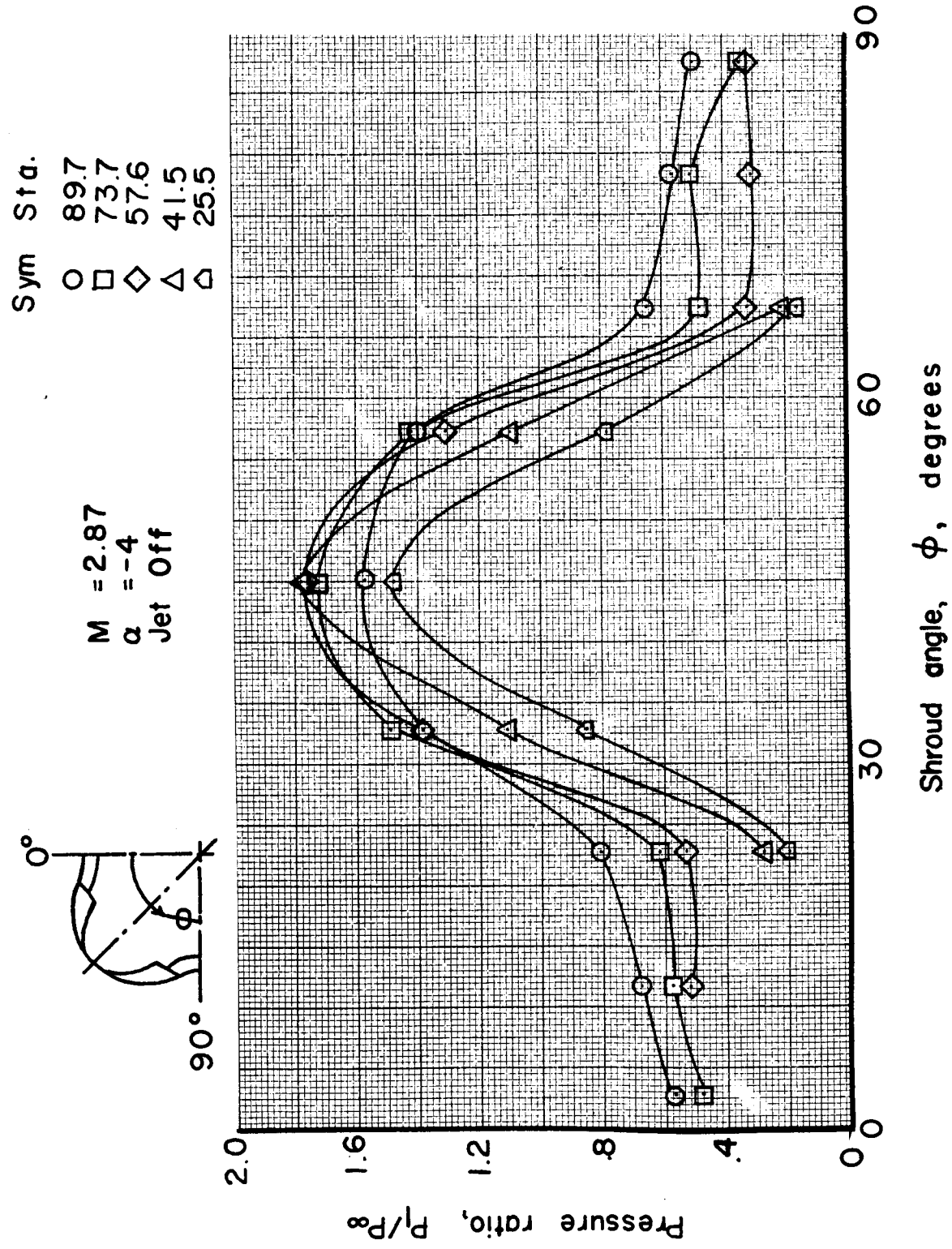


Figure 49c Results of wind tunnel tests showing variation of shroud pressures

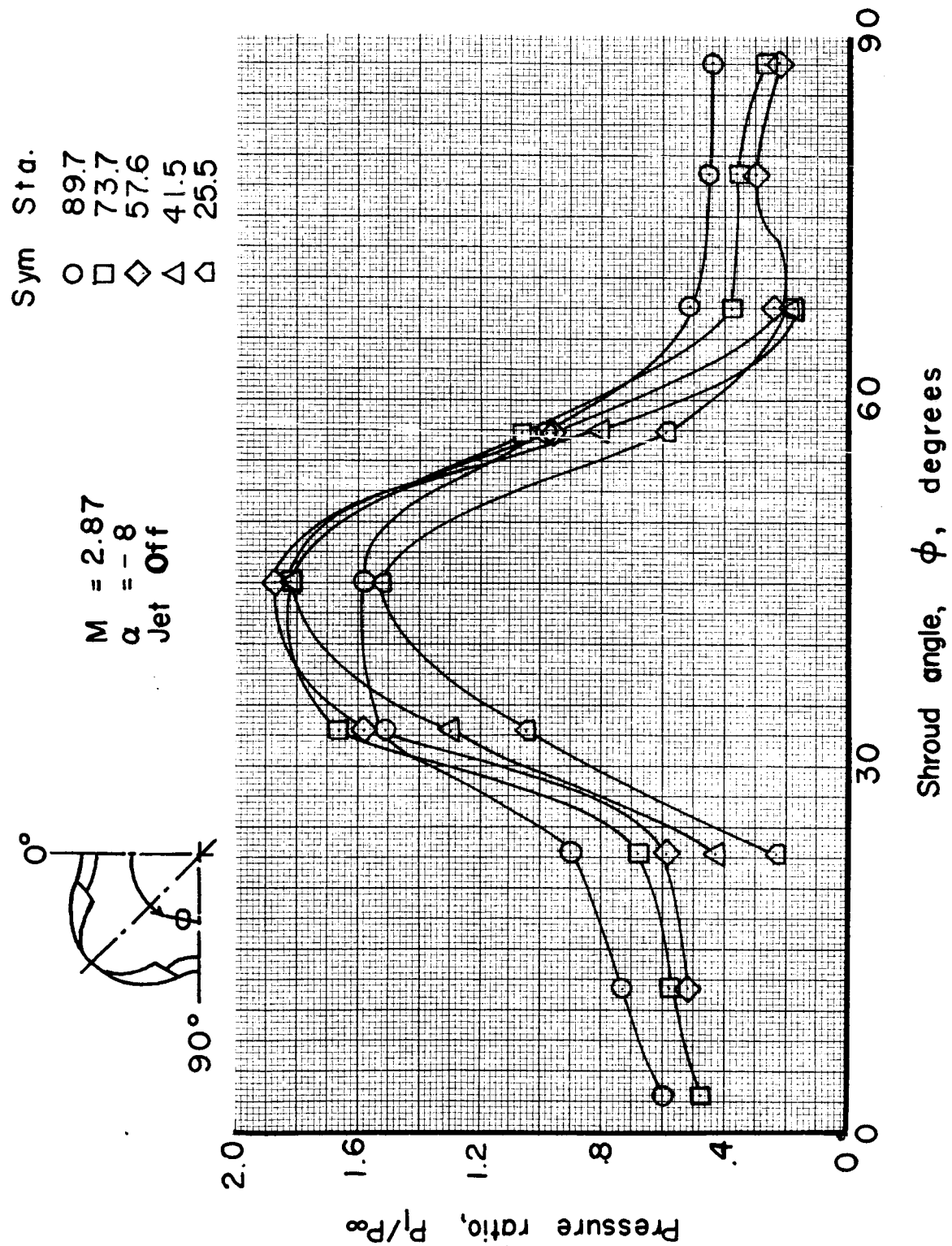


Figure 49d Results of wind tunnel tests showing variation of shroud pressures

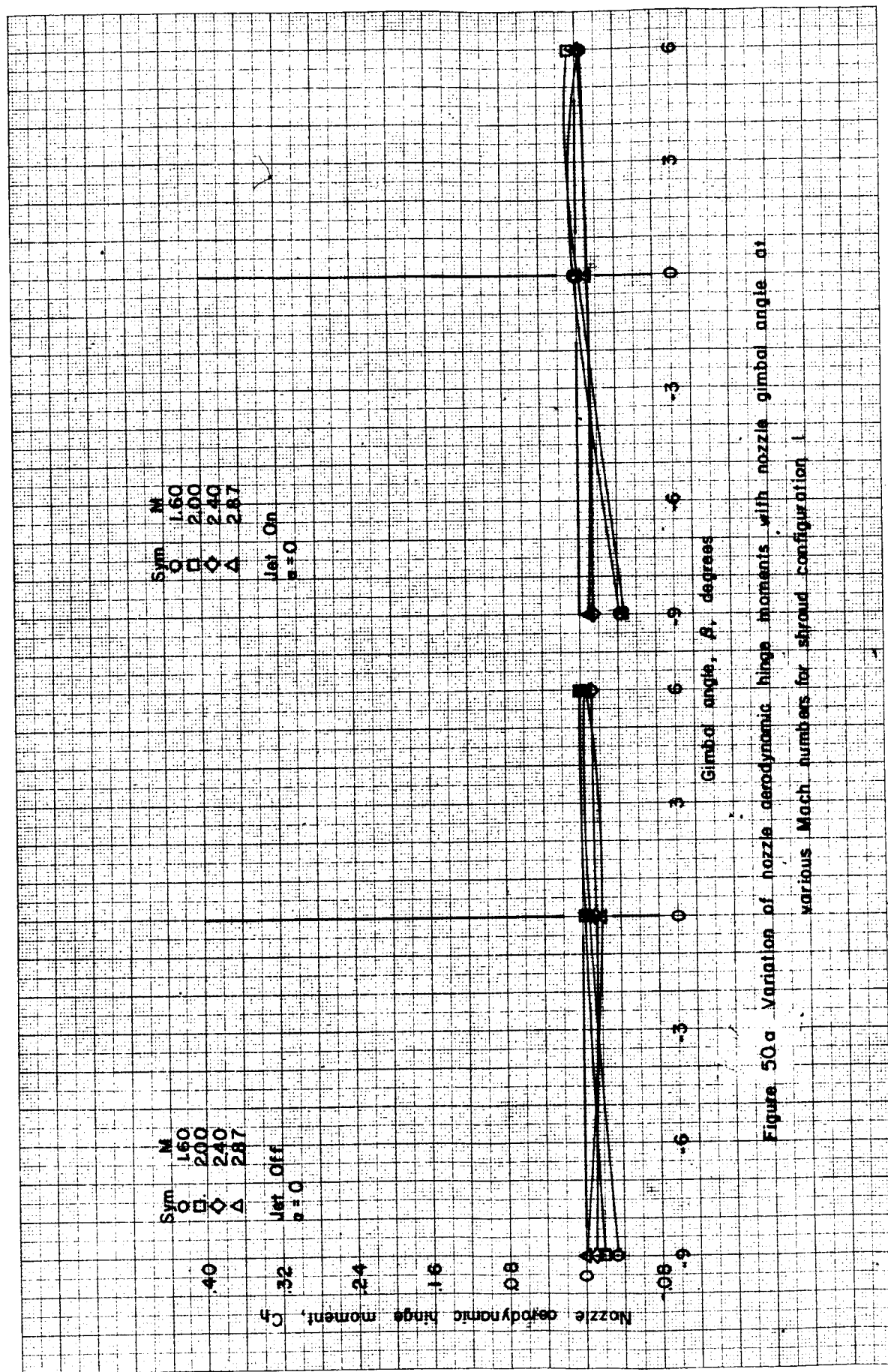


Figure 50a Variation of nozzle aerodynamic hinge moments with nozzle gimbal angle  $\alpha$ ,  
various Mach numbers for shield configuration I.

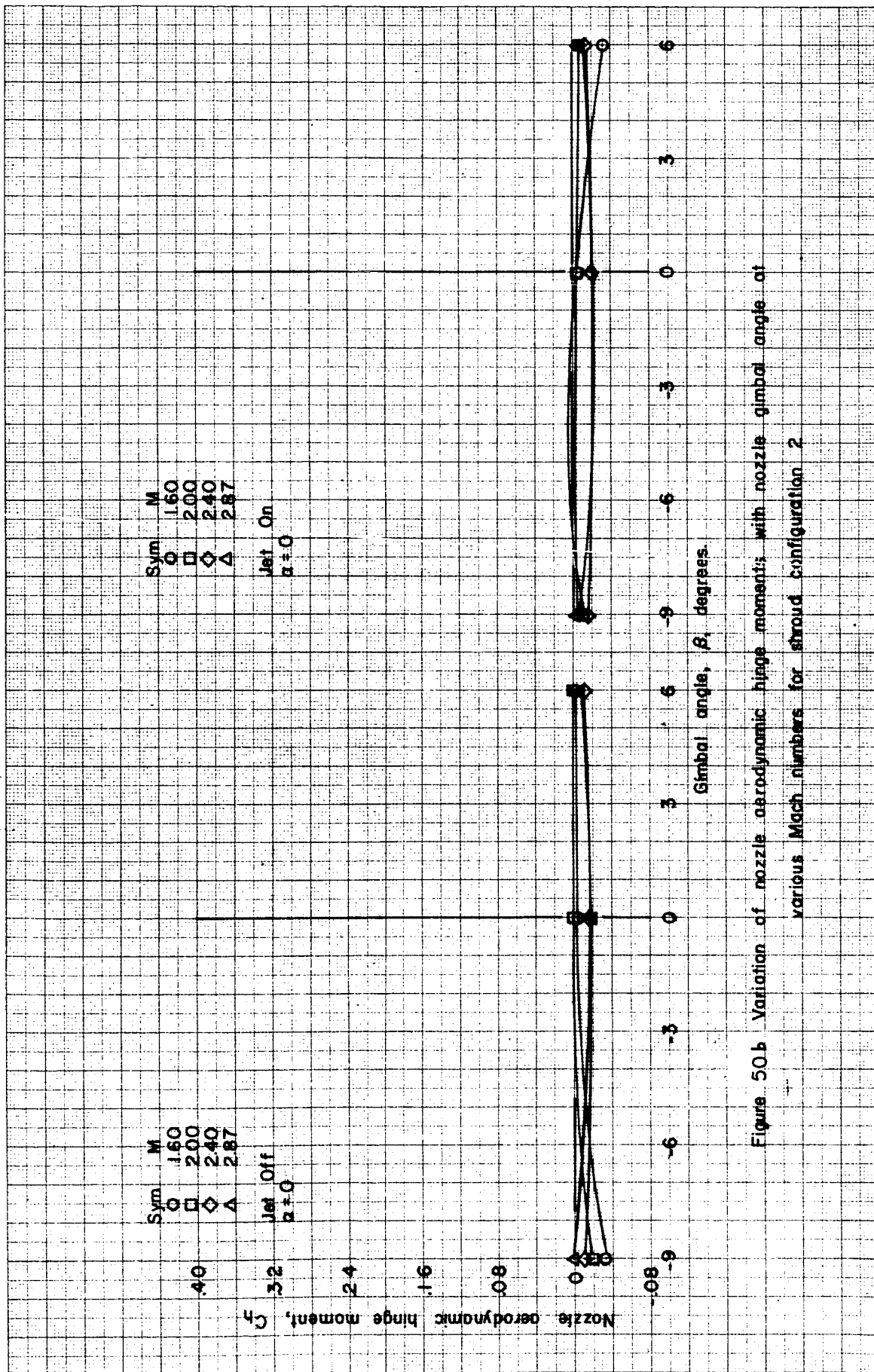


Figure 50b Variation of nozzle aerodynamic hinge moments with nozzle gimbal angle at various Mach numbers for shroud configuration 2

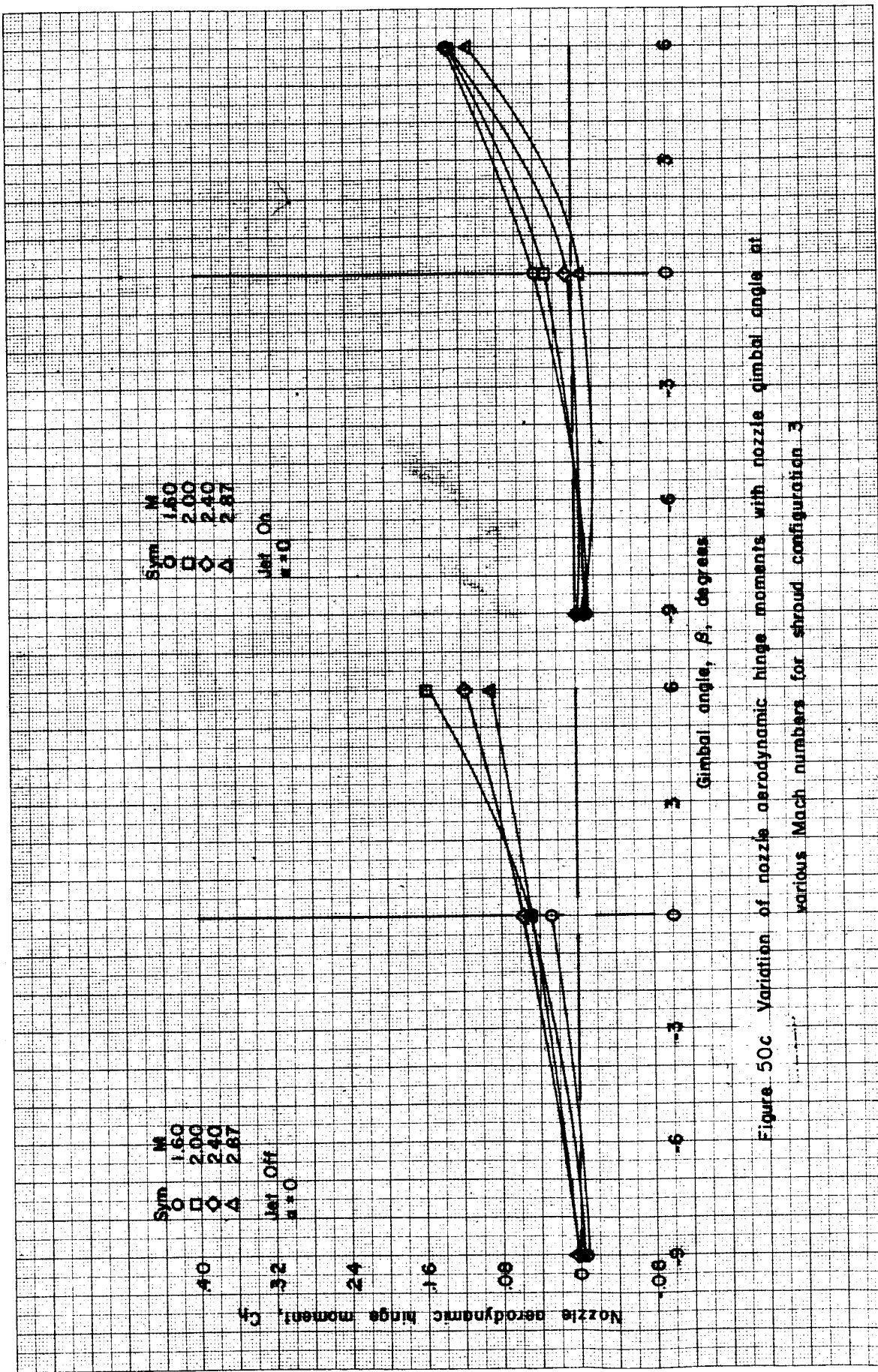


Figure 50c Variation of nozzle aerodynamic hinge moments with nozzle gimbal angle at various Mach numbers for shroud configuration 3

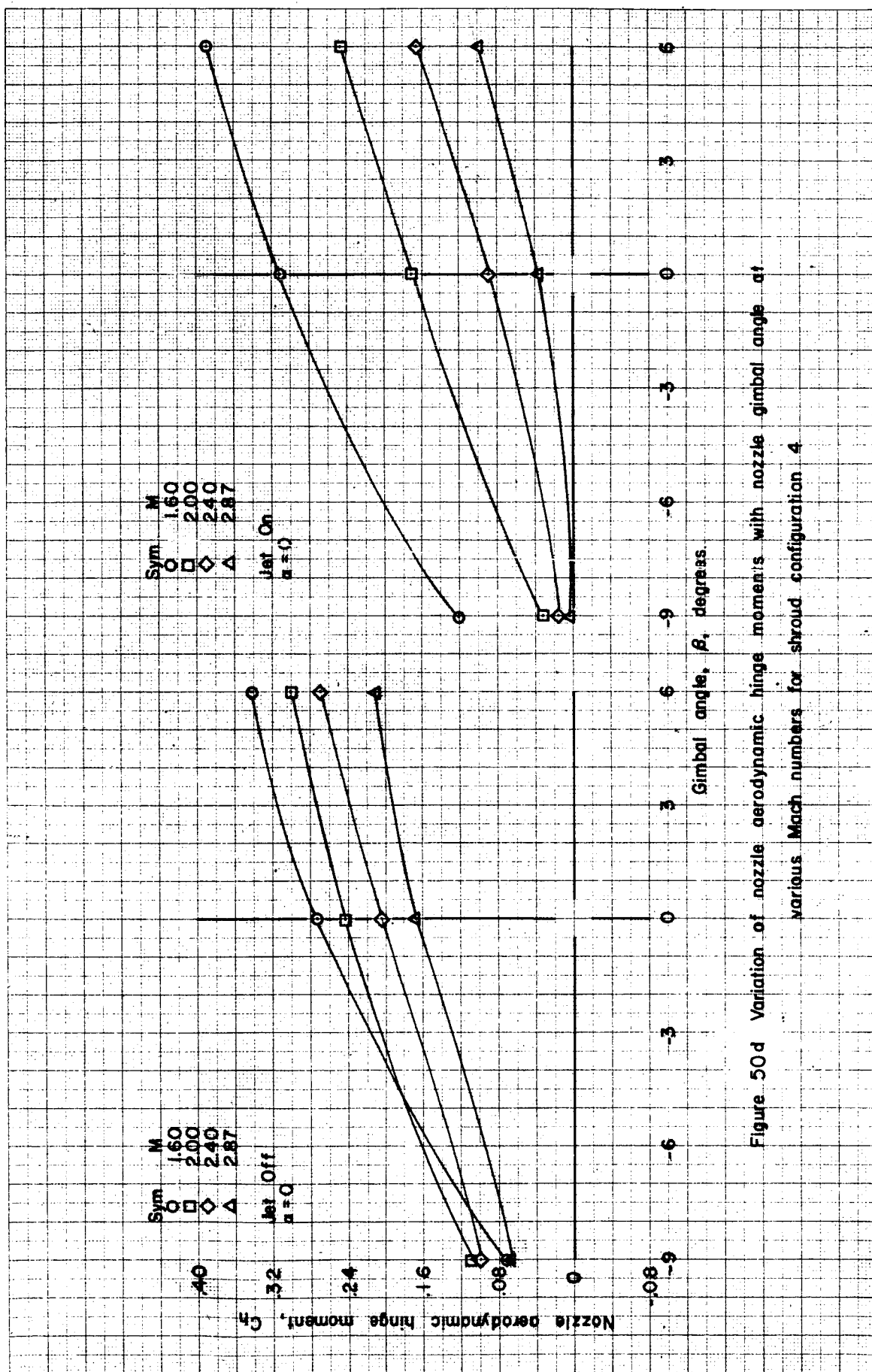


Figure 50d Variation of nozzle aerodynamic hinge moments with nozzle gimbal angle at various Mach numbers for shroud configuration 4

## REFERENCES

1. Goethert, B. H., Symposium Proceedings - Altitude Testing of Rockets and Missile Components - sponsored by Aero, Inc., and Space Technology Labs. March 1960. Subject: "Test Techniques used to Provide Atmospheric and Space Environment Required for Rocket Testing to Measure the Important Rocket Parameters."

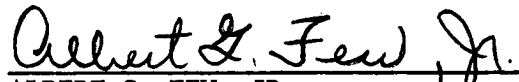
APPROVAL

MTP-AERO-63-31

A WIND TUNNEL INVESTIGATION TO DETERMINE SOME  
AERODYNAMIC HINGE MOMENTS ON THE MODEL ENGINES  
OF A SATURN I, BLOCK I CONFIGURATION

GLENN T. BOYD

The information in this report has been reviewed for security classification. Review of any information concerning Department of Defense or Atomic Energy Commission programs has been made by the MSFC Security Classification Officer. This report, in its entirety, has been determined to be unclassified.



ALBERT G. FEW, JR.  
Chief, Experimental Projects Section



O. C. HOLDERER  
Chief, Experimental Aerodynamics Branch



E. D. GEISSLER  
Director, Aeroballistics Division

## DISTRIBUTION

M-DIR

M-PAT

M-P&VE

Mr. Hunt  
Mr. Blumrich  
Mr. Neighbors  
Mr. Verble  
Mr. Stevens  
Mr. Kroll  
Mr. Showers  
Mr. Connell

M-MS-H

M-HME-P

Scientific and Technical Information  
Facility  
ATTN: NASA Representative (S-AK/RKT)  
P. O. Box 5700  
Bethesda, Md. (2)

M-AERO

Dr. Geissler  
Dr. Hoelker  
Mr. Jean  
Mr. Teague  
Mr. Miner  
Mr. Schmieder  
Mr. Winch  
Mr. Holderer  
Mr. May  
Mr. Few  
Mr. Clark  
Mr. Felix  
Mr. Horn  
Dr. Speer  
Mr. Lindberg  
Mr. Payne  
Mr. Dahm  
Mr. McAnnally  
Mr. Linsley  
Mr. Dunn  
Mr. Weaver  
Mr. Windham  
Mr. Boyd

M-MS-IP

M-MS-IPL (8)